

DISSERTATION

NUMERICAL ANALYSIS OF RIVER SPANNING ROCK U-WEIRS: EVALUATING
EFFECTS OF STRUCTURE GEOMETRY ON LOCAL HYDRAULICS

Submitted by

Christopher Lee Holmquist-Johnson

Department of Civil and Environmental Engineering

In partial fulfillment of the requirements

For the Degree of Doctor of Philosophy

Colorado State University

Fort Collins, Colorado

Summer 2011

Doctoral Committee:

Advisor: Chester C. Watson

Steven R. Abt
Christopher I. Thornton
William Doe

ABSTRACT

NUMERICAL ANALYSIS OF RIVER SPANNING ROCK U-WEIRS: EVALUATING EFFECTS OF STRUCTURE GEOMETRY ON LOCAL HYDRAULICS

River spanning rock weirs are being constructed for water delivery as well as to enable fish passage at barriers and provide or improve the aquatic habitat for endangered fish species. Many design methods are based upon anecdotal information applicable to narrow ranges of channel conditions and rely heavily on field experience and engineering judgment. Without an accurate understanding of physical processes associated with river spanning rock weirs, designers cannot address the failure mechanisms of these structures. This research examined the applicability of a Computational Fluid Dynamics (CFD) model, U²RANS, to simulate the complex flow patterns associated with numerous U-weir configurations.

3D numerical model simulations were used to examine the effects of variations in U-weir geometry on local hydraulics (upstream water surface elevations and downstream velocity and bed shear stress). Variations in structure geometry included: arm angle, arm slope, drop height, and throat width. Various combinations of each of these parameters were modeled at five flow rates: 1/10 bankfull discharge, 1/5 bankfull discharge, 1/3 bankfull discharge, 2/3 bankfull discharge and bankfull discharge. Numerical modeling results duplicated both field observations and laboratory results by quantifying high shear stress magnification near field and lab scour areas and low shear stress magnification near field and lab depositional areas. The results clearly showed that by altering the

structure geometry associated with U-weirs, local flow patterns such as upstream flow depth, downstream velocity, and bed shear stress distributions could be altered significantly. With the range of parameters tested, the maximum increase in channel velocity ranged from 1.24 to 4.04 times the reference velocity in the channel with no structure present. Similarly, the maximum increase in bed shear stress caused by altering structure geometry ranged from 1.57 to 7.59 times the critical bed shear stress in the channel for a given bed material size. For the range of structure parameters and channel characteristics modeled, stage-discharge relationships were also developed utilizing output from the numerical model simulations.

These relationships are useful in the design process when estimating the backwater effect from a structure for irrigation diversion as well as determining the spacing between structures when multiple structures are used in series. Recommendations were also made, based on the analysis and conclusions gathered from the current study, for further research. The analysis and results of the current study as well as laboratory studies conducted by Colorado State University and field reconnaissance by the Bureau of Reclamation provide a process-based method for understanding how structure geometry affects flow characteristics, scour development, fish passage, water delivery, and overall structure stability. Results of the numerical modeling allow designers to utilize the methods and results of the analysis to determine the appropriate U-weir geometry for generating desirable flow parameters (i.e. upstream flow depth and downstream velocity and bed shear stress magnification) to meet project specific goals. The end product of this research provides tools and guidelines for more robust structure design or retrofits based upon predictable engineering and hydraulic performance criteria.

ACKNOWLEDGMENTS

Sincere appreciation and thanks are extended to those who assisted in this study. Special thanks are extended to my advisor, Dr. Chester Watson, for his continuous guidance and technical support throughout the preparation of this dissertation. Special thanks and appreciation are extended to my committee members, Dr. Christopher Thornton, Dr. Steven Abt, and Dr. William Doe, for their insight and critical review of this document

I would also like to thank: Dr. David Mooney for his numerous hours of data collection and assistance with the mesh generation program; Dr. Terry Waddle for his guidance, technical review, and perspectives along the way; Tony Meneghetti and Michael Scurlock for their collaboration and assistance with the laboratory modeling results; and the Bureau of Reclamation who provided funding for this research project. Many thanks are also extended to my fellow colleagues at the Bureau of Reclamation Technical Service Center for their assistance in the field data collection and overall support and long lasting friendships.

I also would like to thank my family for encouraging me to pursue a higher education and sincerely appreciate their support throughout this study. Finally, a special thank you to my wife, Dr. Helen Holmquist-Johnson, for her inspiration, encouragement, love, and understanding throughout this very long journey.

TABLE OF CONTENTS

Abstract.....	ii
Acknowledgments.....	iv
Table of Contents.....	v
List of Figures.....	vii
List of Tables.....	xiv
List of Symbols and Abbreviations.....	xv
1 Introduction.....	1
1.1 General Background.....	1
1.2 Project Background.....	3
1.3 Research Objectives.....	5
1.4 Approach and Methodology.....	6
2 Literature Review.....	10
2.1 Introduction.....	10
2.2 Current Design Practices.....	12
2.2.1 Structure Dimensions.....	12
2.2.2 Location and Spacing.....	19
2.2.3 Stage discharge relationships.....	20
2.2.4 Scour prediction.....	24
2.3 Numerical Modeling.....	28
2.3.1 Previous experiments.....	29
2.4 Summary.....	33
3 Comparison and Validation of Rock Weir Numerical Modeling.....	34
3.1 Qualitative Comparison of 1D, 2D, and 3D numerical modeling methods for rock weirs.....	35
3.2 3D numerical model comparison with observed field conditions.....	41
3.2.1 Site Description.....	41
3.2.2 Data Collection.....	42
3.2.3 Numerical Model Description.....	45
3.2.4 Comparison.....	47
3.3 3D numerical model comparison with observed laboratory conditions.....	55
3.3.1 Physical Model Description.....	56
3.3.2 Data Collection.....	58
3.3.3 Numerical Model Description.....	58
3.3.4 Comparison.....	61
4 Methods: Testing matrix Design and Setup of Numerical Model Simulations.....	74
4.1 Design of Testing Matrix.....	75
4.1.1 Bed material.....	76
4.1.2 Bankfull Channel Geomerty.....	76
4.1.3 Structure Geometry.....	78
4.2 Mesh Generation Program Development.....	84

4.2.1	Introduction.....	84
4.2.2	Structure Definition	84
4.2.3	Input of Channel characteristics and structure geometry.....	86
4.2.4	Mesh Generation.....	90
4.3	3D Model Description.....	94
4.3.1	U ² RANS.....	94
4.3.2	Model Inputs.....	96
4.3.3	Model Output.....	102
4.4	Identifying effects of structure geometry on local hydraulics	104
5	Data Analysis and Results	108
5.1	Introduction.....	108
5.2	Effects of structure geometry on upstream flow depth.....	110
5.3	Effects of structure geometry on velocity and bed shear stress.....	114
5.3.1	Velocity Magnification.....	116
5.3.2	Bed Shear Stress Magnification.....	121
5.4	Stage-Discharge Relationship for Rock Weirs	127
5.4.1	Applicability of Existing Equations.....	127
5.4.2	Modification to Existing Equations	134
5.4.3	Application of modified equation.....	142
5.5	Analysis Summary.....	145
6	Summary and Recommendations	147
6.1	Contributions.....	147
6.2	Research Summary	149
6.3	Recommendations for Further Research.....	153
6.3.1	Comparison with additional field sites and laboratory data.....	153
6.3.2	Investigate effects of pre-excavated scour holes	153
6.3.3	Channel characteristics and mobile bed simulations	154
6.4	Conclusion	155
7	References.....	157
Appendix A	161
Numerical Model Testing Matrix Configurations		161
Appendix B	176
Summary of numerical model results for each structure configuration.....		176

LIST OF FIGURES

Figure 1.1 – Example of multifaceted approach of river spanning rock weir research incorporating mutually supporting field, laboratory, and numerical studies.....	4
Figure 2.1 – Depiction of river spanning rock weir structure types (Mooney et al. 2007b)	11
Figure 2.2 – Conceptual U-weir a) profile view and b) plan view (adapted from Rosgen, 2006).....	13
Figure 2.3 – Minimum rock size as a function of bankfull shear stress (Rosgen 2006)...	18
Figure 2.4 – Rock weir effective length parameters (Scurlock, 2009).....	27
Figure 2.5 – Laboratory free surface comparison with CFD simulations for a broad- crested weir at various flow rates (Hargreaves et al., 2007).....	30
Figure 2.6 – Experimental and simulated velocity profiles at different longitudinal locations for a linear rectangular weir (Bhuiyan and Hey, 2007).....	31
Figure 2.7 – Different weir layouts for U-, V-, and W-weir simulations and approximate mean flow directions (Bhuiyan and Hey, 2007).....	32
Figure 2.8 – Computed shear stress distribution downstream of W-weir and V-weir (Bhuiyan and Hey, 2007).....	32
Figure 3.1 – Example 3D output showing plan view water surface elevation contours obtained from 3D model.....	36
Figure 3.2 – Example 3D output showing plan view velocity vectors and wetted area obtained from 3D model.....	37

Figure 3.3 – Example 3D output showing thalweg profile and velocity magnitude obtained from 3D model.....	38
Figure 3.4 – Meeting 1D water surface criteria fails to meet velocity criteria (a) and vice versa (b). No Method of manipulating 1D transects captures jumps or plunging flow (c).....	40
Figure 3.5 – Map of field site location on South Fork Little Snake River.	41
Figure 3.6 – U-weir located on the South Fork Little Snake River at bankfull flow.....	42
Figure 3.7 – Bridge with sampling platform and field ADV probe used for high flow measurements.....	44
Figure 3.8 – U-weir on South Fork Little Snake River at low flow.	44
Figure 3.9 – Computational mesh for U-weir on South Fork Little Snake River.....	46
Figure 3.10 – Cross section locations for 1D model extraction for U-weir on South Fork Little Snake River.	47
Figure 3.11 – Field and numerical model U-weir centerline water surface profile comparison.....	48
Figure 3.12 – Field U-weir percent error in numerical model water surface elevations. .	49
Figure 3.13 – Field U-weir measured vs. predicted water surface elevation.....	50
Figure 3.14 – Field and numerical model U-weir water surface elevation comparison, percent error along centerline profile.....	51
Figure 3.15 – Field and numerical model U-weir velocity comparison along channel centerline a) velocity magnitude b) percent error.....	52
Figure 3.16 – Field U-weir measured versus predicted velocity.	53

Figure 3.17 – Field U-weir and numerical model velocity percent error comparison for 1D, 2D, and 3D model.....	54
Figure 3.18 – Field U-weir velocity comparison, percent error magnitude box-plot with maximum 1.5 IQR for 1D, 2D, and 3D models.....	55
Figure 3.19 – Plan-View Schematic of Flume (Meneghetti 2009).....	56
Figure 3.20 – Profile-View Schematic of Flume (Meneghetti 2009).....	56
Figure 3.21 – U-weir conceptual design parameters (Meneghetti, 2009).....	57
Figure 3.22 – Schematic of laboratory sampling locations for U-weir (Meneghetti, 2009)	58
Figure 3.23 – 3D numerical model mesh representing physical model test 35.....	59
Figure 3.24 – Cross section locations for 1D model extraction for laboratory U-weir. ...	60
Figure 3.25 – Laboratory and numerical model water surface elevation comparison test 33.....	61
Figure 3.26 – Laboratory and numerical model water surface elevation comparison test 34.....	62
Figure 3.27 – Laboratory and numerical model water surface elevation comparison test 35.....	62
Figure 3.28 – Laboratory and numerical model water surface elevation comparison, percent error along channel centerline for tests 33-35.....	63
Figure 3.29 – Laboratory measured versus predicted water surface elevations for tests 33- 35.....	64
Figure 3.30 – Numerical model water surface elevation percent error comparison for laboratory tests 33-35.....	65

Figure 3.31 – a) Numerical model bed shear stress distribution at Q_{bkf} b) Numerical model surface velocity and stream lines at Q_{bkf} c) Laboratory final bed LIDAR survey d) Laboratory test at Q_{bkf} e) Measured Laboratory vs. 3D model velocity vectors.....	66
Figure 3.32 – Laboratory and numerical model velocity comparison along channel centerline test 33.....	67
Figure 3.33 – Laboratory and numerical model velocity comparison along channel centerline test 34.....	68
Figure 3.34 – Laboratory and numerical model velocity comparison along channel centerline test 35.....	68
Figure 3.35 – Laboratory and numerical model velocity comparison, percent error along centerline for test 35.....	69
Figure 3.36 – Laboratory measured vs. predicted velocity for laboratory tests 33-35.....	70
Figure 3.37 – Laboratory and numerical model velocity percent error comparison.....	71
Figure 3.38 – Laboratory U-weir velocity comparison, percent error magnitude box-plot for 1D, 2D, and 3D models.....	72
Figure 4.1 – U-weir structure parameters a) profile view and b) plan view (adapted from Rosgen, 2006).....	78
Figure 4.2 – Plot of variation in structure parameters for three grain sizes (CG-coarse gravel, SC-small cobble, LC-large cobble) used in design matrix.....	82
Figure 4.3 – 3D Structure Line and Point Definition.....	85
Figure 4.4 – Highly Warped Quadrilateral versus Triangular Boundaries.....	91
Figure 4.5 – Highly Irregular Triangles versus Warped Quadrilateral Boundary.....	91

Figure 4.6 – Example of structure definition lines used by rock weir mesh generator. ...	93
Figure 4.7 – Example computational mesh created using mesh generation program.	94
Figure 4.8 – Computational mesh generated from mesh generator for a U-weir.	98
Figure 4.9 – Numerical representation of trapezoidal channel and U-weir header-footer configuration.	99
Figure 4.10 – Example of 3D Numerical model output showing surface velocity distribution at bankfull flow.	103
Figure 4.11 – Example of 3D numerical model output showing boundary shear stress distribution at bankfull flow.	103
Figure 4.12 – Example of sample point distribution used in comparing flow patterns between numerical model simulations a) structure configuration1 ($L_a/L_{a_{ref}}=1$) and b) structure configuration2 ($L_a/L_{a_{ref}}=1/2$).	106
Figure 5.1 – Depiction of channel and U-weir parameters a) profile view and b) plan view.	109
Figure 5.2 – Flow depth magnification associated with variation in structure geometry at five different discharge ratios.	111
Figure 5.3 – Comparison of flow depth magnification at $1.0Q_{bkf}$ and $0.1Q_{bkf}$ for each structure configuration.	113
Figure 5.4 – Example of flow redirection over weir crest and increase in mid-channel velocity streamlines and bed shear stress associated with U-weir.	115
Figure 5.5 – Maximum velocity magnification associated with variation in structure geometry at five different discharge ratios.	117

Figure 5.6 – Velocity magnification associated with variation in structure arm length at $1/3Q_{bkf}$	118
Figure 5.7 – Maximum velocity magnification comparison between $0.1Q_{bkf}$ and Q_{bkf} for variations in structure geometry.....	119
Figure 5.8 – Maximum velocity magnification location associated with variation in structure geometry.	121
Figure 5.9 – Maximum bed shear stress magnification associated with variation in structure geometry.	122
Figure 5.10 – Bed shear stress magnification associated with variation in structure arm length at Q_{bkf}	123
Figure 5.11 – Maximum bed shear stress magnification comparison between variations in arm angle, throat width, and drop height at bankfull flow.....	124
Figure 5.12 – Maximum bed shear stress magnification location associated with variation in structure geometry for flows greater than $1/3Q_{bkf}$	126
Figure 5.13 – Observed versus predicted flow depth using equation developed by Meneghetti (2009).....	131
Figure 5.14 – Observed versus predicted flow depth using equation developed by Thornton et al. (2011).	132
Figure 5.15 – Percent error magnitude box-plot comparison of stage-discharge relationships developed by Meneghetti (2009) and Thornton et al. (2011).....	133
Figure 5.16 – Observed versus predicted flow depth using original equation developed by Thornton et al. (2011) with new piecewise regression coefficients.....	136

Figure 5.17 – Observed versus predicted flow depth using equation 5.18 regression for all flows.....	139
Figure 5.18 – Observed versus predicted weir flow depth using equations 5.19 and 5.20.	140
Figure 5.19 – Percent error magnitude box-plot comparison of stage-discharge relationships developed by Meneghetti (2009), Thornton et al. (2011), and the current study.....	141
Figure 5.20 – Observed versus Predicted weir flow depth using stage-discharge relationships for field site and laboratory data set.	143
Figure 5.21 – Percent error box-plot comparison of stage-discharge relationships developed by Meneghetti (2009), Thornton et al. (2011), and equations 5.19 and 5.20 applied to a field site and laboratory data set.....	144

LIST OF TABLES

Table 2.1 – Agency fish passage criteria associated with rock weirs.....	15
Table 2.2 - FHWA Boulder diameters for normal summer flows.....	16
Table 2.3 - Rock weir spacing criteria.....	20
Table 3.1 – Summary of laboratory U-weir and channel geometry used in numerical model simulation.....	57
Table 4.1 – Summary of numerical modeling testing matrix throat widths.	79
Table 4.2 – Example of testing matrix configurations.....	83
Table 4.3 – Structure Definition Point Identification	86
Table 4.4 – Summary data from Excel input file: “StructureID” worksheet.....	86
Table 4.5 – Reach geometry input file for generating structure definition points.....	88
Table 4.6 – Structure geometry input file for generating structure definition points.	88
Table 4.7 – Structure definition point data used by mesh generator	89
Table 4.8 – Example 3D output data generated by U ² RANS.....	102
Table 4.9 – Longitudinal sample point distribution.....	105
Table 5.1 – Range of flow depth magnification for each flow range and structure configuration (highest value in red and lowest value in blue).....	112
Table 5.2 – Range of maximum velocity magnification for each discharge ratio.....	118
Table 5.3 – Range of maximum bed shear stress magnification for each structure configuration.....	124
Table 5.4 – Range of variables from laboratory data, field data, and numerical model.	130

LIST OF SYMBOLS AND ABBREVIATIONS

SYMBOLS

d_{50} = grain size that 50% of the particles are finer than

d_s = channel sediment size

D_{50} = median structure rock size

D_{100} = maximum structure rock size

D_{\min} = minimum structure rock size

D_{ref} = normal flow depth reference with no structure present

D_q = flow depth at given discharge

g = acceleration due to gravity

h_{weir} = depth of water over the weir relative to the throat crest

L_a = length of weir arm

L_{ref} = reference arm length

L_T = total weir length along structure crest

L_T' = effective weir length along structure crest based on effective weir height Z_u

n = Manning's roughness coefficient

P_s = the ratio of pool to pool spacing/bankfull width

q = flow rate per unit channel width

Q = volumetric flow rate (discharge)

Q_{bkf} = bankfull volumetric flow rate

Q_r = discharge ratio (Q/Q_{bkf})

R^2 = coefficient of determination

S_o = bed/channel slope

S_f = friction slope

T_w = channel top width

V = average cross-sectional velocity

V_o = normal depth reference velocity

V_{max} = maximum velocity

W_{ss} = wall shear stress in U^2 RANS program (equivalent to bed shear stress)

W_t = weir throat width

W_u = effective weir width associated with effective weir height Z_u

y_{us} = upstream flow depth

y_n = normal depth calculated using Manning's equation

z = elevation

Z_d = weir drop height

Z_u = effective weir height

GREEK

θ = plan view angle of departure from bankline (arm angle)

ϕ = profile angle (arm slope)

γ_s = specific weight of sediment

γ_w = specific weight of water

τ_{max} = maximum bed shear stress

τ_c = critical shear stress for a given bed material size

η = magnification term (i.e. ratio of max velocity/reference velocity)

ABBREVIATIONS

#	number
%	percent
ADV	Acoustic Doppler Velocimeter
cms	cubic meter(s) per second
cfs	cubic feet per second
CFD	Computational Fluid Dynamics
DS	downstream
ft	foot or feet
ft/s	feet per second
kg/m ²	kilogram(s) per square meter
m	meter(s)
m ³ /s	cubic meter(s) per second
mm	millimeter(s)
LWE	water surface elevation at left edge of channel
N	Newton(s)
N/A	not applicable
Pa	Pascal(s) (N/m ²)
RWE	water surface elevation at right edge of channel
US	upstream
WSE	water surface elevation
XS	channel cross section

1 INTRODUCTION

1.1 GENERAL BACKGROUND

The use of in-stream structures for habitat and stream restoration dates back to the early 1900's (Thompson 2005); however, the design, effectiveness, and performance of these types of structures have not been well documented. A review of international literature on grade control structure design by Nagato (1998) found that no official standard guidelines for designing low-head drop structures exist. He found that design guidelines were relatively tentative or provisional and site-specific in nature. While recently there have been a large number of laboratory experiments and empirical relationships developed, efforts to link these relationships with field engineering practices are lacking. Roni et al. (2002) reported that the lack of design guidance stems from limited information on the effectiveness of various habitat restoration techniques.

Providing irrigation diversion, fish passage, and improved aquatic habitat in gravel-bed streams is very important to water resources development. The alternatives to river spanning rock weirs that function efficiently and garner the approval of ecological regulatory agencies are few. When properly designed, river spanning rock structures have the ability to provide sufficient head for irrigation diversion, permit fish passage over barriers, protect banks, stabilize degrading channels, activate side channels, reconnect floodplains, and create in-channel habitat. River spanning rock structures share common performance objectives, which include the ability to withstand high flow events and preserve functionality over a range of flow conditions. Functionality is often

measured by a structures ability to maintain upstream water surface elevation and/or downstream pool depths in conjunction with providing suitable conditions for fish passage. Vertical drop height, lateral constriction, flow depth and velocity, size of rock material, and construction methods are common design considerations for these structures.

Monitoring of in-stream restoration projects has focused primarily on whether structures produce the desired physical response rather than understanding the physical processes that cause the physical response and how that response might change with differing structure configurations. Cox (2005) found that available guidelines and literature related to rock weirs were scarce and consistently lacked investigation of hydraulic effects and/or performance. A number of restoration projects that have been thoroughly evaluated and provide some insight into project effectiveness, or lack thereof, have been highly debated within the scientific community (Frissell and Nawa 1992; Kondolf and Micheli 1995; Kauffman et al. 1997; Reeves et al. 1991; Schmetterling and Pierce 1999; Wohl et al. 2005). Roni et al. (2002) found that reported failure rates for various types of boulder structures were highly variable, ranging from 0% to 76%. These researchers state that the conflicting results are probably due to differences in definitions of “failure” and/or “function,” structure age and type, and design and placement methods. While general monitoring of in-stream restoration projects provides some information pertaining to success and failure rates, monitoring plans usually do not provide enough detailed information to determine the physical processes associated with the success or failure of a given structure geometry. As a result, many design methods are based upon anecdotal information applicable to narrow ranges of channel conditions and rely heavily

on field experience and engineering judgment. Previously, rock weirs have been met with approval of many in the conservation community, but very high maintenance and the lack of engineering performance criteria have limited their use to applications where structure stability and associated liability to the designer were not of primary consideration.

The complex flow patterns and resulting performance of rock weirs are not well understood, and methods and standards based upon predictable engineering and hydraulic performance criteria currently do not exist. Without accurate hydraulic performance criteria, designers cannot address the failure mechanisms of structures. There are no one-dimensional (1D) hydraulic guidelines for rock weirs, field work alone cannot quantify and capture detailed processes, and physical modeling is expensive and time intensive. Collecting enough detailed field and laboratory data to include a wide range of design parameters (structure geometry, grain sizes, channel characteristics, etc) and performing an analysis of structure performance would be costly and take decades to accomplish. To address the paucity of design guidelines and logistical challenges of empirical modeling, this research examines the applicability of a Computational Fluid Dynamics (CFD) model, U²RANS, to simulate the complex flow patterns associated with numerous U-weir configurations.

1.2 PROJECT BACKGROUND

In 2005, while working for the Bureau of Reclamation (Reclamation), other colleagues and I initiated a research program to evaluate the performance of river spanning rock weirs and develop design guidelines using a multi-faceted approach that consists of field reconnaissance, physical modeling, and numerical (CFD) modeling (Figure 1.1).

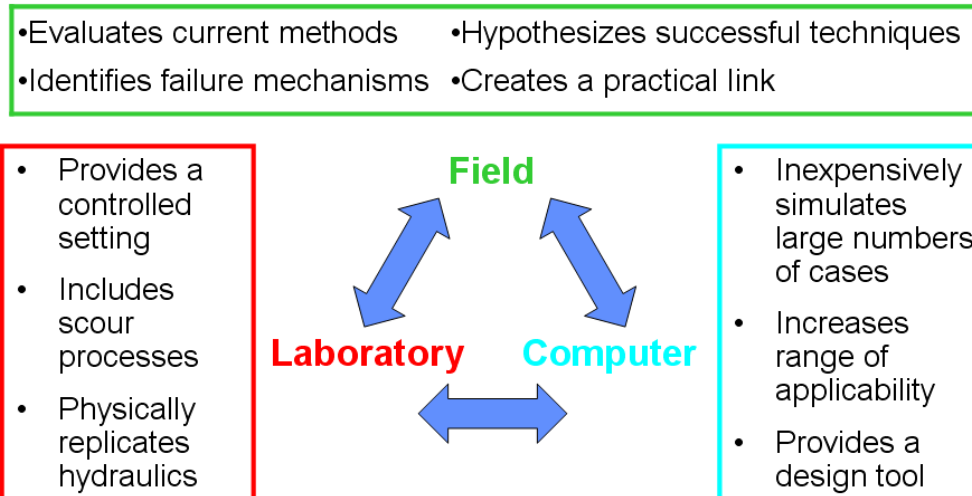


Figure 1.1 – Example of multifaceted approach of river spanning rock weir research incorporating mutually supporting field, laboratory, and numerical studies.

Field reconnaissance provides long term performance data under actual conditions, including how different river processes affect the structures and how the structures in turn affect river processes. Physical laboratory modeling provides information under carefully controlled conditions that isolate one or more variables to test the impact of specific changes on structure performance. Numerical modeling provides a cost effective method for evaluation of a range of structure geometries and channel conditions to develop a more complete understanding of structure performance and optimize structure design. Integration of field, laboratory, and numerical model data sets provides a scientific basis for predicting structure performance under various river conditions and for developing the most-effective design criteria. The physical laboratory modeling was conducted at Colorado State University’s (CSU) Engineering Research Center in Fort Collins, Colorado (Meneghetti 2009 and Scurlock 2009) and the field reconnaissance was conducted by Reclamation’s Technical Service Center in Denver, Colorado (Mooney et al. 2007b, Holburn et al. 2009a, and Holburn et al. 2009b).

1.3 RESEARCH OBJECTIVES

Due to the lack of reliable design guidance for river spanning rock weirs, a numerical model testing matrix was developed to investigate the physical processes associated with river spanning rock weirs and how variations in structure geometry affect the local hydraulics within and around the structures. The testing matrix includes a U-weir with varying structure geometries (arm angle, arm slope, drop height, and throat width) and channel characteristics (bed slope, discharge, and grain size) for an idealized flat bed trapezoidal channel. The objectives of this research are:

- Develop a rock weir mesh generation program that utilizes basic channel characteristics and the design parameters associated with U-weirs to generate a standardized/replicable computational mesh that can be used in the numerical model to describe how variations in individual structure parameters alter local flow patterns.
- Using measured data from a U-weir modeled in the laboratory and a U-weir constructed in the field, demonstrate that a three-dimensional numerical model can be used to simulate the complex flows patterns associated with river spanning rock weir structures.
- Using a three-dimensional numerical model and an idealized flat bed trapezoidal channel, identify how variations in structure geometry (drop height, throat width, and arm length) alter local flow patterns (i.e. velocity and bed shears stress distribution) and develop stage-discharge relationships to describe the changes in upstream water surface elevation as a function of structure geometry.

Thirty three unique weir configurations were generated and numerically modeled at five different flow rates ($1/10Q_{bkf}$, $1/5Q_{bkf}$, $1/3Q_{bkf}$, $2/3Q_{bkf}$, and Q_{bkf}) over the course of the research project for a total of 165 simulations. The following sections document existing design methods and numerical modeling found in the literature, testing matrix design, numerical modeling procedures, numerical model validation, and data analysis and results related to river spanning rock weirs.

1.4 APPROACH AND METHODOLOGY

The general approach and methods used to complete the research were data analysis and numerical modeling. The major tools used were computer-based simulation experiments using CFD code in conjunction with a rock weir mesh generation program written specifically for this project to simplify the process of generating a standardized/replicable computational mesh for each structure configuration.

There were six main tasks that were completed to meet the research objectives: (1) CFD model selection; (2) selection of a field site and laboratory data set for numerical model validation; (3) develop sensitivity testing matrix for numerical modeling; (4) develop a rock weir mesh generation program; (5) conduct numerical model simulations; (6) describe and document the results.

The first task was the selection of a CFD code. The three-dimensional numerical model U^2RANS was used to meet the research objectives. U^2RANS is an Unsteady and Unstructured Reynolds Averaged Navier-Stokes solver that has been tested and validated extensively with a variety of fluid flow problems such as open channel flow in an S-shaped trapezoidal channel, flow through a hydro-turbine draft tube, and simulation of flow in a hydropower reservoir (Lai and Patel, 1999; Lai et al, 2003). U^2RANS is

designed for simulation of unsteady or steady, three-dimensional, turbulent flows, with or without a free surface. The code adopts the framework of unstructured grid technology with arbitrarily shaped elements so that both structured and unstructured grids can be used (Lai, 1999). U²RANS is public domain software developed by Dr. Yong Lai from Reclamation's Technical Service Center in Denver, Colorado. Being able to utilize public domain CFD software that has been previously tested and validated provided an opportunity to conduct the research without having to use commercial software programs (e.g. FLUENT, FLOW-3D) that can be cost-prohibitive. Working with Dr. Yong Lai provided a unique opportunity to learn how the program worked, discuss model output/results, and troubleshoot problems/errors that occurred while using the program.

The second task was the selection of field and laboratory data to demonstrate that U²RANS can simulate the complex flow patterns associate with river spanning rock weirs. The field site selected for this research was a U-weir located on the South Fork of the Little Snake River near Steamboat Springs, Colorado. This site was selected because it contained detailed field measurements (water surface elevations, three-dimensional velocity measurements, and detailed channel and structure topography) that were obtained during a field reconnaissance trip in the summer and fall of 2005. A description of the site and data used are presented in section 3.2. The laboratory data selected for this research was a U-weir that was modeled at Colorado State University. Details of the rock weir physical modeling methods, data analysis, and results are described in Theses by Meneghetti (2009) and Scurlock (2009). A description of the laboratory data used in this research is presented in Section 3.3.

The third task was the development of a test matrix that consists of various U-weir configurations to investigate how flow patterns change as a result of varying structure geometry. The numerical model testing matrix expands on current rock weir design recommendations made by Rosgen (2006) and includes three different channel configurations associated with differing channel slopes and bed material grain sizes. A detailed description of the channel characteristics and range of structure parameters used in the design of the testing matrix is presented in Section 4.1.

The fourth task was the development of a rock weir mesh generation program to simplify the process of generating multiple structure geometries and associated computational meshes in a quick and cost effective manner. The rock weir mesh generation program consists of two parts: (1) an Excel workbook that uses inputs for channel geometry and specified weir design parameters to generate northing, easting, and elevation data for eleven cross sections that define the channel and structure geometry within a prescribed reach; (2) a Visual Basic program that uses data from the eleven prescribed cross sections and generates a detailed computational mesh for input into the numerical model. A description of the mesh generation program is presented in Section 4.2.

The fifth task was to conduct computer simulations using the testing matrix to examine how flow patterns (velocity, bed shear stress, and water surface elevation) are affected by varying structure geometry. Results from the numerical simulations were analyzed to investigate how variations in structure geometry affect flow patterns through the structure and whether hydraulic relationships could be developed to describe changes

in local flow characteristics (e.g. velocity and water surface elevation) based on flow rate and structure design parameters.

The final task was to describe and document the results of this research and provide recommendations for future research based on the current findings.

A review of literature relevant to river spanning rock weirs and numerical modeling is presented in Section 2. Section 3 provides information pertaining to numerical modeling methods associated with river spanning rock weirs and the process used to validate U²RANS for this research project. Development of the testing matrix, mesh generation program, and description of the numerical model is presented in Section 4. Data analysis and results are discussed in Section 5. Conclusions and recommendations are presented in Section 6 and references are listed in Section 7.

2 LITERATURE REVIEW

A literature review was conducted to examine current design methods, effectiveness, and performance of river spanning rock weirs. The following sections review current design practices, definitions, and numerical modeling methods associated with river spanning rock weirs.

2.1 INTRODUCTION

River spanning rock weirs are often constructed to provide irrigation diversion, grade control, or to modify local flow conditions for river restoration and in many cases are used to satisfy multiple objectives (e.g. irrigation diversion with fish passage). According to Rosgen (2006) a properly designed river structure should provide:

- Decreased near-bank velocities while maintaining channel capacity;
- Fish passage at all flows;
- Safe passage or enhanced recreational boating;
- Improved fish habitat;
- Visual compatibility with natural channels; and
- Maintenance-free diversion structures.

He also states that rock weir structures have the ability to reduce near-bank shear stress, velocity, and stream power, while increasing the energy in the center of the channel to retain both flood-flow and sediment transport capacity. While this may be true, design guidelines describing how these local flow patterns are affected by differing

rock weir geometries do not appear to be documented in the literature. Recently, numerous laboratory experiments and numerical modeling studies have been carried out to examine the local flow patterns associated with rock weirs (Meneghetti 2009, Scurlock 2009, Bhuiyan and Hey 2007, Bhuiyan et al. 2007), however, the studies usually focus on the hydraulics associated with a single or limited range of rock weir geometries (e.g throat width, arm angle, arm slope, drop height). Additionally, field experience using rock weirs for stream restoration has been presented by numerous authors (Shields et al. 1995, Rosgen 2006, Kondolf and Micheli 1995, Thompson 2005) but none of these efforts have linked the physical processes associated with rock weir performance to variations in structure geometry.

To study the effects of variations in rock weir geometry on local flow patterns, current design practices related to river spanning rock weirs were identified. Figure 2.1 presents a depiction of various types of river spanning rock weirs.

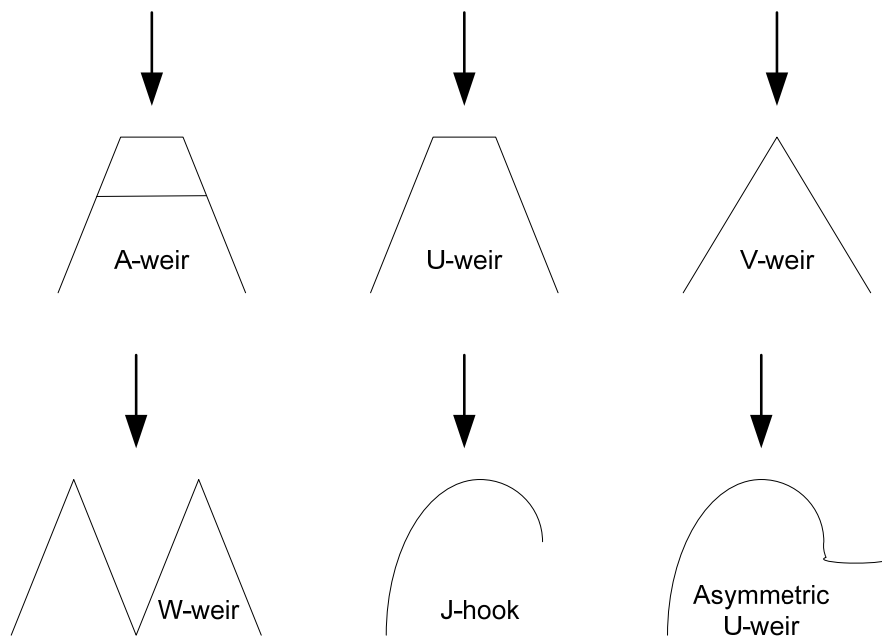


Figure 2.1 – Depiction of river spanning rock weir structure types (Mooney et al. 2007b)

The research focus for this dissertation is related to U-weirs and how variations in design parameters (throat width, drop height, arm angle, and arm slope) affect local flow patterns. The following sections describe current design practices and numerical modeling methods found in the literature pertaining to U-weirs.

2.2 CURRENT DESIGN PRACTICES

Available river spanning rock weir design guidelines typically include geometric shape, structure material and construction techniques with limited guidelines concerning hydraulic effects. Guidelines related to rock weir geometry were limited and more often than not just an adaptation from original designs prescribed by Rosgen (1996 and 2006). The following sections summarize available design guidelines for U-weir structure geometry, spacing, stage discharge relationships, and scour prediction.

2.2.1 STRUCTURE DIMENSIONS

Typical structure parameters associated with river spanning rock weirs include: throat width (W_t), drop height (Z_d), arm plan angle (θ), arm profile slope (ϕ), arm length (L_a), and structure rock size. Figure 2.2 presents profile and plan views of a typical U-weir design.

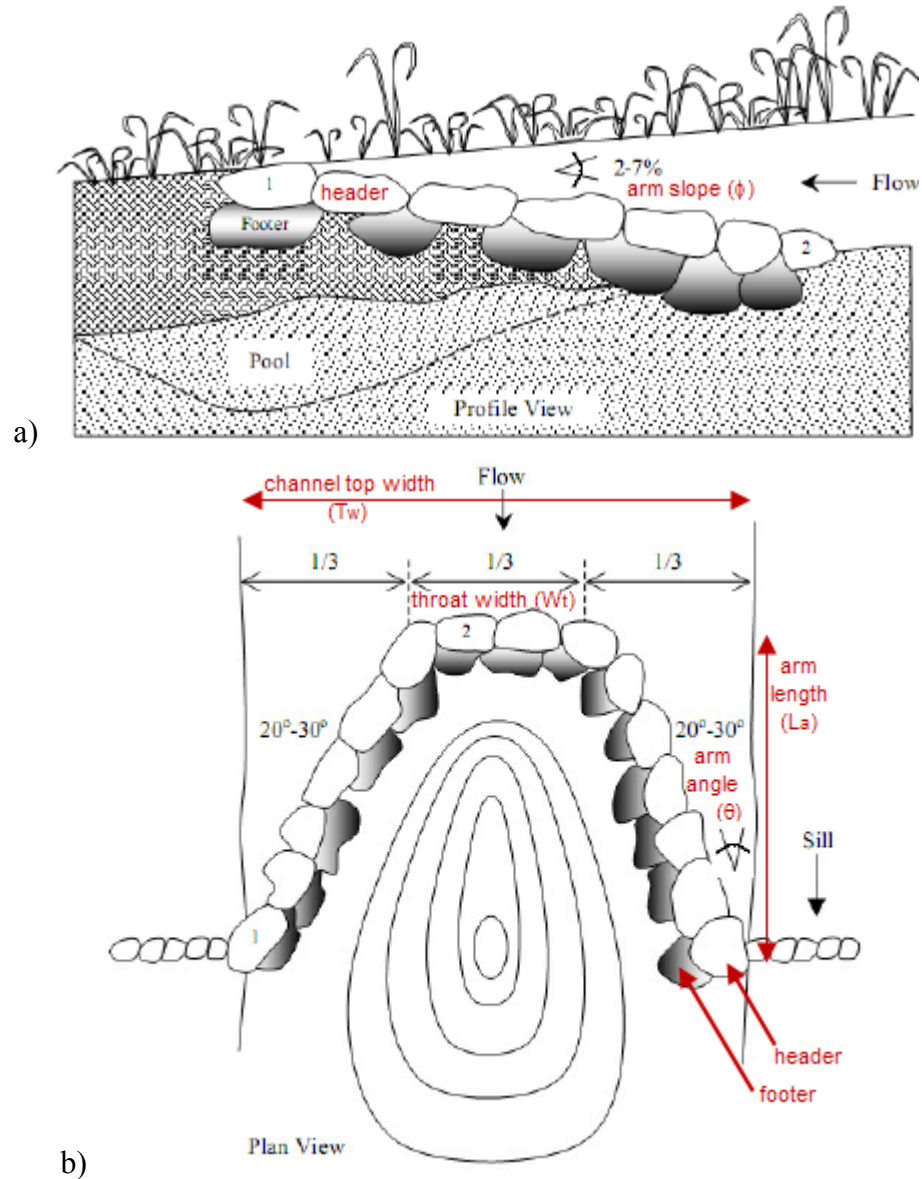


Figure 2.2 – Conceptual U-weir a) profile view and b) plan view (adapted from Rosgen, 2006)

2.2.1.1 ARM ANGLE AND SLOPE

Rosgen (2006) suggests that the structure arms should extend to and tie-in at the bankfull stage elevation. The profile angle (ϕ), or slope, of the weir arm extending from the bank is measured from the top rocks in the direction of the channel and should vary between 2-7 percent (1.15-4.0 degrees). The plan angle (θ) is measured upstream from the tangent line where the weir arm intercepts the bank and should be in the range of 20-

30 degrees. Castro (2000) suggests a plan angle of 20-60 degrees and emphasizes the need for a positive slope towards the center of the channel but does not provide a recommendation for the slope of the arm. The structure arm length (L_a) is measured parallel with the bank from the structure throat to the structure arm tie-in and is dependent on the arm angle and slope (Figure 2.2b).

2.2.1.2 THROAT WIDTH AND DROP HEIGHT

The structure throat (W_t) is typically constructed perpendicular to the channel flow, centered in the middle of the channel laterally and according to Rosgen (2006) should span one-third of the total channel width. He also suggests that center crest rocks should be placed near the streambed elevation to allow adequate fish passage at low discharges. Castro (2000) states that the center of the weir should be at grade with the channel bed to allow for sediment transport and fish passage. The elevation of the center crest rocks depends on the objective of the structure design. If the objective is for irrigation diversion then the elevation of the crest rocks is set by the upstream water surface elevation required for the diversion structure. If the objective is for fish passage, the crest elevation can be adjusted to meet local fish passage criteria. Table 2.1 lists various agency fish passage criteria for maximum drop height requirements associated with diversion structures. While maximum drop height is directly linked to the crest elevation, the resulting local hydraulics for a given structure geometry must meet additional fish passage requirements for maximum velocity, pool depth, and resting areas. These requirements are usually set by local agencies and vary depending on fish species and life stage.

Table 2.1 – Agency fish passage criteria associated with rock weirs.

Agency	Maximum drop height
Washington Department of Fish and Wildlife (WDFW)	0.8 ft (0.244 m)
Oregon Department of Fish and Wildlife (ODFW)	1.0 ft (0.305 m)
Natural Resources Conservation Service (NRCS)	1.0 ft (0.305 m)
National Oceanic and Atmospheric Administration (NOAA) Fisheries	1.0 to 1.5 ft (0.305 to 0.457 m)

2.2.1.3 FOUNDATION – HEADER AND FOOTER CONFIGURATION

Typical construction of rock weirs consists of a header and footer combination with the footer offset approximately one third the structure rock width in the downstream direction (Figure 2.2). Scour downstream of rock weirs increases the depth locally and creates hydraulic diversity, however, the formation of a scour pool can also undermine the rocks comprising the structure if the footer rocks are not placed deep enough; resulting in the structure rocks rolling into the scour hole and failure of the structure.

According to Rosgen (2006), the minimum depth of the footer ranges from three times the drop height to six times the drop height for gravel/cobble bed and sand bed streams respectively. Field reconnaissance of numerous rock weir structures conducted by Mooney et al. (2007b) identified that undermining of the structure foundation was one of the most common failure modes associated with rock weirs. As a result, they suggest foundation depths should remain at a constant elevation across the channel and not decrease near the edge of the channel where the structure arms slope upward and tie-in to the top bank.

2.2.1.4 STRUCTURE MATERIAL

The boulders used in constructing rock weirs must be large enough to simultaneously resist movement and create the desired hydraulic conditions. Mooney et

al. (2007b) found that header and footer rocks surveyed in the field were usually very large, blocky shaped rocks in excess of three feet in diameter. Guidelines for sizing the boulders comprising the structure header and footer are typically based on existing riprap design equations or incipient motion criteria.

Several authors have provided guidelines for the shape and sizing of isolated rocks in gravel bed streams. Though not specific to site conditions, the numbers can provide a check on calculations. For example, Province of Alberta (2001) recommends rock diameters in the range of 2-3 feet (0.61-0.91 meters), Mefford (2005) recommends 4 foot (1.22 meter) rocks, and the Federal Highway Administration (FHWA, 1979) provides a table for sizing rocks based on channel width and bankfull flow depth (Table 2.2).

Table 2.2 - FHWA Boulder diameters for normal summer flows

Channel Width (ft)	Bankfull Flow Depth(ft)	Rock Diameter (ft)
<20	1.0-2.5	2-4
20-40	1.0-3.0	3-8
40-60	1.5-4.0	4-12
>60	1.5-5.0	5 +

Incipient motion can determine the likely flow required to move an isolated rock. Critical shear stress, Shields parameter, or stream power methods provide an empirical approach to sizing rocks. Julien (2002) describes shear stress and Shields parameter approaches while Yang (1973) describes the stream power approach. Fischenich and Seal (1999) recommend using incipient motion for an initial size and then performing a momentum balance to determine the required diameter of the rock to resist motion.

A study of eight, steep, coarse grained mountain streams in Colorado by Thomas et al. (2000) found the average size of boulders to be 2 feet (0.61 meters). To determine the size of boulders for construction of man-made step-pool structures, Thomas et al. (2000) suggest using the U.S. Army Corps of Engineers “steep slope riprap design” method (COE, 1991) with the 25-year unit discharge (Equation 2.1), but note that these should be supplemented with anchor boulders (footers) that should be placed along the base of the step-pool structure to provide additional support and stability.

$$D_{30} = \frac{1.95 \cdot S^{0.555} \cdot q^{2/3}}{g^{1/3}} \quad \text{Equation 2.1}$$

Where:

- S = slope of the rock ramp (ft/ft);
- q = design unit discharge (cfs/ft);
- g = acceleration due to gravity (ft/s²); and
- D₃₀ = characteristic stone size 30 percent quantile.

Rosgen (2006) provides an empirical relationship for calculating weir rock size as a function of bankfull shear stress with the caveat that it is only applicable for streams with a bankfull discharge range of 0.5-114 cms and bankfull channel depths of 0.3-1.5 meters (Figure 2.3).

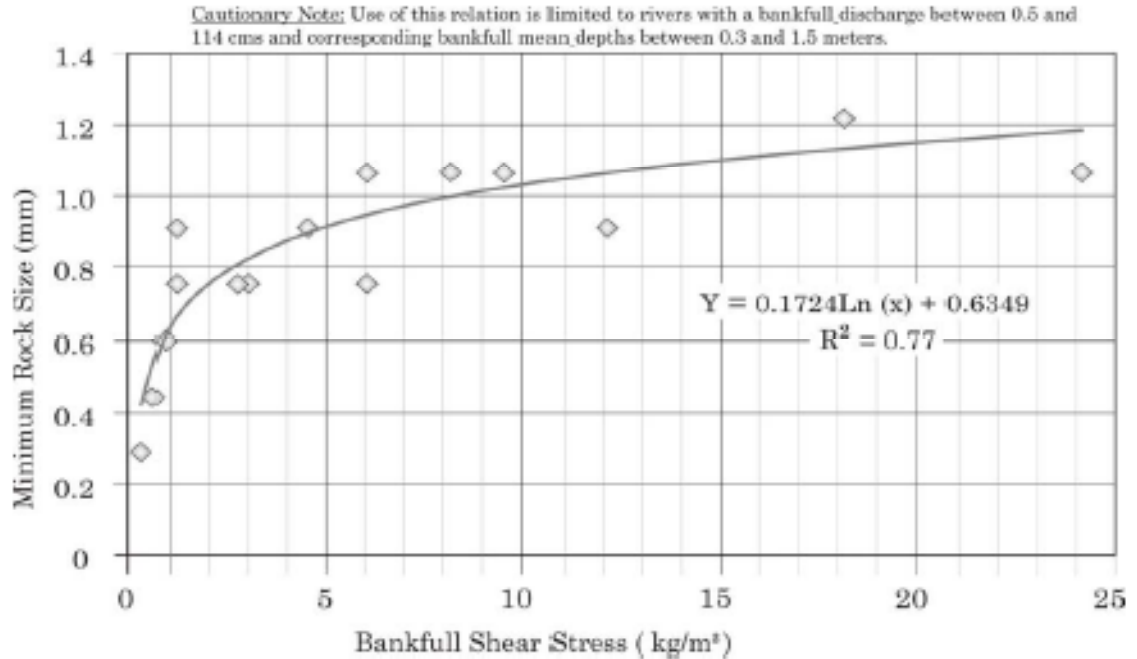


Figure 2.3 – Minimum rock size as a function of bankfull shear stress (Rosgen 2006)

Castro (2000) suggests using rock that is angular to sub-rounded in shape and provides several formulas linked to the Far West States-Lane Method (Lane 1955) for sizing riprap (Equation 2.2 through 2.5).

$$D_{50-riprap} = \frac{3.5}{C \times K} \gamma_w D S_f \quad \text{Equation 2.2}$$

$$D_{50-weir} = 2D_{50-riprap} \quad \text{Equation 2.3}$$

$$D_{100-weir} = 2D_{50-weir} \quad \text{Equation 2.4}$$

$$D_{min} = 0.75D_{50-riprap} \quad \text{Equation 2.5}$$

Where:

$D_{50-riprap}$ = median rock size (in.) from Far West States-Lane Method;

C = correction for channel curvature;

K = correction for side slope;

S_f = channel friction slope (ft/ft);

D = flow depth (ft);

- γ_w = density of water (lb/ft³);
 $D_{50\text{-weir}}$ = median structure rock size;
 $D_{100\text{-weir}}$ = maximum structure rock size; and
 D_{\min} = minimum structure rock size.

Given the limited design criteria available for sizing the boulders used in constructing rock weirs, designers tend to calculate the minimum rock size required for their site using one or more of the methods listed above in order to assure stability and then construct the weir using the largest rock available in the area (Humbles, 2009, personal communication). Mooney et al. (2007b) noted that the majority of structures found in the field were constructed using boulders much larger than required by any riprap sizing equation or force balance calculation. This suggests that the size of the boulders used in the construction of the structure may have been determined by the conservative approach of using the largest available rock dimensions at a site to minimize rock movement rather than by design calculations using channel hydraulics.

2.2.2 LOCATION AND SPACING

The various methods for calculating rock weir spacing found in the literature are presented in Table 2.3. Castro (2000) recommends placing cross-vanes in areas where pools would naturally form and if the elevation change is greater than one foot (0.3048 meters) they should be used in series to meet fish passage criteria. He also states that for grade control, it is recommended that rock weirs be placed no closer than the net drop divided by the channel slope. Additional methods (Humbles, 2009, personal communication) include estimating the backwater effects from a structure and placing the next upstream structure at a location where the required tail water elevation for the

upstream structure is met. If the structures are placed too close together they may become submerged and not function as intended.

Table 2.3 - Rock weir spacing criteria

Method	Reference
$L=0.31*S^{-1.19}$ Where: L=step-pool spacing (m) S=channel slope	Whitaker 1987
Step-Pool spacing = 2-3 channel widths	Knighton 1998
$L=f(H, ACW, S_o, q_{design})$ Where: H=Weir Drop Height ACW=Active Channel Width S_o =Channel Slope q_{design} =Design unit discharge	Thomas et al. 2000
Step-pool spacing = 0.43-2.4 channel widths	Chin 1989
$H/L=1.5*S$	Abrahams et al. 1995
$Ps = 8.2513 S_{\%}^{-0.9799}$ Where: Ps = pool spacing/bankfull width	Rosgen 2006

2.2.3 STAGE DISCHARGE RELATIONSHIPS

Stage-discharge relationships define a unique relationship between water-surface stage and the corresponding discharge and have been used in a number of ways for over a century (Schmidt, 2002). The most common application of stage discharge relationships involves calculating a flow rate based on a measured stage or water surface elevation at a prescribed channel cross section or flow measuring device (e.g. partial flume, rectangular weir, broad crested weir). In the case of river spanning rock weirs, Meneghetti (2009) describes how the stage-discharge relationship is applied in an inverse way, for a given discharge the corresponding stage above the weir crest is used to determine the water surface elevation upstream of the structure. This calculated water surface elevation can then be used to determine the backwater effects of the structure for a given flow in the

river. The backwater effects are of particular importance when multiple structures are used in series to determine the proper spacing between each structure. When structures are used in series, the backwater from the downstream structure provides the tail water elevation (hydraulic control) for the upstream structure. If the structures are spaced to far apart then the hydraulic control is no longer linked to the backwater effects and will revert back to normal or critical depth, causing each structure to function independently. The relevant scientific literature has very limited data describing the development of stage-discharge relationships for river spanning rock weirs (Meneghetti, 2009).

Given the lack of stage-discharge relationships for river spanning rock weirs, many design engineers resort to using equations developed for broad crested weirs as a method for estimating the backwater effects of rock weirs (Humbles, 2009, personal communication). Other methods for calculating backwater include using 1D models such as HEC-RAS and modeling the rock weir using increased roughness values, cross sections aligned parallel to the structure crest, modification of expansion and contraction coefficients, and ineffective flow areas. However, with no standard guidelines available regarding how to model these types of structures using a 1D model, the results are highly dependent on the methods used by each designer and their experience with river spanning rock weirs.

Cox (2005) modeled cross-vane structures in a sand-bed flume to study their hydraulic effects, stability thresholds and scour formations. Multiple variations in bed slope, structure material, weir height, and weir length were included in the model and stage-discharge equations were developed to predict the upstream flow depth for cross-vane structures (Equation 2.6).

$$\frac{y_{us}}{y_b} = 2.43 \left(\frac{qL_w^{1.11}}{g^{0.5} \bar{h}_w^{(2.61)}} \right)^{-0.172} \quad \text{Equation 2.6}$$

Where:

- y_{us} = flow depth upstream of rock weir (ft);
- q = volumetric flow rate per unit width (cfs/ft);
- L_w = weir length (ft);
- h_w = average weir height (ft);
- y_b = base-line flow depth (ft); and
- g = acceleration due to gravity (ft/s²).

Ruttenburg (2007) developed a spreadsheet based model to simulate flow over U-weirs at several study sites using the general form of the Poleni equation from Chow (1959) with a slight modification that included a contraction coefficient to account for contraction due to the weir length perpendicular to the channel flow direction (Equation 2.7 and 2.8). The equations developed by Ruttenburg were designed to calculate the discharge in the river based on the wetted weir length along the weir crest (B) which is a function of the water stage and weir geometry.

$$Q_{weir} = \frac{2}{3} \mu \cdot C_w \cdot B \cdot \sqrt{2g} \cdot h_{weir}^{1.5} \quad \text{Equation 2.7}$$

$$C_w = \frac{W_t + (B - W_t) \sin \theta}{B} \quad \text{Equation 2.8}$$

Where:

- Q_{weir} = discharge for weir flow (m³/s);
- μ = weir coefficient, function of the geometry, varies from 0.6 to 0.8;
- C_w = contraction coefficient for weir crest profile length;
- B = wetted weir profile length along boulder crest, function of water stage and weir geometry (m);
- g = acceleration due to gravity (m/s²);

h_{weir} = water depth at the rock vortex weir crest (m);

W_t = structure throat width (m); and

θ = structure plan arm angle relative to stream bank (degrees).

Meneghetti (2009) modeled rock weir structures in a gravel-bed flume to study their hydraulic effects at three different discharges. Variations in bed material, slope, and structure geometry were included in the model and stage-discharge equations were developed to predict the upstream flow depth for a given U-weir geometry (Equation 2.9).

$$y_{us} = 0.830 \left(Q \frac{y_n}{L_t} \right)^{0.223} \left(\frac{L_A}{L} \right) \quad \text{Equation 2.9}$$

Where:

y_n = normal depth (ft);

L_T = total weir length (ft);

L_A = angled weir arm length (ft); and

L = weir arm length (ft).

Using the laboratory data from Meneghetti (2009), Thornton et al. (2011) conducted further analysis and using the general form of the broad crested weir equation developed a stage-discharge relationship which included a coefficient to reflect the geometry of the rock weir and the channel in which it was placed (Equations 2.10 and 2.11).

$$Q_{weir} = \frac{2}{3} b_u \cdot C_d \cdot \sqrt{2g} \cdot (y_{us} - z_u)^{1.5} \quad \text{Equation 2.10}$$

$$C_d = 0.652 \cdot \left(\frac{D_{50weir}}{z_u} \right)^{-0.708} \left(\frac{b_u}{B} \right)^{0.587} \quad \text{Equation 2.11}$$

Where:

- Q_{weir} = discharge for weir flow;
- C_d = contraction coefficient for weir crest profile length;
- b_u = effective weir length, function of the structure geometry;
- z_u = effective weir height, function of the structure geometry;
- g = acceleration due to gravity;
- B = stream width; and
- y_{us} = water depth upstream of rock weir.

2.2.4 SCOUR PREDICTION

Scour prediction equations related to river spanning rock weirs were found to be very limited in the reviewed literature. Castro (1999) provides methods for estimating the scour depth downstream of cross-vane structures for gravel and sand bed channels (Equations 2.12). However, this is a very rough estimate since it is based only on the structure drop height and does not take into account the effects that changes in arm angle or slope might have on the scour depth.

$$d_s = k \cdot h \quad \text{Equation 2.12}$$

Where:

- d_s = depth of scour;
- k = 2.5 for gravel/cobble and 3 to 3.5 for sand; and
- h = height of exposed rock relative to the bed elevation.

Cox (2005) modeled rock weir structures in a sand-bed flume to study their hydraulic effects and scour formations. Multiple variations in bed slope, structure material, weir height, and weir length were included in the model and scour prediction equations were developed to predict the maximum scour depth based on variations on rock weir geometry in a sand bed stream (Equation 2.13).

$$d_s + y_b = 3.98 \left(\frac{q L_w \bar{h}_w^{0.39}}{g^{0.5} b^{2.89}} \right)^{0.381} \quad \text{Equation 2.13}$$

Where:

d_s = maximum scour depth (ft);

q = volumetric flow rate per unit width (cfs/ft);

L_w = weir length (ft);

h_w = average weir height (ft);

y_b = base-line flow depth (ft);

g = acceleration due to gravity (ft/s²); and

b = channel width (ft).

Similarly, Scurlock (2009) modeled rock weir structures in a gravel-bed flume to study their hydraulic effects and scour development. After completing an extensive literature review of scour depth prediction methods, he determined that equation 2.14 developed by D'Agostino and Ferro (2004) was best suited for the development of an equation to predict scour downstream of rock weirs because the form of the equation allowed for representation of all variables manipulated during the test matrix in a single, verified equation.

$$\frac{y_{SE}}{z} = 0.540 \left(\frac{b}{z} \right)^{0.593} \left(\frac{y_t}{H} \right)^{-0.126} \left(\frac{Q}{bz\sqrt{g(\Delta-1)d_{50}}} \right)^{0.544} \left(\frac{d_{90}}{d_{50}} \right)^{-0.856} \left(\frac{b}{B} \right)^{-0.751} \quad \text{Equation 2.14}$$

Where:

y_{SE} = equilibrium scour depth;

B = channel width;

d_{50} = mean sediment diameter;

d_{90} = sediment diameter where 90% of total is smaller by size;

g = gravitational acceleration;

H = piezometric drop across structure;

Q = discharge;

y_t = tailwater depth;

b = weir width; and

z = fall height.

Because the original equation was developed for scour downstream from linear grade control structures, Schurlock (2009) used an effective weir length (b_u) to represent the weir width (b) and a mean weir height above the bed (z_u) to represent the drop over the structure (z). Variations in bed material, slope, and structure geometry were included in the laboratory model and scour equations were developed to predict the maximum scour depth for a given weir geometry, bed size, and flow rate as described in equation 2.15 below:

$$\frac{y_{SE}}{z_u} = 9074.589 \left(\frac{b_u}{z_u} \right)^{-2.958} \left(\frac{y_t}{H} \right)^{-0.491} \left(\frac{Q}{b_u z_u \sqrt{g(\Delta-1)d_{90}}} \right)^{1.254} \left(\frac{d_{90}}{d_{50}} \right)^{20.299} \left(\frac{b_u}{B} \right)^{87.9} \quad \text{Equation 2.15}$$

Where:

b_u = effective weir length for u-weir as defined in Figure 2.4;

z_u = mean weir height above bed for u-weir as defined in Figure 2.4;

and all other terms previously described.

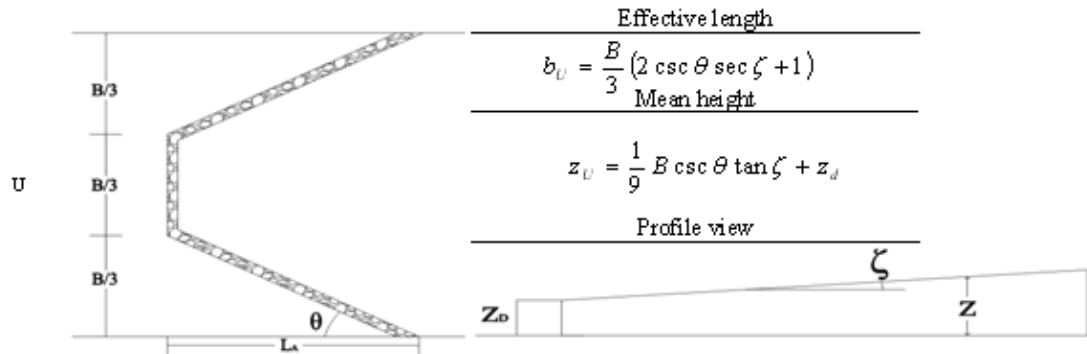


Figure 2.4 – Rock weir effective length parameters (Scurlock, 2009)

Using field data collected between 2005 and 2008, Holburn et al. (2009a) applied the scour equation developed by Scurlock (2009) to two field sites to investigate how well the equation applied to full-scale rock weirs measured in the field. Their results showed that the equation developed by Scurlock (2009) tended to over predict the scour measured in the field by more than three hundred percent. After further investigation they identified that the range of values measured in the field were outside the narrow range of values tested in the laboratory. Given that the original D'Agostino and Ferro (2004) equation was developed across a much wider range of laboratory conditions, Holburn et al. (2009a) modified the original scour equation (equation 2.14) slightly by only replacing weir width (b) with effective weir length (b_u), drop height (z) with effective weir height (z_u), and replacing d_{50} in the third term with d_{90} as recommended by Scurlock (2009) and leaving all the coefficients and exponents unchanged. The modified equation is presented as follows:

$$\frac{y_{SE}}{z_u} = 0.540 \left(\frac{b_u}{z_u} \right)^{0.593} \left(\frac{y_t}{H} \right)^{-0.126} \left(\frac{Q}{b_u z_u \sqrt{g(\Delta-1)d_{90}}} \right)^{0.544} \left(\frac{d_{90}}{d_{50}} \right)^{-0.856} \left(\frac{b_u}{B} \right)^{-0.751} \quad \text{Equation 2.16}$$

The modified equation provided by Holburn et al. (2009a) proved to have results that were within a reasonable range of expectation, less than fifty percent difference in measured versus predicted scour depth, for the two cases examined. However, they note that further validation of the equation is necessary to determine its suitability for all rock weirs, but the preliminary results hold promise of its application for foundation depth design.

2.3 NUMERICAL MODELING

Numerical modeling provides a design tool for analyzing how hydraulics in a channel are affected by changes in channel geometry, flow rate, and the presence of structures (weirs, culverts, bridges). The type of numerical model used in an analysis must capture significant flow patterns and replicate the important processes. One-dimensional (1D) numerical simulations model downstream changes in hydraulics while neglecting vertical and lateral variation. Two-dimensional (2D) models incorporate lateral differences in velocity and water surface elevation, but neglect variations in the vertical velocity component. Three-dimensional (3D) modeling simulates the motion of water in all directions and most accurately captures complex flow patterns. Estimating channel hydraulics with lower dimensional methods requires understanding the impact of representing a feature with methods that may oversimplify real world processes. Flow characteristics that are not captured in 1D or 2D models such as jets, near bed velocities, recirculation, and plunging flow associated with river spanning rock weirs govern scour pool development and overall structure performance.

Current methodologies for the modeling of rock weirs utilizing 1D and 2D models revolve around manipulation of cross-section geometry, contraction and expansion loss coefficients, Manning roughness values, cross-section spacing, and cross-section survey point resolution (Cox 2005, Scurlock 2009, Humbles 2009 personal communication). Flow through the structures is rapidly varied and therefore violates the 1D model cross-section averaged parameter assumption necessary for the direct application of a standard step methodology in determining water surface and energy profiles. Additionally, velocity components downstream of the structure crest and in the scour hole contain plunging flow which violates 2D modeling assumptions that velocity vectors are parallel to the bed. 3D numerical models capture these patterns without requiring the prior and possibly incorrect assumptions of lower order models.

2.3.1 PREVIOUS EXPERIMENTS

Until recently, the use of 3D numerical modeling in studying complex river structures such as river spanning rock weirs has been minimal and mostly limited to comparisons with laboratory experiments. Jia et al. (2005) conducted numerical modeling to study the helical secondary current and near-field flow distribution around a submerged bendway weir. Their results show good agreement between the simulations and the physical model data for velocity and secondary flow distributions.

Hargreaves et al. (2007) conducted a number of simulations for the free surface flow over a broad-crested weir for comparison with data from a previous laboratory experiment carried out by Hager and Schwalt (1994). Comparisons of free surface profiles (Figure 2.5) and velocity profiles for a range of input flows were found to be in good agreement between the numerical model and measured laboratory data.

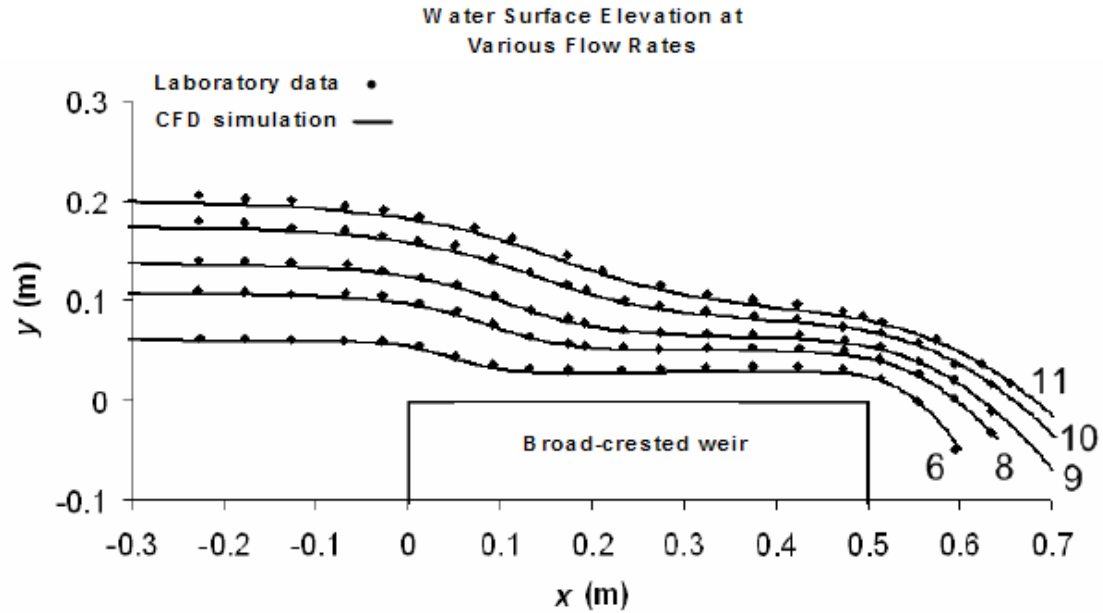


Figure 2.5 – Laboratory free surface comparison with CFD simulations for a broad-crested weir at various flow rates (Hargreaves et al., 2007)

Through the validation process, Hargreaves et al. (2007) proved the validity of CFD software in the modeling of free surface flows over hydraulic structures such as the broad-crested weir. They point out that through their validation process, modeling of more complex geometries and flow configurations can now be addressed with more confidence by themselves and others.

Bhuiyan and Hey (2007) conducted laboratory tests for a linear rectangular weir in a straight sand bed channel and for a W-weir in a meandering sand bed channel. They also conducted numerical model simulations of the laboratory tests and for a U-, V-, and W-weir in a straight channel to examine the mean flow directions associated with folder weirs. A good correspondence was observed among the computed flow patterns, surface jet characteristics, and laboratory measurements. Comparing the simulated and measured velocity profiles downstream from the linear rectangular weir at various locations (Figure 2.6), Bhuiyan and Hey (2007) demonstrated that the numerical model was able to simulate the mean flow patterns observed in the laboratory. After validating the

numerical model for the linear rectangular weir, they used the numerical model to examine the mean flow patterns associated with folded weirs in a straight channel. Numerical simulations were conducted for four different layouts consisting of U-, V-, and W-weirs as shown in Figure 2.7.

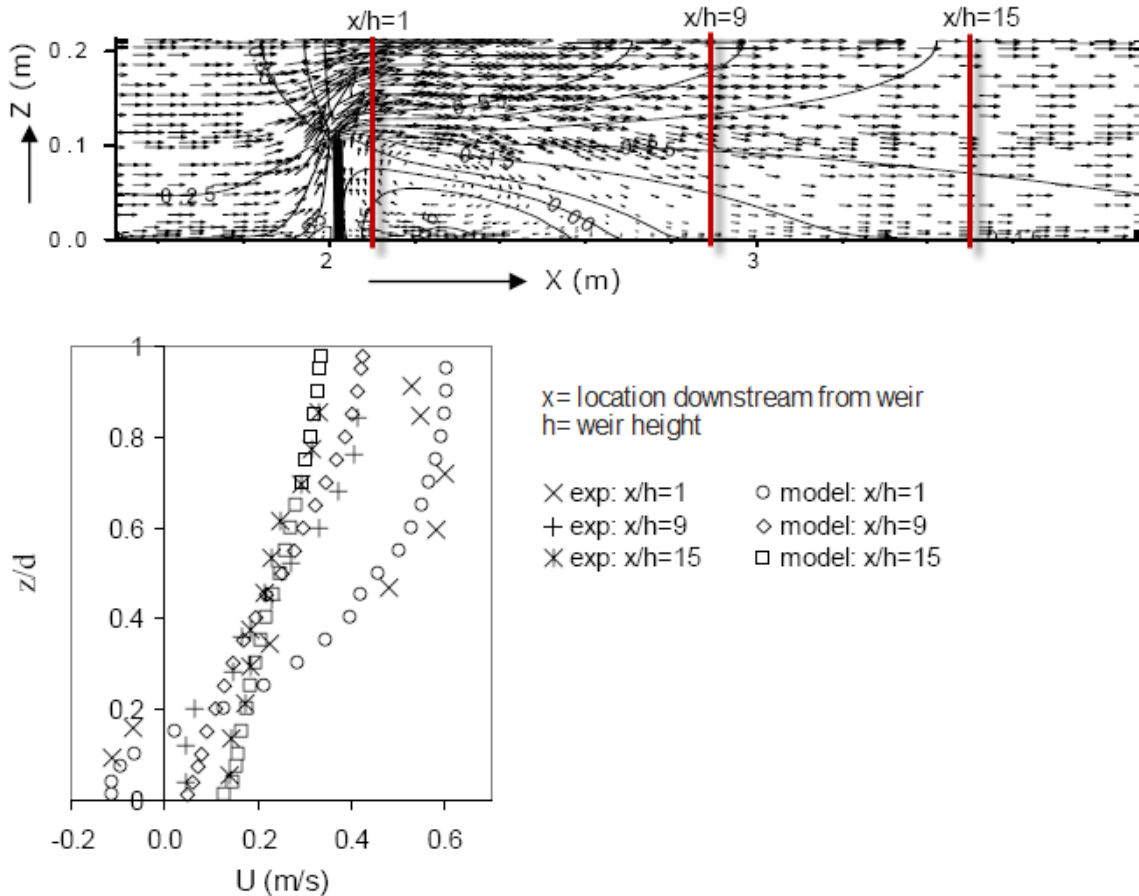


Figure 2.6 – Experimental and simulated velocity profiles at different longitudinal locations for a linear rectangular weir (Bhuiyan and Hey, 2007)

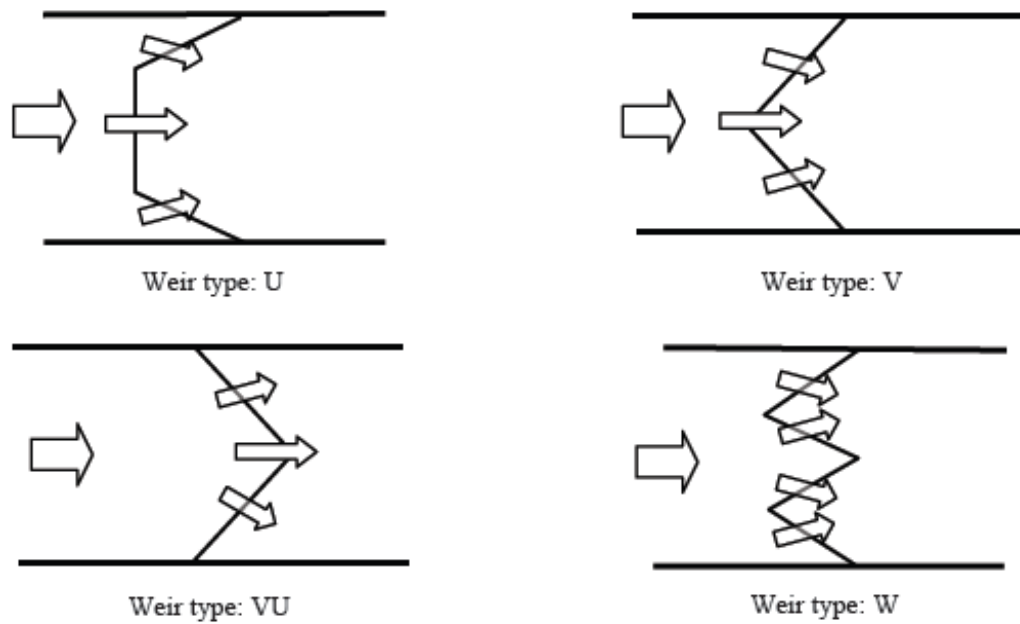


Figure 2.7 – Different weir layouts for U-, V-, and W-weir simulations and approximate mean flow directions (Bhuiyan and Hey, 2007)

Bhuiyan and Hey (2007) point out that another important parameter for folded weirs is the pitch (slope) of the arms and that sloping crest weirs provide higher flow diversification across the channel and increased bed shear stress in the middle of the channel. Two examples of distribution of simulated bottom shear stresses from their study are shown in Figure 2.8. They point out that bed shear stresses are higher in two pockets in the middle of the channel so that two adjacent scour holes are formed downstream of the weir which they also observed in the laboratory experiments.

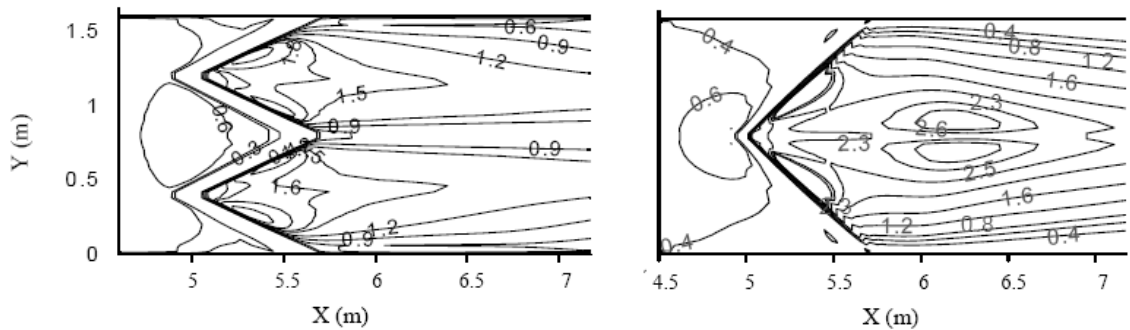


Figure 2.8 – Computed shear stress distribution downstream of W-weir and V-weir (Bhuiyan and Hey, 2007)

Through their numerical simulations, they found that the secondary flow strength and bed shear stress magnification associated with U-, V-, and W-weirs were enhanced significantly (28% and 5 times respectively) downstream of the structures compared to those of a linear weir layout. The results of their study clearly show the sensitivity of flow patterns to changes in weir layout.

2.4 SUMMARY

A review of available literature pertaining to river spanning rock weirs has been presented including design guidance, stage-discharge relationships, scour prediction equations, and numerical modeling methods. Information concerning local flow patterns associated with river spanning rock weirs such as changes in channel velocities, bed shear stress, and length of structure effects for differing structure geometries was limited in the reviewed literature. The work presented by Bhuiyan and Hey (2007) provided the most information and insight related to numerical modeling of folded weirs and how different types of weirs (U-, V-, and W-weirs) with and without sloping crests alter local flow patterns. While their study provided information related to changes in flow patterns for flat and sloping weir crests, they did not investigate how local flow patterns change for an individual weir type due to variations in structure geometry (drop height, throat width, arm angle, and arm slope).

3 COMPARISON AND VALIDATION OF ROCK WEIR NUMERICAL MODELING

Numerical modeling of river spanning rock weirs provides a design tool for analyzing how hydraulic phenomena in a channel are affected by variations in channel characteristics and structure geometry. The type of numerical model used in the analysis (1D, 2D, or 3D) must capture significant flow patterns and replicate the important processes. As mentioned in Section 2.3, estimating channel hydraulic phenomena with lower dimensional methods requires understanding the impact of representing a feature with methods that are increasingly removed from real world processes as the order of the model decreases. Flow through a river spanning rock weir is rapidly varied and therefore violates the 1D model cross-section averaged parameter assumption necessary for the direct application of a standard step methodology in determining water surface and energy profiles. Additionally, velocity components downstream of the structure crest and within the scour hole contain plunging flow which violates 2D modeling assumptions that velocity vectors are parallel to the bed. 3D numerical models capture these patterns without requiring the prior and possibly incorrect assumptions of lower order models. To better understand the applicability and limitations of 1D, 2D, and 3D numerical modeling for rock weirs, a comparison of predicted water surface elevations and corresponding velocities from each of the numerical models was conducted for a field site as well as a laboratory test case. The results of the numerical model comparisons for the field data as well as the laboratory tests are presented in the following sections.

3.1 QUALITATIVE COMPARISON OF 1D, 2D, AND 3D NUMERICAL MODELING METHODS FOR ROCK WEIRS

Flow through rock weirs exhibit highly three-dimensional, rapidly-varied flow, with a hydraulic jump that occurs downstream of the weir crest and is dependent upon the geometry of the weir crest and discharge. Furthermore, velocities and water surface elevations vary across the channel near the weir where relatively stagnant water near the outer arms is contrasted with the fast moving, plunging flow found in the middle portion of the weir entering the scour pool. To better understand the limitations of representing the complex flows associated with river spanning rock weirs using lower order models, output from a 3D numerical model simulation for a U-weir measured in the field is presented below and used to illustrate flow patterns associated with river spanning rock weirs and describe why current methods used in lower order models, 1D and 2D, are not able to properly represent the 3D flow patterns.

Figure 3.1 shows a plan view of a U-weir with water surface elevation contours obtained from the 3D model. The areas upstream and downstream of the structure show little lateral variation. The water surface drops rapidly over the structure and follows the weir crest topology. As a result, a transect located within the structure results in multiple water surface elevations along the transect, violating 1D model assumptions of gradually varied flow and constant water surface elevation across a transect. Methods to meet 1D water surface requirements include constructing cross sections tracing water surface elevation contours or coding multiple cross sections perpendicular to the flow. Since 2D and 3D models account for lateral variations in flow, they are able to properly simulate variations in water surface elevations along a transect. Therefore, when simulating flow conditions that result in lateral variations in water surface elevations, 2D and 3D models

can be applied directly without requiring additional manipulation of cross section placement and calibration required with a 1D model as described above.

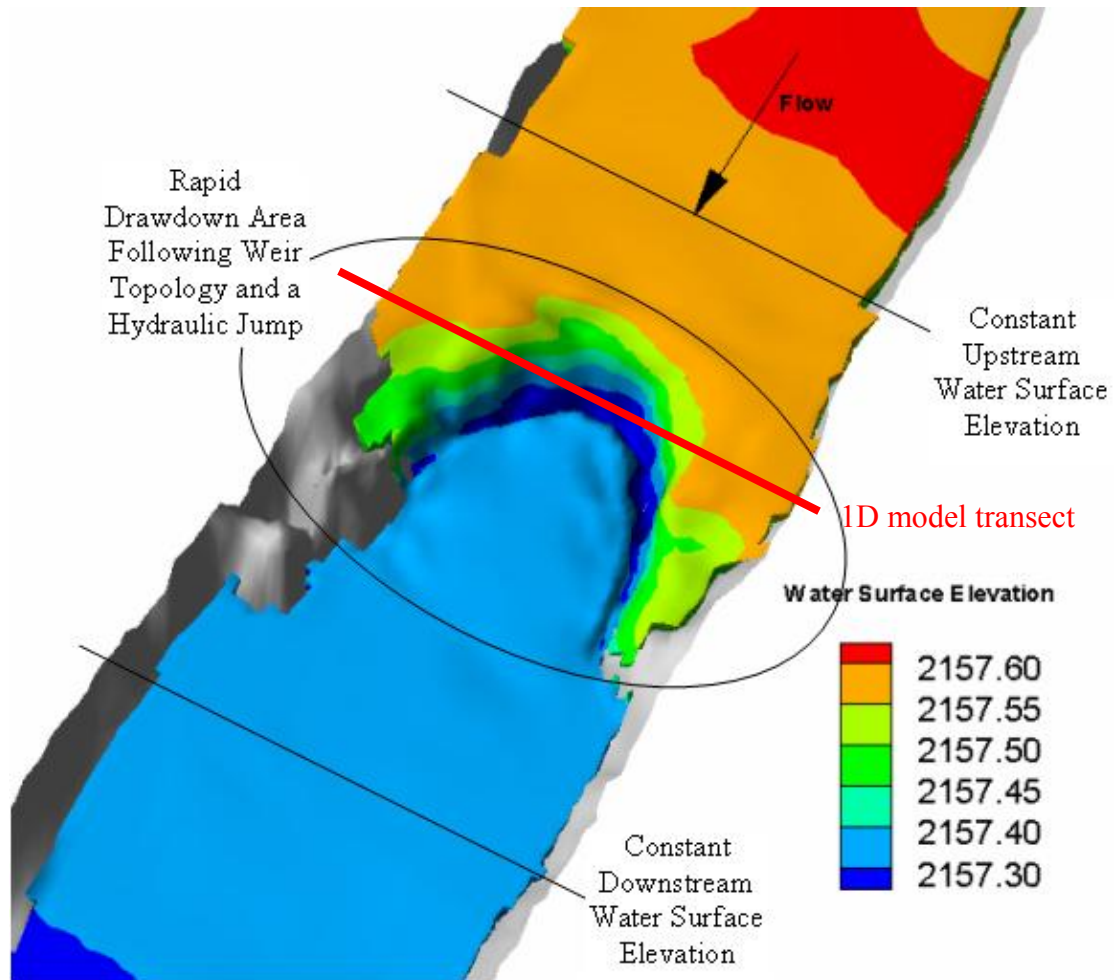


Figure 3.1 – Example 3D output showing plan view water surface elevation contours obtained from 3D model.

Figure 3.2 shows a plan view of a U-weir with surface velocity vectors obtained from the 3D numerical model. In the channel upstream and downstream of the structure water flows parallel to the banks. Over the weir, the flow paths rapidly converge and then slowly expand. A jet through the center of the channel creates abrupt lateral changes in velocity. As a result, a transect located within the structure results in the velocity vectors not being perpendicular to the transect, violating 1D model assumptions for velocity. In a 1D model, lateral velocity components are disregarded entirely and all

hydraulic properties and parameters are cross-section averaged. Methods to meet 1D velocity requirements include bending the cross section perpendicular to anticipated velocity vectors in order to accommodate lateral variability. However, since the re-direction of flow associated with rock weirs varies with discharge, there is not one unique cross section orientation that will satisfy 1D modeling assumptions for a range of flows. Since 2D and 3D models utilize a computational mesh that links channel topography both longitudinally and laterally, the models are able to simulate lateral changes in flow conditions for a range of flows by calculating hydraulics at individual mesh points throughout the reach.

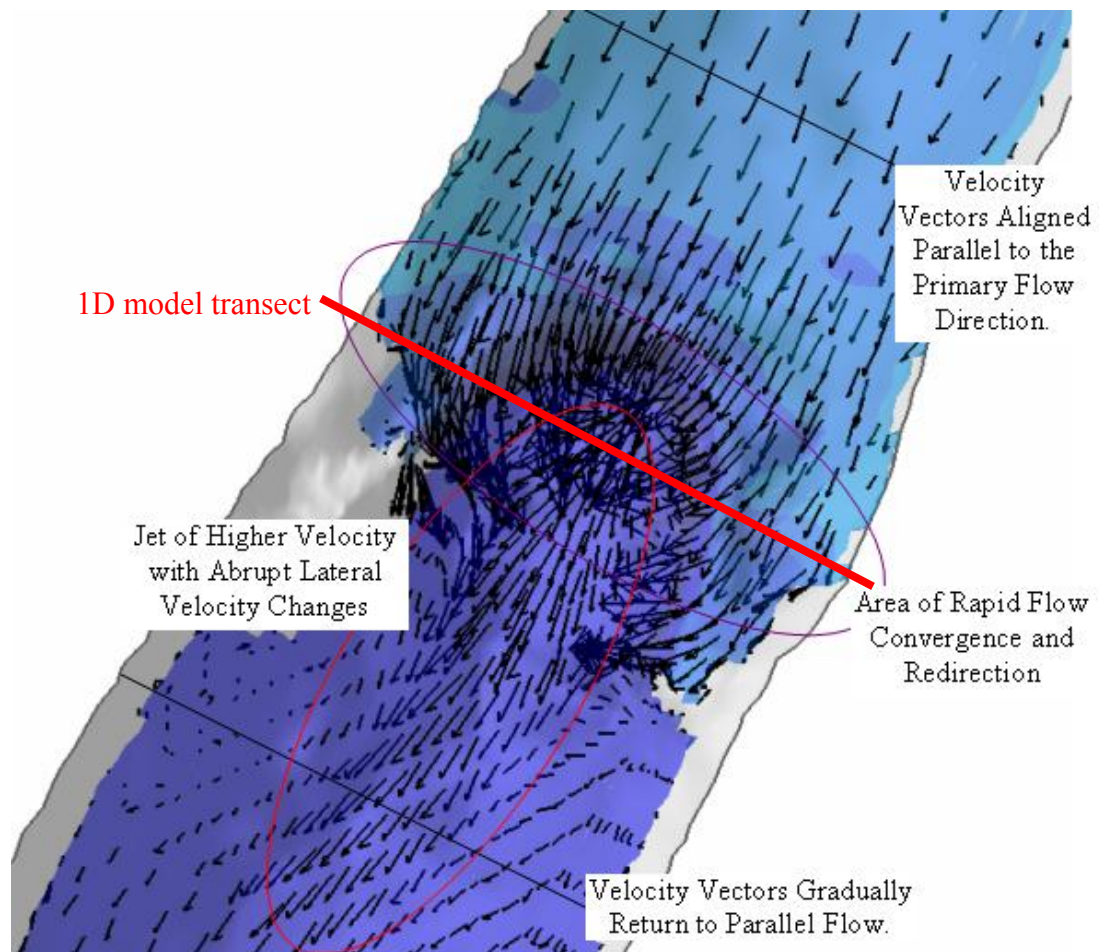


Figure 3.2 – Example 3D output showing plan view velocity vectors and wetted area obtained from 3D model.

Figure 3.3 shows a profile view for a U-weir with velocities in a longitudinal cut along the thalweg. Water flows parallel to the bed upstream and downstream of the structure. The stream lines rapidly converge and diverge vertically through the structure near the structure crest. The velocity profile contains a jet midway through the water column rather than the logarithmic profile of a typical river section. Vertical velocity components downstream of the structure crest show plunging flow. The vertical velocity components found downstream of the structure violate both 1D and 2D modeling assumptions that require velocity vectors perpendicular to the vertical plane. Additionally, while the 3D model calculates velocity vectors along the vertical, 1D and 2D models compute an average cross section and vertically depth-averaged velocity respectively.

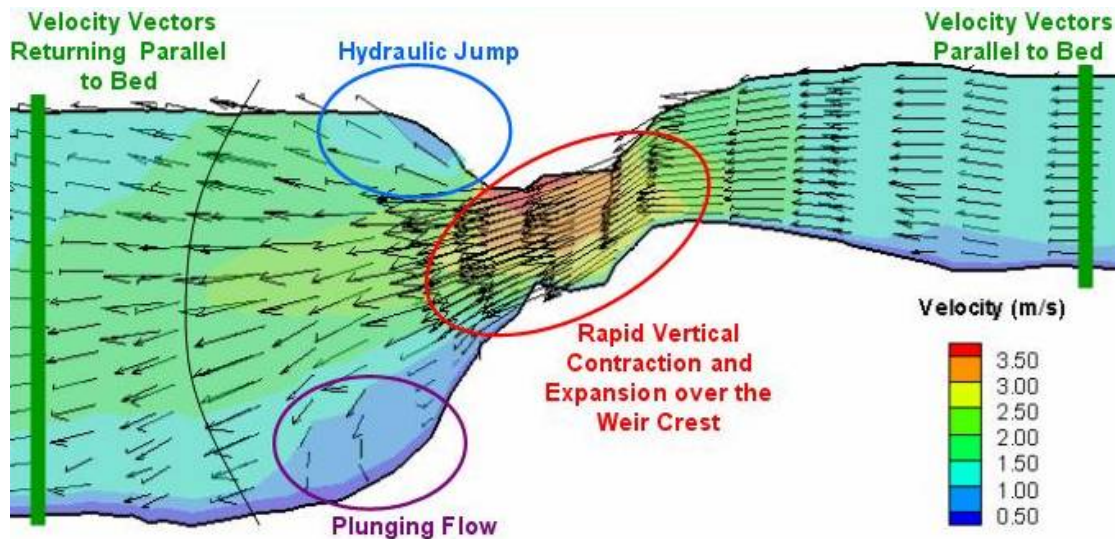


Figure 3.3 – Example 3D output showing thalweg profile and velocity magnitude obtained from 3D model.

Unlike 1D and 2D models, three-dimensional models account for flow that is not parallel to the stream bed, such as flows through a hydraulic jump or river training feature, and therefore more adequately capture the depths and associated velocities immediately downstream from a rock weir. Additionally, 3D models compute velocity

for each grid point control volume within the computational mesh, and therefore incorporate both the horizontal and vertical components of velocity. Figure 3.4 shows attempts to reconcile 1D modeling requirements for rock weirs with the results obtained from the 3D numerical model. A 1D cross section model for rock weirs can meet either water surface requirements or velocity requirements, but not both. Figure 3.4 demonstrates the need for a 1D model to incorporate adjustments for multi-dimensional effects. HEC-RAS contains placeholders to account for multi-dimensional effects (e.g. expansion/contractions coefficients, weir equations, roughness, ineffective flow, etc.), but the magnitudes of the adjustments are unknown for rock weirs. The adjustments will depend on the throat width, profile and plan arm angle, structure length, drop height, bed material, and more. After understanding the 3D processes associated with rock weirs, 1D adjustment parameters can be tested and developed where required. Outside of the plunge pool, where there is less of a vertical flow component, 2D modeling provides a method for estimating the lateral changes in flow and is described in more detail in sections 3.2 and 3.3.

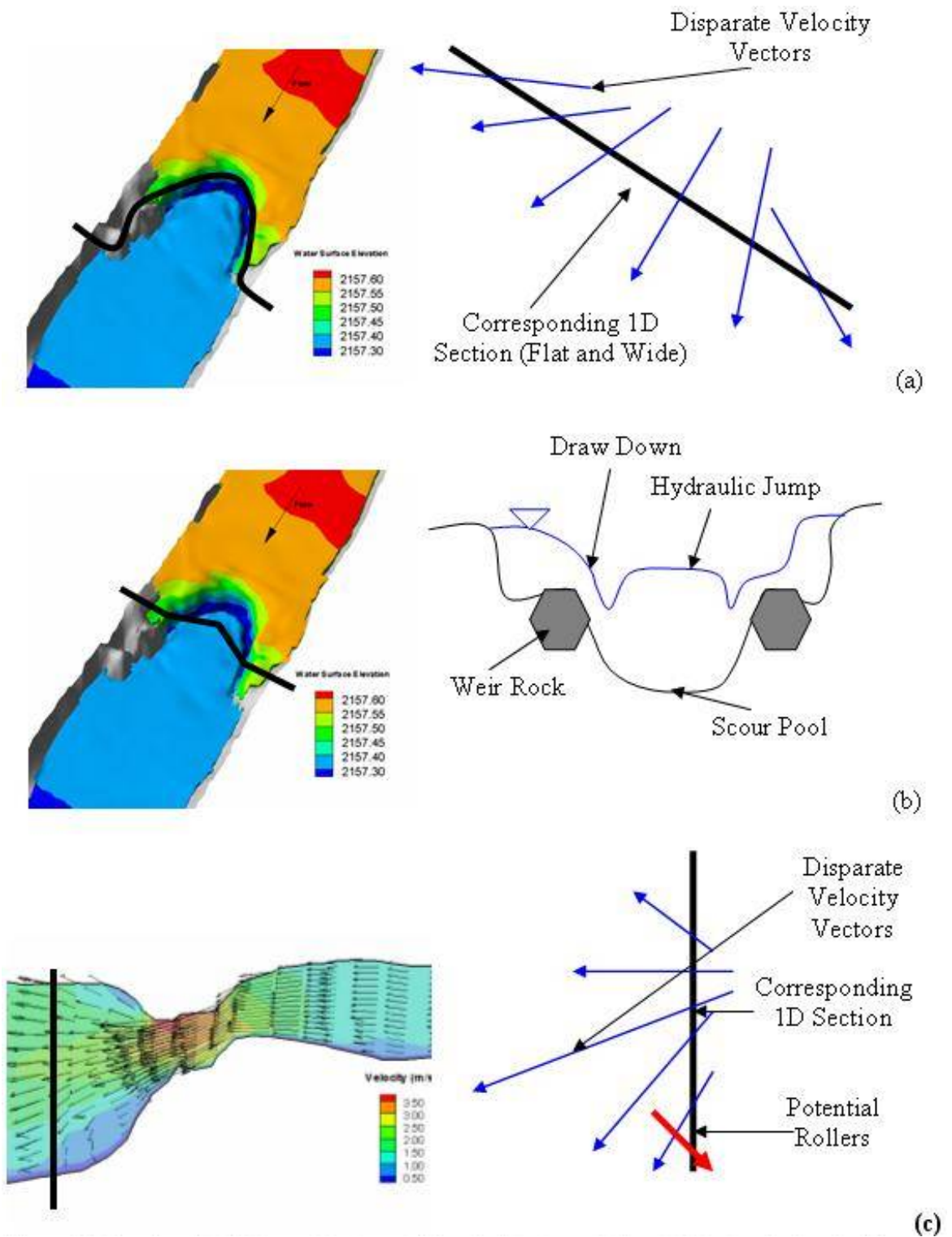


Figure 3.4 – Meeting 1D water surface criteria fails to meet velocity criteria (a) and vice versa (b). No Method of manipulating 1D transects captures jumps or plunging flow (c).

The use of three-dimensional models to evaluate hydraulics through river spanning rock weirs has not been extensively documented in available literature. To determine the ability of a three-dimensional model to adequately capture hydraulic processes associated with river spanning rock weirs, two test cases were modeled utilizing physical laboratory data from Meneghetti (2009) and Scurlock (2009) and a field reconnaissance conducted on the South Fork Little Snake River near Steamboat Springs, Colorado.

3.2 3D NUMERICAL MODEL COMPARISON WITH OBSERVED FIELD CONDITIONS

Using field data collected on the South Fork of the Little Snake River, measured water surface elevations, velocities, and bed topography were analyzed and compared with results from each of the numerical modeling methods (1D, 2D, and 3D).

3.2.1 SITE DESCRIPTION

The field site is located in the Upper Yampa River Basin in Northwestern Colorado on the South Fork of the Little Snake River on the property of Three Forks Ranch Corporation (Figure 3.5).

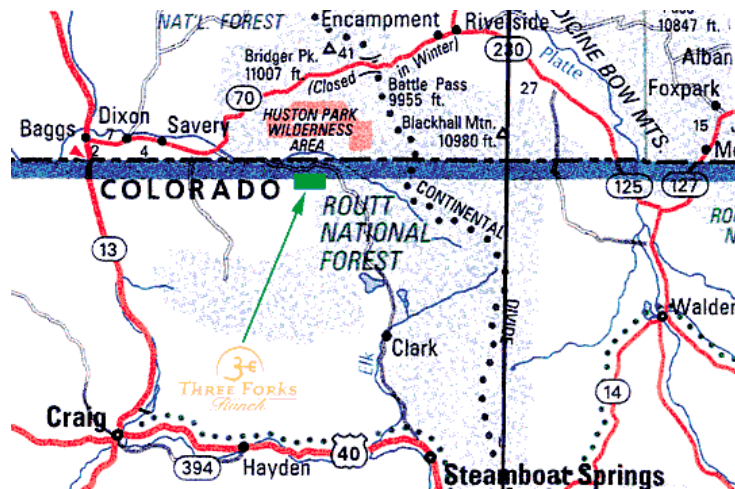


Figure 3.5 – Map of field site location on South Fork Little Snake River.

The field site was selected because of the large number of river spanning rock weirs present along this stretch of river and the ability to collect detailed velocity and topographic data from a portable bridge constructed in the field. Selection Criteria for the U-weir included accessibility, symmetry of the weir arms, plunging flow, intact weir crest, and well defined bank tie-ins. Using the selection criteria, two U-weir structures in close proximity of one another were located (Figure 3.6). Both structures altered the local flow patterns at bankfull flow and exhibited plunging flow conditions.



Figure 3.6 – U-weir located on the South Fork Little Snake River at bankfull flow.

3.2.2 DATA COLLECTION

Field reconnaissance took place in June and September of 2005. Data collection during the June 2005 site visit included topographic surveys of the structures and surrounding features (e.g. banks, scour pools, thalweg, water surface elevation), 3D velocity measurements, discharge measurements, and qualitative information related to vegetation, bank condition, and structure performance. Detailed topographic survey data was collected along transects that were spaced approximately every 1.5 meters. In

addition to the topographic survey data, each structure included six sampling transects for measuring velocity:

1. Upstream of the flow disturbance;
2. Upstream of the weir crest;
3. Beginning of the weir crest (throat);
4. Half way through the length of the structure ($0.5*La$);
5. End of the structure extent at arm tie-in location ($1.0*La$); and
6. End of the downstream flow disturbance.

Five sampling locations were placed at evenly spaced intervals across each transect and three dimensional velocity measurements were collected at 20, 60, and 80 percent of the depth (as measured down from the water surface) with additional depth measurements taken along the centerline. At each transect a bridge placed perpendicular to the flow and spanning 36 feet supported a sliding sampling platform. Stationing was marked on the bridge relative to the bridge endpoints. The sampling platform held a mounting bracket on the upstream face of the bridge with a 3.5 meter long 3 centimeter square solid aluminum rod to hold a Sontek field ADV probe (Figure 3.7). 25 Hz three dimensional velocity measurements were take for 60 seconds at the centerline and 30 seconds everywhere else unless high turbulence, low correlations, or interference from air entrainment required longer sampling intervals.

In September of 2005, the site was re-visited and survey data was collected at a lower flow (Figure 3.8) to document structure conditions and surrounding topographic features including a detailed survey of the structure crest rocks, bank lines, channel thalweg, scour pools, and adjacent bed topography.

Survey data collected during both field visits was used in generating the bed topography used in the 3D numerical model described in the next section. Measured

velocities and water surface elevations were used in validating the numerical model and are described in Section 3.3.4.



Figure 3.7 – Bridge with sampling platform and field ADV probe used for high flow measurements.



Figure 3.8 – U-weir on South Fork Little Snake River at low flow.

3.2.3 NUMERICAL MODEL DESCRIPTION

3D modeling requires detailed bed topography through the entire reach modeled as well as a vertically distributed mesh between the bed and water surface elevation to describe flow patterns in three dimensions. Using the topographic survey data from both the June and September field visits, a scatter point data set containing northing (y), easting (x), and elevation (z) was generated and used as a base map for creating the numerical model computational mesh. The mesh was generated using quadrilateral and triangular elements to describe the structure and channel bathymetry in the numerical model (Figure 3.9).

Measured water surface elevations and discharge observed during the site visits were used for input boundary conditions in the numerical model. The upstream boundary condition was set by specifying a discharge measured in the field using a Sontek FlowTracker Handheld-ADV® (acoustic doppler velocimeter) and the downstream boundary condition was set by specifying the corresponding water surface elevation measured in the field using Trimble GPS survey equipment.

While the focus of this dissertation is related to 3D modeling of rock weirs, results from 1D and 2D model simulations are also presented in this section for comparison purposes. Comparing the results from each of the numerical models with observed values provides insight into the applicability and limitations of each numerical modeling method in simulating the complex flow patterns associated with rock weirs. The 1D model HEC-RAS, developed by the U.S. Army Corps of Engineers (2006) and the 2D model SRH-2D, developed by Reclamation (2008) were selected to model the field U-weir described above.

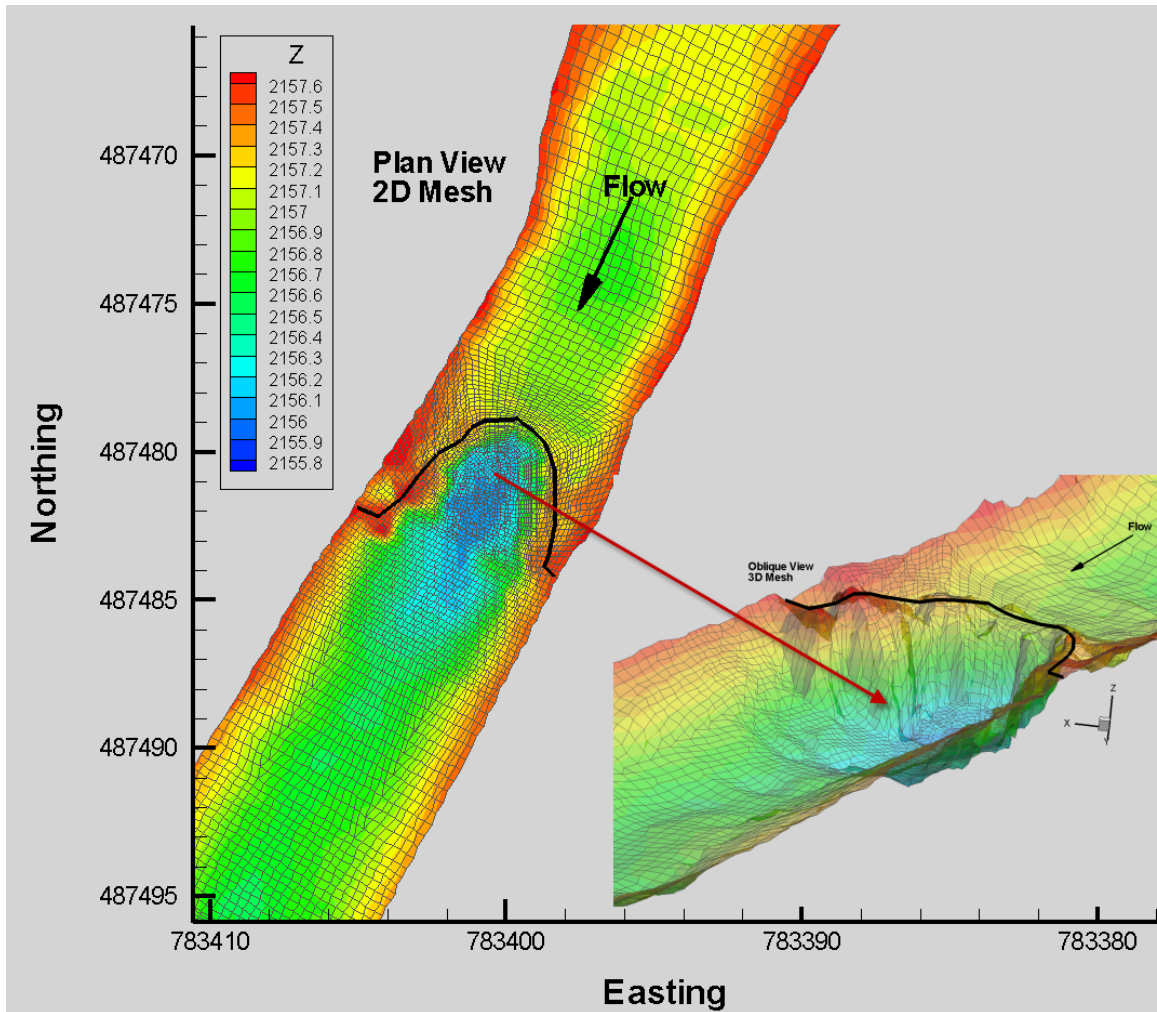


Figure 3.9 – Computational mesh for U-weir on South Fork Little Snake River.

The 2D model, SRH-2D was selected because it was used to provide input (water surface elevation) for the 3D model solid lid approximation for steady state free surface flows and additional output such as depth and velocity were readily available for comparison purposes. Since the computed water surface elevation from the 2D model provides input to the 3D model, water surface elevations for the 2D and 3D model are the same and will be referred to as 2D/3D for comparison purposes.

The 1D model, HEC-RAS was selected because of the wide range of use in river restoration/channel design and popularity of the model among hydraulic engineers and designers. Channel geometry for the 1D model was generated by extracting station-

elevation data along twenty-two transects from the 2D computational mesh as shown in Figure 3.10 below. Six of the twenty-two transects correspond to field data collection locations. Boundary conditions used in the 1D model were consistent with the measured values used in the 2D and 3D model for discharge and downstream water surface elevation.

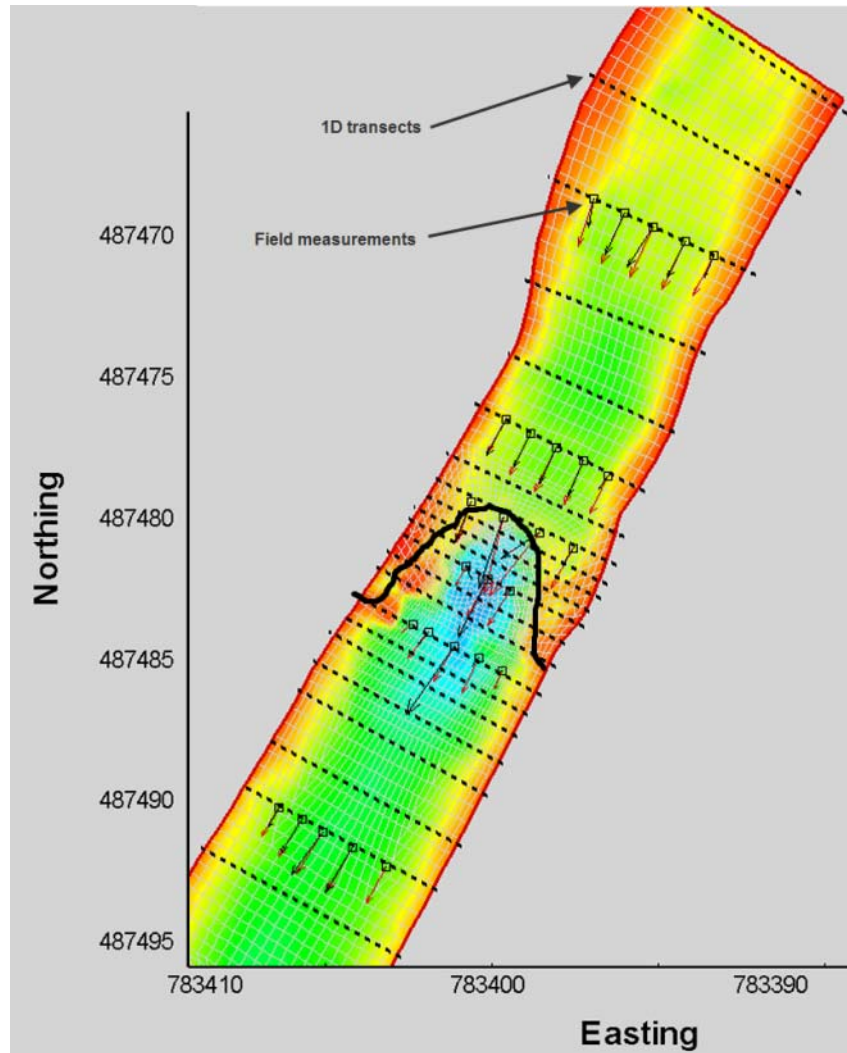


Figure 3.10 – Cross section locations for 1D model extraction for U-weir on South Fork Little Snake River.

3.2.4 COMPARISON

Using the field data collected on the South Fork of the Little Snake River, measured water surface elevations, velocities, and bed topography were analyzed and

compared with results from the numerical models (1D, 2D, and 3D). Verification of the 3D model was performed by comparing results from the 3D model with measured water surface elevations and velocities collected on the South Fork of the Little Snake River.

Comparisons between numerical model results and measured water surface elevations (Figure 3.11) show that the 2D/3D numerical model was able to replicate field measurements by matching measured water surface elevations within 7.5% (Figure 3.12) for bankfull discharge at measured depths ranging from 0.3 meters to 1.3 meters. Figure 3.12 also shows that for the bankfull flow, the 1D model was able to replicate field measurements within 12.5% with the exception of a 25% error near the structure crest.

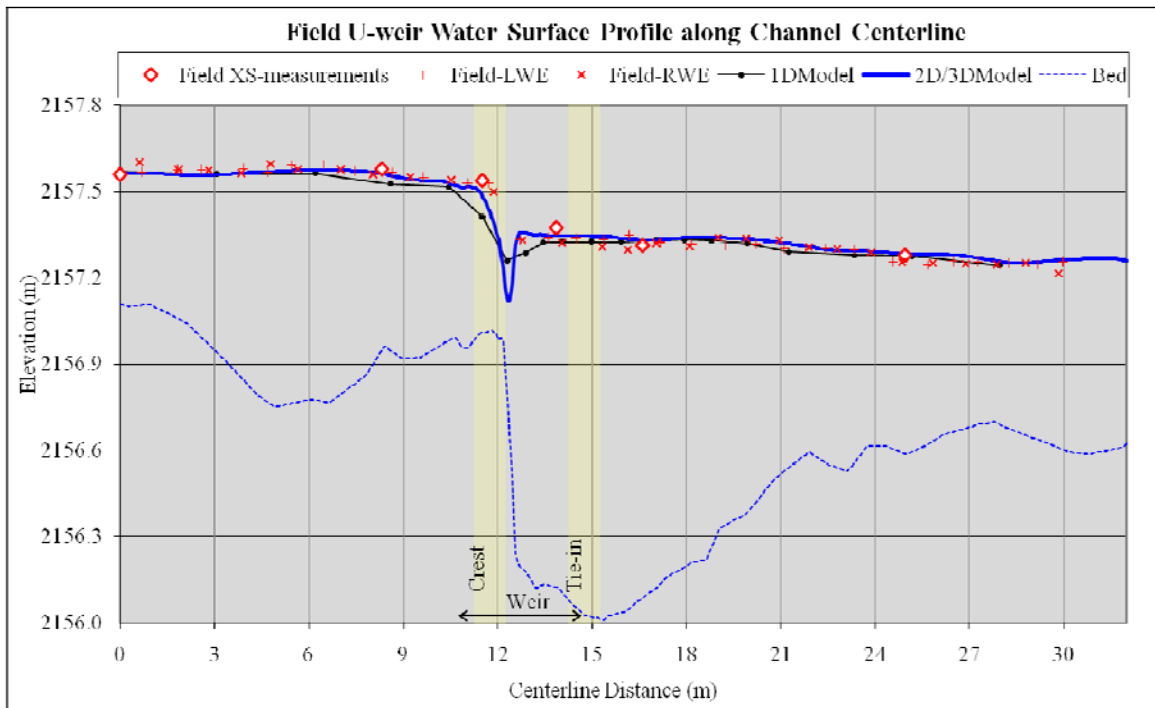


Figure 3.11 – Field and numerical model U-weir centerline water surface profile comparison.

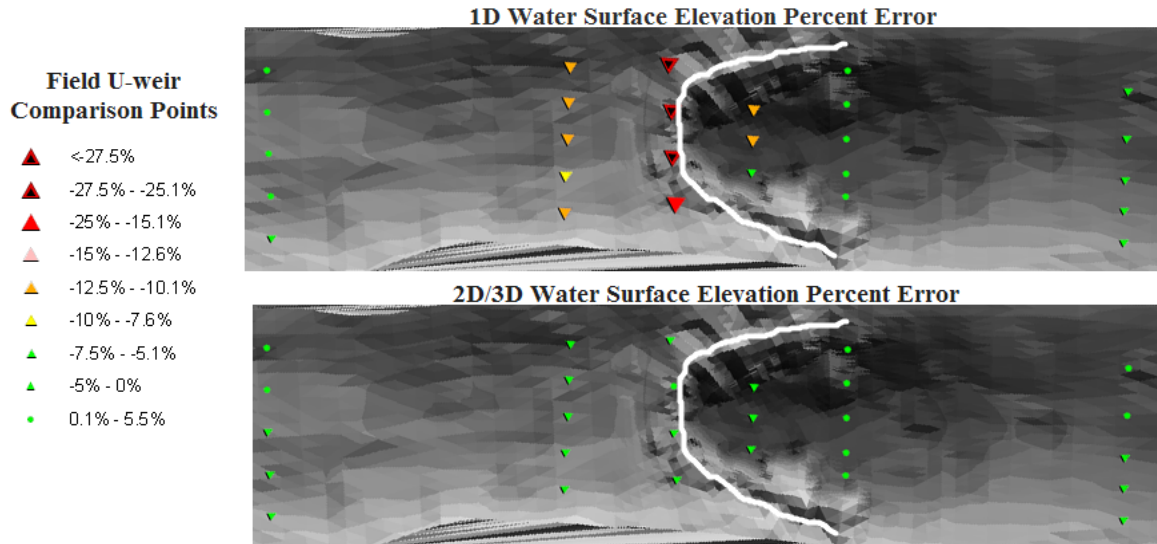


Figure 3.12 – Field U-weir percent error in numerical model water surface elevations.

Figure 3.13 shows the observed (true) water surface elevation measurements plotted against predicted values from the numerical models for the same locations. The linear correlation coefficients of 0.84 for the 1D model and 0.98 for the 2D/3D model show relatively good overall agreement (with no regard to the spatial component in the data) between predicted and measured values for all models. The residuals of the water surface elevation predictions have a slight negative bias with a mean= -0.03m (n = 27).

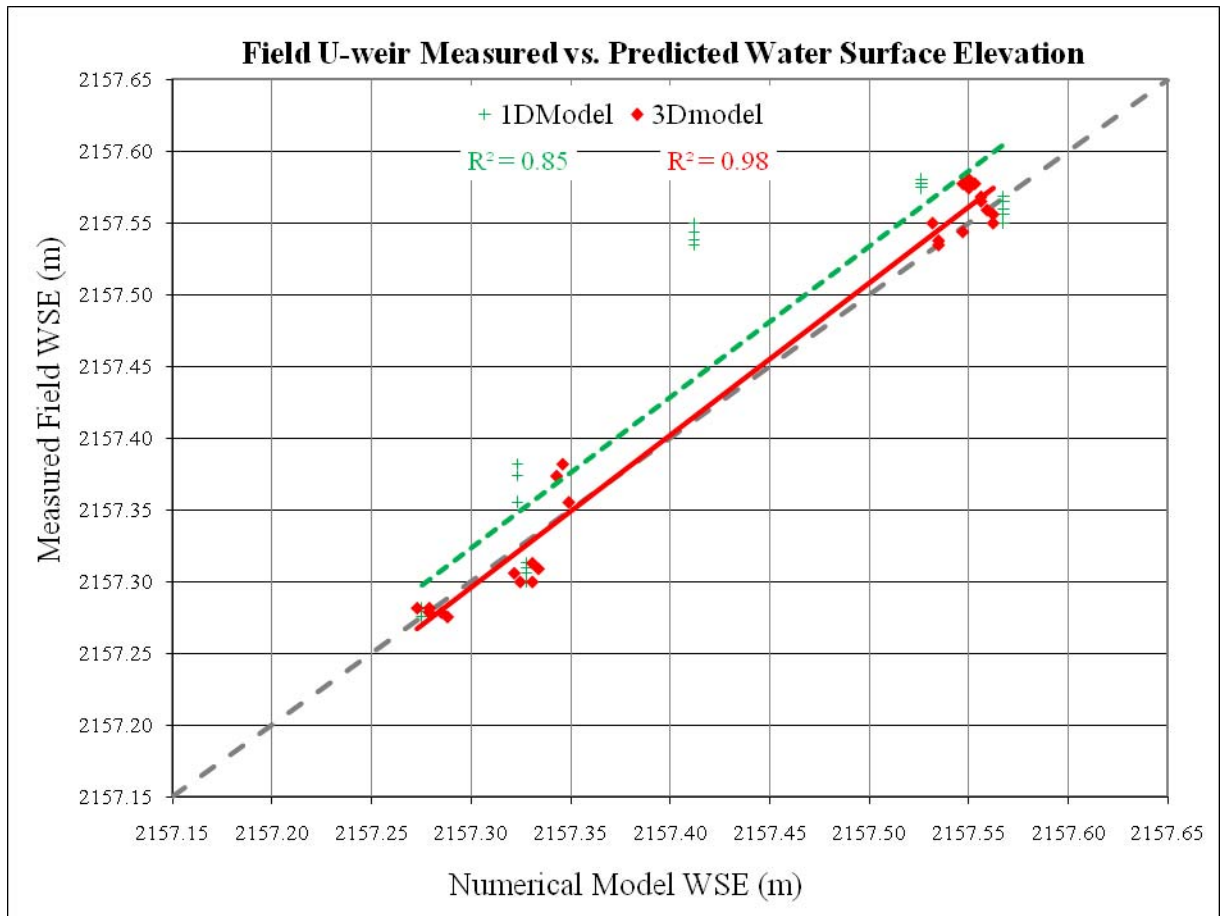


Figure 3.13 – Field U-weir measured vs. predicted water surface elevation.

However, when the spatial component of the data is considered (Figure 3.14), it is evident that the 2D/3D model provides a much better prediction of the water surface elevation near the crest of the structure. While the error in the predicted water surface elevations from the 2D/3D model are all less than 7.5% (0.036m), the 1D model shows more than a 25% error (0.138m) at the structure crest. The large error in the 1D model is due to the rapidly varied flow condition that exists along the crest of the structure; which the 1D model is unable to accurately simulate.

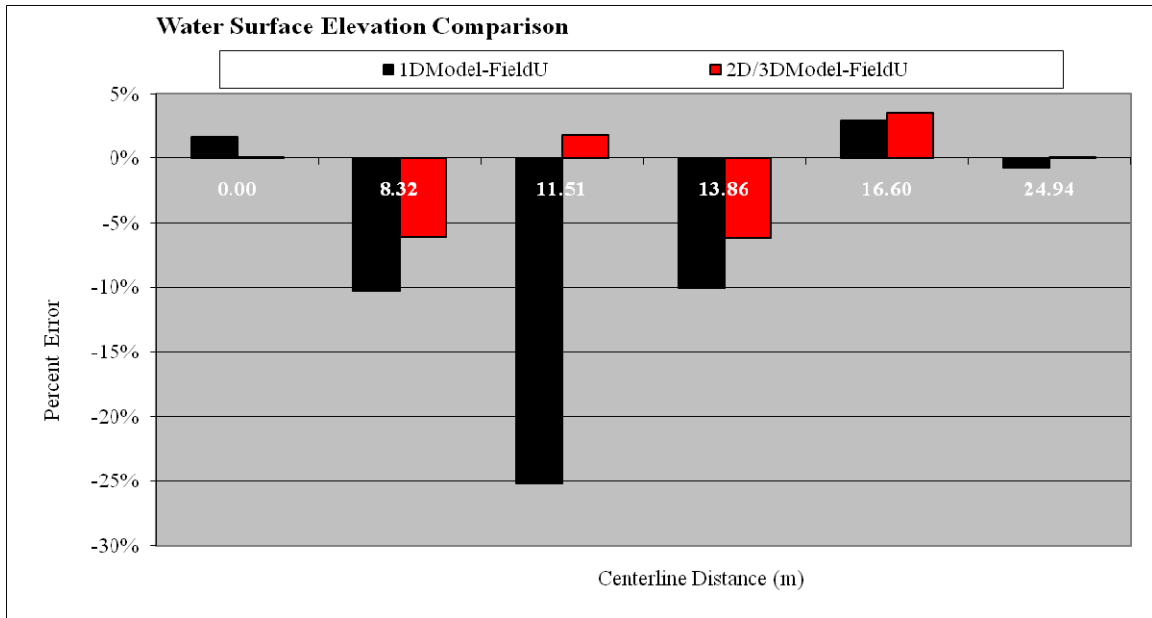


Figure 3.14 – Field and numerical model U-weir water surface elevation comparison, percent error along centerline profile.

Comparisons between numerical model results and measured velocities along the channel center line show that the numerical models also differ in their ability to replicate field measurements, especially downstream from the structure crest (Figure 3.15). From Figure 3.15 it is evident that the 3D model provides a much better prediction of the velocities downstream from the crest of the structure. While the maximum error in the predicted channel centerline velocity from the 3D model is 11% (0.168 m/s), the 1D and 2D models have much greater errors at 56% (0.97 m/s) and 41% (0.71 m/s) respectively. The 1D and 2D models are not able to properly simulate the vertical components of the velocity vectors that occur downstream of the structure crest. The high variability in the velocity predictions is a result of the plunging flow that occurs along the structure crest causing the flow downstream of the structure to have a strong vertical velocity component which violates 1D and 2D model assumptions that require velocity vectors perpendicular to the vertical plane. Additionally, while the 3D model calculates velocity vectors along the vertical, 1D and 2D models compute average cross section and depth-

averaged velocity respectively. Since the 1D model provides an average cross sectional velocity, predicting changes in flow patterns around the structure both longitudinally and laterally is not feasible. Hence the need for higher order models (2D and 3D) that incorporate lateral changes in flow.

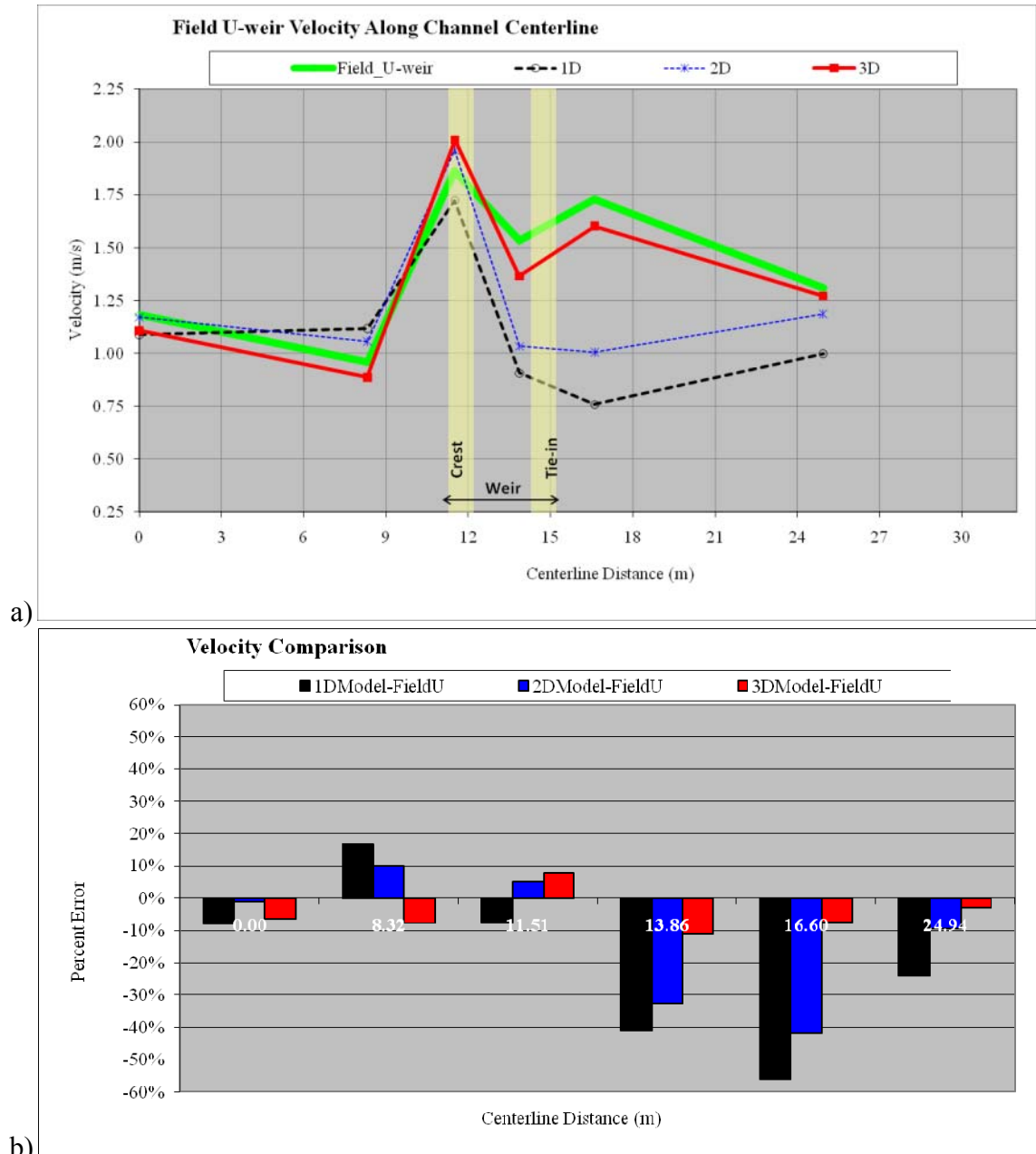


Figure 3.15 – Field and numerical model U-weir velocity comparison along channel centerline a) velocity magnitude b) percent error.

Figure 3.16 shows the observed (true) velocity measurements plotted against predicted velocities from the numerical model for the same locations measured in the field. The linear correlation coefficients of 0.14 for the 1D model, 0.46 for the 2D model, and 0.93 for the 3D model show that only the 3D model provides reasonable overall agreement (with no regard to the spatial component in the data) between predicted and measured values. The residuals of the 3D velocity predictions have a slight positive bias with a mean= 0.055 m/s (n = 27).

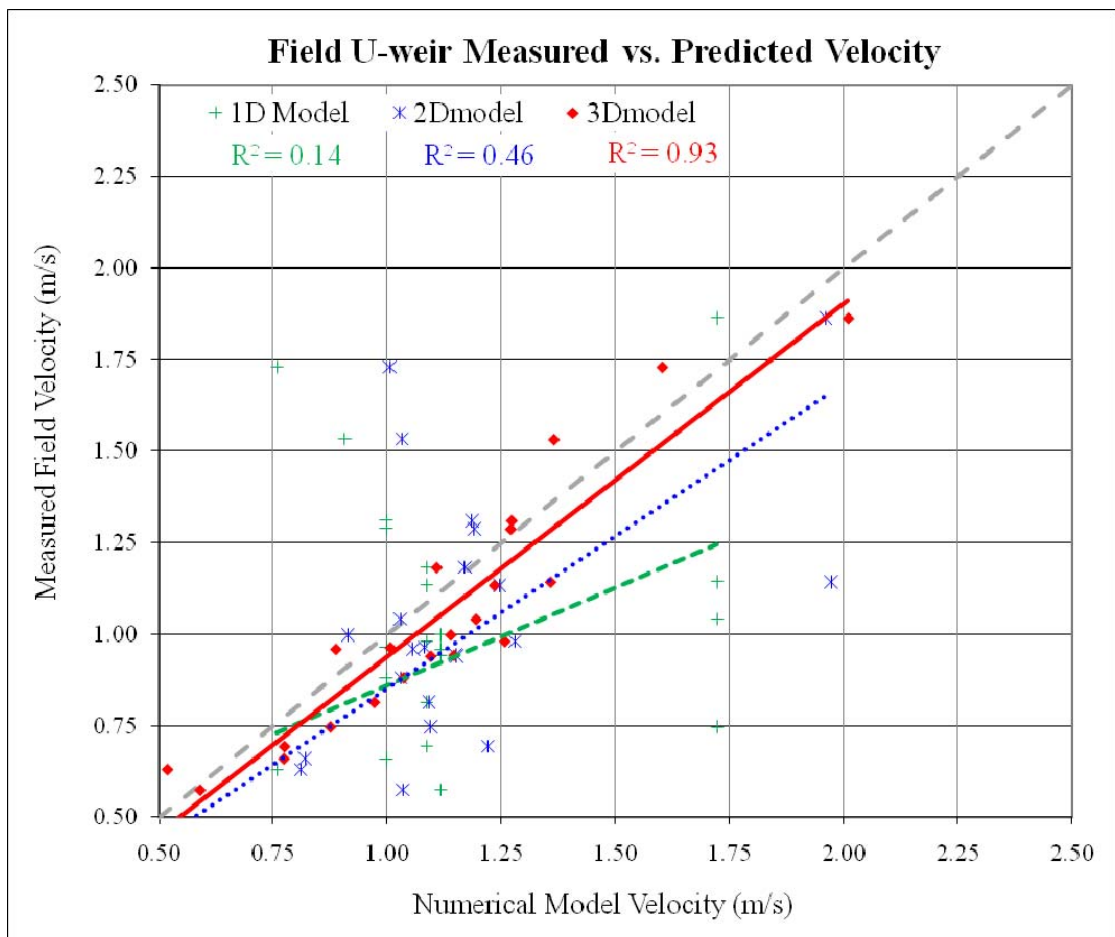


Figure 3.16 – Field U-weir measured versus predicted velocity.

When the spatial component of the data is considered (Figure 3.17), it is evident that the 3D model provides a much better prediction of the velocities across the channel and downstream from the crest of the structure. Figure 3.17 shows the percent error in the

predicted velocities from each of the numerical models for the sample locations measured in the field. The results of the velocity comparison show that only the 3D model was able to properly simulate the complex flow patterns associated with U-weirs with a maximum velocity error of 28%. While the maximum error in the predicted velocity from the 3D model is 0.276 m/s (28%), the 1D and 2D models have much greater errors at 0.976 m/s (130%) and 0.83 m/s (73%) respectively. The 1D and 2D models are not able to properly simulate the vertical velocity vectors that occur downstream of the structure crest. Variations between the predicted 3D model velocities and measured values are likely attributable to minor differences in the modeled topography, high turbulence downstream of the structure from the plunging flow over the structure crest and arms, accuracy of the instruments used in the measurements, and field measurement error.

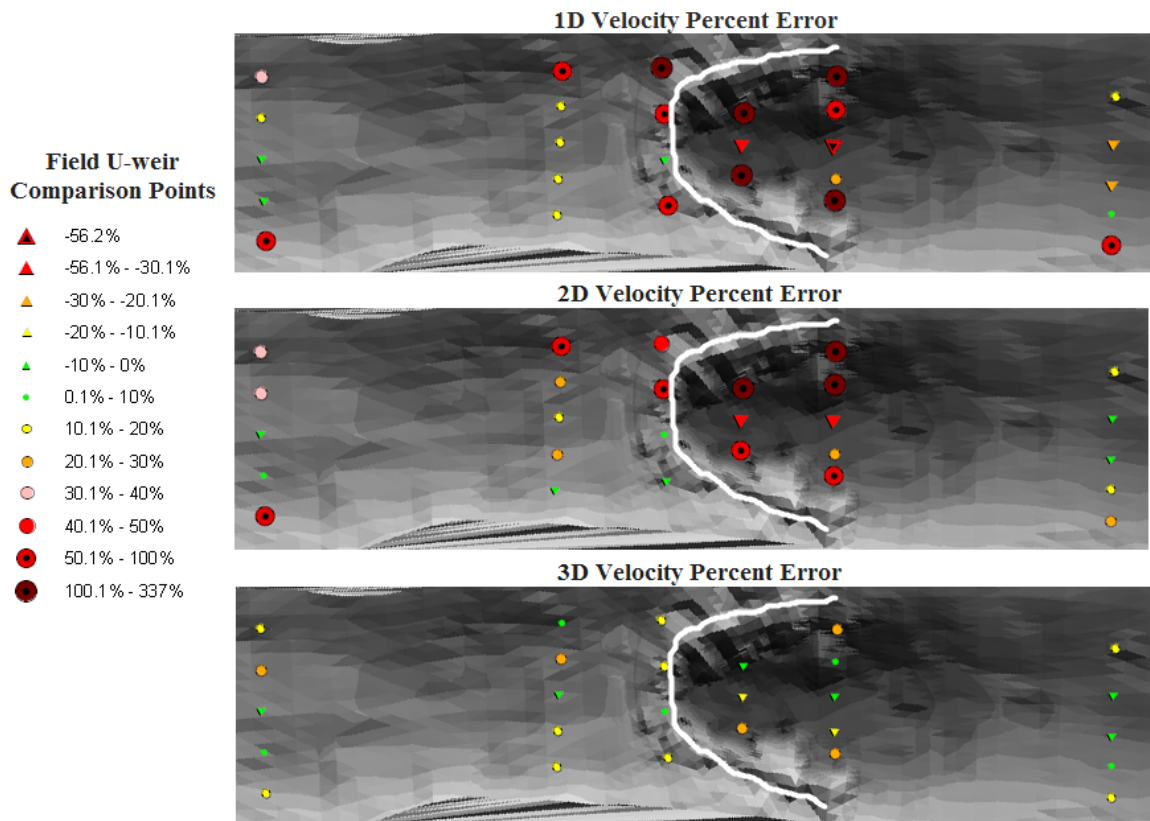


Figure 3.17 – Field U-weir and numerical model velocity percent error comparison for 1D, 2D, and 3D model.

A box and whisker plot showing the variation between the 1D, 2D, and 3D model percent error magnitude in velocity is presented in Figure 3.18 below. It is evident from the comparison that of the three numerical models, the 3D model provides a better overall prediction of the velocities throughout the study reach with a 95% confidence interval of 7.5%-18% compared to 17%-66% and 10%-54% for the 1D and 2D model respectively.

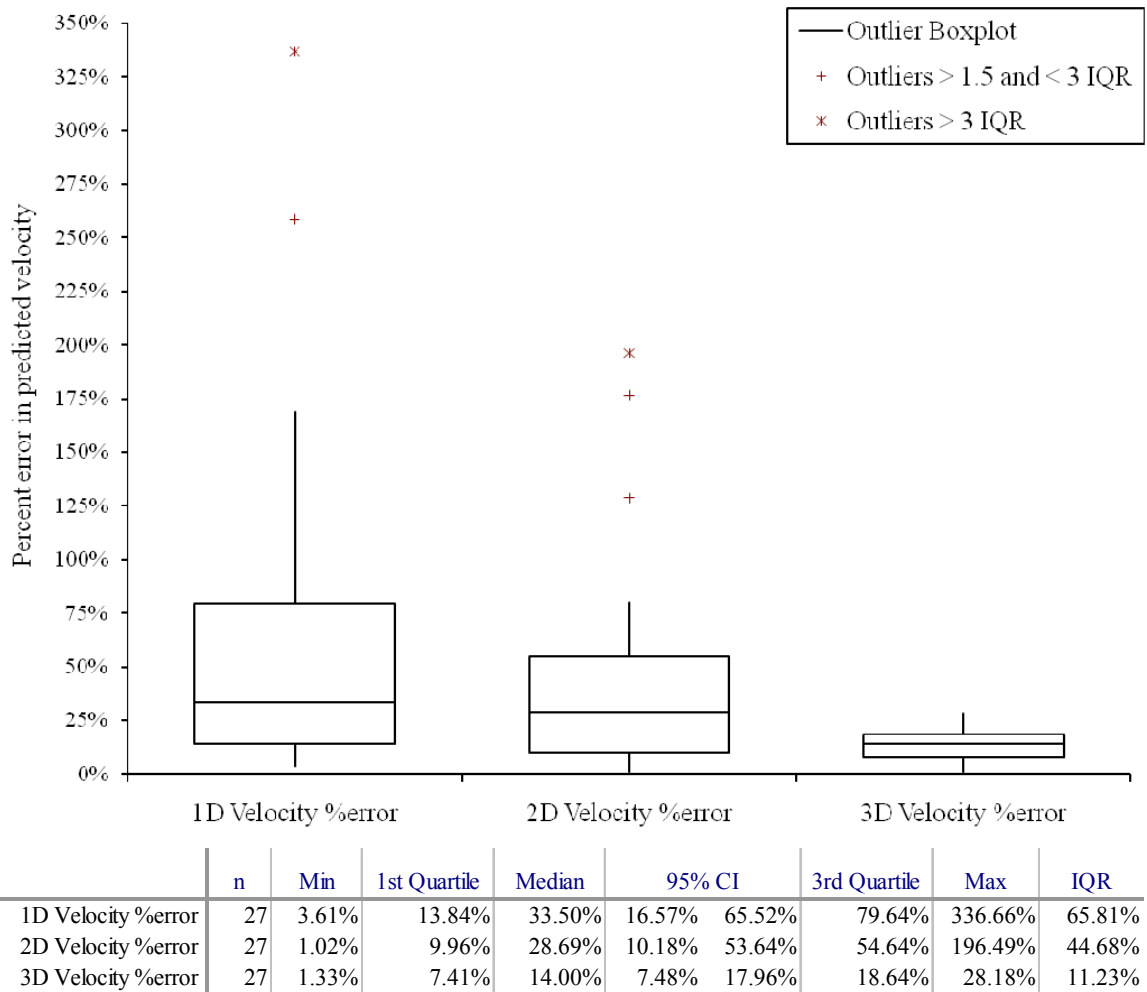


Figure 3.18 – Field U-weir velocity comparison, percent error magnitude box-plot with maximum 1.5 IQR for 1D, 2D, and 3D models.

3.3 3D NUMERICAL MODEL COMPARISON WITH OBSERVED LABORATORY CONDITIONS

Using data collected during laboratory studies conducted by Colorado State University (Meneghetti 2009 and Scurlock 2009), measured water surface elevations,

velocities, and bed topography were analyzed and compared with results from each of the numerical modeling methods (1D, 2D, and 3D).

3.3.1 PHYSICAL MODEL DESCRIPTION

The laboratory experiments were conducted in a 4.88 meter (16 ft) wide by 15.24 meter (50 ft) flume (Figure 3.19 and Figure 3.20). The channel width was equal to the flume width and the geometry of the weir was designed such that the parameters for the throat width, arm angle, and arm slope were near the median of the design range of values recommended by Rosgen (2006).

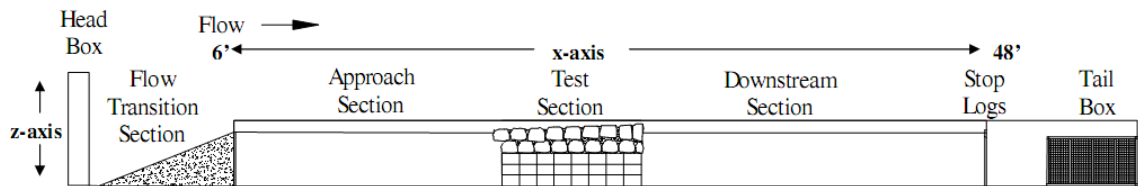


Figure 3.19 – Plan-View Schematic of Flume (Meneghetti 2009)

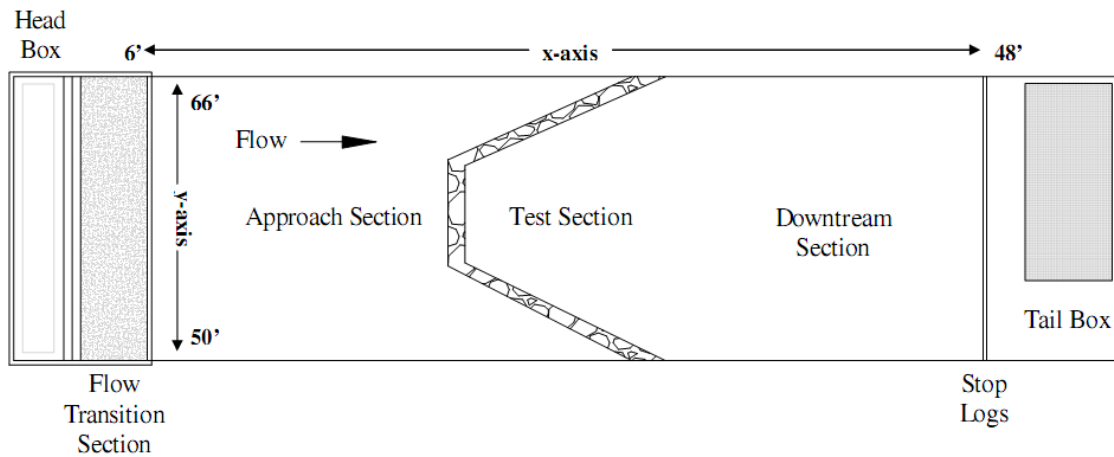


Figure 3.20 – Profile-View Schematic of Flume (Meneghetti 2009)

The U-weir consists of a horizontal sill constructed perpendicular to the flow, centered in the lateral dimension and spanning 1/3 of the total channel width (Figure 3.21). Arms extend from each side of the sill at a 23 degree angle with the bank and rising upwards at a 3.6 percent slope intersecting at the overbank elevation. The selected

U-weir geometry and channel characteristics used for the numerical model validation are presented in Table 3.1 along with the test numbers and associated discharge. Details regarding the design process for model scaling, flume construction, and testing procedures are presented in Meneghetti (2009).

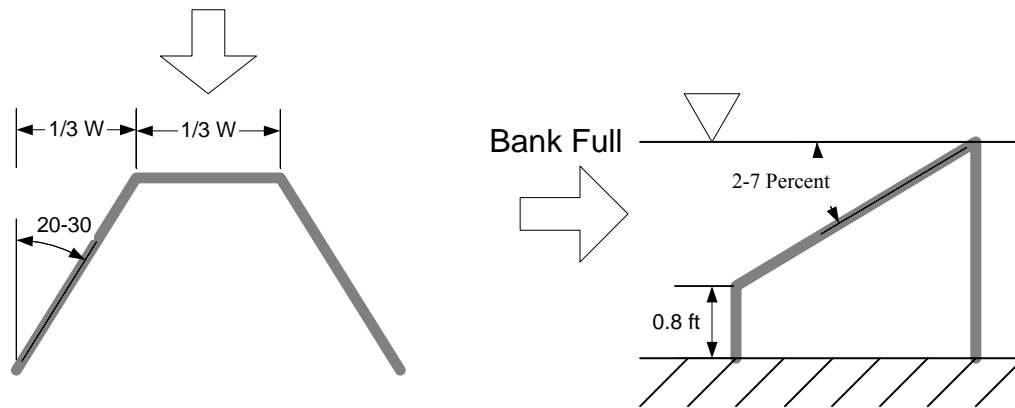


Figure 3.21 – U-weir conceptual design parameters (Meneghetti, 2009)

Table 3.1 – Summary of laboratory U-weir and channel geometry used in numerical model simulation

Channel Conditions					
	Width (m)	Slope	Grain size (mm)	Discharge (cms)	Depth (m)
Prototype	22.55	0.003	45.25	38.5	0.93
Model	4.88	0.003	9.8	0.85	0.20
Weir Geometry					
	Throat width (m)	Arm angle (degrees)	Arm slope (percent)	Drop height (m)	Rock size (m)
Prototype	7.5	23	3.6	0.24	1.03
Model	1.62	23	3.6	0.05	0.22
Laboratory Test					
Reference Discharge	Test ID	Discharge (cms)	Downstream WSE (m)		
1/3 Bankfull	Test33	0.28	26.548		
2/3 Bankfull	Test34	0.57	26.602		
Bankfull	Test35	0.85	26.654		

3.3.2 DATA COLLECTION

Data collection locations were determined based on the geometry of the structure and were designed to best quantify the hydraulic and scour variables associated with the U-weir structure. At each data-collection location, bed elevation, water-surface elevation, and 3-D velocity data were collected. Water surface elevation and velocity data were collected along 8 transects for the U-weir and are presented in Figure 3.22.

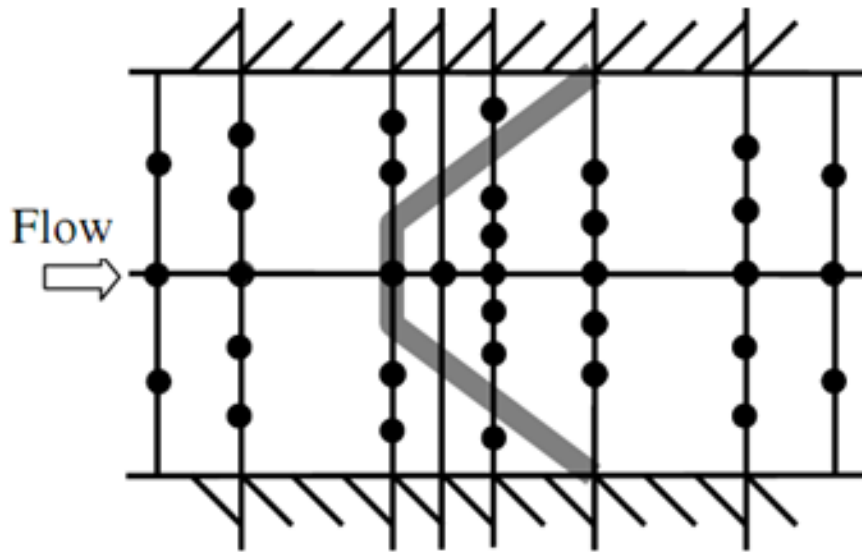


Figure 3.22 – Schematic of laboratory sampling locations for U-weir (Meneghetti, 2009)

Detailed LIDAR survey data of the bed before and after the test were collected using a Leica Scan Station™. A scan consisting of a 2 centimeter grid in the horizontal was conducted for the entire flume to define the initial and final bed topography that would be used in the numerical model simulation. The vertical resolution of the survey data was +/- 4 mm.

3.3.3 NUMERICAL MODEL DESCRIPTION

The numerical model was used to model a simple U-weir with discharges varying between one-third bankfull flow, two-thirds bankfull flow, and bankfull flow. Using the topographic LIDAR survey data from the laboratory, a scatter point data set containing

northing (y), easting (x), and elevation (z) was generated and used in creating the computational mesh for the numerical model. The 3D mesh was generated using the LiDAR data collected for each test case with a node spacing ranging from 0.45 meters to 0.03 meters in both the x- and y-direction and 0.03 meters in the z-direction (Figure 3.23). The 3D model was extended 5.5 meters upstream and 11.5 meters downstream of the laboratory model with a slope of 0.003 to provide boundary conditions that were outside the influence of the structure itself.

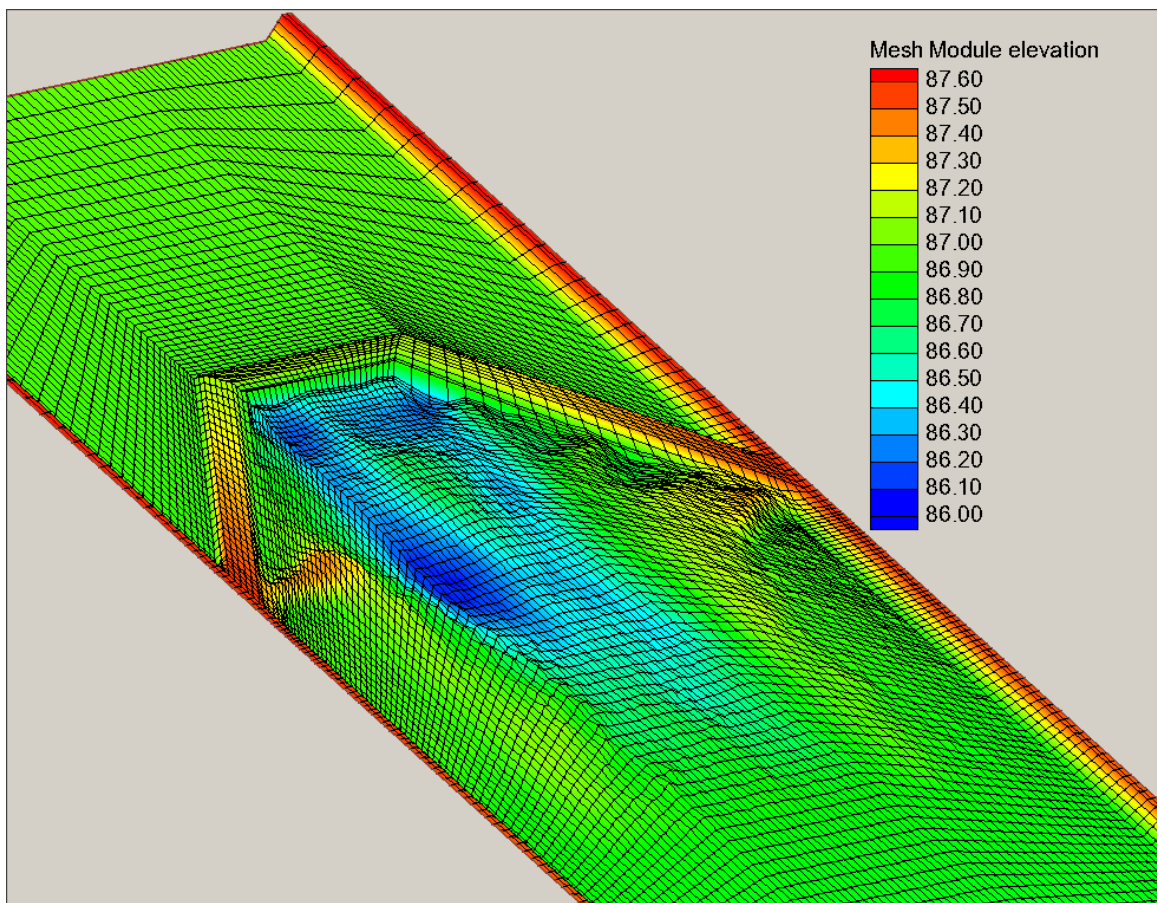


Figure 3.23 – 3D numerical model mesh representing physical model test 35.

Measured water surface elevations and discharge from the laboratory experiments were used for input boundary conditions in the numerical model. The upstream boundary condition was set by specifying the discharge used in the laboratory and the downstream

boundary condition was set by specifying the corresponding water surface elevation measured during the laboratory experiment.

As mentioned in Section 3.2, while the focus of this dissertation is related to 3D modeling of rock weirs, results from 1D and 2D model simulations are also presented in this section for comparison purposes. Comparing the results from each of the numerical models with observed values provides insight into the applicability and limitations of each numerical modeling method in simulating the complex flow patterns associated with rock weirs.

Channel geometry for the 1D model was generated by extracting station-elevation data along twenty-one transects from the 2D computational mesh as shown in Figure 3.24. Eight of the twenty-one transects correspond to laboratory data collection locations. Boundary conditions used in the 1D model were consistent with the measured values used in the 2D and 3D model for discharge and downstream water surface elevation.

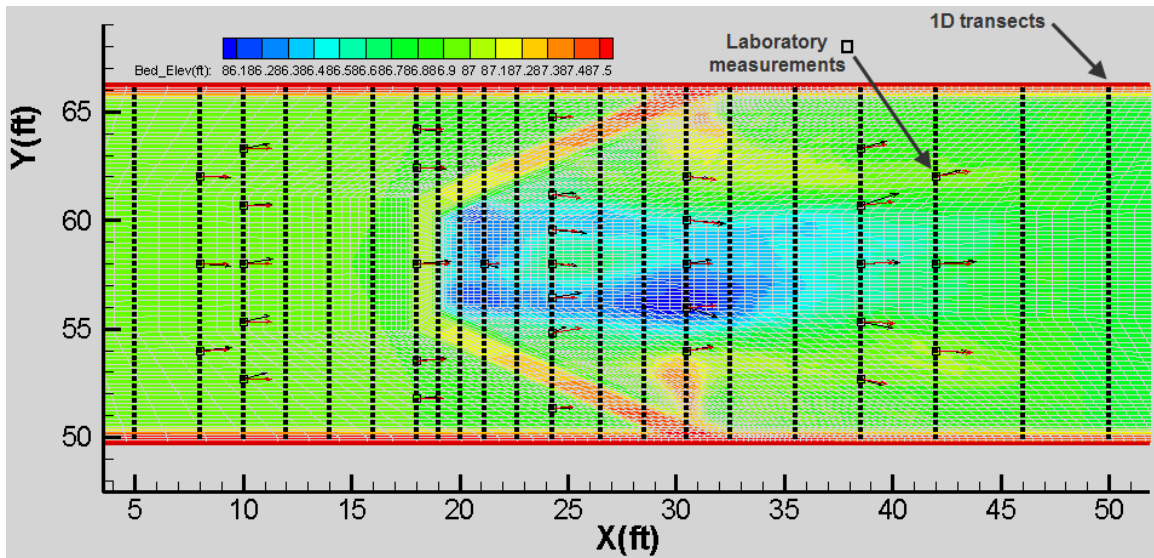


Figure 3.24 – Cross section locations for 1D model extraction for laboratory U-weir.

3.3.4 COMPARISON

Verification of the 3D model was performed by comparing results from the 3D model with measured water surface elevations and velocities collected in the laboratory physical model by Meneghetti (2009) and Scurlock (2009).

Analysis of the numerical model output shows that the water surface elevations along the channel centerline from each of the models matched reasonably well with the measured values from the physical model (Figure 3.25, Figure 3.26, and Figure 3.27).

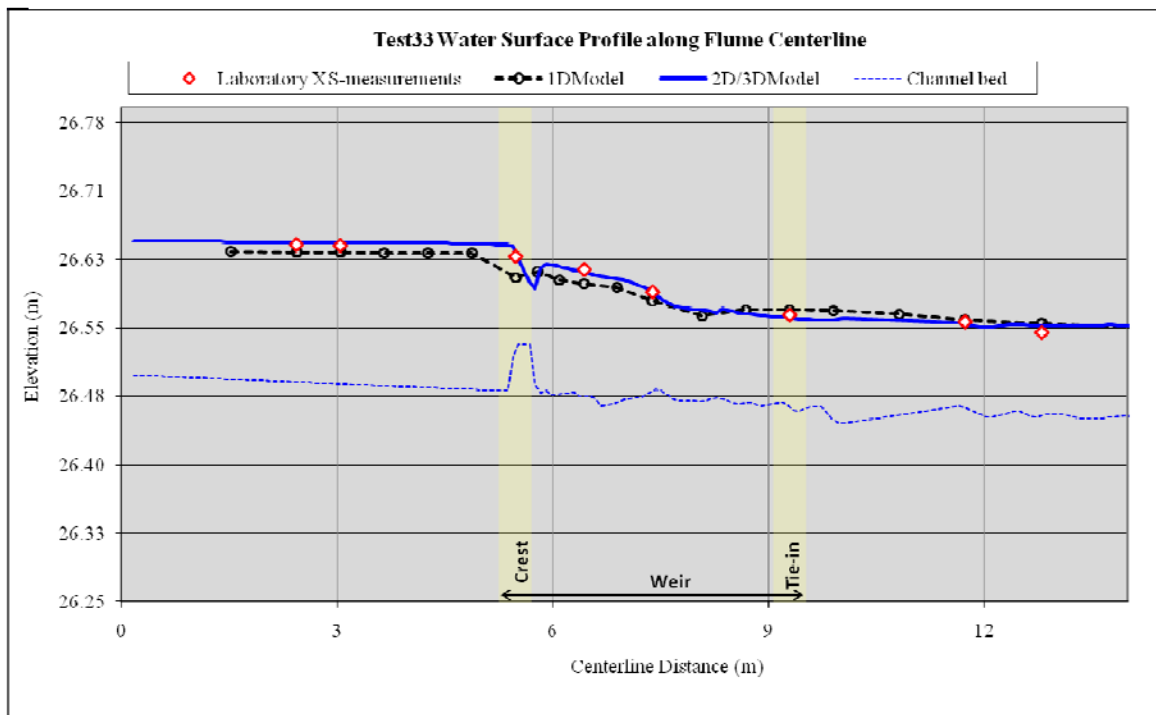


Figure 3.25 – Laboratory and numerical model water surface elevation comparison test 33.

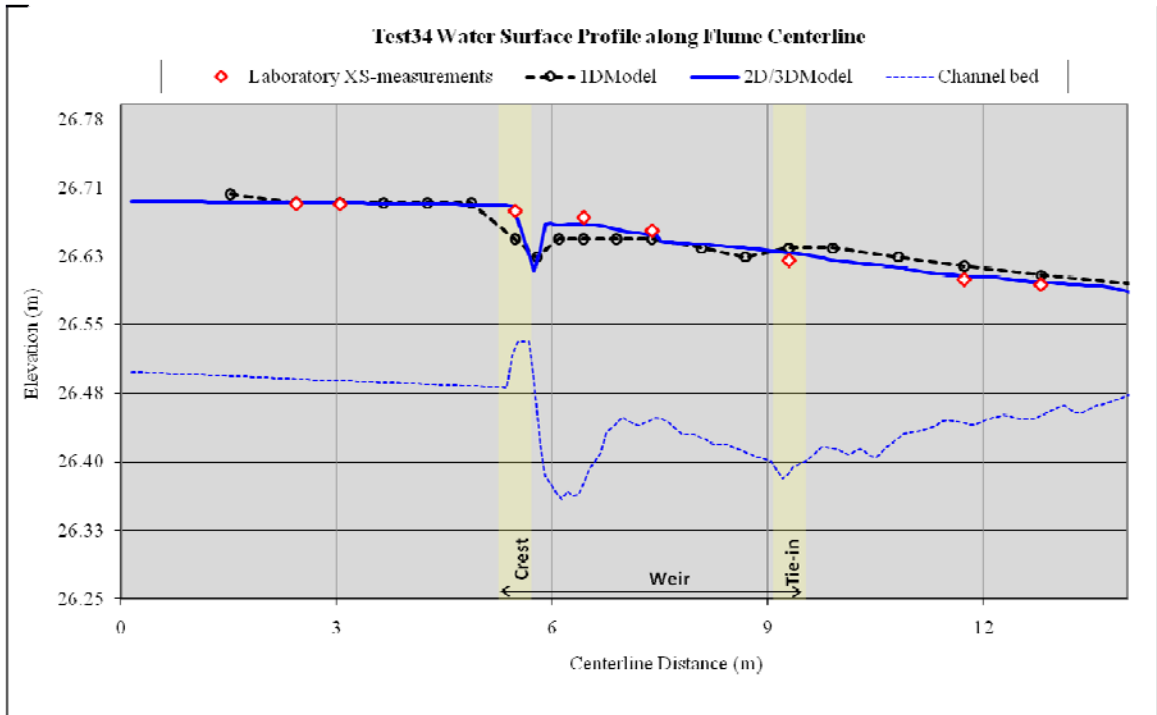


Figure 3.26 – Laboratory and numerical model water surface elevation comparison test 34.

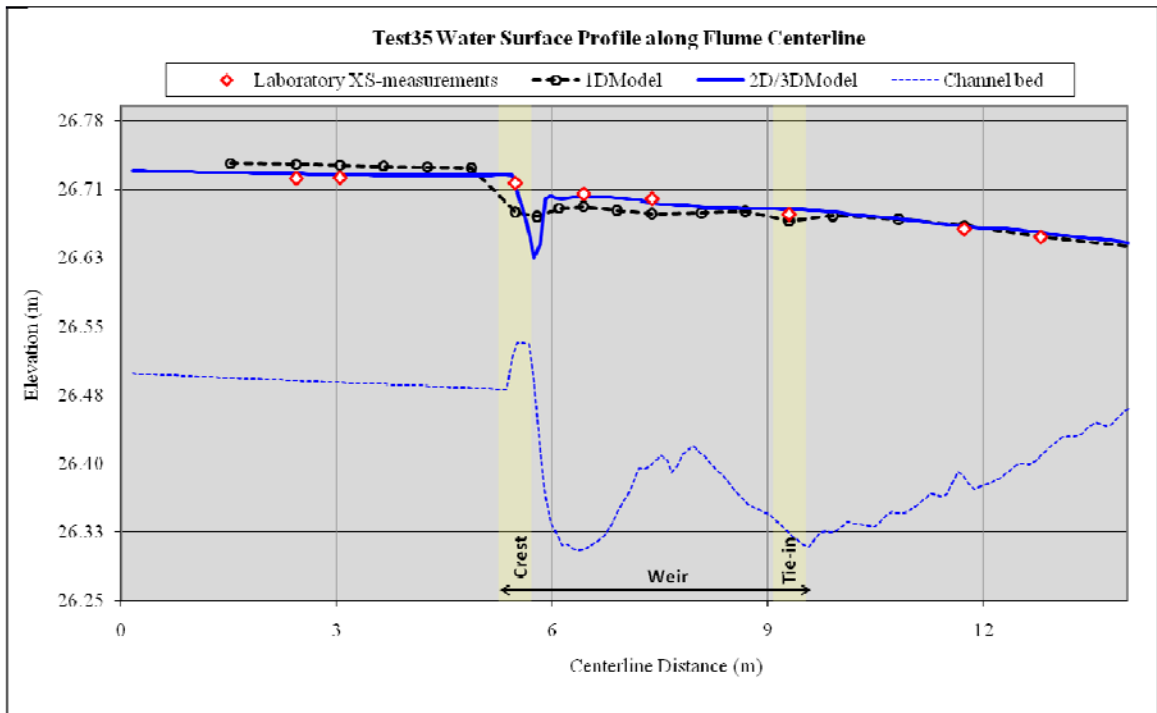


Figure 3.27 – Laboratory and numerical model water surface elevation comparison test 35.

While the percent error in the predicted water surface elevations from the 2D/3D model is less than 5% (0.011m), the 1D model shows a 15% error (0.031m) near the structure crest (Figure 3.28). The large error in the 1D model is due to the rapidly varied flow condition that exists along the crest of the structure. The 1D model is not able to properly simulate such conditions.

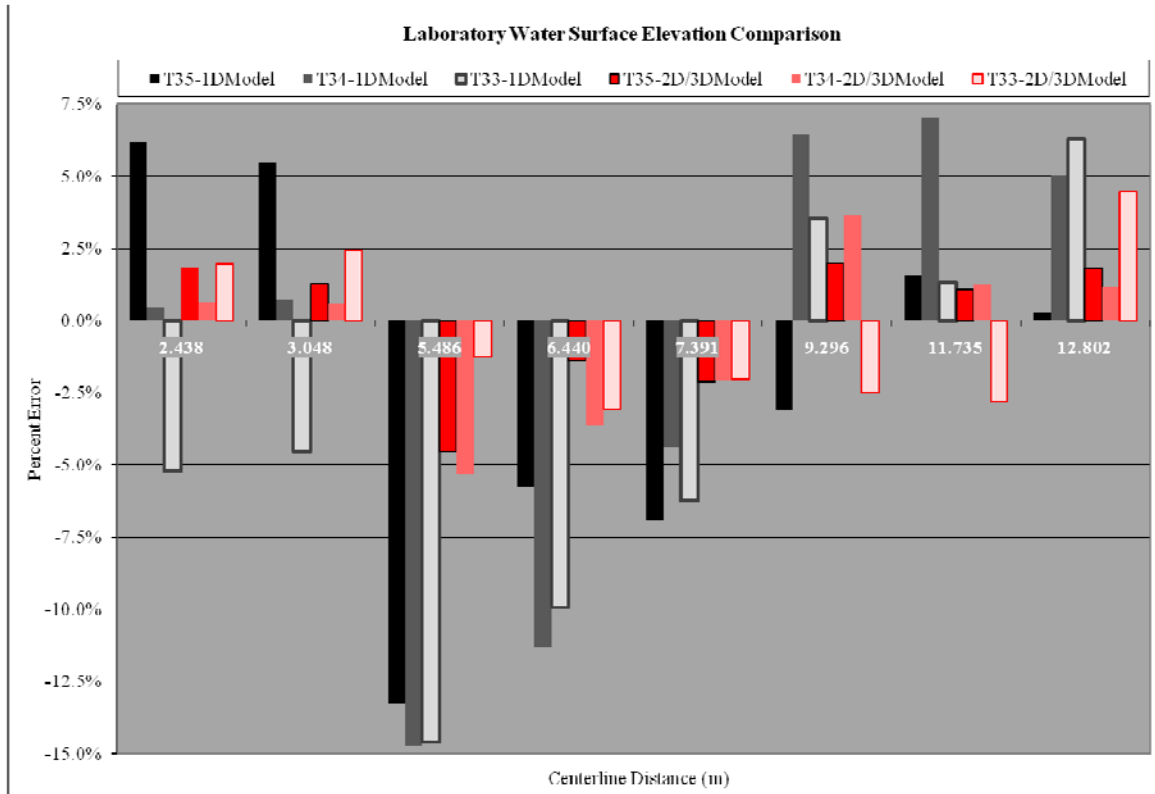


Figure 3.28 – Laboratory and numerical model water surface elevation comparison, percent error along channel centerline for tests 33-35.

Figure 3.29 shows the observed (true) water surface elevation measurements plotted against predicted ones from the numerical model for the same locations. The linear correlation coefficients of 0.84 for the 1D model and 0.98 for the 2D/3D model show good overall agreement (with no regard to the spatial component in the data) between predicted and measured values for all models. The residuals of the 2D/3D water surface elevation predictions have a slight positive bias with a mean= 0.003m (n = 102).

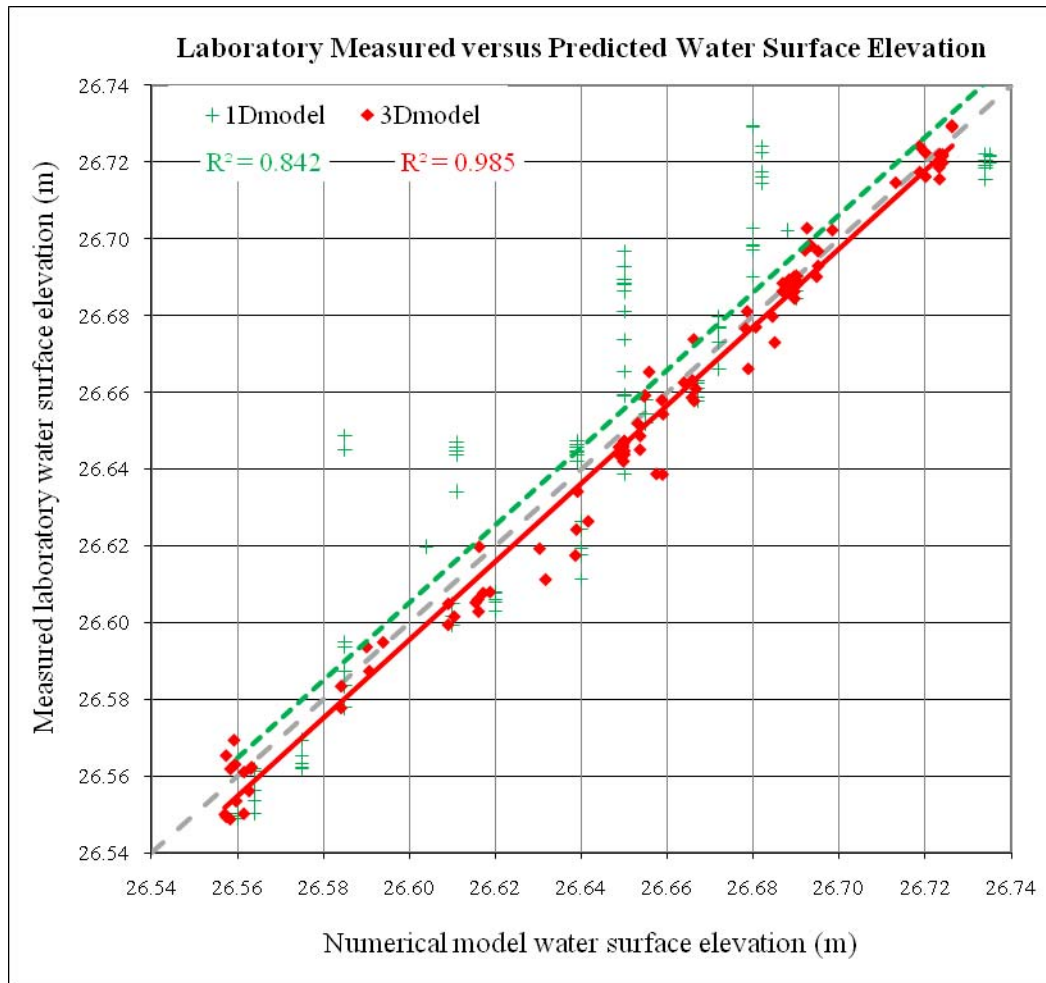


Figure 3.29 – Laboratory measured versus predicted water surface elevations for tests 33-35.

However, when the spatial component of the data is considered (Figure 3.30), it is evident that the 2D/3D model provides a better prediction of the water surface elevations near the structure. Figure 3.30 shows that the predicted water surface elevations from the 2D/3D model were within 10% for all three tests (n=102 observations) with measured depths ranging from 0.061 meters to 0.427 meters. The 1D model was able to replicate field measurements within 23% with the exception of a 40% error in the middle of the structure where multiple water surface elevations were present along the transect due to the structure arm. The greatest differences occurred from the throat of the structure to a distance approximately equal to the half the length of the structure’s longitudinal extent.

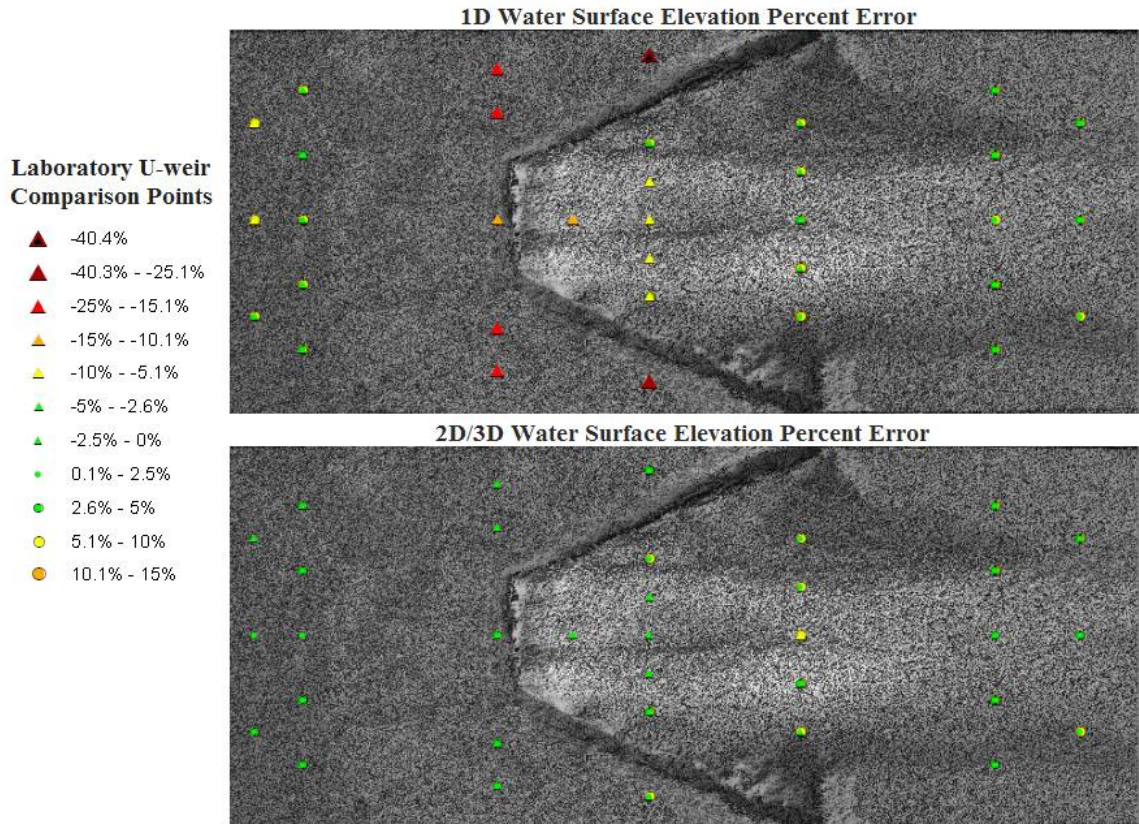


Figure 3.30 – Numerical model water surface elevation percent error comparison for laboratory tests 33-35.

In addition to matching water surface elevation within 10%, the 3D model results show that the numerical model is able to simulate conditions measured in the laboratory by quantifying high shear zones near scour areas and low shear zones near depositional areas as well as the surface velocity and redirection of stream lines over the arms of the weir (Figure 3.31).

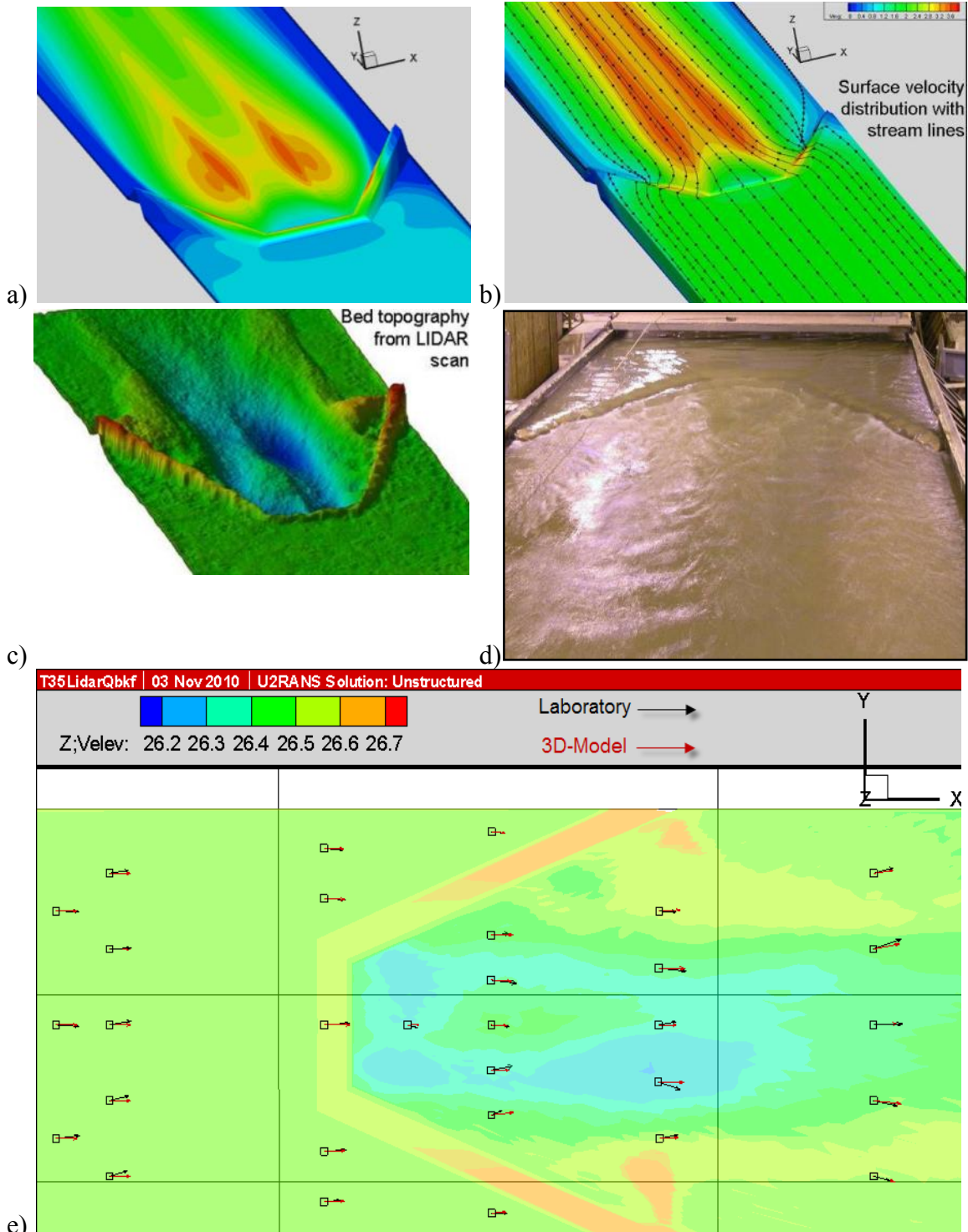


Figure 3.31 – a) Numerical model bed shear stress distribution at Q_{bkf} b) Numerical model surface velocity and stream lines at Q_{bkf} c) Laboratory final bed LIDAR survey d) Laboratory test at Q_{bkf} e) Measured Laboratory vs. 3D model velocity vectors.

Comparisons between numerical model results and measured laboratory velocities (Figure 3.32, Figure 3.33, and Figure 3.34) show that the numerical models differ in their ability to replicate laboratory measurements throughout the reach. The high variability in the 1D velocity predictions is a result of the flow convergence and plunging flow that occurs along the structure crest causing the flow downstream of the structure to have a strong vertical velocity component which provides energy dissipation. The variation in the 1D model velocities is also attributed to the resulting cross section averaged velocity that is calculated rather than point velocities which are calculated with the higher order models (2D and 3D).

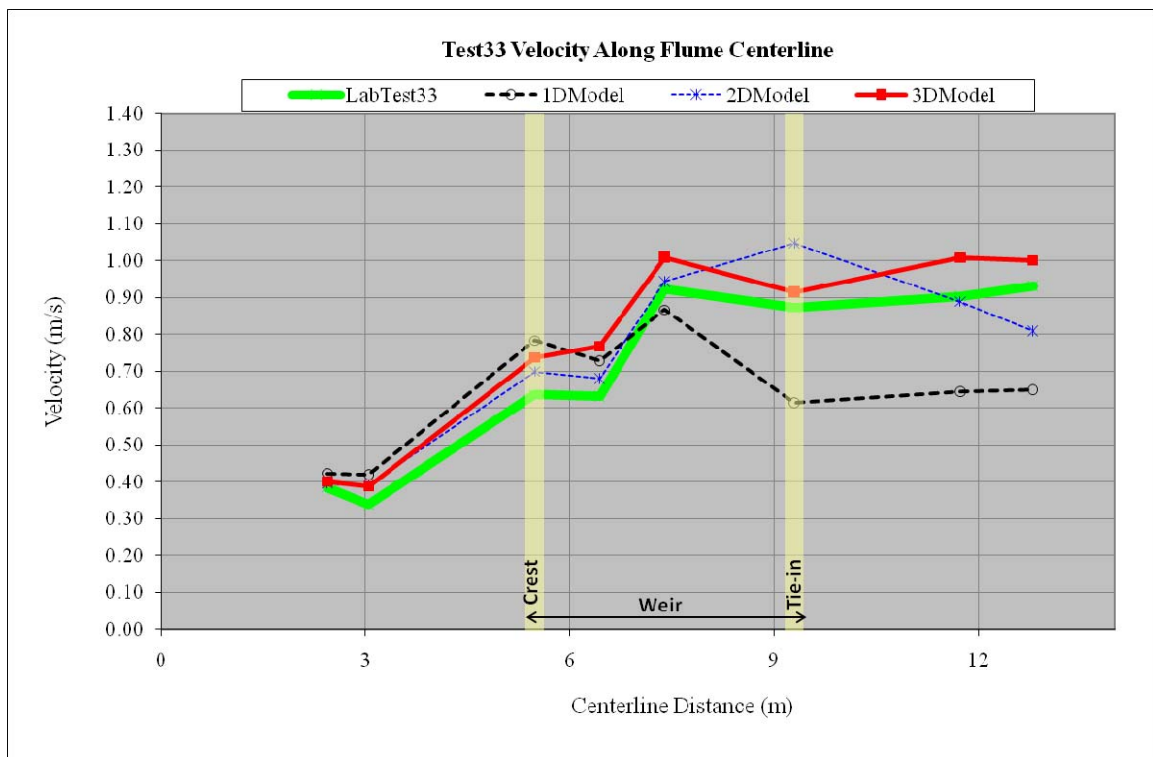


Figure 3.32 – Laboratory and numerical model velocity comparison along channel centerline test 33.

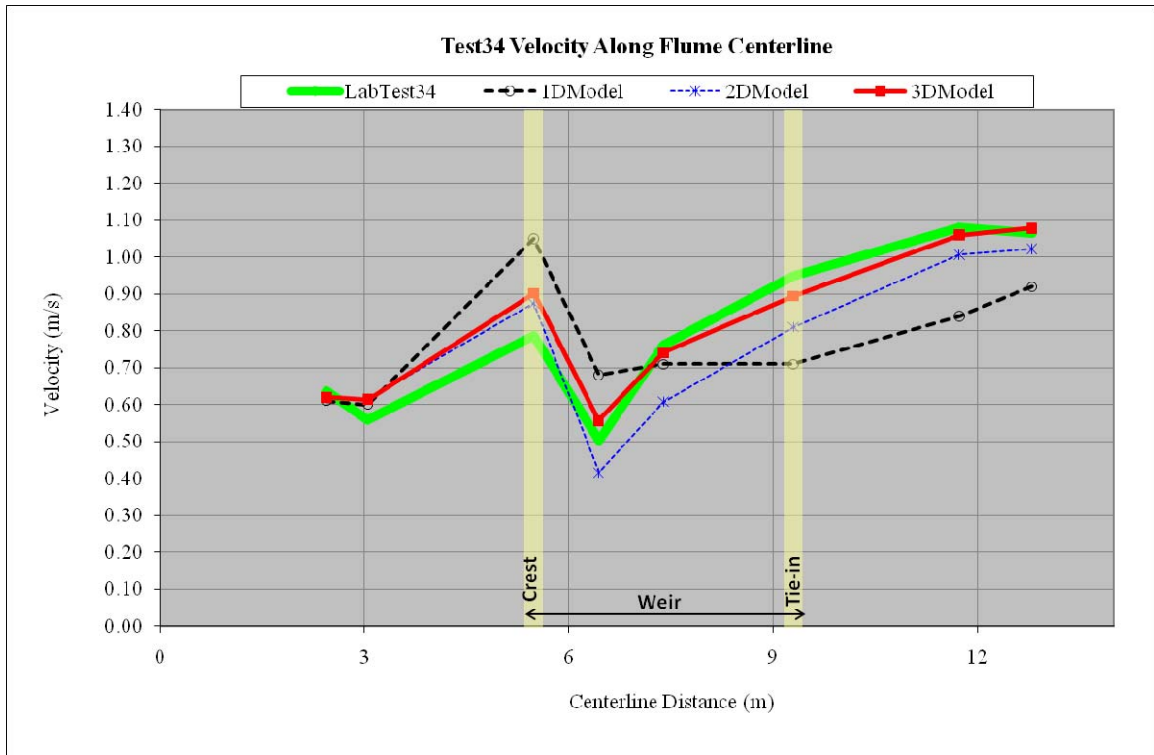


Figure 3.33 – Laboratory and numerical model velocity comparison along channel centerline test 34.

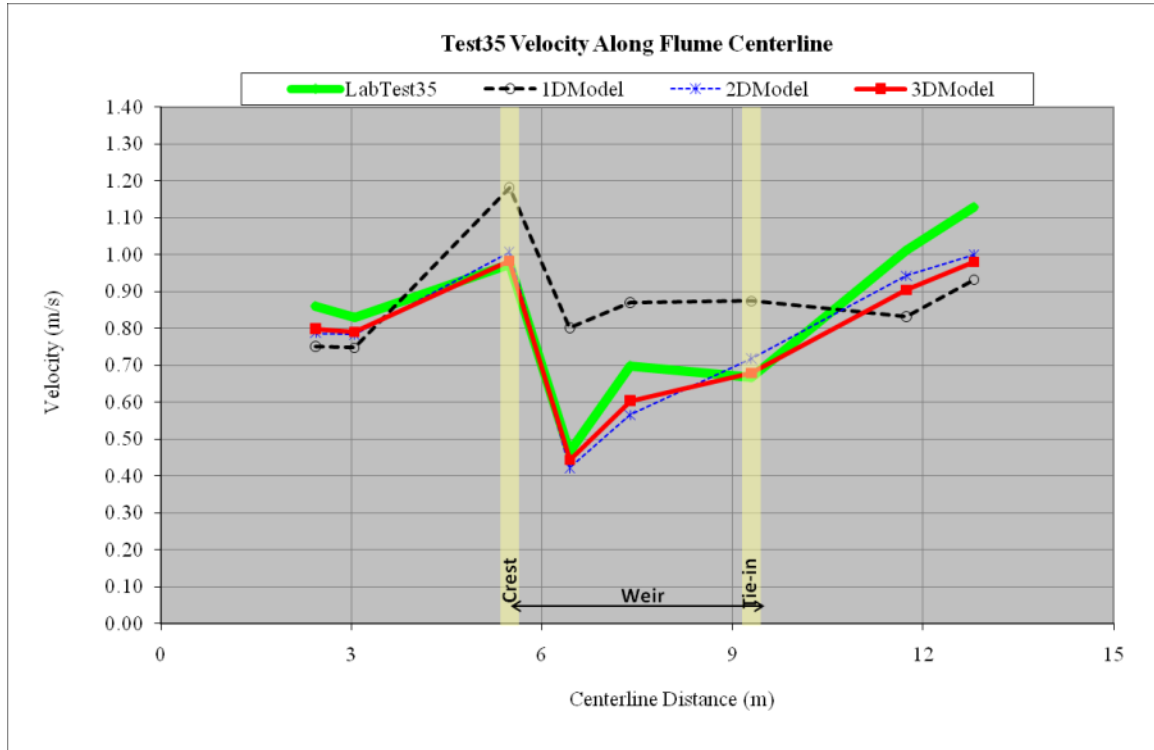


Figure 3.34 – Laboratory and numerical model velocity comparison along channel centerline test 35.

From Figure 3.35 it is evident that the 3D model provides a much better prediction of the velocities downstream from the crest of the structure compared with the 1D and 2D models. While the maximum error in the predicted channel centerline velocity from the 2D and 3D model is 0.133 m/s (19%) and 0.094 m/s (13%) respectively, the 1D model has a much greater error at 0.336 m/s (72%). The 1D model is not able to properly simulate the flow convergence and vertical component of the velocity vectors that occur downstream of the structure crest. Since the 1D model provides an average cross sectional velocity, predicting changes in flow patterns around the structure both longitudinally and laterally is not feasible.

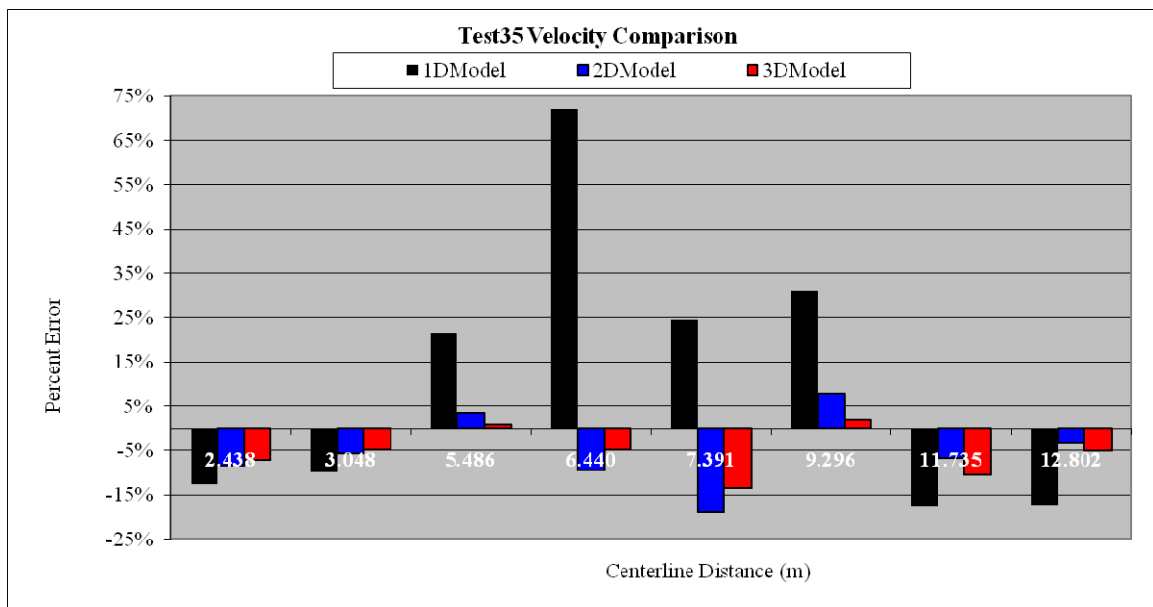


Figure 3.35 – Laboratory and numerical model velocity comparison, percent error along centerline for test 35.

Figure 3.36 shows the laboratory (true) velocity measurements plotted against predicted velocities from the numerical models for the same locations. It appears that both the 2D and 3D models provide relatively good overall agreement (with no regard to the spatial component in the data) between predicted and measured values. The residuals of the 3D velocity predictions have a slight negative bias with a mean= -0.012m/s (n =

102). The differences likely result from the three-dimensional hydraulic effects of the plunging flow over the structure crest and arms and the high turbulence encountered downstream of the structure crest.

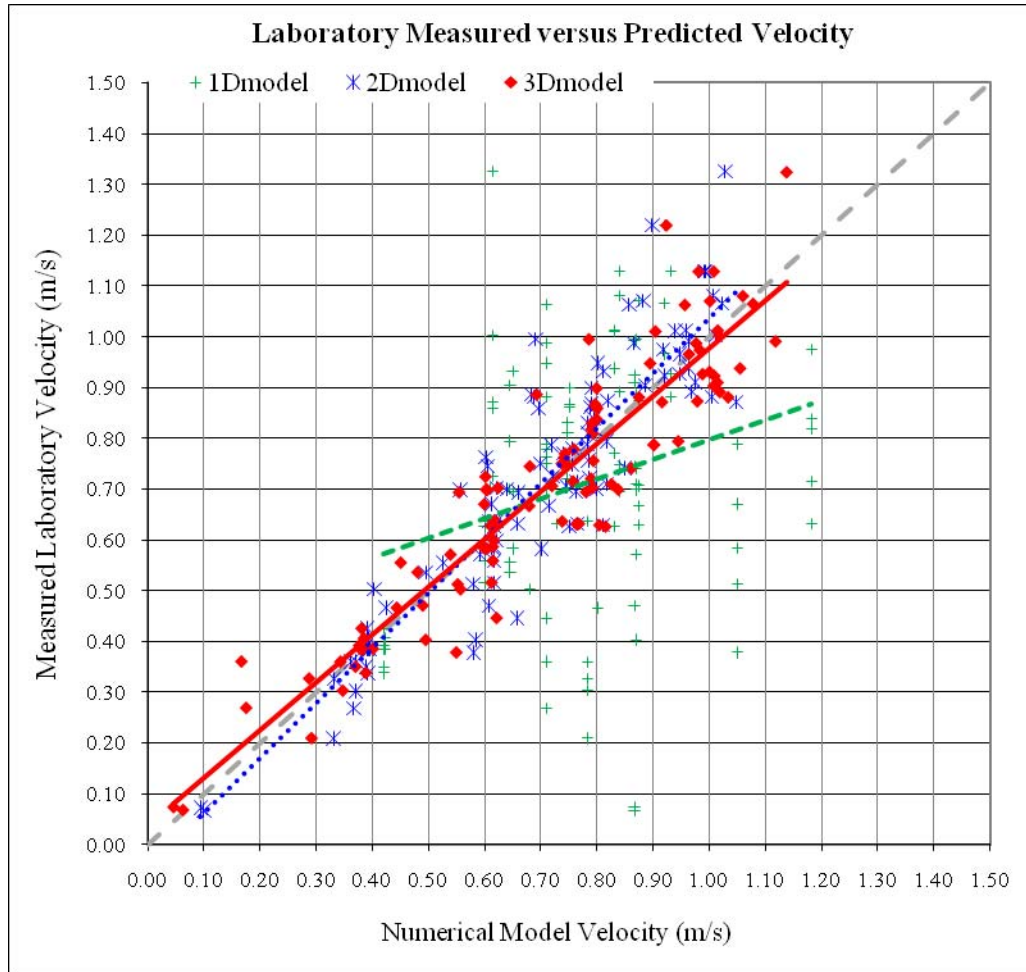


Figure 3.36 – Laboratory measured vs. predicted velocity for laboratory tests 33-35.

When the spatial component of the data is considered (Figure 3.37), it is evident that the 3D model provides a much better prediction of the velocities near the crest of the structure. While the maximum error in the predicted velocity from the 2D and 3D models is around 53% (0.19 m/s) and 39% (0.13 m/s) respectively, the 1D model has a much greater error at 177% (0.57 m/s). As mentioned in section 3.2.1, a 1D cross section model for rock weirs can meet either water surface requirements or velocity requirements, but

not both. The 1D model is not able to properly simulate the vertical velocity vectors and associated energy dissipation that occur downstream of the structure crest. Additionally, the 1D model computes an average cross section velocity and therefore cannot account for the lateral variations in velocity caused by the redirection of flow over the weir crest.

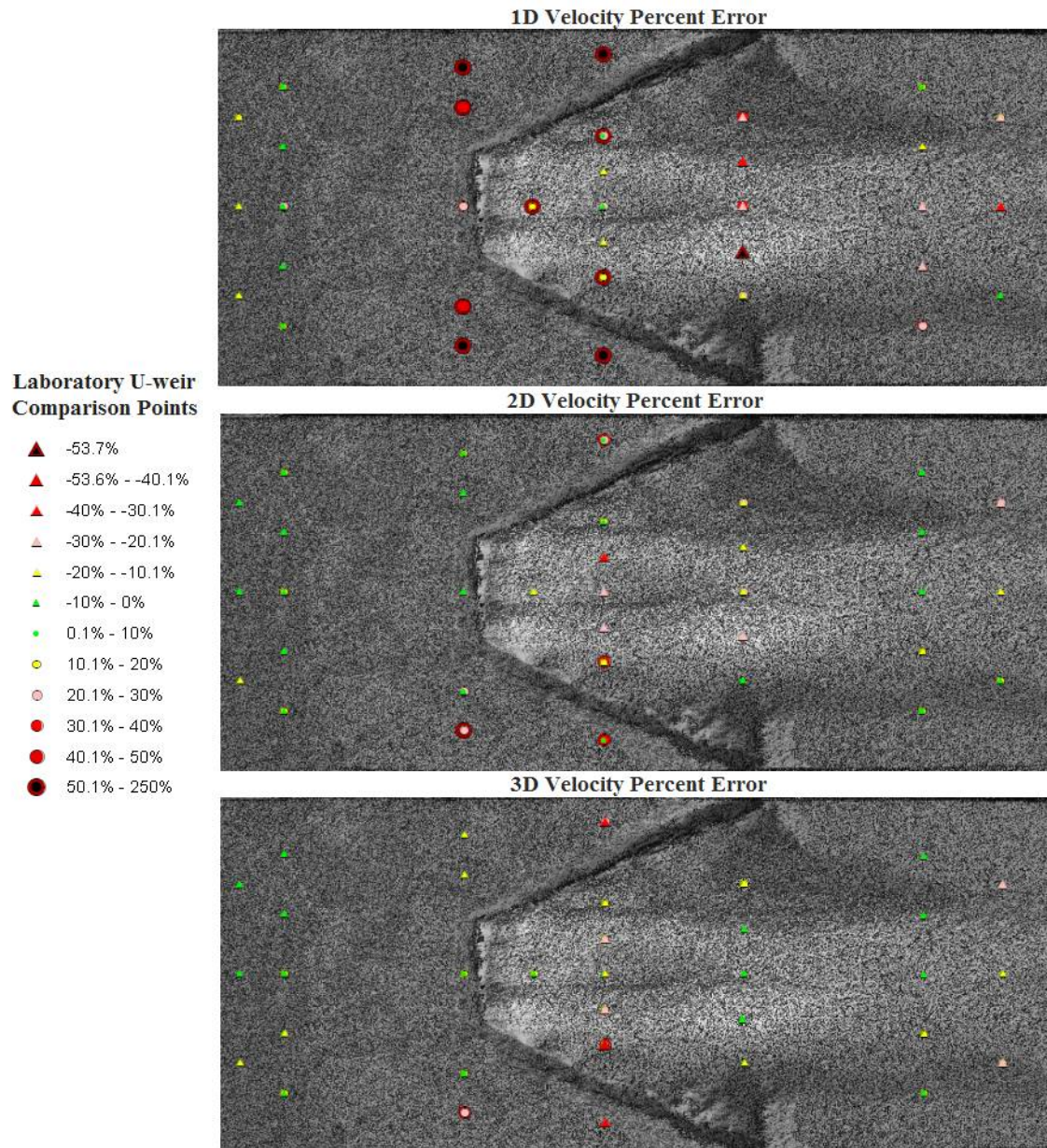
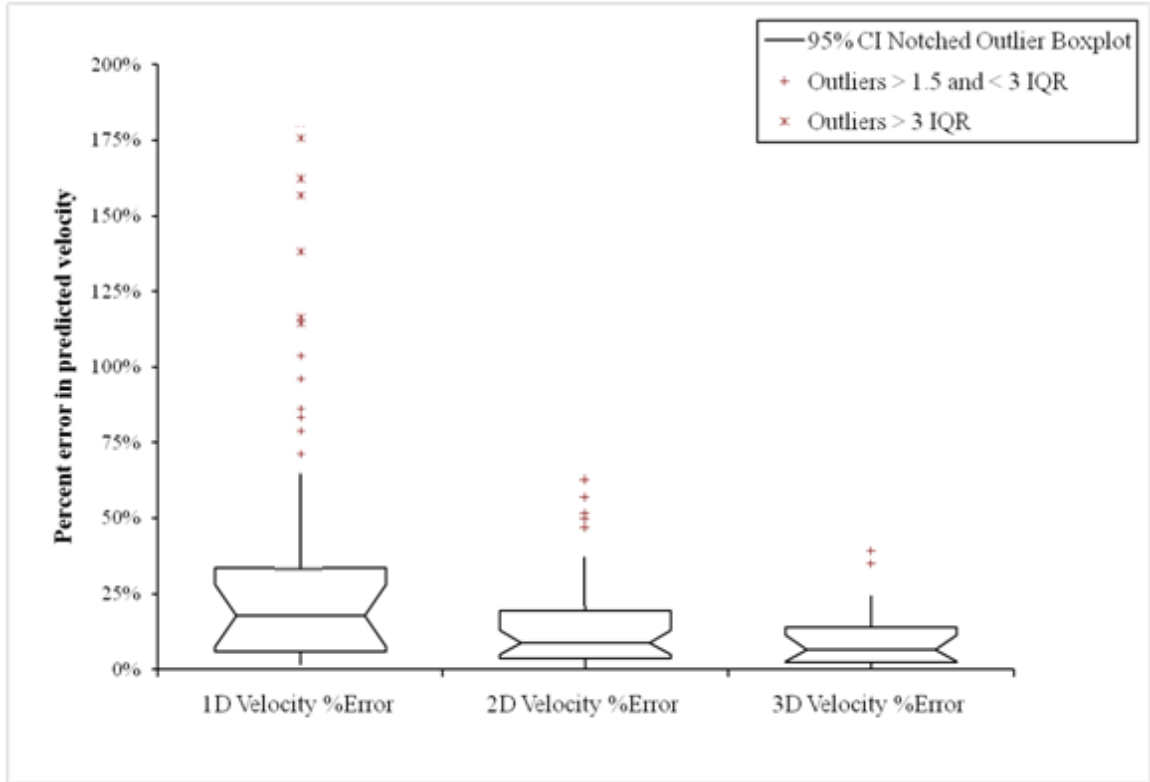


Figure 3.37 – Laboratory and numerical model velocity percent error comparison.

Box and whisker plots showing the magnitude of 1D, 2D, and 3D model percent error in velocity are presented in Figure 3.38 below. It is evident from the comparison that of the three numerical models, the 3D model provides a better overall prediction of the velocities throughout the study reach with 95% confidence interval of 3%-11% compared to 13%-28% for the 1D model.



	n	Min	1st Quartile	Median	95% Confidence Interval	3rd Quartile	Max	IQR
1D Velocity %Error	102	0.07%	5.82%	17.88%	13.40% to 28.10%	33.43%	177.84%	27.61%
2D Velocity %Error	102	0.52%	3.65%	8.69%	5.75% to 13.85%	19.41%	53.46%	15.76%
3D Velocity %Error	102	0.16%	2.30%	6.64%	2.68% to 11.29%	13.91%	39.20%	11.61%

Figure 3.38 – Laboratory U-weir velocity comparison, percent error magnitude box-plot for 1D, 2D, and 3D models.

The results from the field and laboratory comparison described above provides validation that by utilizing a computational mesh that defines the critical features associated with river spanning rock weirs (drop height, throat width, arm angle, arm slope, and bed topography), the 3D numerical model is capable of representing the

complex flow patterns associated with U-weirs. Therefore, the following section describes the design process used in conducting the 3D numerical model simulations to investigate how local flow patterns are affected by variations in structure geometry associated with U-weirs.

4 METHODS: TESTING MATRIX DESIGN AND SETUP OF NUMERICAL MODEL SIMULATIONS

The amount of field data required to evaluate the effects different rock weir geometries (e.g. throat width, arm angle, arm slope, and drop height) have on local flow conditions and overall structure performance is substantial. Collecting the quantity of data required to evaluate a large range of design parameters using field reconnaissance or laboratory testing alone is cost prohibitive and could take decades. However, using data collected in the field and from laboratory studies in conjunction with numerical model simulations provides a scientific basis for predicting structure performance under various river conditions and for developing the most-effective design criteria.

Field reconnaissance provides long term performance data under actual conditions, including the effect of river processes on the structure and the effect of the structure on river processes. Physical laboratory modeling provides information under carefully controlled conditions that isolate one or more variables to test the impact of specific changes on structure performance. Numerical modeling provides a cost effective method for evaluation of a range of structure geometries and channel conditions to develop a more complete understanding of structure performance and to optimize structure design.

The approach of this research was to apply a verified and validated three-dimensional numerical model, U²RANS, to investigate how local flow patterns are affected by variations in structure geometry associated with a U-weir. To understand how

this type of structure affects local flow conditions, an analysis of a wide range of structure geometries was conducted. The following section describes the numerical model testing matrix design.

4.1 DESIGN OF TESTING MATRIX

To understand the effects variations in structure geometry have on local flow patterns through U-weirs, the following variables were included in the testing matrix and are described in more detail in the sections below:

- Bed material
- Discharge
- Channel geometry (slope, width, and depth)
- Structure throat width
- Structure drop height
- Structure arm length (incorporates arm angle and slope)

The scope of this research was focused on the effects of variations in structure geometry on local flow patterns and not on the effects of variations in channel characteristics. Therefore, regime equations (described in Section 4.1.2) were used as a method for determining a characteristic shape for bankfull channel geometry used in the testing matrix. All model simulations were conducted at bankfull discharge or less, no overbank flows were simulated. The following elements were considered but not included in the design of the testing matrix:

- Meandering channel: Radius of curvature was not part of the study scope and therefore only straight prismatic channels were investigated.

- Non-linear weirs: Asymmetric geometries were not investigated because they were beyond the scope of this research.
- Pre-excavated scour holes: pre-excavated scour holes were not investigated due to the lack of design criteria and use of a fixed bed numerical model and therefore were beyond the scope of this research.

4.1.1 BED MATERIAL

Grain sizes were selected to match field conditions in which river spanning rock weirs are most commonly used (e.g. gravel bed rivers). The three d_{50} grain diameters were selected using the geometric mean of the American Geophysical Union (AGU) classification system (Lane, 1947), a log base 2 scale. The distributions for the d_{84} and d_{16} were set to plus and minus one phi class as listed below:

- Coarse Gravel: $d_{50} = 22.63$ mm, $d_{84} = 45.25$ mm, $d_{16} = 11.31$ mm
- Small Cobble: $d_{50} = 90.51$ mm, $d_{84} = 181.0$ mm, $d_{16} = 45.25$ mm
- Large Cobble: $d_{50} = 181$ mm, $d_{84} = 256$ mm, $d_{16} = 90.51$ mm

4.1.2 BANKFULL CHANNEL GEOMETRY

Previous research has shown that it is possible to define a “bankfull channel geometry” (Leopold and Maddock, 1953; Leopold et al., 1964) in terms of a bankfull width, bankfull depth and down-channel bed slope. More recently, Parker et al. (2007) used a baseline data set consisting of four differing stream reaches from Canada, the USA, and Britain to determine bankfull hydraulic relations for alluvial, single-thread gravel bed streams with definable channels and floodplains (Equations 4.1, 4.2, and 4.3). Their results show a considerable degree of universality and the exponents of Q_{bf} in the equations below are similar to those found by other authors (e.g., Millar, 2005).

$$S \cong 0.101 \cdot \left(\frac{Q_{bkf}}{\sqrt{gd_{50}d_{50}^2}} \right)^{-0.344} \quad \text{Equation 4.1}$$

$$W_{bkf} \cong \frac{4.63}{g^{1/5}} Q_{bkf}^{0.4} \left(\frac{Q_{bkf}}{\sqrt{gd_{50}d_{50}^2}} \right)^{0.0667} \quad \text{Equation 4.2}$$

$$H_{bkf} \cong \frac{0.382}{g^{1/5}} Q_{bkf}^{2/5} \quad \text{Equation 4.3}$$

Where:

S = bed slope;

Q_{bkf} = bankfull discharge (m^3/s);

d_{50} = median particle diameter, (m);

W_{bkf} = bankfull width (m); and

H_{bkf} = bankfull depth (m).

Additionally, Parker et al. (2007) applied the regression relations to three other data sets, one from Maryland, one from Colorado, and one from Britain, confirming this tendency toward universality. The degree of universality and ease of use of the hydraulic geometry equations presented by Parker et al. (2007) were the reasons that they were selected for determining the bankfull hydraulic geometry used in this study. Given the bed material grain sizes listed above and a range of representative bankfull discharges that match field conditions in which river spanning rock weirs are most commonly used, Equations 4.1, 4.2, and 4.3 above were used to compute central width, depth, and channel slope tendency in the design matrix. To analyze each structure configuration and the effects on the local flow patterns, the discharge for each structure configuration was varied to include 1/10, 1/5, 1/3, 2/3, and bankfull discharges.

4.1.3 STRUCTURE GEOMETRY

Structure geometry consists of three major components (Figure 4.1); throat width (W_t), drop height (Z_d), and structure arm length (L_a) which is a function of the departure angle (θ) from the bank and slope of the arm (ϕ). The following sections describe how each of these components was altered in the numerical model testing matrix.

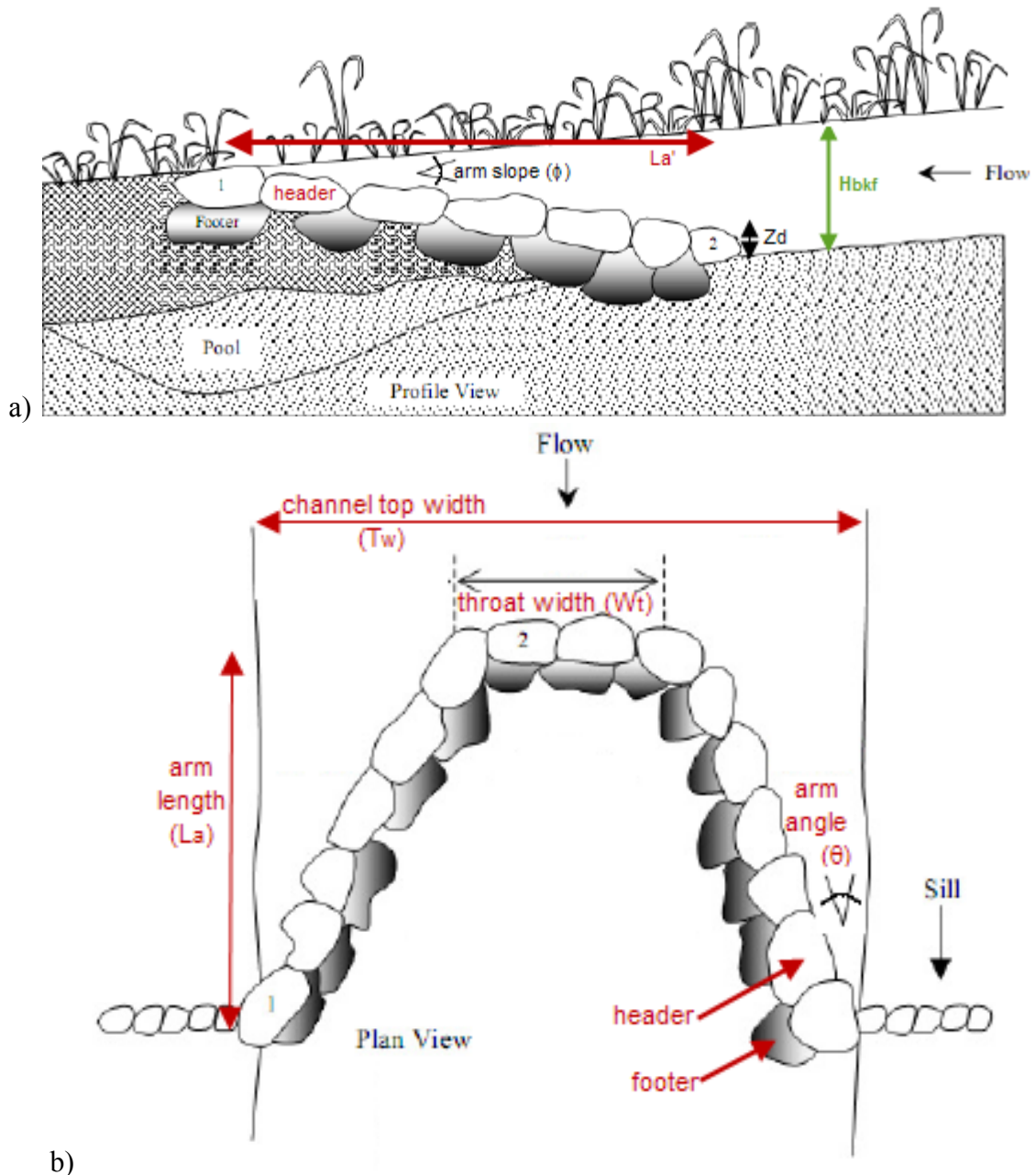


Figure 4.1 – U-weir structure parameters a) profile view and b) plan view (adapted from Rosgen, 2006)

4.1.3.1 THROAT WIDTH

Initial structure throat width was set to 1/3 the bankfull width as specified by Rosgen (2006). To study how flow patterns are affected by changes in structure throat width, the throat width was varied over 1/4, 1/3, and 1/2 the bankfull top width for each of the three grain sizes and corresponding channel geometry. Table 4.1 provides a summary of structure throat width associated with each of the three channel geometries.

Table 4.1 – Summary of numerical modeling testing matrix throat widths.

Q (cms)	D50 (mm)	S_o	H_{bkf} (m)	T_w (m)	W_t/T_w	W_t (m)
162	22.63	0.001	1.850	54.919	0.25	13.730
162	22.63	0.001	1.850	54.919	0.33	18.306
162	22.63	0.001	1.850	54.919	0.50	27.459
92	90.51	0.004	1.475	33.470	0.25	8.368
92	90.51	0.004	1.475	33.470	0.33	11.157
92	90.51	0.004	1.475	33.470	0.50	16.735
36	181	0.01	1.015	19.242	0.25	4.811
36	181	0.01	1.015	19.242	0.33	6.414
36	181	0.01	1.015	19.242	0.50	9.621

4.1.3.2 DROP HEIGHT

Structure drop height (Z_d) was defined as the elevation difference between the bed elevation and the structure crest. Depending on the purpose of the structure, drop height can vary from a zero drop if the structure crest is level with the channel bed to a predetermined height based on fish passage criteria and/or irrigation requirements. Given the increased need to meet fish passage criteria associated with diversion type structures such as rock weirs, initial drop height was set to 0.8 feet (0.24 meters) as prescribed by

WDFW (2003) for the maximum drop height allowed for fish passage. Since the focus of this research was related to overall structure performance and not specifically fish passage, additional fish passage criteria were not considered and are outside the scope of this study. To evaluate how the drop height over the structure affected flow patterns, the structure drop height was varied by 1/2 and 1.5 times the initial value of 0.8 feet (0.24 meters). This resulted in a range of drops heights of 0.4, 0.8, and 1.2 feet (0.12, 0.24, and 0.36 meters).

4.1.3.3 ARM LENGTH

Weir arm length (L_A) was defined as the length of the weir along the channel bank. For a given weir arm length, the resulting structure arm angle (θ) and arm slope (ϕ) are a function of channel width (T_w), bank height (H_{bkf}), drop height (Z_d), and throat width (W_t) as presented in Equations 4.4 and 4.5. The arm angle (θ) is defined as the angle between the channel bank and weir arm. The profile angle (ϕ) is defined as the angle between the horizontal plane and the weir arm that slopes downward from the tie-in elevation to the weir crest at the throat of the structure as shown in Figure 4.1.

$$\theta = \text{Tan}^{-1} \left(\frac{\frac{T_w - W_t}{2}}{L_a} \right) \quad \text{Equation 4.4}$$

$$\phi = \text{Tan}^{-1} \left(\frac{H_{bkf} - Z_d - L_a S_o}{\sqrt{\left(\frac{T_w - W_t}{2}\right)^2 + L_a^2}} \right) \quad \text{Equation 4.5}$$

Where:

T_w = channel top width;

W_t = structure throat width;

L_a = structure arm length;

H_{bkf} = channel bank height;

Z_d = structure drop height; and

S_o = channel bed slope.

Initial structure arm lengths were designed such that the arm angle and arm slope for a given channel geometry, structure drop height, and throat width approached as close as possible the midpoint of the design ranges specified in Rosgen (2006). Recommended arm angles were between 20 and 30 degrees and arm slopes between 2 and 7 percent. Target angles were 25 degrees for arm angles and 4.5 percent for arm slopes. The solver function in Microsoft Excel® was then used to calculate the weir arm length that minimized the relative distances on the planform and profile angles of the weir arms. This minimized solution was then used to calculate the arm length ranges that would be used in the numerical modeling in two ways; multiplying the minimized values by ½ and 2. This provided a wide range of arm angles (10.31 to 48.35 degrees) and corresponding arm slopes (1.47 to 10.11 percent) that were tested (Figure 4.2).

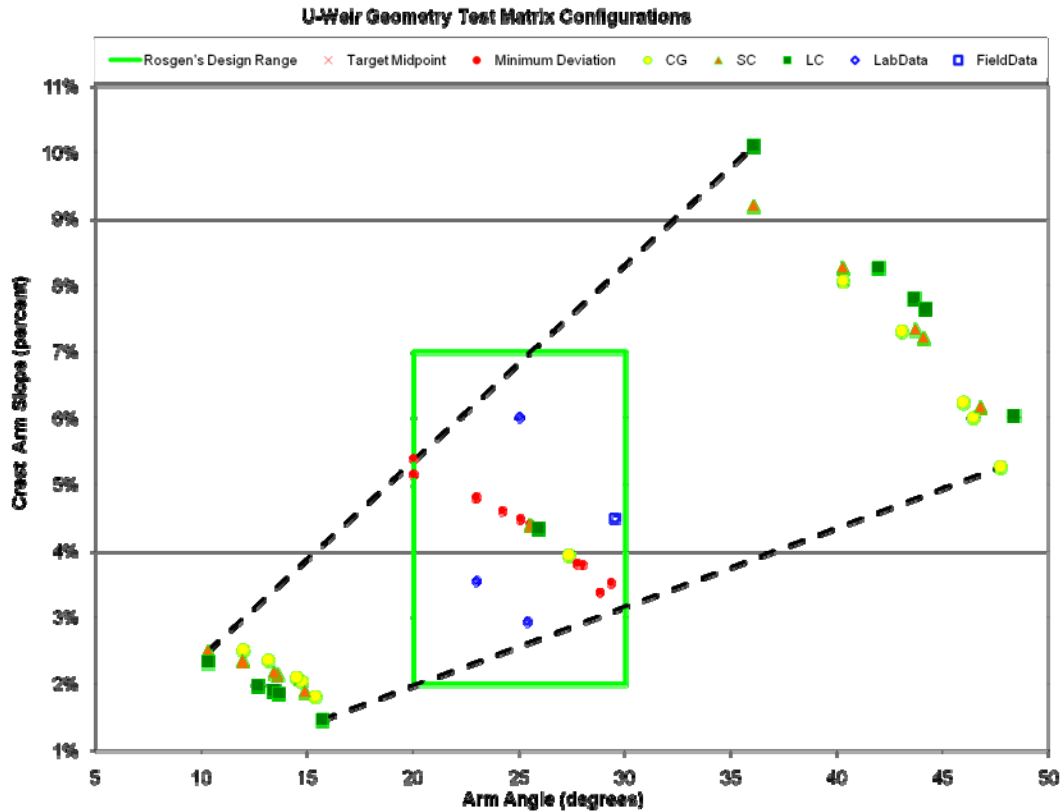


Figure 4.2 – Plot of variation in structure parameters for three grain sizes (CG-coarse gravel, SC-small cobble, LC-large cobble) used in design matrix.

Structure arm angle and arm slope for both the U-weir tested in the laboratory and the U-weir measured in the field are also shown in Figure 4.2 and fall within the range of values included in the testing matrix design.

Using the methods described above to define the channel geometry for the three selected grain sizes and variations in structure geometry (drop height, throat width, and arm length), a total of 33 unique weir configurations were generated and numerically modeled at five different flow rates ($1/10Q_{bkf}$, $1/5Q_{bkf}$, $1/3Q_{bkf}$, $2/3Q_{bkf}$, and Q_{bkf}) for a total of 165 simulations. Table 4.2 provides an example of testing matrix configurations used in the numerical modeling. A complete list of the testing matrix configurations used in the numerical modeling is presented in Appendix A.

Table 4.2 – Example of testing matrix configurations.

Config ID	Ref Description (d ₅₀ -Q _r -DropHt-ThoatW-ArmLength)	Q (m ³ /s)	Grain Size (m)	Top Width (m)	Slope	Bank height (m)	Drop Height (m)	Throat Width (m)	Arm Length (m)	Arm Angle	Arm Slope	Arm Slope (%)
1.01_1	22.63mm-Qb_0.8ft-.3W-1ArmL	162	0.023	54.92	0.001	1.85	0.24	18.31	35.40	27.34	2.26	3.94%
1.01_2	22.63mm-2/3Qb_0.8ft-.3W-1ArmL	108	0.023	54.92	0.001	1.85	0.24	18.31	35.40	27.34	2.26	3.94%
1.01_3	22.63mm-1/3Qb_0.8ft-.3W-1ArmL	54	0.023	54.92	0.001	1.85	0.24	18.31	35.40	27.34	2.26	3.94%
1.01_4	22.63mm-1/5Qb_0.8ft-.3W-1ArmL	32	0.023	54.92	0.001	1.85	0.24	18.31	35.40	27.34	2.26	3.94%
1.01_5	22.63mm-1/10Qb_0.8ft-.3W-1ArmL	16	0.023	54.92	0.001	1.85	0.24	18.31	35.40	27.34	2.26	3.94%
1.10_46	22.63mm-Qb_0.8ft-.3W-0.5ArmL	162	0.023	54.92	0.001	1.85	0.24	18.31	17.70	45.96	3.57	6.24%
1.10_47	22.63mm-2/3Qb_0.8ft-.3W-0.5ArmL	108	0.023	54.92	0.001	1.85	0.24	18.31	17.70	45.96	3.57	6.24%
1.10_48	22.63mm-1/3Qb_0.8ft-.3W-0.5ArmL	54	0.023	54.92	0.001	1.85	0.24	18.31	17.70	45.96	3.57	6.24%
1.10_49	22.63mm-1/5Qb_0.8ft-.3W-0.5ArmL	32	0.023	54.92	0.001	1.85	0.24	18.31	17.70	45.96	3.57	6.24%
1.10_50	22.63mm-1/10Qb_0.8ft-.3W-0.5ArmL	16	0.023	54.92	0.001	1.85	0.24	18.31	17.70	45.96	3.57	6.24%
1.11_51	22.63mm-Qb_0.8ft-.3W-2ArmL	162	0.023	54.92	0.001	1.85	0.24	18.31	70.81	14.50	1.20	2.10%
1.11_52	22.63mm-2/3Qb_0.8ft-.3W-2ArmL	108	0.023	54.92	0.001	1.85	0.24	18.31	70.81	14.50	1.20	2.10%
1.11_53	22.63mm-1/3Qb_0.8ft-.3W-2ArmL	54	0.023	54.92	0.001	1.85	0.24	18.31	70.81	14.50	1.20	2.10%
1.11_54	22.63mm-1/5Qb_0.8ft-.3W-2ArmL	32	0.023	54.92	0.001	1.85	0.24	18.31	70.81	14.50	1.20	2.10%
1.11_55	22.63mm-1/10Qb_0.8ft-.3W-2ArmL	16	0.023	54.92	0.001	1.85	0.24	18.31	70.81	14.50	1.20	2.10%
1.02_6	22.63mm-Qb_0.4ft-.25W-0.5ArmL	162	0.023	54.92	0.001	1.85	0.12	13.73	19.58	46.44	3.44	6.02%
1.02_7	22.63mm-2/3Qb_0.4ft-.25W-0.5ArmL	108	0.023	54.92	0.001	1.85	0.12	13.73	19.58	46.44	3.44	6.02%
1.02_8	22.63mm-1/3Qb_0.4ft-.25W-0.5ArmL	54	0.023	54.92	0.001	1.85	0.12	13.73	19.58	46.44	3.44	6.02%
1.02_9	22.63mm-1/5Qb_0.4ft-.25W-0.5ArmL	32	0.023	54.92	0.001	1.85	0.12	13.73	19.58	46.44	3.44	6.02%
1.02_10	22.63mm-1/10Qb_0.4ft-.25W-0.5ArmL	16	0.023	54.92	0.001	1.85	0.12	13.73	19.58	46.44	3.44	6.02%
1.03_11	22.63mm-Qb_0.4ft-.25W-2ArmL	162	0.023	54.92	0.001	1.85	0.12	13.73	78.34	14.73	1.17	2.04%
1.03_12	22.63mm-2/3Qb_0.4ft-.25W-2ArmL	108	0.023	54.92	0.001	1.85	0.12	13.73	78.34	14.73	1.17	2.04%
1.03_13	22.63mm-1/3Qb_0.4ft-.25W-2ArmL	54	0.023	54.92	0.001	1.85	0.12	13.73	78.34	14.73	1.17	2.04%
1.03_14	22.63mm-1/5Qb_0.4ft-.25W-2ArmL	32	0.023	54.92	0.001	1.85	0.12	13.73	78.34	14.73	1.17	2.04%
1.03_15	22.63mm-1/10Qb_0.4ft-.25W-2ArmL	16	0.023	54.92	0.001	1.85	0.12	13.73	78.34	14.73	1.17	2.04%
1.04_16	22.63mm-Qb_0.4ft-.5W-0.5ArmL	162	0.023	54.92	0.001	1.85	0.12	27.46	16.19	40.29	4.61	8.07%
1.04_17	22.63mm-2/3Qb_0.4ft-.5W-0.5ArmL	108	0.023	54.92	0.001	1.85	0.12	27.46	16.19	40.29	4.61	8.07%
1.04_18	22.63mm-1/3Qb_0.4ft-.5W-0.5ArmL	54	0.023	54.92	0.001	1.85	0.12	27.46	16.19	40.29	4.61	8.07%
1.04_19	22.63mm-1/5Qb_0.4ft-.5W-0.5ArmL	32	0.023	54.92	0.001	1.85	0.12	27.46	16.19	40.29	4.61	8.07%
1.04_20	22.63mm-1/10Qb_0.4ft-.5W-0.5ArmL	16	0.023	54.92	0.001	1.85	0.12	27.46	16.19	40.29	4.61	8.07%
1.05_21	22.63mm-Qb_0.4ft-.5W-2ArmL	162	0.023	54.92	0.001	1.85	0.12	27.46	64.78	11.97	1.44	2.51%
1.05_22	22.63mm-2/3Qb_0.4ft-.5W-2ArmL	108	0.023	54.92	0.001	1.85	0.12	27.46	64.78	11.97	1.44	2.51%
1.05_23	22.63mm-1/3Qb_0.4ft-.5W-2ArmL	54	0.023	54.92	0.001	1.85	0.12	27.46	64.78	11.97	1.44	2.51%
1.05_24	22.63mm-1/5Qb_0.4ft-.5W-2ArmL	32	0.023	54.92	0.001	1.85	0.12	27.46	64.78	11.97	1.44	2.51%
1.05_25	22.63mm-1/10Qb_0.4ft-.5W-2ArmL	16	0.023	54.92	0.001	1.85	0.12	27.46	64.78	11.97	1.44	2.51%

Using the testing matrix described above, structure definition points were generated for each of the 33 weir configurations and utilized by the rock weir mesh generation program to generate the computational mesh used in the numerical modeling. The following section describes the process used in generating the structure definition points and computational mesh for this project.

4.2 MESH GENERATION PROGRAM DEVELOPMENT

4.2.1 INTRODUCTION

The development of a rock weir mesh generation program simplifies the process of numerical modeling by allowing the generation of multiple computational meshes describing individual changes in structure geometry in a quick and cost effective manner. The rock weir mesh generation process for this project consisted of two parts: (1) an Excel workbook used to provide input for generation of structure definition points based on given channel geometry and structure parameters and (2) a Visual Basic program that used the output from the excel definition points to generate the computational mesh.

4.2.2 STRUCTURE DEFINITION

To describe channel characteristics and structure geometry for a given configuration, a total of eleven lateral definition lines were located throughout the study reach to represent the critical changes in channel and structure geometry (Figure 4.3). Six lateral definition lines were used to describe the structure: upstream bed, upstream header, downstream header, upstream footer, downstream footer, and downstream bed. Five lateral definition lines were used to describe the channel: upstream boundary condition, upstream pool, downstream pool, downstream bed, and downstream boundary condition. Overbank, topbank, toe, and throat lines describe the location across the channel. Each lateral definition line consists of eight definition points. Figure 4.3 shows the conceptualized structure with definition lines and definition points.

Combinations of river left or river right, throat or toe, topbank or overbank, upstream or downstream, bed, header or footer, and pool uniquely identify each definition point. Dashed lines show the intersection of the structure with the channel

bank. Thin grey lines show breaks in direction. Each definition point can be uniquely identified through selecting one item from each column in Table 4.3.

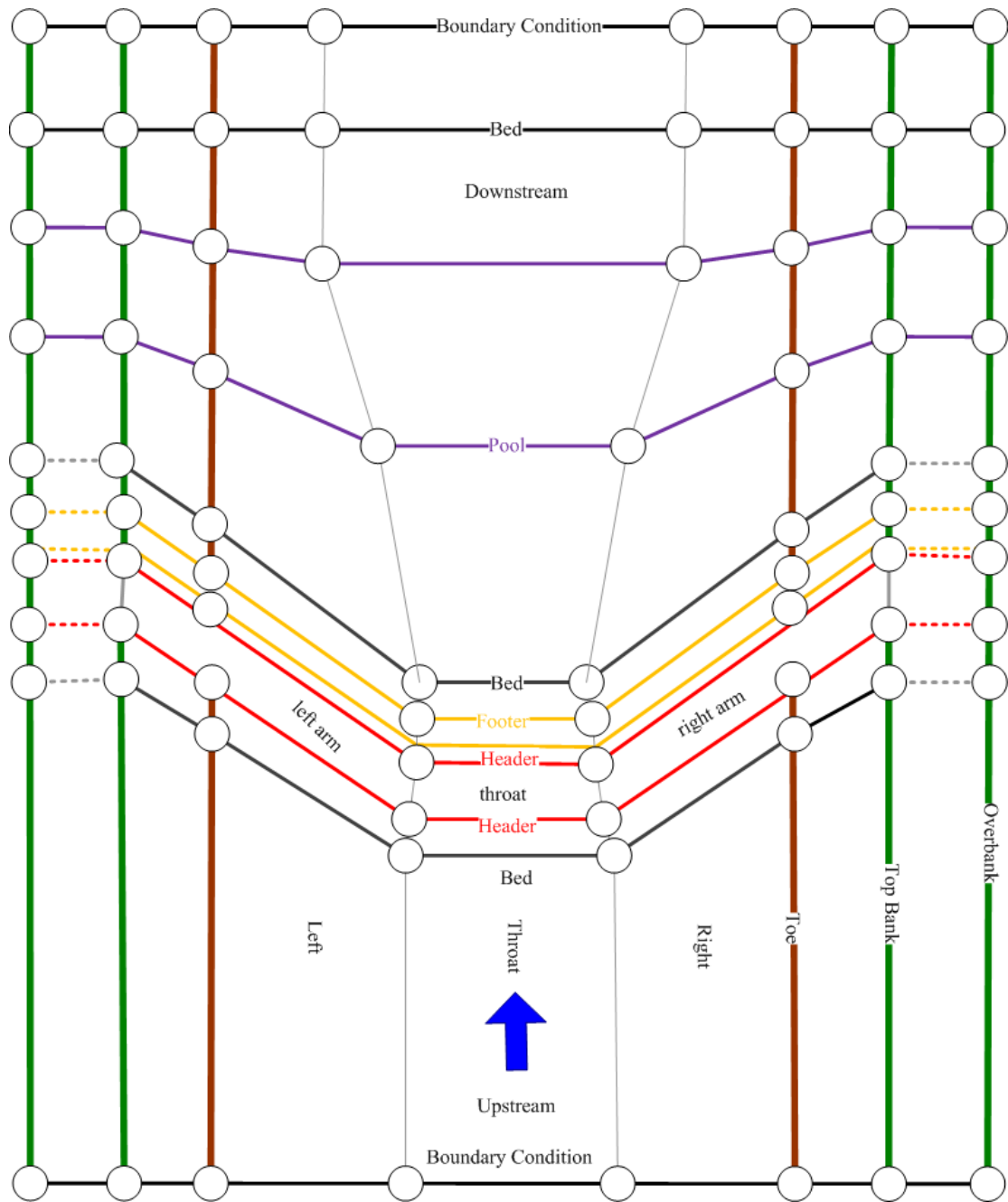


Figure 4.3 – 3D Structure Line and Point Definition

Table 4.3 – Structure Definition Point Identification

Flow-Reference	Bank-Reference	Structure-Reference	Lateral-Reference
Upstream	Left	Bed	Throat
Downstream	Right	Header	Toe
		Footer	Top bank
		Pool	Overbank

4.2.3 INPUT OF CHANNEL CHARACTERISTICS AND STRUCTURE GEOMETRY

To simplify the process of generating the definition lines and corresponding points described above, an Excel file containing input data from the testing matrix was generated. The Excel file contains six worksheets; 1) StructureID, 2) ReachGeometry, 3) Uweir, 4) StructurePoints, 5) zVectors, and 6) 3Dworksheet. The “StructureID” worksheet contains a summary of the testing matrix configuration identifier (ID) and associated bed-material, discharge, and structure reference (Table 4.4).

Table 4.4 – Summary data from Excel input file: “StructureID” worksheet.

Record ID	Configuration ID	River	Reach	Structure Reference	Structure Type	Comment
1	1.01	P1.01_1	22.63mm-Qb	0.8ft-.3W-1ArmL	U	
2	1.01	P1.01_2	22.63mm-2/3Qb	0.8ft-.3W-1ArmL	U	
3	1.01	P1.01_3	22.63mm-1/3Qb	0.8ft-.3W-1ArmL	U	
4	1.01	P1.01_4	22.63mm-1/5Qb	0.8ft-.3W-1ArmL	U	
5	1.01	P1.01_5	22.63mm-1/10Qb	0.8ft-.3W-1ArmL	U	
6	1.02	P1.02_6	22.63mm-Qb	0.4ft-.25W-0.5ArmL	U	
7	1.02	P1.02_7	22.63mm-2/3Qb	0.4ft-.25W-0.5ArmL	U	
8	1.02	P1.02_8	22.63mm-1/3Qb	0.4ft-.25W-0.5ArmL	U	
9	1.02	P1.02_9	22.63mm-1/5Qb	0.4ft-.25W-0.5ArmL	U	
10	1.02	P1.02_10	22.63mm-1/10Qb	0.4ft-.25W-0.5ArmL	U	
11	1.03	P1.03_11	22.63mm-Qb	0.4ft-.25W-2ArmL	U	
12	1.03	P1.03_12	22.63mm-2/3Qb	0.4ft-.25W-2ArmL	U	
13	1.03	P1.03_13	22.63mm-1/3Qb	0.4ft-.25W-2ArmL	U	
14	1.03	P1.03_14	22.63mm-1/5Qb	0.4ft-.25W-2ArmL	U	
15	1.03	P1.03_15	22.63mm-1/10Qb	0.4ft-.25W-2ArmL	U	

For each record ID provided on the “StructureID” worksheet, additional data related to reach characteristics (e.g. bed slope, channel width, channel depth, grain size, etc.) and structure parameters (throat width, arm length, drop height, rock size, etc.) are required to generate the final structure definition points described in Section 4.2.2. Reach characteristics are included in the “ReachGeometry” worksheet and include:

- Design discharge
- Channel width
- Overbank width
- Channel slope
- Channel depth
- Top width
- Side slope
- Grain size
- Mannings-n
- Normal depth

Structure parameters are included in the “StructureGeometry” worksheet and include:

- US boundary station
- Crest station
- DS boundary station
- Structure rock size width
- Structure rock size height
- Weir crest elevation
- Drop height
- Throat width
- Left arm length
- Left arm angle
- Left arm slope
- Right arm length
- Right arm angle
- Right arm slope

An example input sheet for the reach characteristics and structure geometry are presented in Table 4.5 and Table 4.6. A summary of all the parameters used in the testing matrix is presented in Appendix A.

Table 4.5 – Reach geometry input file for generating structure definition points.

Record ID	Configuration ID	River	Reach	Design Discharge (cfs)	Oberbank Width (ft)	Slope	Channel Width (ft)	Channel Depth (ft)	Top Width (ft)	Side Slope (H/V)	Grain size (d50mm)	Manning n	Normal Depth (ft)	Comment
1	1.01	P1.01_1	22.63mm-Qb	5721	0.25	0.001	171.08	6.07	180.18	.75	22.63	0.024	5.61	
2	1.01	P1.01_2	22.63mm-2/3Qb	3814	0.25	0.001	171.08	6.07	180.18	.75	22.63	0.025	4.49	
3	1.01	P1.01_3	22.63mm-1/3Qb	1907	0.25	0.001	171.08	6.07	180.18	.75	22.63	0.027	3.08	
4	1.01	P1.01_4	22.63mm-1/5Qb	1144	0.25	0.001	170.95	6.07	180.18	.76	22.63	0.027	2.26	
5	1.01	P1.01_5	22.63mm-1/10Qb	572	0.25	0.001	170.83	6.07	180.18	.77	22.63	0.027	1.49	
6	1.02	P1.02_6	22.63mm-Qb	5721	0.25	0.001	171.08	6.07	180.18	.75	22.63	0.024	5.60	
7	1.02	P1.02_7	22.63mm-2/3Qb	3814	0.25	0.001	171.08	6.07	180.18	.75	22.63	0.025	4.49	
8	1.02	P1.02_8	22.63mm-1/3Qb	1907	0.25	0.001	171.08	6.07	180.18	.75	22.63	0.027	3.08	
9	1.02	P1.02_9	22.63mm-1/5Qb	1144	0.25	0.001	171.08	6.07	180.18	.75	22.63	0.027	2.26	
10	1.02	P1.02_10	22.63mm-1/10Qb	572	0.25	0.001	171.08	6.07	180.18	.75	22.63	0.027	1.49	
11	1.03	P1.03_11	22.63mm-Qb	5721	0.25	0.001	171.08	6.07	180.18	.75	22.63	0.024	5.60	
12	1.03	P1.03_12	22.63mm-2/3Qb	3814	0.25	0.001	171.08	6.07	180.18	.75	22.63	0.025	4.49	
13	1.03	P1.03_13	22.63mm-1/3Qb	1907	0.25	0.001	171.08	6.07	180.18	.75	22.63	0.027	3.08	
14	1.03	P1.03_14	22.63mm-1/5Qb	1144	0.25	0.001	171.08	6.07	180.18	.75	22.63	0.027	2.26	
15	1.03	P1.03_15	22.63mm-1/10Qb	572	0.25	0.001	171.08	6.07	180.18	.75	22.63	0.027	1.49	

88

Table 4.6 – Structure geometry input file for generating structure definition points.

Record ID	Configuration ID	River	Reach	Structure Reference	US XS Station (ft)	Crest Station (ft)	DS XS Station (ft)	Structure Rock Size Width (ft)	Structure Rock Size Height (ft)	Weir Crest Elevation (ft)	Drop Height (ft)	Throat Width (ft)	Lft Arm Angle (degrees)	Lft Arm Slope (degrees)	Lft Arm Length (ft)	Rt Arm Angle (degrees)	Rt Arm Slope (degrees)	Rt Arm Length (ft)
1	1.01	P1.01_1	22.63mm-Qb	0.8ft-.3W-1Arml	-540.54	0	900.9	4	2.67	100.8	0.8	60.06	27.34	2.26	116.15	27.34	2.26	116.15
2	1.01	P1.01_2	22.63mm-2/3Qb	0.8ft-.3W-1Arml	-540.54	0	900.9	4	2.67	100.8	0.8	60.06	27.34	2.26	116.15	27.34	2.26	116.15
3	1.01	P1.01_3	22.63mm-1/3Qb	0.8ft-.3W-1Arml	-540.54	0	900.9	4	2.67	100.8	0.8	60.06	27.34	2.26	116.15	27.34	2.26	116.15
4	1.01	P1.01_4	22.63mm-1/5Qb	0.8ft-.3W-1Arml	-540.54	0	900.9	4	2.67	100.8	0.8	60.06	27.34	2.26	116.15	27.34	2.26	116.15
5	1.01	P1.01_5	22.63mm-1/10Qb	0.8ft-.3W-1Arml	-540.54	0	900.9	4	2.67	100.8	0.8	60.06	27.34	2.26	116.15	27.34	2.26	116.15
6	1.02	P1.02_6	22.63mm-Qb	0.4ft-.25W-0.5Arml	-540.54	0	900.9	4	2.67	100.4	0.4	45.04	46.44	3.44	64.25	46.44	3.44	64.25
7	1.02	P1.02_7	22.63mm-2/3Qb	0.4ft-.25W-0.5Arml	-540.54	0	900.9	4	2.67	100.4	0.4	45.04	46.44	3.44	64.25	46.44	3.44	64.25
8	1.02	P1.02_8	22.63mm-1/3Qb	0.4ft-.25W-0.5Arml	-540.54	0	900.9	4	2.67	100.4	0.4	45.04	46.44	3.44	64.25	46.44	3.44	64.25
9	1.02	P1.02_9	22.63mm-1/5Qb	0.4ft-.25W-0.5Arml	-540.54	0	900.9	4	2.67	100.4	0.4	45.04	46.44	3.44	64.25	46.44	3.44	64.25
10	1.02	P1.02_10	22.63mm-1/10Qb	0.4ft-.25W-0.5Arml	-540.54	0	900.9	4	2.67	100.4	0.4	45.04	46.44	3.44	64.25	46.44	3.44	64.25
11	1.03	P1.03_11	22.63mm-Qb	0.4ft-.25W-2Arml	-540.54	0	1028.04	4	2.67	100.4	0.4	45.04	14.73	1.17	257.01	14.73	1.17	257.01
12	1.03	P1.03_12	22.63mm-2/3Qb	0.4ft-.25W-2Arml	-540.54	0	1028.04	4	2.67	100.4	0.4	45.04	14.73	1.17	257.01	14.73	1.17	257.01
13	1.03	P1.03_13	22.63mm-1/3Qb	0.4ft-.25W-2Arml	-540.54	0	1028.04	4	2.67	100.4	0.4	45.04	14.73	1.17	257.01	14.73	1.17	257.01
14	1.03	P1.03_14	22.63mm-1/5Qb	0.4ft-.25W-2Arml	-540.54	0	1028.04	4	2.67	100.4	0.4	45.04	14.73	1.17	257.01	14.73	1.17	257.01
15	1.03	P1.03_15	22.63mm-1/10Qb	0.4ft-.25W-2Arml	-540.54	0	1028.04	4	2.67	100.4	0.4	45.04	14.73	1.17	257.01	14.73	1.17	257.01

Using the input data provided above, location (x and y) and elevation (z) data for the structure definition points are generated using vector analysis and the “zVectors” worksheet. Results of the vector analysis are summarized in the “StructurePoints” worksheet (Table 4.7) and are used to provide input to the rock weir mesh generation program in order to generate the computational mesh based on the eleven lateral definition lines shown previously in Figure 4.3.

Table 4.7 – Structure definition point data used by mesh generator

River	Reach	Structure Reference	PI	x	y	z	Pt description
P1.01_1	22.63mm-Qb	0.8ft-.3W-1ArmL	1	9.66	-540.54	106.613	lft-us-bc-ob
P1.01_1	22.63mm-Qb	0.8ft-.3W-1ArmL	2	9.91	-540.54	106.611	lft-us-bc-topbank
P1.01_1	22.63mm-Qb	0.8ft-.3W-1ArmL	3	12.03	-540.54	103.783	lft-us-bc-bank
P1.01_1	22.63mm-Qb	0.8ft-.3W-1ArmL	4	14.472	-540.54	100.541	lft-us-bc-toe
P1.01_1	22.63mm-Qb	0.8ft-.3W-1ArmL	5	49.789	-540.54	100.541	lft-us-bc-chanpt
P1.01_1	22.63mm-Qb	0.8ft-.3W-1ArmL	6	63.964	-540.54	100.536	lft-us-bc-throat
P1.01_1	22.63mm-Qb	0.8ft-.3W-1ArmL	7	100	-540.54	100.516	us-bc-midpt
P1.01_1	22.63mm-Qb	0.8ft-.3W-1ArmL	8	136.036	-540.54	100.536	rt-us-bc-throat
P1.01_1	22.63mm-Qb	0.8ft-.3W-1ArmL	9	150.211	-540.54	100.541	rt-us-bc-chanpt
P1.01_1	22.63mm-Qb	0.8ft-.3W-1ArmL	10	185.528	-540.54	100.541	rt-us-bc-toe
P1.01_1	22.63mm-Qb	0.8ft-.3W-1ArmL	11	187.97	-540.54	103.783	rt-us-bc-bank
P1.01_1	22.63mm-Qb	0.8ft-.3W-1ArmL	12	190.09	-540.54	106.611	rt-us-bc-topbank
P1.01_1	22.63mm-Qb	0.8ft-.3W-1ArmL	13	190.34	-540.54	106.613	rt-us-bc-ob
P1.01_1	22.63mm-Qb	0.8ft-.3W-1ArmL	14	9.66	108.906	105.961	lft-us-bed-ob
P1.01_1	22.63mm-Qb	0.8ft-.3W-1ArmL	15	9.91	108.906	105.959	lft-us-bed-topbank
P1.01_1	22.63mm-Qb	0.8ft-.3W-1ArmL	16	12.03	104.805	103.136	lft-us-bed-bank
P1.01_1	22.63mm-Qb	0.8ft-.3W-1ArmL	17	14.473	100.101	99.898	lft-us-bed-toe
P1.01_1	22.63mm-Qb	0.8ft-.3W-1ArmL	18	49.789	31.814	99.966	lft-us-bed-chanpt
P1.01_1	22.63mm-Qb	0.8ft-.3W-1ArmL	19	67.941	-3.334	99.996	lft-us-bed-throat
P1.01_1	22.63mm-Qb	0.8ft-.3W-1ArmL	20	100	-3.333	99.976	us-bed-midpt
P1.01_1	22.63mm-Qb	0.8ft-.3W-1ArmL	21	132.059	-3.333	99.996	rt-us-bed-throat
P1.01_1	22.63mm-Qb	0.8ft-.3W-1ArmL	22	150.211	31.815	99.966	rt-us-bed-chanpt
P1.01_1	22.63mm-Qb	0.8ft-.3W-1ArmL	23	185.528	100.102	99.898	rt-us-bed-toe
P1.01_1	22.63mm-Qb	0.8ft-.3W-1ArmL	24	187.97	104.806	103.136	rt-us-bed-bank
P1.01_1	22.63mm-Qb	0.8ft-.3W-1ArmL	25	190.09	108.907	105.959	rt-us-bed-topbank
P1.01_1	22.63mm-Qb	0.8ft-.3W-1ArmL	26	190.34	108.907	105.961	rt-us-bed-ob
P1.01_1	22.63mm-Qb	0.8ft-.3W-1ArmL	27	9.744	111.652	105.956	lft-us-header-ob
P1.01_1	22.63mm-Qb	0.8ft-.3W-1ArmL	28	9.994	111.652	105.954	lft-us-header-topbank
P1.01_1	22.63mm-Qb	0.8ft-.3W-1ArmL	29	12.114	107.55	105.772	lft-us-header-bank
P1.01_1	22.63mm-Qb	0.8ft-.3W-1ArmL	30	14.556	102.846	105.563	lft-us-header-toe
P1.01_1	22.63mm-Qb	0.8ft-.3W-1ArmL	31	49.872	34.559	102.529	lft-us-header-chanpt
P1.01_1	22.63mm-Qb	0.8ft-.3W-1ArmL	32	68.753	-2	100.795	lft-us-header-throat
P1.01_1	22.63mm-Qb	0.8ft-.3W-1ArmL	33	100	-2	100.775	us-header-midpt
P1.01_1	22.63mm-Qb	0.8ft-.3W-1ArmL	34	131.247	-2	100.795	rt-us-header-throat
P1.01_1	22.63mm-Qb	0.8ft-.3W-1ArmL	35	150.128	34.559	102.529	rt-us-header-chanpt
P1.01_1	22.63mm-Qb	0.8ft-.3W-1ArmL	36	185.444	102.846	105.563	rt-us-header-toe
P1.01_1	22.63mm-Qb	0.8ft-.3W-1ArmL	37	187.886	107.55	105.772	rt-us-header-bank
P1.01_1	22.63mm-Qb	0.8ft-.3W-1ArmL	38	190.006	111.652	105.954	rt-us-header-topbank
P1.01_1	22.63mm-Qb	0.8ft-.3W-1ArmL	39	190.256	111.652	105.956	rt-us-header-ob

4.2.4 MESH GENERATION

Once structure definition points were generated from the reach characteristics and structure geometry described in Section 4.2.3, a Visual Basic code was used to describe how each of the definition points were connected and define the longitudinal and lateral spacing (number of vertexes) used to generate the final computational mesh.

A mesh consisting of quadrilateral and/or triangular elements represents the structure and surrounding trapezoidal channel. Use of triangular or quadrilateral elements depends upon the interior angles created by the mesh elements surrounding a node. In U^2 RANS, a perfect quality mesh element would contain a face oriented normal to the direction of flow entering the element and a second face normal to the flow leaving the element. The remaining faces would lie parallel to stream lines. Unfortunately, a perfect mesh would require a priori knowledge of model results. Areas of concern occur along breaks in geometry where the structure transitions from one face to another, e.g. the structure definition lines.

Regular geometries cannot create a perfect representation of all features. A combination of quadrilaterals and triangles can be used to better approach regular shapes. The intersection of the structure and flat bank can create a situation where filling a mesh entirely with quadrilaterals may result in a large amount of warping while an edge of triangles would create more regular shaped cells as shown in Figure 4.4.

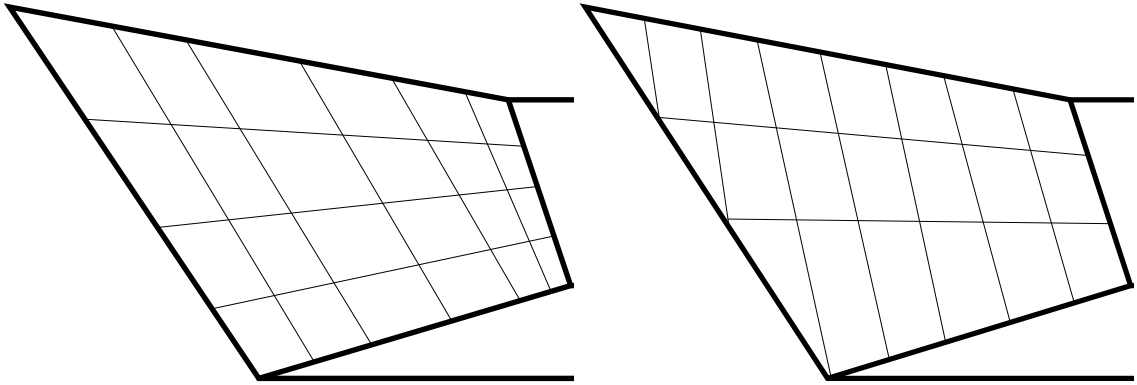


Figure 4.4 – Highly Warped Quadrilateral versus Triangular Boundaries

However applying a triangular edge can create irregular cell sizes in certain cases. A steeply sloped bank will create very small interior angles for triangular edges as shown in Figure 4.5.

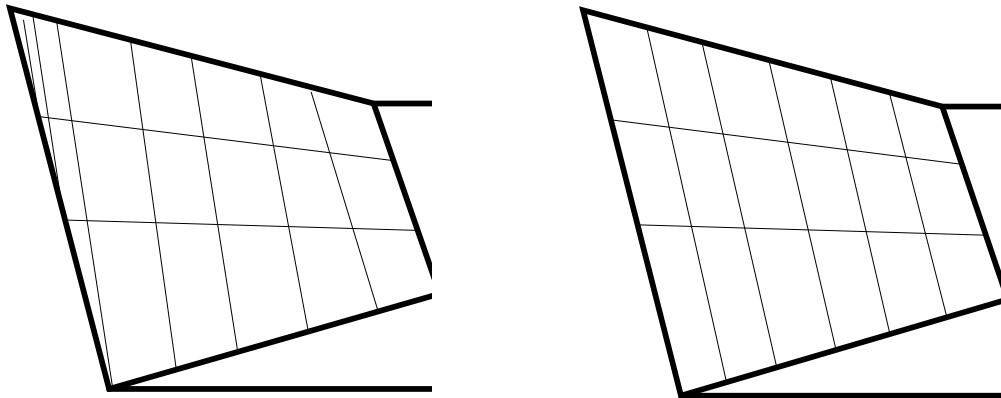


Figure 4.5 – Highly Irregular Triangles versus Warped Quadrilateral Boundary

The longitudinal and lateral spacing of each element also affects the shape and overall density of the mesh. A decision must occur along each structure definition line as to whether a triangle or quadrilateral provides the best representation based on the element spacing and resulting shape. The rock weir mesh generator seeks to create the most regular shape possible by comparing the interior angles of the shapes formed by each element along each definition line.

Using the structure definition points generated from the reach characteristics and structure geometry, the visual basic program was used to generate a computational mesh

using the methods described above. A script file that describes how each point is connected and defines the longitudinal and lateral spacing (number of vertexes) used by the mesh generation program was created for input to U²RANS. Alterations to the input script for mesh spacing and point definitions provide a fast and efficient method for generating computational meshes of various configurations and densities. Each mesh was designed to have a much higher nodal density near the weir than in the upstream and downstream parts of the channel with smooth transitions in mesh density. An example of the lateral definition lines for a given weir geometry and the resulting rock weir mesh generation output are shown in Figure 4.6 and Figure 4.7. The output from the mesh generation program provides the computational mesh required to conduct the numerical simulations using U²RANS. The following section provides information about the CFD program U²RANS, input requirements, and data output options.

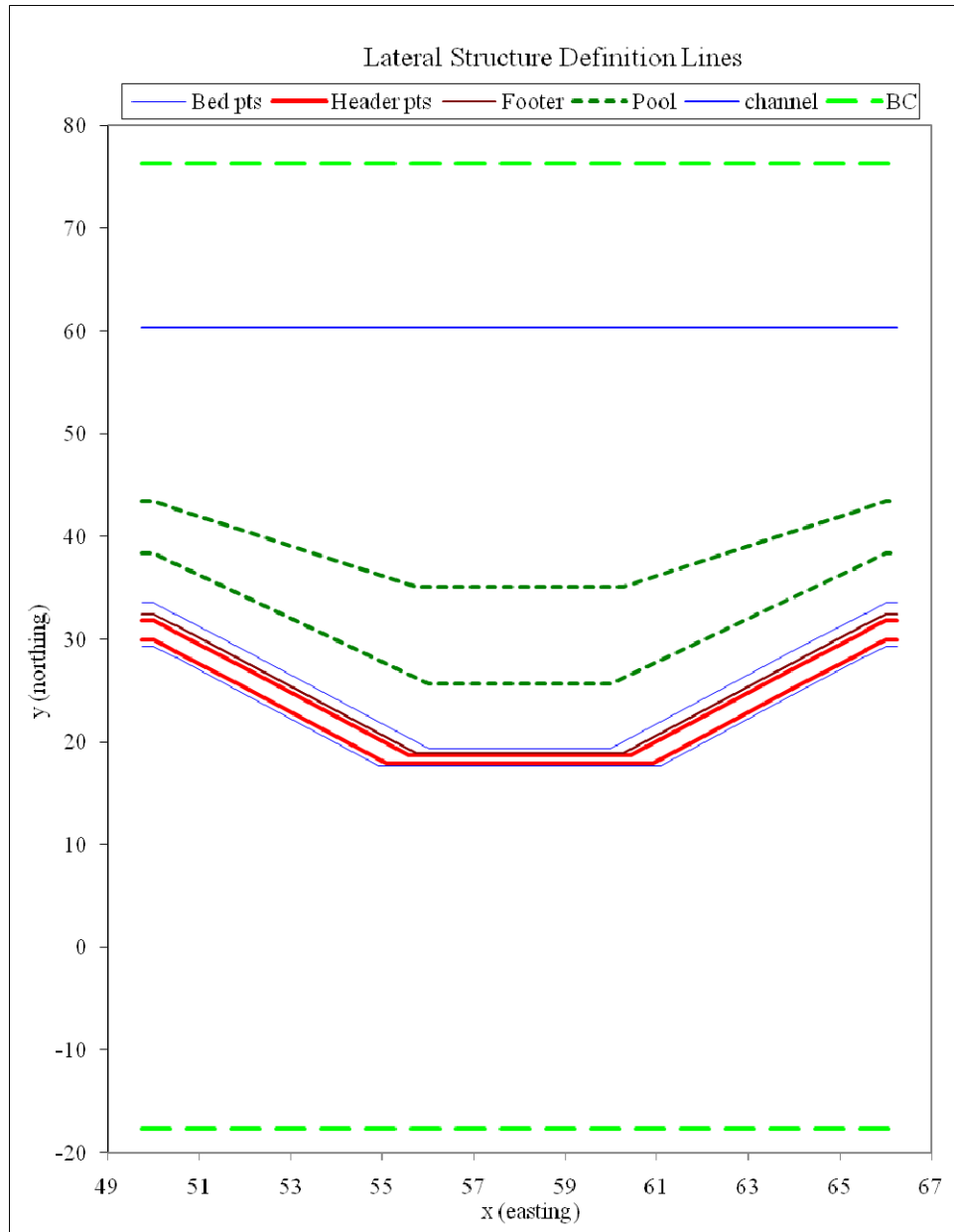


Figure 4.6 – Example of structure definition lines used by rock weir mesh generator.

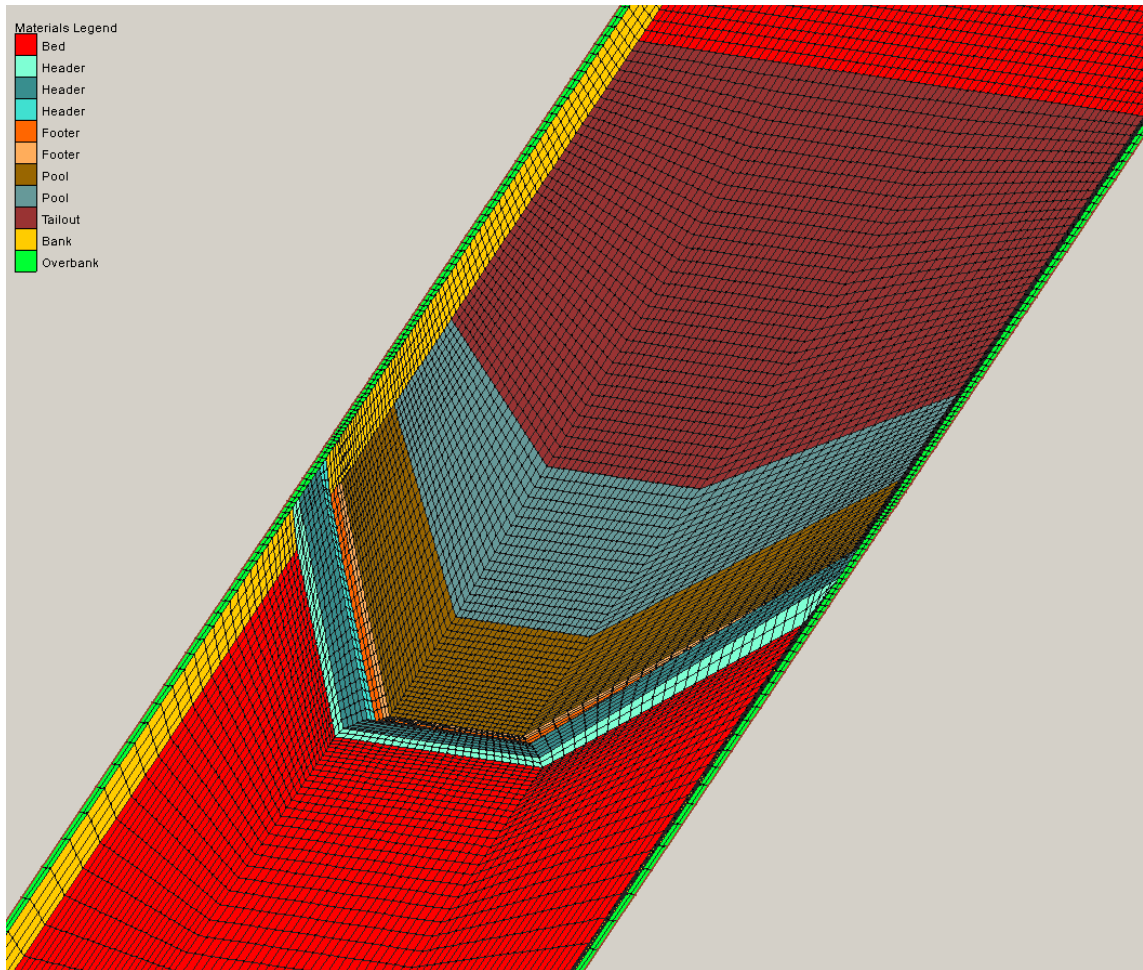


Figure 4.7 – Example computational mesh created using mesh generation program.

4.3 3D MODEL DESCRIPTION

4.3.1 U²RANS

U²RANS is an Unsteady and Unstructured Reynolds Averaged Navier-Stokes solver that can be used to solve a variety of practical flow and thermal problems. It is a general-purpose CFD code for modeling fluid flow, heat transfer, multi-fluid transport, and chemically reacting flows. The code has been extensively used to solve various hydraulic flows in rivers, hydropower dams, hydraulic structures, and power station thermal discharges (Lai, 2001). U²RANS currently consists of two programs: *u2pre* and *u2rans*.

u2pre is a text-based interactive user interface which guides a user to set up the fluid flow problem. *u2pre* has an error checking mechanism so that most input data errors are expected to be detected before going to the *u2rans* solver. *u2rans* is the main solver module which reads the input files generated by *u2pre*, performs the simulation, and outputs final results to data files in a format specified by the user. The output data files store the final results and can be viewed and processed using corresponding graphic packages.

The numerical model involves the solution of the Reynolds Averaged Navier-Stokes (RANS) equations based on the conservation of mass and momentum equations. The mass and momentum equations are concisely written in Cartesian tensor form by Lai et al. (2003) as presented in Equations 4.6 and 4.7 below:

$$\frac{\partial(\rho U_j)}{\partial x_j} = 0 \quad \text{Equation 4.6}$$

$$\frac{\partial(\rho U_i)}{\partial t} + \frac{\partial(\rho U_i U_j)}{\partial x_j} = -\frac{\partial P}{\partial x_i} + \frac{\partial}{\partial x_j} \left(\mu \frac{\partial U_i}{\partial x_j} - \overline{\rho u_i u_j} \right) \quad \text{Equation 4.7}$$

Where

- U = mean velocity;
- u = fluctuating velocities;
- P = mean pressure;
- ρ = fluid density;
- μ = fluid viscosity; and
- $u_i u_j$ = Reynolds stress.

In the above equation, a turbulence model is required for the Reynolds stress ($\overline{\rho u_i u_j}$). U²RANS uses the k-ε turbulence model to solve for Reynolds stress. In the k-ε turbulence model, the eddy viscosity is expressed in terms of turbulent kinetic energy (k)

and turbulent dissipation (ϵ). Details pertaining to the derivation and solution of the above equations using numerical techniques are presented in Ferziger and Peric (1997).

In solving the RANS equations, the numerical model uses the pressure-based finite volume technique and an element-centered storage scheme. The SIMPLE (Semi-Implicit Method for Pressure-Linked Equations) algorithm is used for the pressure coupling. In this algorithm, the continuity equation is converted into a discrete Poisson equation for pressure and then the pressure field is determined (Ferziger and Peric 1997). The momentum equation is then solved using the pressure field to calculate velocities. The computed velocities satisfy momentum, but not continuity. Therefore, resultant continuity errors are calculated and used to adjust the pressure and velocity fields to satisfy continuity. After that adjustment the velocities will not satisfy momentum, so this process is repeated iteratively until both continuity and momentum errors are acceptably small. Additional information related to CFD theory and a more detailed description of the numerical techniques used in CFD models like U²RANS can be found in the literature (i.e. Ferziger and Peric, 1997).

4.3.2 MODEL INPUTS

Input data required by U²RANS consists mostly of a computational mesh and boundary conditions associated with the type of model simulation being conducted. *u2pre* allows a user to set up the simulation by reading an existing script input file (run_SIF) or through an on-screen interactive session by entering the inputs one-by-one as directed by the preprocessor. The pre-processor commands and data entered by the user are saved to a script file named run_SOF (Script Output File). It is recommended that the script file run.SOF be copied and saved to a file named run_SIF (Script Input File) for future model

simulations. There are two important benefits in having the input commands saved to a script file:

- (1) Provides a permanent record of model inputs once the simulation is complete and provides a method in which the simulation can be repeated later if needed.
- (2) Allows a user to edit the script file directly for simulation setup. This is particularly useful when only minor changes are needed for carrying out a parametric analysis such as the present study (e.g. computational mesh, flow rate, and exit conditions for a given structure configuration).

After executing *u2pre*, an output file named run.GRD is generated which contains the computational mesh and associated model input parameters required to execute U²RANS. The following sections provide a description of the geometry (computational mesh) and boundary conditions used for this project.

4.3.2.1 GEOMETRY

The computational mesh (trapezoidal channel and structure geometry) used in the numerical modeling was generated from the rock weir mesh generation program described in section 4.2. The channel consisted of a simplified trapezoidal channel with a 0.75 horizontal to vertical side slope and the width and depth of the channel calculated from hydraulic geometry regime equations presented in section 4.1.2. Figure 4.8 shows the computational mesh that was generated using the rock weir mesh generator for a structure configuration with a throat width equal to one third the channel top width, arm angle of 27 degrees, and arm slope of 4 percent.

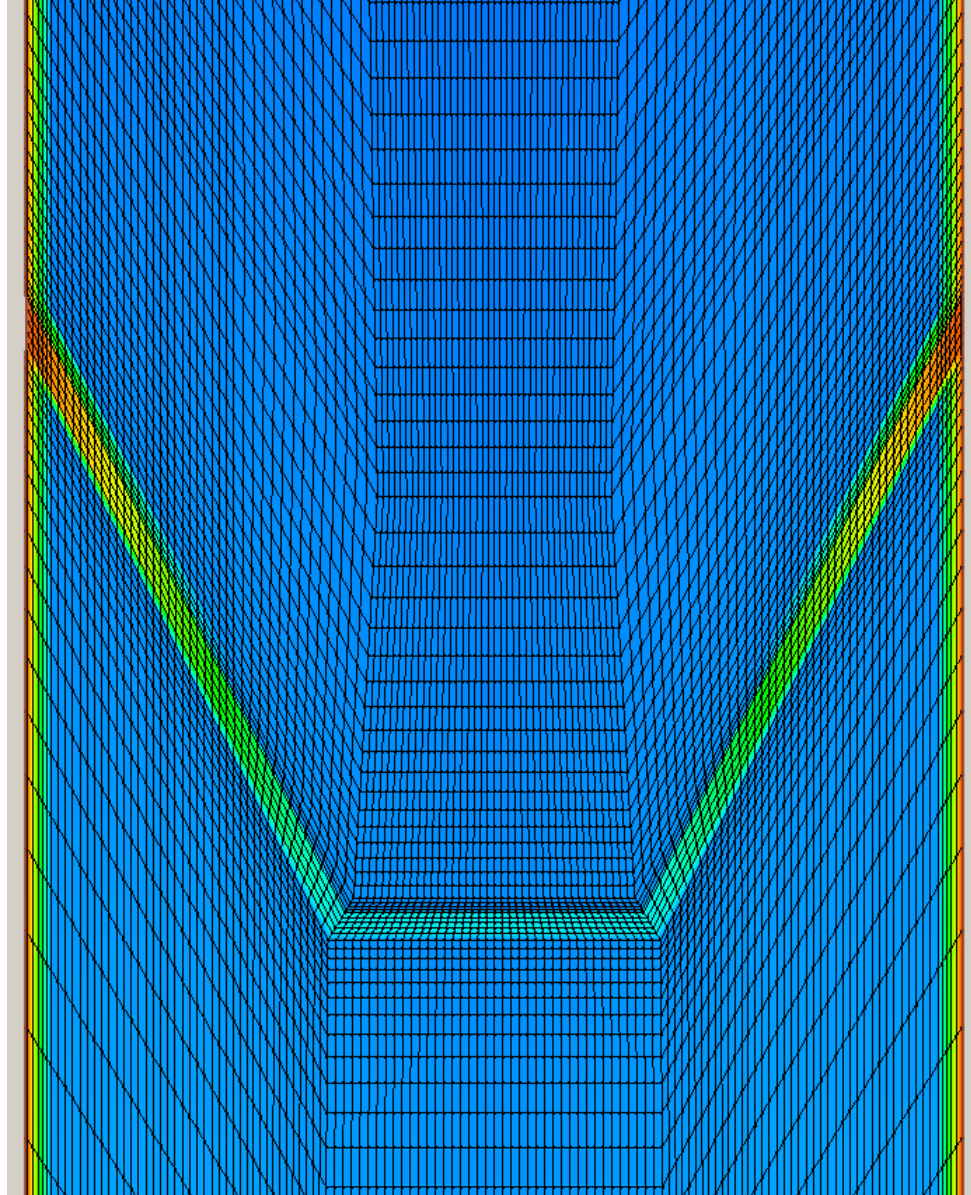


Figure 4.8 – Computational mesh generated from mesh generator for a U-weir.

Figure 4.9 shows the numerical representation of the trapezoidal channel looking downstream at the structure crest/throat of the U-weir and how the arms tie-in to the top bank. Notice how the downstream footer begins to show as the arm elevation increases and the footer elevation becomes greater than the bed elevation.

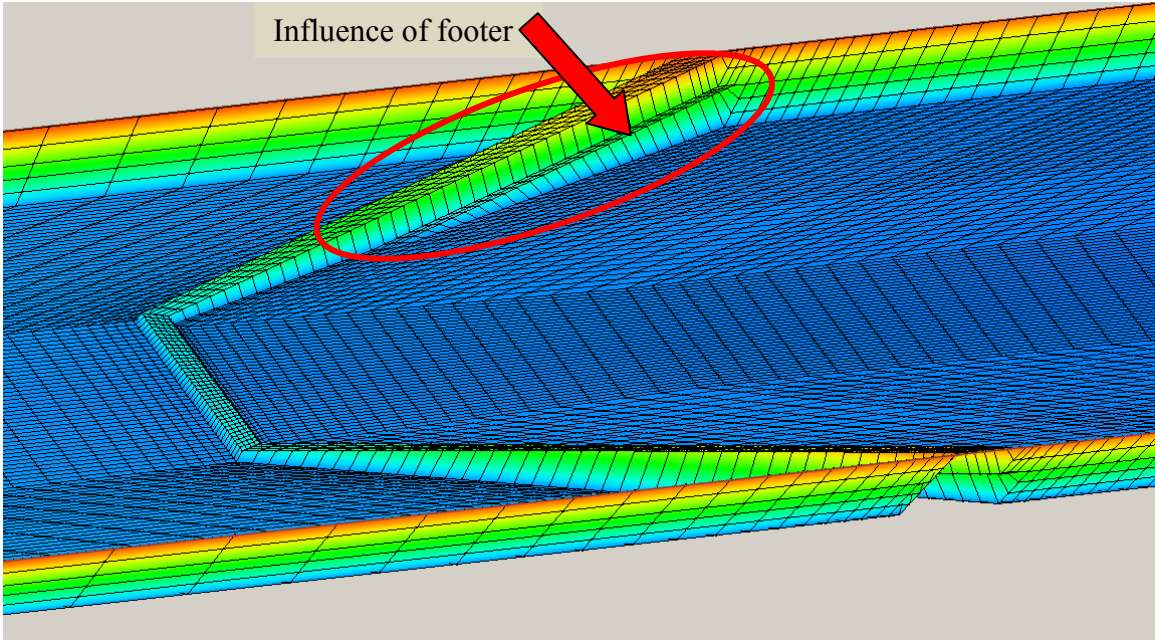


Figure 4.9 – Numerical representation of trapezoidal channel and U-weir header-footer configuration.

Utilizing the mesh generation program, a sensitivity test was conducted to determine whether the specified computational mesh had sufficient density for simulating the flow patterns associated with U-weirs. Simulation results of four mesh resolutions ranging from a low density mesh (mesh#1) to a high density mesh (mesh#4) were compared. The number of lateral, longitudinal, and vertical elements associated with each mesh density was as follows: mesh#1-50x120x12, mesh#2-75x180x12, mesh#3-50x120x18, and mesh#4-100x240x12. Each mesh was designed to have a much higher nodal density near the weir with smooth transitions between the upstream and downstream portion of the channel. The second and fourth mesh densities were increased by 1.5 times and 2 times the lateral and longitudinal resolution of the first mesh respectively. The increase in mesh density resulted in a much greater element concentration around the structure. The third mesh density was increased in the vertical direction by 1.5 times the number of vertical elements of the first mesh. Simulations of

the same channel characteristics, structure geometry, and discharge were conducted and the computational results were compared to see if significant improvements were gained through increasing the density of the computational mesh. No significant difference was found in the computed flow conditions by increasing the number of vertical cells between the first and third meshes. The lateral and longitudinal increase in the second and fourth mesh densities resulted in a more detailed recirculation zone near the structure arms compared to the coarser first and third meshes. Comparisons between the second and fourth mesh resulted in less than a two percent difference in the computed velocities and no apparent differences in the definition of the recirculation zones near the arms. The greatest difference between the second and fourth mesh densities was related to the computation time. The computation time using the fourth mesh (greatest density) was almost five times longer (~34hrs) than that of the second mesh (~8hrs) using a PC with a Xeon 2.66 GHz Quad-Core processor and 4 GB of RAM. Given the large increase in computation time using the fourth mesh with no apparent differences in the computed flow conditions compared to that of the second mesh, the second mesh density was selected to define the channel and rock weir geometry used in the numerical simulations. Therefore, the computational mesh and numerical modeling results presented in this dissertation were obtained by using the algorithm associated with the second mesh.

4.3.2.2 BOUNDARY CONDITIONS

Boundary conditions required by U^2 RANS depend on the type of flow simulation being conducted. For the rock weir modeling, the main input parameters included but were not limited to the following:

- Type of flow: 3D steady flow with solid lid approximation

- Inflow: Discharge
- Exit Condition: downstream water surface elevation
- Input mesh: mesh file name and number of vertical cells
- Roughness height: roughness height associate with bed material size

Boundary conditions for each numerical simulation were dependent on the associated channel characteristics, structure geometry, and discharge associated with the testing matrix configuration ID. Inflow for each configuration was based on a fraction of the design bankfull discharge and included a total of five variations ($1/10Q_{\text{bkf}}$, $1/5Q_{\text{bkf}}$, $1/3Q_{\text{bkf}}$, $2/3Q_{\text{bkf}}$, and Q_{bkf}). For each discharge and structure configuration an exit condition (downstream water surface elevation) was determined based on the downstream channel elevation and estimated normal depth. Normal depth was estimated using Manning's equation for each of the channel characteristics (slope, grain size, and channel geometry) and associated discharges. The input mesh for each configuration was generated from the mesh generation program as well as specifying the number of vertical cells to include in the simulation. Finally, the roughness height was based on the bed material size (d_{50} in meters) associated with each configuration.

The input parameters listed above were defined using a script input file (*run_SIF.dat*) that was read by the U²RANS pre-processor. A number of other input parameters are included in the script file; however, since these parameters remained constant for all the numerical model simulations, they are not discussed here. Detailed information pertaining to input parameters used in the numerical modeling code can be referenced in the user's manual (Lai, 2001).

4.3.3 MODEL OUTPUT

Output generated by U²RANS includes 3D spatially distributed velocity magnitude and flow direction, bed shear stress, and water surface elevation. Output data from the model can be used to analyze how flow patterns are affected by changes in structure geometry. Table 4.8 provides an example of the data that can be extracted from U²RANS. Figure 4.10 and Figure 4.11 are examples of U²RANS output visualized in TEC-PLOT.

Table 4.8 – Example 3D output data generated by U²RANS.

X (m)	Y (m)	Z (m)	WSE (m)	Depth (m)	Velev (m)	Vx (m/s)	Vy (m/s)	Vz (m/s)	Tk (m ² /s ²)	Td (m ² /s ³)	Vmag (m/s)	Wss (Pa)
19.495	-5.493	30.476	32.351	1.878	31.225	0.167	1.682	-0.001	0.007	0.001	1.691	3.816
24.988	-5.493	30.464	32.345	1.884	31.216	0.088	1.756	-0.002	0.007	0.001	1.758	4.214
30.480	-5.493	30.458	32.342	1.890	31.209	0.000	1.784	-0.002	0.007	0.001	1.784	4.285
19.495	7.081	30.467	32.287	1.823	31.194	0.560	1.928	-0.145	0.017	0.006	2.014	5.374
24.988	7.081	30.455	32.278	1.826	31.183	0.230	2.230	-0.019	0.011	0.002	2.242	5.510
30.480	7.081	30.446	32.278	1.835	31.178	0.000	2.233	-0.010	0.011	0.002	2.233	5.163
19.495	14.161	30.461	32.223	1.765	31.165	0.457	2.211	-0.091	0.033	0.009	2.260	9.064
24.988	14.161	30.449	32.227	1.780	31.159	0.238	2.644	-0.034	0.009	0.001	2.655	9.223
30.480	14.161	30.440	32.230	1.792	31.155	0.000	2.574	-0.009	0.011	0.002	2.574	8.028
19.495	21.242	30.452	32.150	1.701	31.130	0.219	2.475	-0.043	0.050	0.011	2.486	12.254
24.988	21.242	30.443	32.169	1.728	31.132	0.164	3.036	-0.046	0.008	0.001	3.041	12.491
30.480	21.242	30.431	32.172	1.743	31.126	0.000	2.901	-0.010	0.012	0.002	2.901	10.826
19.495	28.322	30.446	32.095	1.652	31.105	0.000	2.635	-0.014	0.055	0.011	2.635	13.608
24.988	28.322	30.437	32.111	1.679	31.103	0.080	3.294	-0.050	0.007	0.001	3.295	14.551
30.480	28.322	30.424	32.117	1.695	31.100	0.000	3.143	-0.009	0.012	0.002	3.143	12.705
19.495	35.403	30.440	32.062	1.625	31.088	-0.067	2.683	-0.001	0.054	0.009	2.684	13.566
24.988	35.403	30.431	32.074	1.646	31.087	0.014	3.421	-0.040	0.006	0.001	3.422	15.141
30.480	35.403	30.418	32.077	1.661	31.081	0.000	3.276	-0.006	0.012	0.002	3.276	13.362

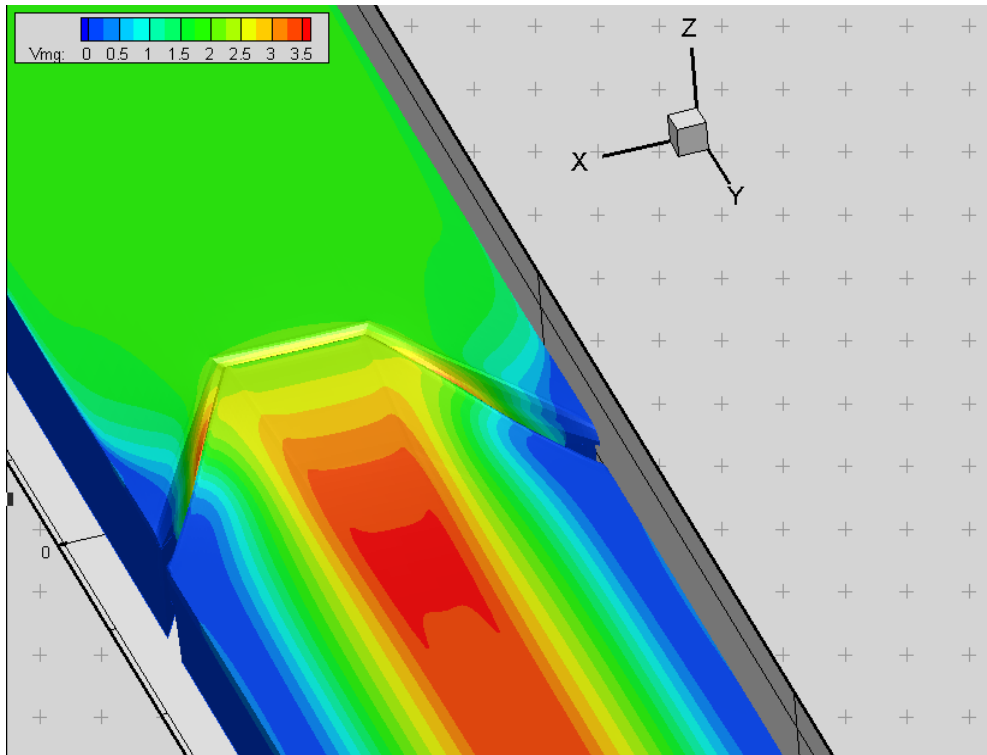


Figure 4.10 – Example of 3D Numerical model output showing surface velocity distribution at bankfull flow.

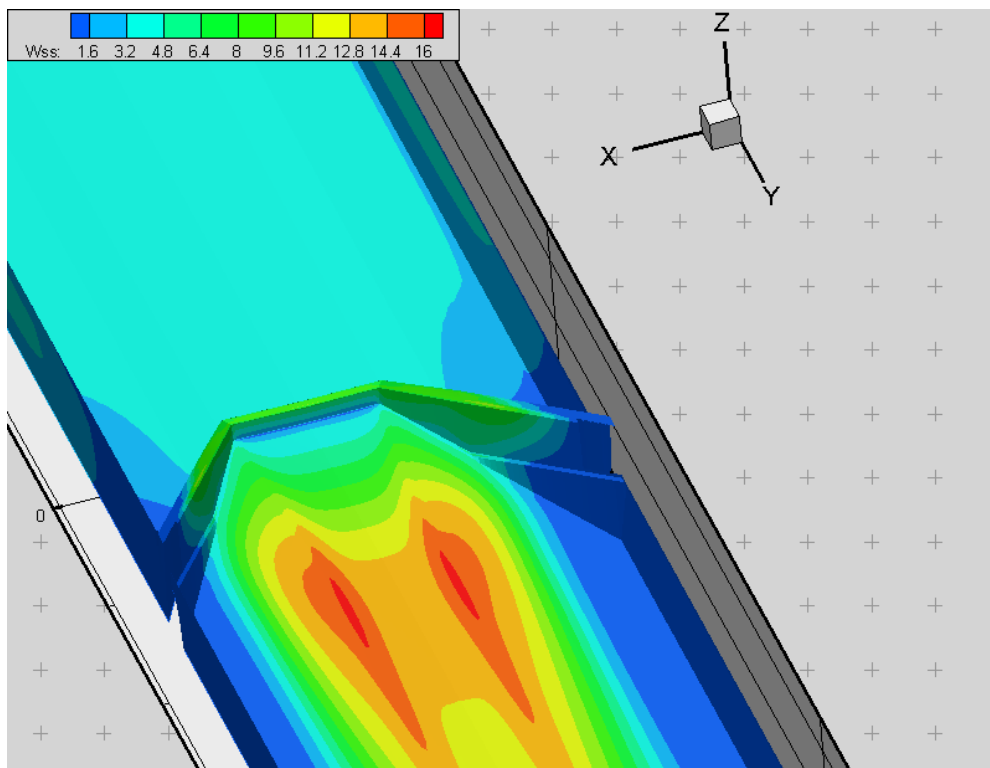


Figure 4.11 – Example of 3D numerical model output showing boundary shear stress distribution at bankfull flow.

Utilizing the testing matrix and mesh generation program described above, 3D numerical modeling was conducted for an idealized flat bed trapezoidal channel. Output from the numerical modeling was analyzed to quantify the effects that variations in structure geometry had on local flow patterns.

4.4 IDENTIFYING EFFECTS OF STRUCTURE GEOMETRY ON LOCAL HYDRAULICS

In conducting an analysis of flow patterns associated with differing structure geometries, a common reference point or plane is needed to compare the results from different configurations. Reference sample points were based on a fraction of the channel width and structure length. Since the channel geometry consists of an idealized flat bed trapezoidal channel and symmetric weir geometry, only half of the channel in the lateral direction was sampled. Sample points across the channel were located at 5% intervals of the channel top width starting at the left overbank location and spanned half of the channel width. Sample points along the channel were located at specified intervals of the channel top width for locations upstream of the structure, 10% intervals of the arm length (L_a) within the structure, and 25% intervals of the arm length downstream from the structure. Table 4.9 shows the longitudinal sample point distribution used.

Utilizing a sampling grid with 10 points across the channel and 28 points along the channel resulted in a total of 280 sample points. An example of the sampling grid distribution for two different weir configurations is provided in Figure 4.12. While a flat bed trapezoidal channel is not indicative of real world conditions, it provides an opportunity to investigate how specific variations in structure geometry affect local flow patterns by holding the bed topography constant.

Table 4.9 – Longitudinal sample point distribution.

Longitudinal Reference Location	Starting Point Number	Ending Point Number	Reference Cross Section Number
Upstream Tw	1	10	1
0.5Tw	11	20	2
0.25Tw	21	30	3
0.1Tw	31	40	4
Structure throat	41	50	5
0.1La	51	60	6
0.2La	61	70	7
0.3La	71	80	8
0.4La	81	90	9
0.5La	91	100	10
0.6La	101	110	11
0.7La	111	120	12
0.8La	121	130	13
0.9La	131	140	14
La	141	150	15
1.1La	151	160	16
1.25La	161	170	17
1.5La	171	180	18
1.75La	181	190	19
2La	191	200	20
2.25La	201	210	21
2.5La	211	220	22
2.75La	221	230	23
3La	231	240	24
3.25La	241	250	25
3.5La	251	260	26
3.75La	261	270	27
Downstream 4La	271	280	28

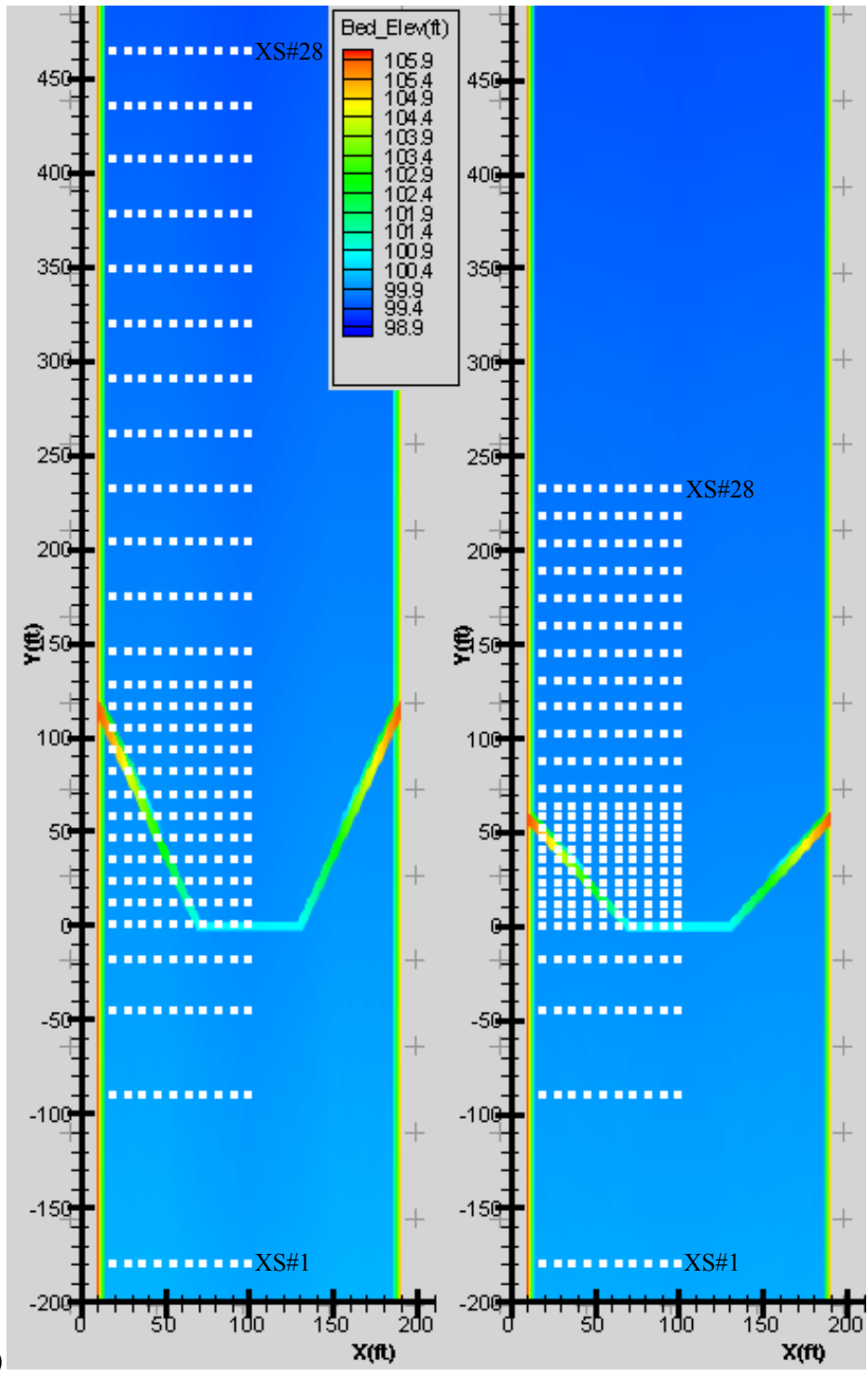


Figure 4.12 – Example of sample point distribution used in comparing flow patterns between numerical model simulations a) structure configuration1 ($L_a/L_{a_{ref}}=1$) and b) structure configuration2 ($L_a/L_{a_{ref}}=1/2$).

Using the sampling point distribution described above, water surface elevation, velocity, and bed shear stress data were extracted from the 3D numerical modeling results for each configuration. Through the analysis process, changes in local flow patterns such as variations in velocity and bed shear stress distributions and stage-discharge relationships related to variations in U-weir structure geometry were investigated.

5 DATA ANALYSIS AND RESULTS

5.1 INTRODUCTION

Utilizing the testing matrix described in Section 4.1, thirty three unique weir configurations were generated and numerically modeled at five different flow rates ($1/10Q_{bkf}$, $1/5Q_{bkf}$, $1/3Q_{bkf}$, $2/3Q_{bkf}$, and Q_{bkf}) for a total of 165 test cases. Output from the numerical modeling was analyzed to quantify the effects that variations in structure geometry had on upstream water surface elevation, downstream velocity magnification, and maximum bed shear stress magnification. Throughout the analysis process it should be noted that since all the structures tie-in at the bankfull channel elevation, a change in drop height or throat width directly affects the arm angle and arm slope that are associated with a given structure arm length. Due to this intercorrelation, each arm length ratio (0.5, 1, and 2) produces a range of arm angles and arm slopes associated with variations in drop height and throat width. Figure 5.1 provides a depiction of the U-weir parameters and channel definitions used in the analysis and results described in the following sections.

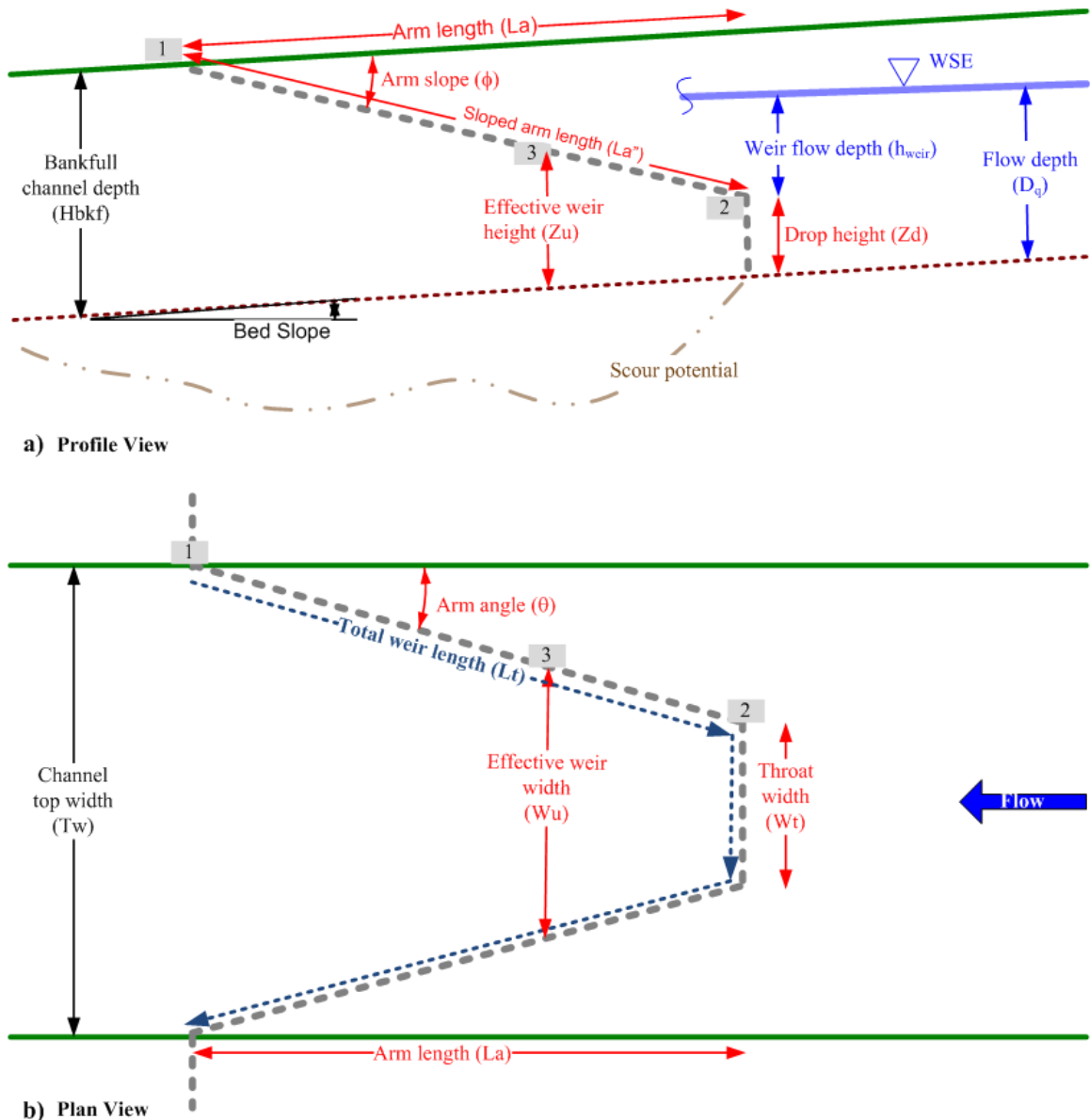


Figure 5.1 – Depiction of channel and U-weir parameters a) profile view and b) plan view.

Each structure configuration provides varying degrees of flow redirection over the weir crest and flow constriction within the channel. Sections 5.2 and 5.3 discuss how variations in structure geometry affected the hydraulic conditions upstream and downstream of the structure. Section 5.4 describes the analysis and development of the stage-discharge relationship for estimating the backwater effects associated with various U-weir geometries and Section 5.5 provides a summary of the analysis.

5.2 EFFECTS OF STRUCTURE GEOMETRY ON UPSTREAM FLOW DEPTH

As mentioned in Section 4.4, when conducting an analysis of flow patterns associated with differing structure geometries, a common reference point or plane must be identified to compare the results from one configuration to another. Utilizing the sample point distribution described in section 4.4, upstream water surface elevation and associated flow depth were identified in the center of the channel at a location one quarter of the channel top width upstream from the weir. Comparing the flow depth upstream of the weir for each configuration and specified flow rate provided insight about how variations in structure geometry affect upstream water surface elevations. To compare how variations in structure geometry alter the flow depth upstream of the weir, normal depth was calculated using Manning's equation (Equation 5.1) for each of the three channels and five discharges to determine the channel flow depths with no structure.

$$Q = \frac{\Phi}{n} (b \cdot y_n) (S_o)^{1/2} \left(\frac{b \cdot y_n}{b + 2 y_n} \right)^{2/3} \quad \text{Equation 5.1}$$

Where:

y_n = normal depth;

n = Manning's roughness coefficient calculated using Strickler's relationship ($n=0.421 \cdot d_{50}^{1/6}$);

Q = discharge;

b = channel width;

S_o = bed slope; and

Φ = conversion coefficient, 1 for SI units and 1.486 for English units.

Using the calculated normal depth from each configuration as a base line reference for pre-structure conditions, the ratio of the flow depth upstream of the weir divided by the reference pre-structure normal depth was used to determine the relative

increase in flow depth (i.e. flow depth magnification) caused by the structure as described in Equation 5.2.

$$\eta_{depth} = \frac{D_q}{D_{nref}} \quad \text{Equation 5.2}$$

Where:

η_{depth} = upstream flow depth magnification;

D_q = flow depth at $0.25 \cdot T_w$ upstream of the weir for a given discharge; and

D_{nref} = reference flow depth associated with normal depth conditions (y_n) with no structure present.

The effects that variations in structure arm length, throat width, and drop height had on the upstream flow depth magnification is presented in Figure 5.2 for each of the five discharge ratios. The greatest flow depth magnification occurred at the lowest range of flows and varied from 1.19 to 2.95 times the pre-structure normal flow depth condition. At the higher range of flows (i.e. bankfull discharge) the effects of variations in structure geometry on flow depth magnification were much less (1.03 to 1.52).

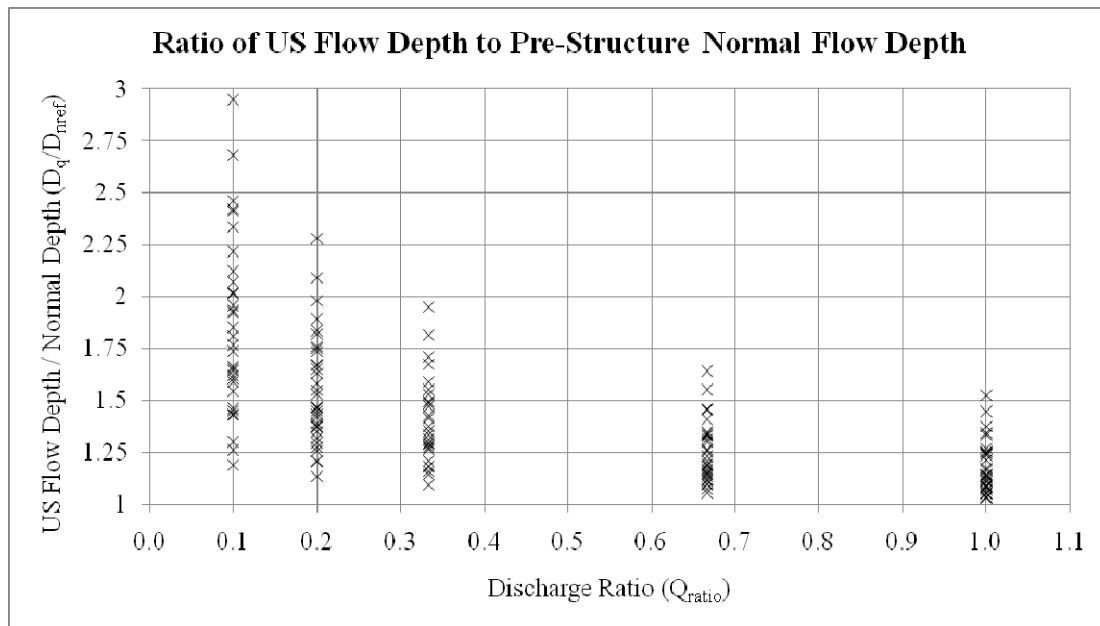


Figure 5.2 – Flow depth magnification associated with variation in structure geometry at five different discharge ratios.

At the higher flows variations in structure geometry have less of an impact on the upstream flow depth compared to the lower flows (i.e. $0.1Q_{bkr}$) where the effects of changes in structure drop height, arm length, and throat width are much more predominant. To understand how variations in structure geometry affected flow depth magnification at each flow rate, the minimum and maximum flow depth magnifications were determined for each structure parameter and are summarized in Table 5.1.

Table 5.1 – Range of flow depth magnification for each flow range and structure configuration (highest value in red and lowest value in blue).

	ds=22.6mm		ds=90.51mm		ds=181mm		$Z_d=0.12$		$Z_d=0.24$		$Z_d=0.366$	
	min	max	min	max	min	max	min	max	min	max	min	max
D_q/D_{nref} (all flows included)	1.03	2.02	1.04	2.42	1.07	2.95	1.03	2.01	1.05	2.33	1.06	2.95
D_q/D_{nref} ($1.0Q_{bkr}$)	1.03	1.21	1.04	1.34	1.07	1.52	1.03	1.33	1.05	1.37	1.06	1.52
D_q/D_{nref} ($0.6Q_{bkr}$)	1.06	1.30	1.07	1.46	1.10	1.64	1.06	1.41	1.10	1.45	1.10	1.64
D_q/D_{nref} ($0.3Q_{bkr}$)	1.09	1.47	1.14	1.71	1.18	1.95	1.09	1.59	1.18	1.67	1.18	1.95
D_q/D_{nref} ($0.2Q_{bkr}$)	1.13	1.67	1.21	1.98	1.26	2.28	1.13	1.74	1.27	1.89	1.32	2.28
D_q/D_{nref} ($0.1Q_{bkr}$)	1.19	2.02	1.30	2.42	1.43	2.95	1.19	2.01	1.46	2.33	1.62	2.95
	$W_t/T_w=0.25$		$W_t/T_w=0.3$		$W_t/T_w=0.5$		$La_{ref}=0.5$		$La_{ref}=1$		$La_{ref}=2$	
	min	max	min	max	min	max	min	max	min	max	min	max
D_q/D_{nref} (all flows included)	1.07	2.95	1.05	2.33	1.03	2.68	1.08	2.95	1.11	2.22	1.03	2.46
D_q/D_{nref} ($1.0Q_{bkr}$)	1.07	1.52	1.05	1.37	1.03	1.45	1.08	1.52	1.11	1.27	1.03	1.27
D_q/D_{nref} ($0.6Q_{bkr}$)	1.12	1.64	1.10	1.45	1.06	1.55	1.11	1.64	1.17	1.35	1.06	1.34
D_q/D_{nref} ($0.3Q_{bkr}$)	1.21	1.95	1.18	1.67	1.09	1.82	1.16	1.95	1.27	1.55	1.09	1.55
D_q/D_{nref} ($0.2Q_{bkr}$)	1.30	2.28	1.27	1.89	1.13	2.09	1.21	2.28	1.38	1.76	1.13	1.84
D_q/D_{nref} ($0.1Q_{bkr}$)	1.43	2.95	1.46	2.33	1.19	2.68	1.26	2.95	1.59	2.22	1.19	2.46

The greatest flow depth magnification was associated with the structure geometry that provided the largest flow constriction which relates to the structure with the greatest drop height, shortest arm length, and narrowest throat width ($Z_d=0.366m$, $La=0.5*La_{ref}$, and $W_t=0.25*T_w$). This structure configuration provided the greatest flow depth magnification for each of the five flow ranges, especially during the lowest flow ($0.1Q_{bkr}$) when the structure drop height becomes greater than the normal depth of flow in the channel (Figure 5.3). From Figure 5.3 it can be shown that for a given drop height and throat width, decreasing the arm length from $2*La_{ref}$ (solid markers) to $0.5*La_{ref}$ (open

markers) increased the flow depth magnification. By decreasing the arm length, the slope of the arm must be increased in order to tie-in at the bankfull elevation resulting in a greater flow constriction and increased backwater effects. At low flows, the additional increase in flow depth magnification caused by altering the length of the structure arm ranged from 6 to 26 percent. Similarly, for a given drop height and arm length, decreasing the throat width from $0.5 \cdot T_w$ to $0.25 \cdot T_w$ (variation within series markers, example shown in Figure 5.3) increased the flow depth magnification. At low flows, this additional increase in flow magnification by altering the throat width ranged from 2 to 26 percent.

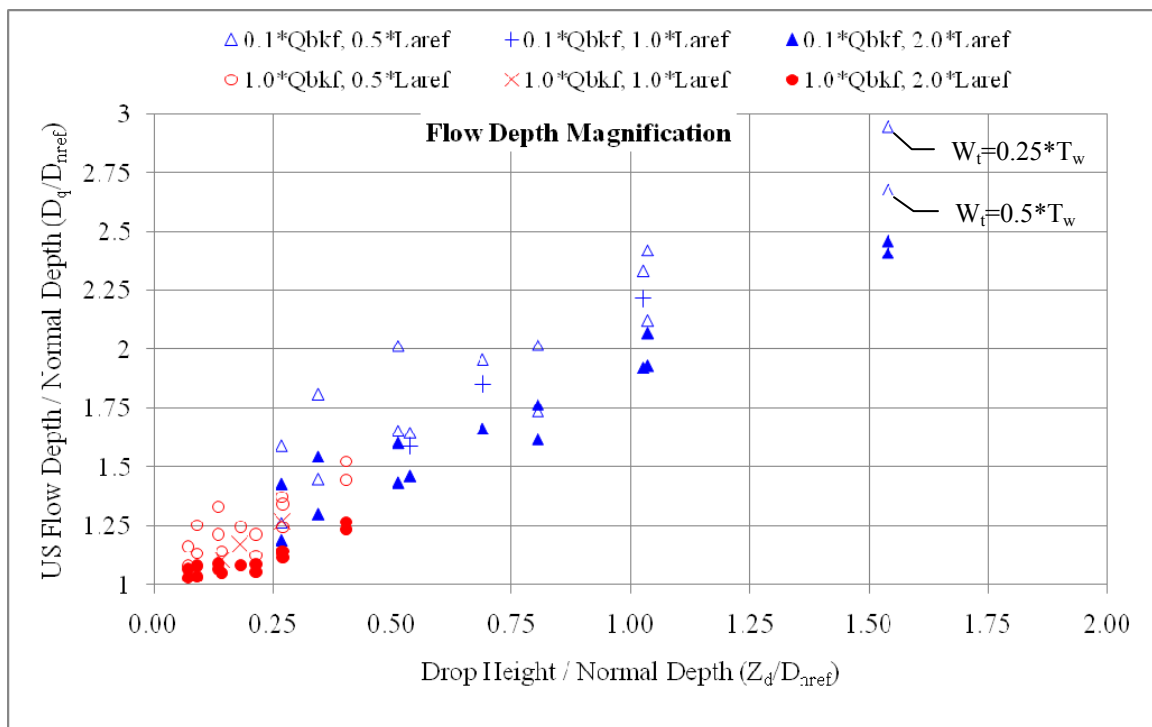


Figure 5.3 – Comparison of flow depth magnification at $1.0Q_{bkf}$ and $0.1Q_{bkf}$ for each structure configuration.

The range of flow depth magnification that was found to be associated with changes in structure geometry provides insight into how numerous structure parameters might be adjusted to provide the necessary water elevation for irrigation diversions and/or

tailwater conditions for an upstream structure. Results of the flow depth magnification analysis show that for the range of conditions tested, the depth of flow upstream of U-weirs was altered by 1.03 to 2.95 times the pre-structure flow depths. Being able to estimate the depth of flow upstream of U-weirs based on structure geometry and channel discharge is essential in designing rock weirs. Due to the complexity and intercorrelations associated with variations in weir geometries and related effects on local hydraulics (i.e. flow depth magnification), the applicability of stage-discharge relationships associated with U-weirs was investigated. The analysis and results of the stage-discharge comparison as well as the development of new stage-discharge relationships utilizing results from the current study are described in Section 5.4. The following section describes how variations in structure geometry affected the hydraulic conditions (i.e. velocity and bed shear stress) downstream of U-weirs.

5.3 EFFECTS OF STRUCTURE GEOMETRY ON VELOCITY AND BED SHEAR STRESS

As water flows over a U-weir it is redirected at a right angle to the structure crest and results in a concentration of flow in the center of the channel and away from the stream banks (Figure 5.4). As a result, near bank velocities and bed shear stresses are reduced while those in the middle of the channel are increased. The magnitude and location of these increases are important in the design of rock weirs because they can affect sediment transport through the structure, scour development, fish passage, and overall structure performance. To determine the location and magnitude of the maximum velocity and bed shear stress downstream of the U-weir for each structure configuration, the sample point distribution described in Section 4.4 was used. Identifying the maximum

velocity and bed shear stress for each configuration provided a method for analyzing how variations in structure geometry altered the local flow patterns.

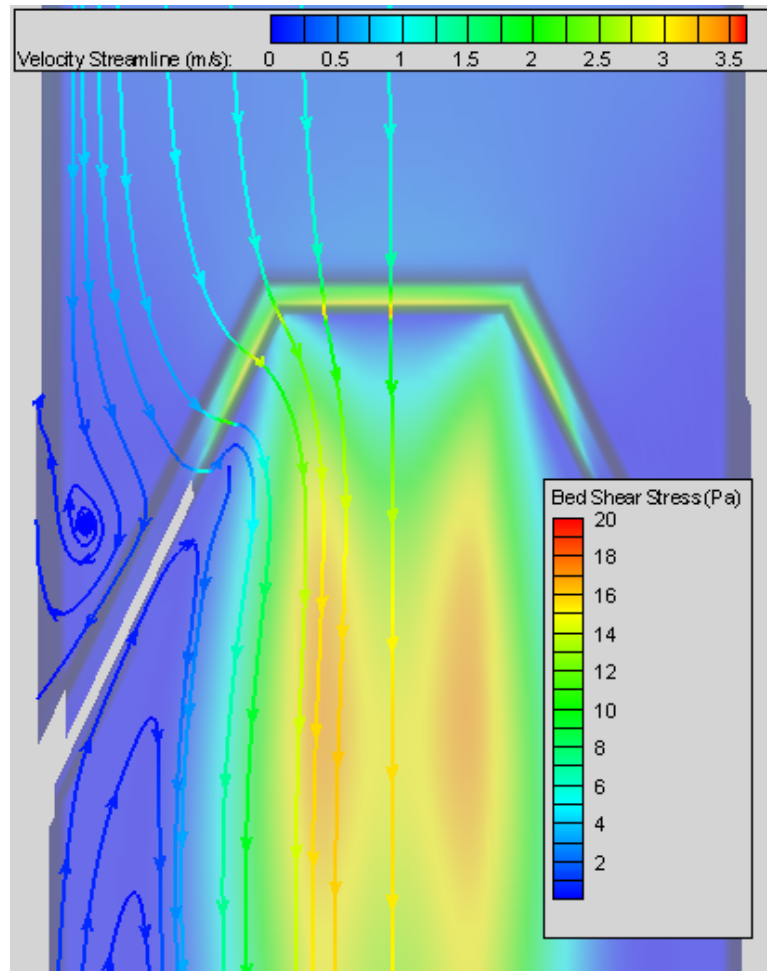


Figure 5.4 – Example of flow redirection over weir crest and increase in mid-channel velocity streamlines and bed shear stress associated with U-weir.

The maximum velocity and bed shear stress for each configuration was used to calculate the ratio of maximum velocity divided by pre-structure reference velocity and maximum bed shear stress divided by the critical shear stress associated with the median bed material size as described in Equations 5.3 and 5.4.

$$\eta_{v\max} = \frac{V_{\max}}{V_o} \quad \text{Equation 5.3}$$

$$\eta_{\tau \max} = \frac{\tau_{\max}}{\tau_c} \quad \text{Equation 5.4}$$

Where:

$\eta_{v\max}$ = maximum velocity magnification;

$\eta_{\tau\max}$ = maximum critical shear stress magnification;

V_{\max} = maximum channel velocity;

V_o = channel velocity associated with normal depth conditions (i.e. no structure);

τ_{\max} = maximum bed shear stress; and

τ_c = critical shear stress (i.e. incipient motion) for a specified bed material grain size ($\tau_c = 0.5 * (\gamma_s - \gamma_w) * d_{50}$).

The effects that variations in structure arm length, throat width, and drop height had on velocity and bed shear stress magnification downstream of the U-weirs are described in sections 5.3.1 and 5.3.2 respectively.

5.3.1 VELOCITY MAGNIFICATION

The maximum velocity magnification (V_{\max}/V_o) was calculated utilizing equation 5.3 described above for each numerical simulation to quantify the effects that variations in structure geometry had on velocity distributions downstream of U-weirs. Since the maximum velocity magnification is dependent on the reference velocity associated with pre-structure conditions for a given discharge, each flow ratio provides insight into the effects that variations in structure geometry have at each flow rate. Similar to the flow depth magnification, the greatest velocity magnification occurred at the lowest range of flows and varied from 1.72 to 4.04 times the reference channel velocity with no structure present (Figure 5.5).

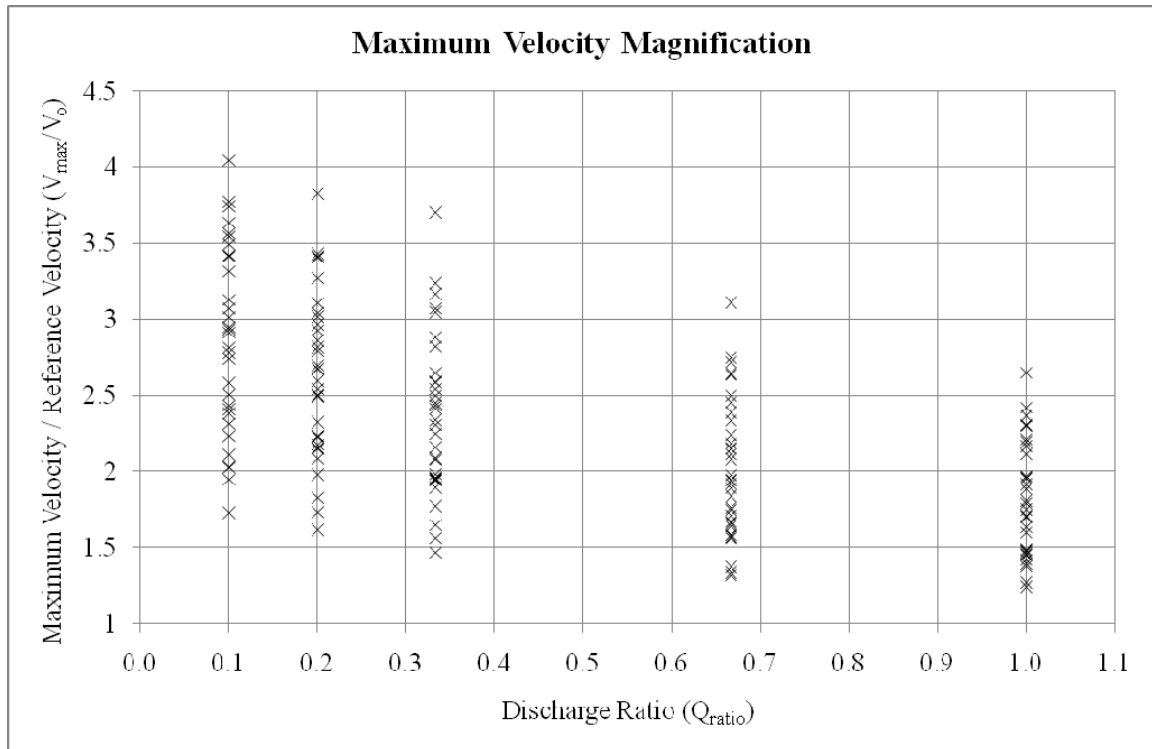


Figure 5.5 – Maximum velocity magnification associated with variation in structure geometry at five different discharge ratios.

At the higher range of flows (i.e. bankfull discharge) the effects of variations in structure geometry on maximum velocity magnification were much less (1.24 to 2.64). Figure 5.6 shows the velocity magnification associated with a 1/3 bankfull flow and varying structure arm length while holding throat width and drop height constant. From Figure 5.6 it is evident that reducing the length of the structure arm increases the mid-channel velocities significantly due to the increased flow constriction and redirection of flow. The maximum velocity magnification for the shorter weir arm length ($L_a=0.5*L_{a_{ref}}$) was 40% greater than that of the longer weir arm ($L_a=2.0*L_{a_{ref}}$). Table 5.2 provides a summary of the maximum velocity magnification for each U-weir configuration and associated discharge.

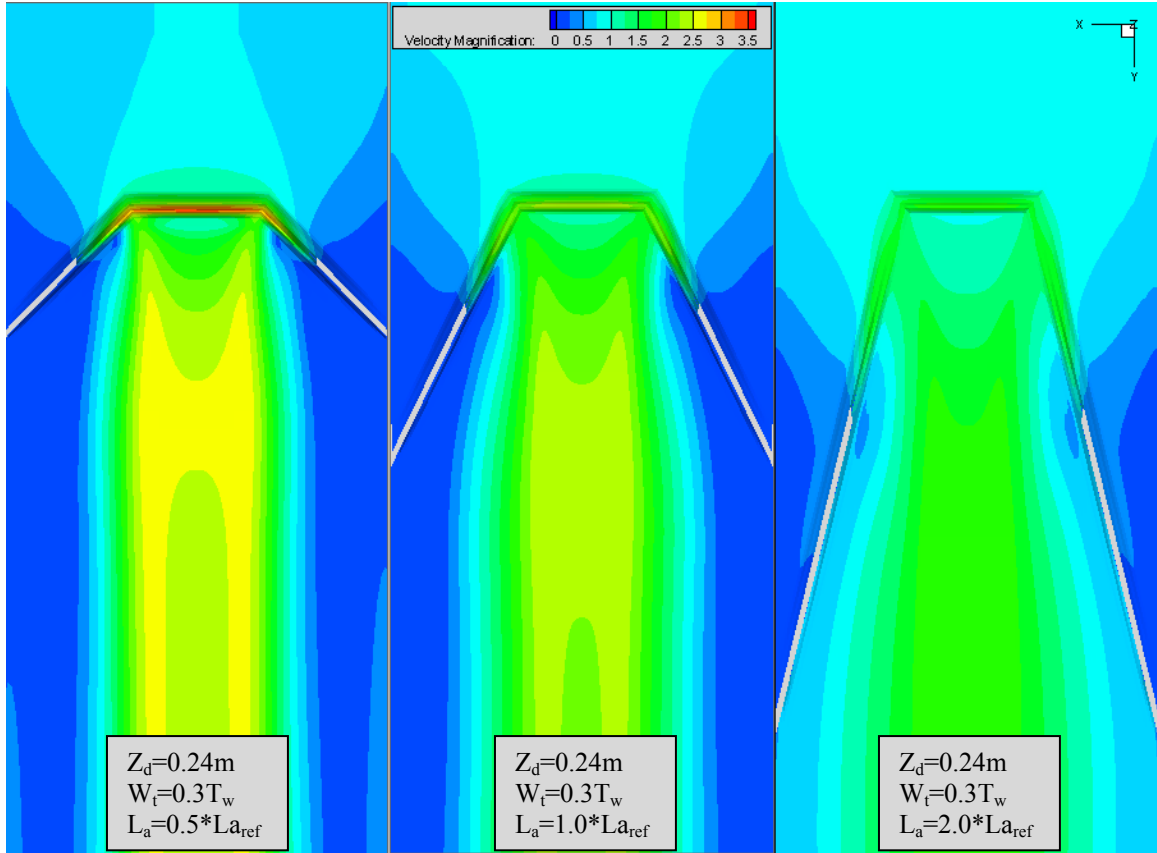


Figure 5.6 – Velocity magnification associated with variation in structure arm length at $1/3Q_{bkf}$.

Table 5.2 – Range of maximum velocity magnification for each discharge ratio.

	ds=22.6mm		ds=90.51mm		ds=181mm		Zd=0.12		Zd=0.24		Zd=0.366	
	min	max										
V_{max}/V_o (all flows included)	1.24	3.82	1.24	3.63	1.27	4.04	1.24	3.74	1.46	3.56	1.37	4.04
V_{max}/V_o ($1.0Q_{bkf}$)	1.24	1.65	1.24	2.42	1.27	2.29	1.24	2.36	1.46	2.30	1.37	2.65
V_{max}/V_o ($0.6Q_{bkf}$)	1.37	3.11	1.33	2.75	1.32	2.63	1.32	2.72	1.66	2.64	1.57	3.11
V_{max}/V_o ($0.3Q_{bkf}$)	1.64	3.70	1.56	3.24	1.17	3.07	1.47	3.17	1.89	3.04	1.94	3.70
V_{max}/V_o ($0.2Q_{bkf}$)	1.83	3.82	1.73	3.41	1.61	3.41	1.61	3.43	2.15	3.27	2.15	3.82
V_{max}/V_o ($0.1Q_{bkf}$)	2.03	3.77	1.94	3.63	1.73	4.04	1.73	3.74	2.41	3.56	2.02	4.04
	Wt/Tw=0.25		Wt/Tw=0.3		Wt/Tw=0.5		Laref=0.5		Laref=1		Laref=2	
	min	max										
V_{max}/V_o (all flows included)	1.42	4.04	1.46	3.56	1.24	3.54	1.70	4.04	1.81	3.41	1.24	3.49
V_{max}/V_o ($1.0Q_{bkf}$)	1.42	2.65	1.46	2.30	1.24	1.97	1.70	2.65	1.81	1.91	1.24	1.70
V_{max}/V_o ($0.6Q_{bkf}$)	1.56	3.11	1.66	2.64	1.32	2.18	1.83	3.11	2.08	2.24	1.32	1.97
V_{max}/V_o ($0.3Q_{bkf}$)	1.77	3.70	1.89	3.04	1.47	2.54	1.96	3.70	2.34	2.65	1.47	2.58
V_{max}/V_o ($0.2Q_{bkf}$)	1.98	3.82	2.15	3.27	1.61	3.02	2.08	3.82	2.59	2.97	1.61	2.93
V_{max}/V_o ($0.1Q_{bkf}$)	2.23	4.04	2.41	3.56	1.73	3.54	2.11	4.04	2.74	3.41	1.73	3.49

The maximum velocity magnification was associated with the structure geometry providing the greatest flow constriction ($Z_d=0.366$, $La_{ref}=0.5$, and $W_t=0.25$). This structure configuration provided the maximum velocity magnification for each of the five flow ranges with an average velocity magnification of 2.45 times the reference channel velocity for high flows and 3.81 times the reference channel velocity for low flows. Figure 5.7 shows that for a given drop height, decreasing the arm length from $2*La_{ref}$ to $0.5*La_{ref}$ increases the velocity magnification. The additional increase in velocity magnification ranged from 4 to 54 percent for low flows and 34 to 66 percent for the high flows. Similarly, decreasing the throat width from $0.5*T_w$ to $0.25*T_w$ (variation within series markers, example shown in Figure 5.7) provided an increase in velocity magnification. At low flows, the additional increase in velocity magnification associated with a narrower throat ranged from 14 to 62 percent and 11 to 35 percent for the high flows.

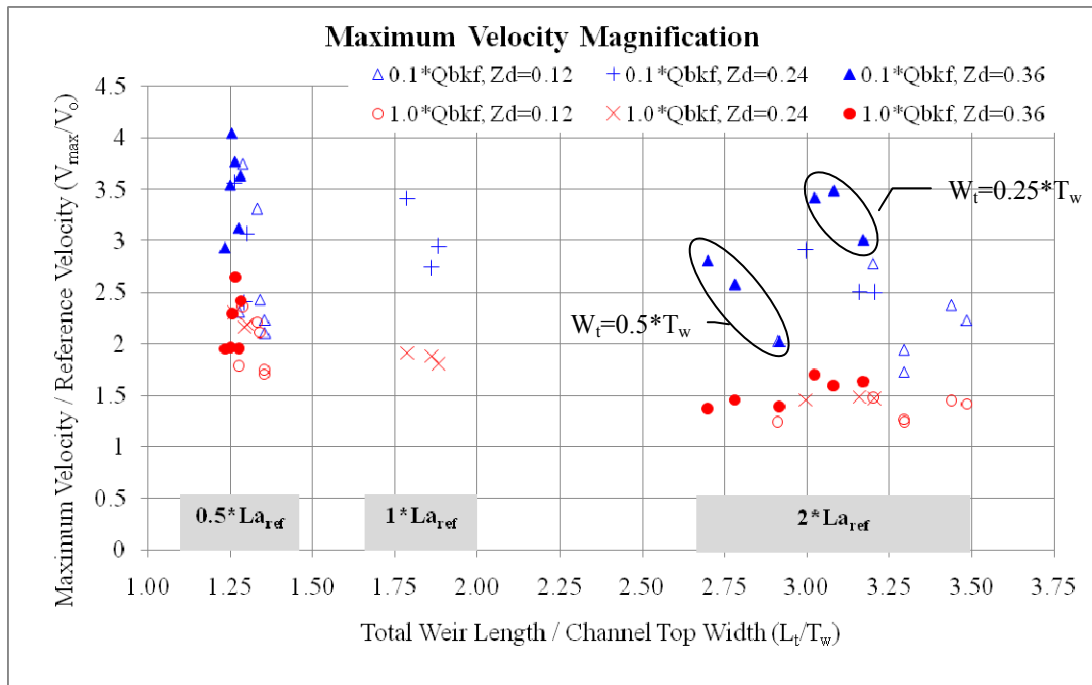


Figure 5.7 – Maximum velocity magnification comparison between $0.1Q_{bkf}$ and Q_{bkf} for variations in structure geometry.

Variations in structure geometry not only affect the magnitude of the maximum velocity magnification but also the distribution of flows downstream of the weir. Figure 5.6 shows that velocities downstream of the U-weir converge creating a high velocity zone in the center of the channel. The resulting velocity distribution provides insight into how velocities near the bank and in the center of the channel may develop for a given weir geometry and how that might influence the stability of the structure, fish passage, and bank erosion. From Figure 5.8 it can be seen that a shorter structure arm ($L_a=0.5L_{a_{ref}}$) generally results in a greater flow constriction causing higher velocities to be focused in the center portion of the channel and located farther downstream from the structure crest compared to a structure with a longer arm ($L_a=2.0*L_{a_{ref}}$). It should be noted that since these results are for a simplified flat bed trapezoidal channel the velocity distributions and magnitudes presented are considered to be a conservative estimate and will vary as scour develops and alters the downstream channel geometry and resulting channel hydraulics.

Results of the velocity magnification analysis show that, for the range of conditions tested the velocity downstream from U-weirs was altered by 1.24 to 4.04 times the original channel velocity with no structure present. Identifying the location of the maximum velocity magnification provided insight into how varying structure geometry can have a large influence on where the maximum velocity occurs within the structure. For the conditions tested, the location of the maximum velocity magnification was found to vary from 0.1 to 1.5 times the arm length downstream of the structure crest by varying the geometry of the structure.

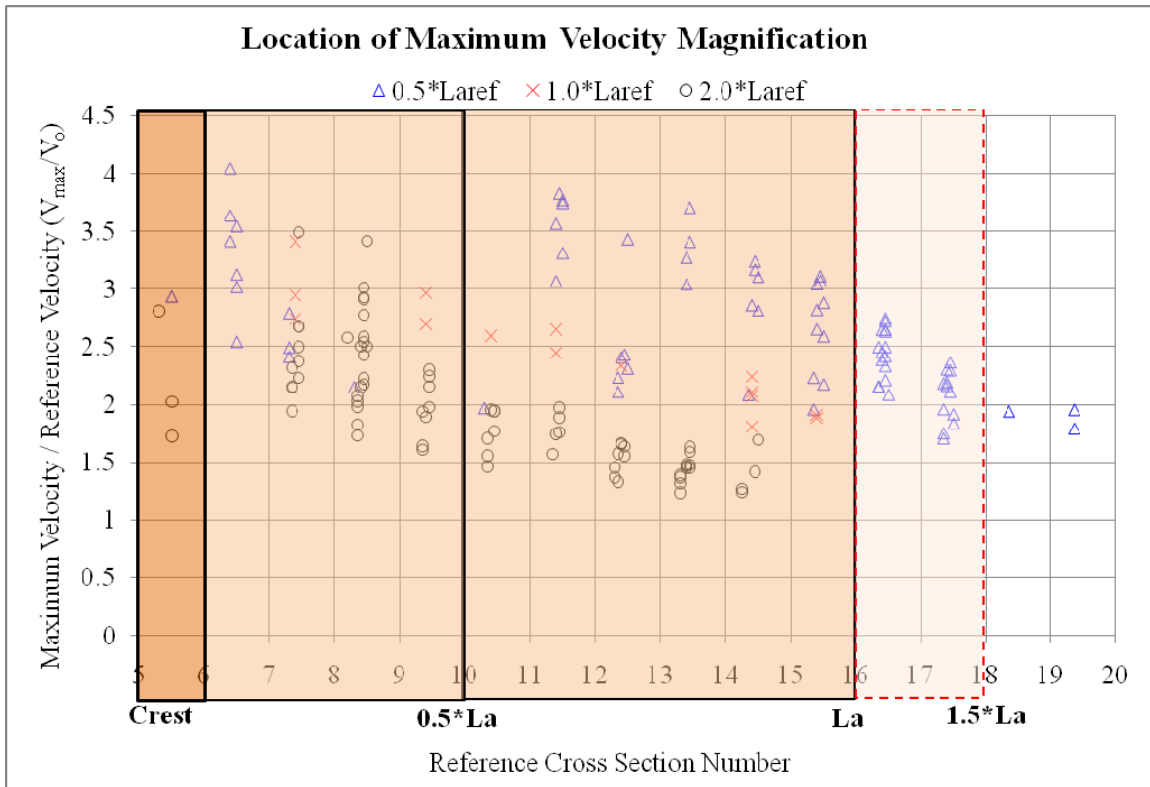


Figure 5.8 – Maximum velocity magnification location associated with variation in structure geometry.

Being able to estimate the differences in channel velocities associated with various U-weir geometries is important in the design process to ensure that the resulting hydraulic characteristics in and around the structure are within a specified design range and meet project goals.

5.3.2 BED SHEAR STRESS MAGNIFICATION

The maximum bed shear stress magnification (τ_{max}/τ_c) was calculated utilizing equation 5.4 described above for each numerical simulation to quantify the effects that variations in structure geometry had on bed shear stress distributions downstream of U-weirs. Since the maximum bed shear stress magnification is a function of critical shear stress (i.e. incipient motion) for a given bed material size, each flow ratio provides insight into the potential scour that may occur due to variations in structure geometry. From

Figure 5.9 it is evident that the largest bed shear stress magnification occurs at bankfull flow ($7.59 \cdot \tau_c$), with similar effects at the 2/3 bankfull flow ($7.32 \cdot \tau_c$). Maximum bed shear stress magnification for the lower flow ranges was much lower, between 0.28 and 3.5 times the critical shear stress. Therefore, analysis pertaining to maximum bed shear stress magnification and variations in structure geometry were conducted using the 2/3 bankfull and bankfull flow ranges for each of the three bed material sizes and associated channel geometry.

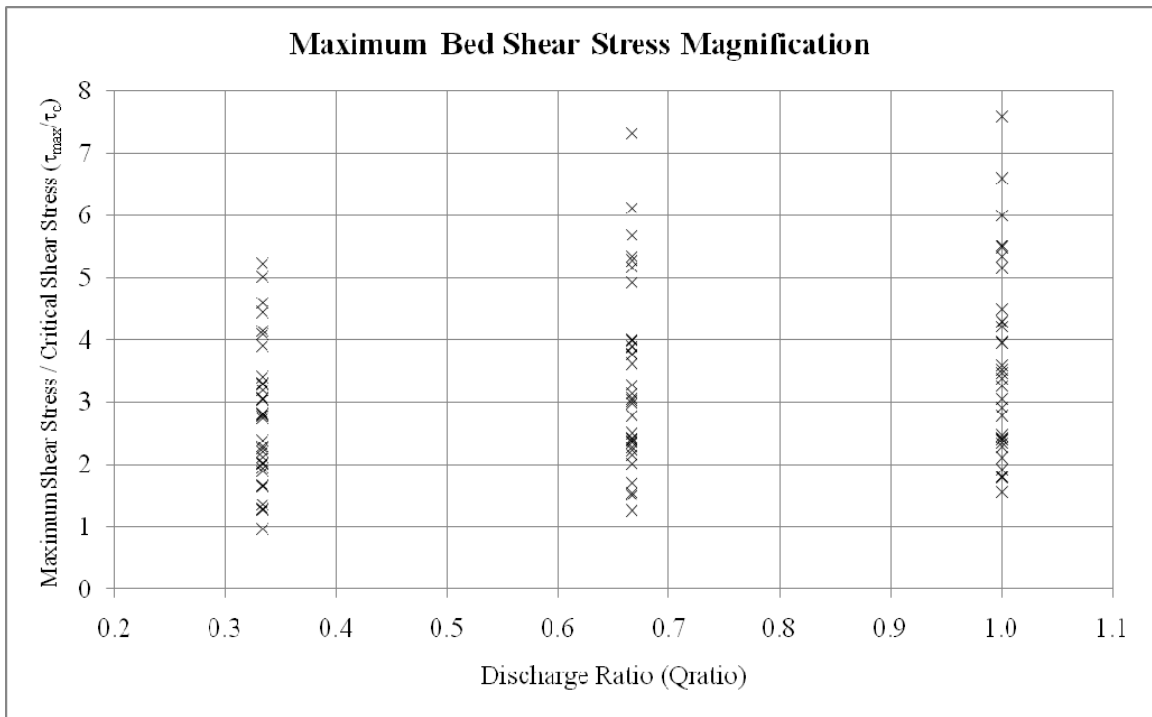


Figure 5.9 – Maximum bed shear stress magnification associated with variation in structure geometry.

Figure 5.10 shows the bed shear stress magnification associated with bankfull flow and varying structure arm length while holding throat width and drop height constant. From Figure 5.10 it is evident that reducing the length of the structure arm increases the bed shear stress significantly due to the increased flow constriction and redirection of flow toward the center of the channel. The maximum bed shear stress

magnification for the shorter weir arm length ($\eta_{\tau_{\max}}=4.29$) was approximately double that of the longer weir arm ($\eta_{\tau_{\max}}=2.11$). This is a result of the increase in flow constriction caused by the shorter arm length and greater arm slope forcing more flow through the center of the channel with a greater velocity.

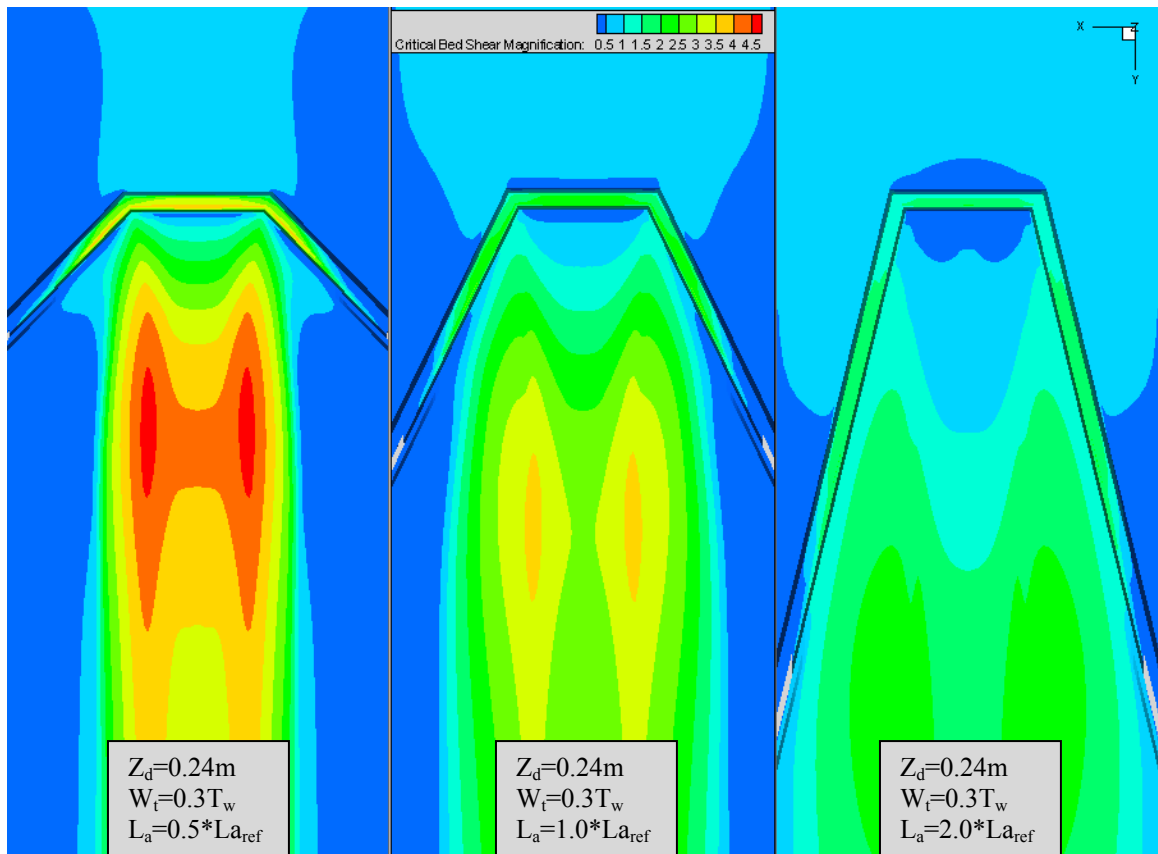


Figure 5.10 – Bed shear stress magnification associated with variation in structure arm length at Q_{bkf} .

To understand how variations in structure geometry affect the maximum bed shear stress magnification downstream of U-weirs, the range of maximum bed shear stress magnification for each configuration was calculated and is presented in Table 5.3 and Figure 5.11. From Figure 5.11 it is evident that variations in the structure geometry greatly affect the maximum bed shear stress and variability in scour potential downstream of U-weirs. The results show that for a given structure drop height and throat width,

maximum bed shear stress magnification can be increased 2 to 2.5 times by shortening the structure arm length from $2 \cdot L_{a_{ref}}$ to $0.5 \cdot L_{a_{ref}}$.

Table 5.3 – Range of maximum bed shear stress magnification for each structure configuration.

	ds=22.6mm		ds=90.51mm		ds=181mm		Zd=0.12		Zd=0.24		Zd=0.366	
	min	max										
τ_{max}/τ_c (all flows included)	1.28	7.59	1.24	6.47	0.96	5.36	0.96	6.00	1.65	5.48	1.94	7.59
τ_{max}/τ_c ($1.0Q_{bkf}$)	1.79	7.59	1.77	6.47	1.57	5.36	1.57	6.00	2.11	5.48	2.28	7.59
τ_{max}/τ_c ($0.6Q_{bkf}$)	1.54	7.32	1.48	6.01	1.26	5.29	1.26	5.68	2.02	5.33	2.15	7.32
τ_{max}/τ_c ($0.3Q_{bkf}$)	1.28	5.10	1.24	5.13	0.96	4.61	0.96	4.45	1.65	4.14	1.94	5.13
τ_{max}/τ_c ($0.2Q_{bkf}$) ¹	1.01	3.50	0.97	3.38	0.78	2.85	0.78	3.02	1.18	3.26	1.81	3.50
τ_{max}/τ_c ($0.1Q_{bkf}$) ¹	0.89	1.80	0.72	1.67	0.63	1.27	0.63	1.38	0.88	1.72	0.97	1.80

	Wt/Tw=0.25		Wt/Tw=0.3		Wt/Tw=0.5		Laref=0.5		Laref=1		Laref=2	
	min	max										
τ_{max}/τ_c (all flows included)	1.35	7.59	1.65	5.48	0.96	4.41	1.67	7.59	2.39	4.00	0.96	3.27
τ_{max}/τ_c ($1.0Q_{bkf}$)	1.92	7.59	2.11	5.48	1.57	4.41	2.79	7.59	3.39	3.96	1.57	3.20
τ_{max}/τ_c ($0.6Q_{bkf}$)	1.71	7.32	2.02	5.33	1.26	3.92	2.38	7.32	3.07	4.00	1.26	3.27
τ_{max}/τ_c ($0.3Q_{bkf}$)	1.35	5.13	1.65	4.14	0.96	3.41	1.67	5.13	2.39	3.30	0.96	3.19
τ_{max}/τ_c ($0.2Q_{bkf}$) ¹	1.08	3.50	1.26	2.87	0.78	2.23	1.34	3.50	1.96	3.10	0.78	2.84
τ_{max}/τ_c ($0.1Q_{bkf}$) ¹	0.86	1.80	1.04	1.26	0.63	1.24	1.01	1.80	1.40	1.63	0.63	1.16

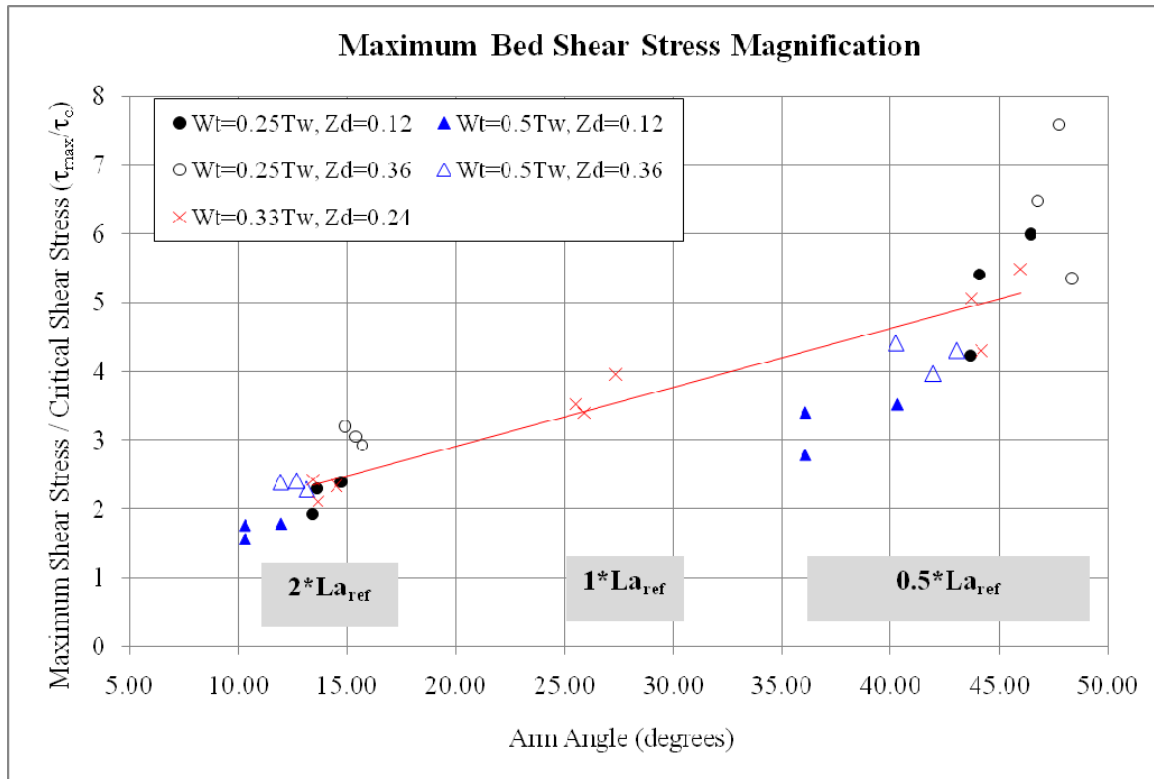


Figure 5.11 – Maximum bed shear stress magnification comparison between variations in arm angle, throat width, and drop height at bankfull flow.

Variations in structure geometry not only affect the magnitude of the maximum bed shear stress but also where it is located and the overall bed shear stress distribution downstream of the weir. Figure 5.10 showed bed shear stresses were higher in two distinct pockets located on each side of the channel centerline. Scour development measured in the laboratory by Scurlock (2009) showed a similar phenomenon with two distinct scour holes located downstream of the weir crest located on either side of the channel centerline (previously shown in Figure 3.31). The resulting bed shear stress distribution provides insight into how scour may develop for a given weir geometry and how that might influence the stability of the structure. From Figure 5.10 it can be seen that a shorter structure arm ($L_a=0.5L_{a_{ref}}$) results in higher bed shear which is focused in the center portion of the channel and further from the structure crest compared to the structure with a longer arm ($L_a=2.0*L_{a_{ref}}$). Similarly, Figure 5.12 shows that as structure arm length is increased, the maximum bed shear stress magnification is decreased and is located closer to the structure crest. It should be noted that since these results are for a simplified flat bed trapezoidal channel the bed shear stress distributions and magnitudes presented are considered to be a conservative estimate and will vary as scour develops and alters the downstream channel geometry. The development of scour downstream of the structure results in an increased flow depth which provides additional energy dissipation and a reduction in shear stress along the bed. Observations from the laboratory testing conducted at Colorado State University found that scour downstream of rock weirs tended to progress in stages; an initial rapid phase immediately after installation followed by development, stabilization and, eventually, an equilibrium phase.

The final equilibrium scour configuration will depend on inflowing sediment, magnitude and duration of the flows encountered, and the geometry of the rock weir.

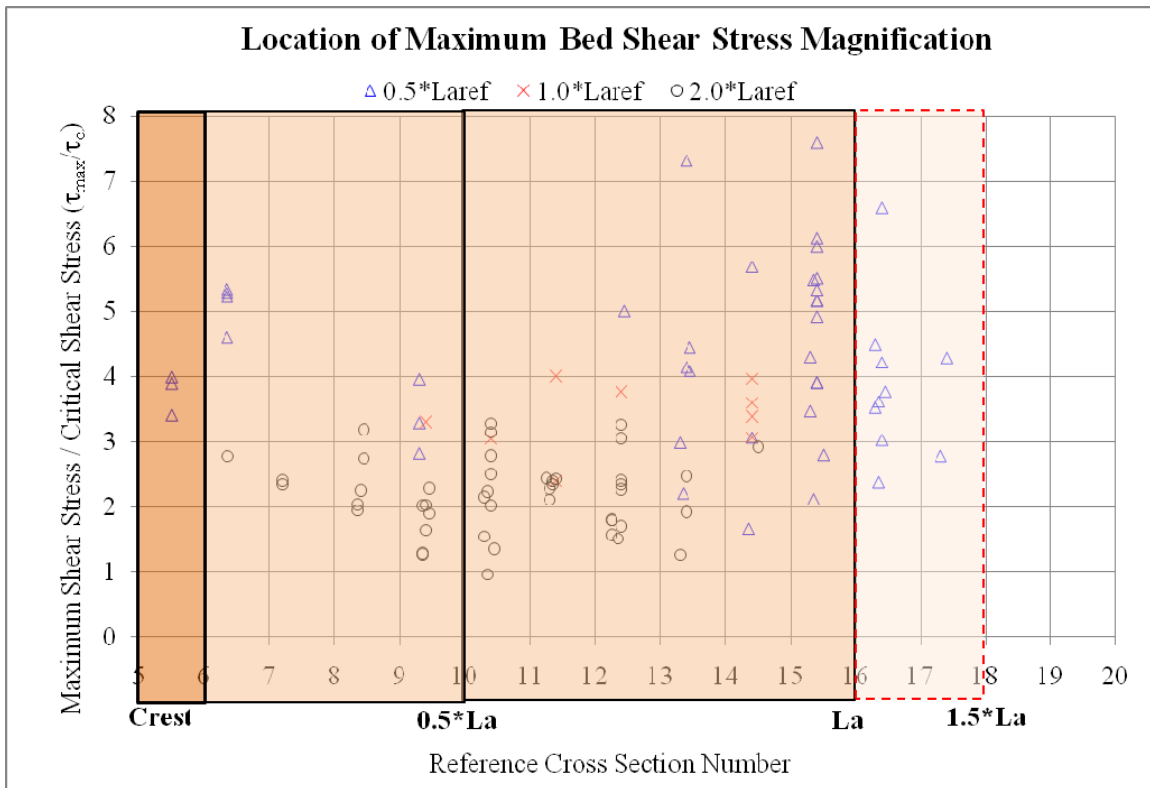


Figure 5.12 – Maximum bed shear stress magnification location associated with variation in structure geometry for flows greater than $1/3Q_{bkf}$.

Results of the bed shear stress magnification analysis show that, for the range of conditions tested the maximum bed shear stress downstream from U-weirs was altered by 1.57 to 7.59 times the critical bed shear stress. Identifying the location of the maximum bed shear stress magnification provided insight into how varying structure geometry can have a large influence on where initial scour might occur within the structure. For the conditions tested, the location of the maximum bed shear stress magnification was found to vary from 0.1 to 1.25 times the arm length downstream of the structure crest depending on the geometry of the structure. Being able to compare the location and differences in channel bed shear stress associated with various weir geometries is important in the

design process to ensure that the structure is not undermined by scour and is able to maintain sediment transport through the reach and the structure itself. While the current study did not include mobile bed simulations or investigate variations in pre-excavated scour holes downstream from rock weirs, it does provide a process based method for understanding how varying structure geometry alone alters local flow patterns.

5.4 STAGE-DISCHARGE RELATIONSHIP FOR ROCK WEIRS

The stage upstream of structures is an important variable used to determine water surface elevations required by irrigation diversions and when multiple weirs are used in series. A stage-discharge relationship allows a designer to estimate stage upstream of a structure for diversion purposes in addition to spacing between structures to ensure that tail water conditions for an upstream structure are met. The following sections describe the stage-discharge analysis and results. Section 5.4.1 identifies current stage-discharge relationships for U-weirs developed by Ruttenburg (2007), Meneghetti (2009), and Thornton et al. (2011) and describes their applicability to the current study. Section 5.4.2 describes modifications that were made to the equation developed by Thornton et al. (2011) to increase the range of applicability to the current study as well as the development of a new stage-discharge relationship utilizing results from the numerical modeling. Finally, Section 5.4.3 provides a comparison of predicted weir flow depth utilizing the new stage-discharge relationship with measured field and laboratory data.

5.4.1 APPLICABILITY OF EXISTING EQUATIONS

A review of the literature pertaining to stage-discharge relationships associated with river spanning rock weirs found three recent studies that specifically addressed this topic. Studies by Ruttenburg (2007), Meneghetti (2009), and Thornton et al. (2011)

developed stage-discharge relationships specifically related to river spanning rock weirs. Ruttenburg (2007) developed a stage-discharge relationship for U-weirs using measured field data for three sites along Beaver Creek in north central Washington. The equations developed by Ruttenburg (2007) were designed to calculate the discharge in the river based on the geometry of the weir, specifically the wetted weir length along the weir crest. However, his equations cannot be utilized in the design process since the wetted weir length is a function of the weir geometry and water stage, which is the variable we are trying to predict. Therefore, the equation developed by Ruttenburg (2007) is not included in the analysis.

The equations developed by Meneghetti (2009) and Thornton et al. (2011) were specifically developed using laboratory data to calculate the upstream flow depth for a given weir geometry and flow rate. Since both of the equations utilize variables that can be determined prior to construction of a rock weir, they can be used in the design process to estimate whether a given weir geometry provides the appropriate water elevation upstream of the weir to meet project goals. Using the stage-discharge relationships developed by Meneghetti (2009) and Thornton et al. (2011), flow depth upstream of the weir was calculated using Equations 5.5 and 5.8 respectively.

$$\text{Meneghetti (2009) } y_{us} = 0.830 \left(Q \frac{y_n}{L_t} \right)^{0.223} \left(\frac{L_a''}{L_a} \right) \quad \text{Equation 5.5}$$

$$L_a'' = \left(\frac{(T_w - W_t)}{2} \cdot \frac{1}{\sin \theta \cdot \cos \phi} \right) \quad \text{Equation 5.6}$$

$$L_t = W_t + 2 \cdot L_a'' \quad \text{Equation 5.7}$$

Where:

y_{us} = water depth upstream of rock weir;

Q = channel flow rate (discharge);

y_n = normal depth;

L_a = sloped weir arm length, function of structure geometry;

L_t = total weir length, function of the structure geometry; and

L_a = weir arm length.

$$\text{Thornton et al. (2011)} \quad y_{us} = \left(\frac{Q}{\frac{2}{3} L_t \cdot C_d \cdot \sqrt{2g} \cdot} \right)^{\frac{2}{3}} + Z_u \quad \text{Equation 5.8}$$

$$C_d = 0.652 \cdot \left(\frac{D_{50}}{Z_u} \right)^{-0.708} \left(\frac{L_t}{T_w} \right)^{0.587} \quad \text{Equation 5.9}$$

$$Z_u = \frac{1}{3} \left(\frac{(T_w - W_t)}{2} \cdot \frac{\tan \phi}{\sin \theta} \right) + Z_d \quad \text{Equation 5.10}$$

Where:

C_d = contraction coefficient for weir crest profile length;

g = acceleration due to gravity;

D_{50} = mean weir rock width;

T_w = stream width;

Z_u = effective weir height, function of the structure geometry;

W_t = weir throat width;

Z_d = structure drop height; and all other terms previously defined.

The depth of flow over the weir (h_{weir}) was determined using the upstream flow depth and corresponding structure drop height as described in Equation 5.11 below:

$$h_{weir} = Y_{us} - Z_d \quad \text{Equation 5.11}$$

Where:

h_{weir} = flow depth over the weir crest;

Y_{us} = flow depth at a location $0.25 \cdot T_w$ upstream of the weir crest; and

Z_d = structure drop height.

Computed weir flow depths were compared with output from the numerical model simulations to examine the applicability of existing U-weir stage-discharge equations to the range of parameters included in the current study. Table 5.4 provides a summary of the range of variables from the laboratory data used by Meneghetti (2009) and Thornton et al. (2011) and the range of variables utilized in the current study. Table 5.4 shows that both the laboratory and field data fall within the range of values examined in the numerical model testing.

Table 5.4 – Range of variables from laboratory data, field data, and numerical model.

	Numerical Model current study		Laboratory Data Meneghetti (2009) and Thornton et al. (2011)		Field Data Holburn et al. (2009a and 2009b)	
	<i>min</i>	<i>max</i>	<i>min</i>	<i>max</i>	<i>min</i>	<i>max</i>
Bankfull Q_{ratio}	0.1	1	0.33	1	N/A	
Discharge - Q (cms)	3.6	162	22.5	90	6.5	87.78
Grain Size - d_s (mm)	22.63	181	22.63	90.51	43	162
Bed Slope - S_o	0.001	0.01	0.0021	0.0047	0.004	0.014
Bankfull Depth - H_{bkf} (m)	1.015	1.85	0.73	1.36	0.53	1.82
Channel Top Width - T_w (m)	19.2	55	21.25	28	8.62	42.6
Weir D50 (m)	0.61	1.22	1	1.11	0.68	1.2
Drop Height - Z_d (m)	0.122	0.366	0.24	0.24	0	0.52
Throat Width - W_t (m)	4.8	27.5	7.08	9.33	4.059	12.02
W_t/T_w	0.25	0.5	0.33	0.33	0.11	0.65
Arm Length - L_a (m)	5.35	78.34	14.9	20.07	3.01	30.85
ArmAngle (degrees)	10.31	48.35	22.97	28.48	12.07	51.8
ArmSlope (degrees)	0.84	5.77	1.7	4.08	0.86	6.52
ArmSlope %	1.5%	10.1%	3.0%	6.3%	1.5%	11.4%
Total Weir Length - L_t (m)	24.06	175.76	38.95	53.73	12.8	78.03
Effective Weir Height - Z_u (m)	0.32	0.856	0.4	0.7	0.28	0.84
Effective Weir Width - W_u (m)	9.62	36.61	11.81	15.6	3.05	15.27
US Flow Depth - D_q (m)	0.34	2.07	0.67	1.56	N/A	
Normal Depth - D_{nref} (m)	0.24	1.71	0.36	1.3	N/A	
Weir Flow Depth - h_{weir} (m)	0.207	1.865	0.42	1.3	N/A	
L_t/T_w	1.23	3.48	1.62	2.04	1.27	3.58
W_u/Z_u	17.17	54.11	22.26	28.99	5.32	47.05
W_u/L_t	0.14	0.54	0.27	0.29	0.13	0.43
Z_d/H_{bkf}	0.07	0.36	0.17	0.334	0.01	0.31

Figure 5.13 and Figure 5.14 show observed versus predicted weir flow depth using the equations developed by Meneghetti (2009) and Thornton et al. (2011) respectively.

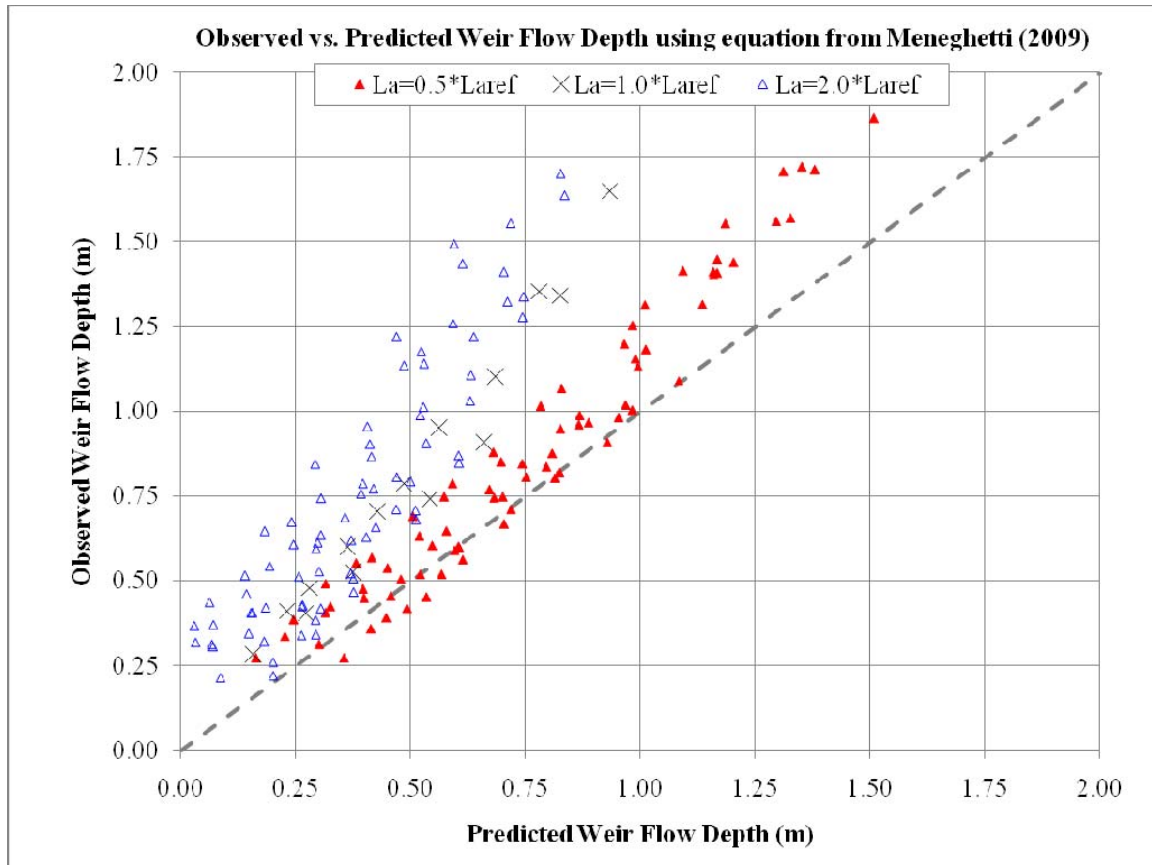


Figure 5.13 – Observed versus predicted flow depth using equation developed by Meneghetti (2009).

Application of the stage-discharge equation developed by Meneghetti (2009) appears to consistently under predict the upstream weir flow depth for the current data set with an absolute mean percent error of 32.2 percent and standard deviation of 23.3 percent. Figure 5.13 shows a distinct separation in the predicted weir flow depths due to variations in arm length. As the arm length was increased, the error in the predicted weir flow depth also increased.

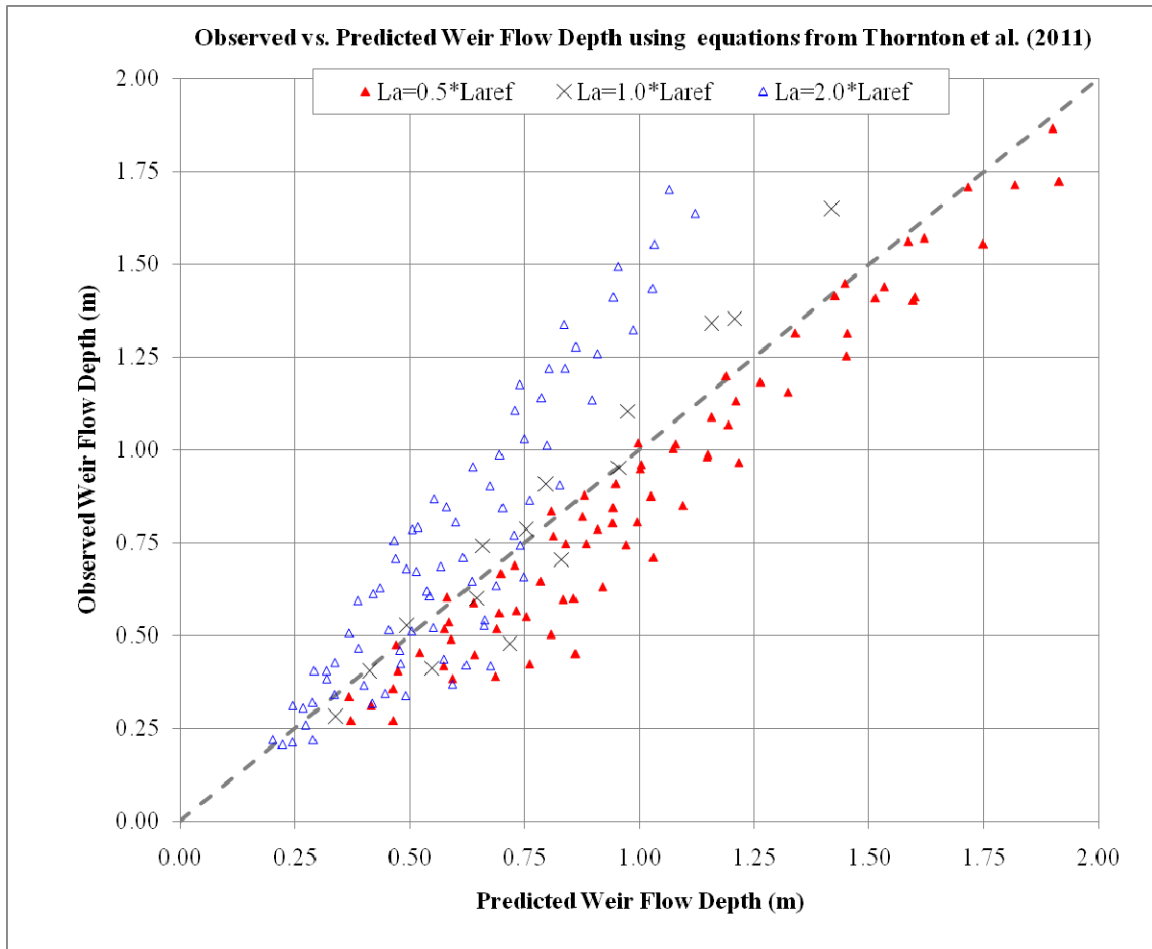
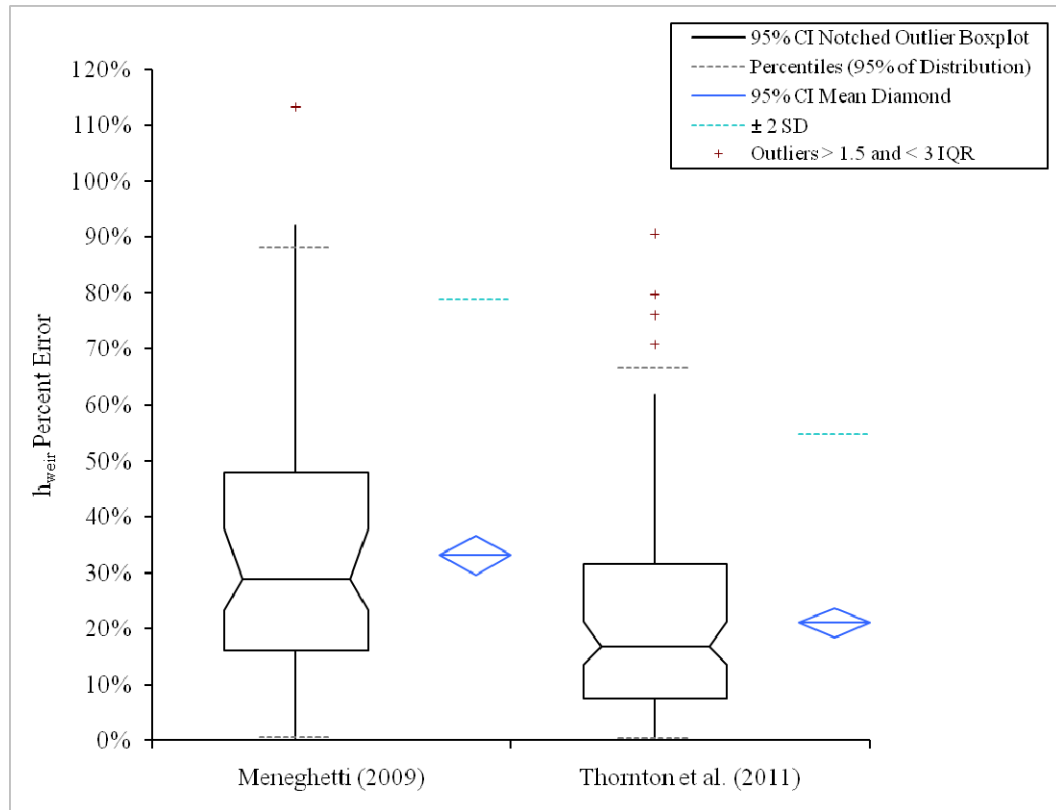


Figure 5.14 – Observed versus predicted flow depth using equation developed by Thornton et al. (2011).

Application of the stage-discharge equation developed by Thornton et al. (2011) provides a better overall prediction for weir flow depth with an absolute mean percent error of 21.1 percent and standard deviation of 16.8 percent. However, Figure 5.14 shows a similar separation in the predicted weir flow depths for varying structure arm lengths. The stage-discharge relationship tends to under predict the weir flow depth for a structure with a long arm ($L_a=2.0*L_{a_{ref}}$) and over predict the weir flow depth for a structure with a short arm ($L_a=0.5*L_{a_{ref}}$). Box and whisker plots showing percent error magnitude in predicted weir flow depth using the stage-discharge relationships developed by Meneghetti (2009) and Thornton et al. (2011) are presented in Figure 5.15.



	n	Mean	95% Confidence Interval	Standard Error	Standard Deviation
Meneghetti (2009)	165	33.17%	29.66% to 36.69%	1.78%	22.86%
Thornton et al. (2011)	165	21.09%	18.51% to 23.68%	1.31%	16.83%

Figure 5.15 – Percent error magnitude box-plot comparison of stage-discharge relationships developed by Meneghetti (2009) and Thornton et al. (2011).

From the above comparison, it is evident that the existing stage-discharge equations produce a large variability in the calculated flow depth over the weir for the range of structure parameters and reach characteristics examined in the current study. The large error can be partially explained by the fact that these equations were developed from laboratory data for a limited range of variability in structure geometry and flow rates as shown in Table 5.4. Since the main objective of the laboratory testing was to determine maximum scour associated with rock weirs, flows less than one-third bankfull flow were not tested. Therefore, predicting weir flow depth for flows less than those tested in the laboratory are expected to have a greater error. Another limiting factor in the

laboratory data set is due to the range of variations in structure geometry tested. The range of arm lengths tested in the laboratory was limited since the arm length was set to the minimized arm length ratio ($L_a=1.0*L_{a_{ref}}$) as described in Section 3.3.1. To increase the range of applicability of these equations and reduce the amount of scatter, additional analyses were needed and are described in the following section.

5.4.2 MODIFICATION TO EXISTING EQUATIONS

Using the stage-discharge relationship developed by Thornton et al. (2011) to predict the weir flow depth resulted in a large error (mean error of 21.2%) for the range of structure geometries included in the current study. Given the limited range of structure parameters tested in the laboratory for which these equations were originally developed, additional analysis were conducted using data from the current study to try and increase the range of applicability and reduce the amount of scatter. Utilizing the original stage-discharge equation developed by Thornton et al. (2011), a new logistic regression was conducted using output from the numerical model for the larger range of structure parameters and flow rates from the current data set to determine the coefficients in the Cd term presented in Equation 5.12.

$$Cd = a \left(\frac{D_{50}}{Z_u} \right)^b \left(\frac{L_t}{T_w} \right)^c \quad \text{Equation 5.12}$$

Using the output from the numerical model and conducting a multivariate nonlinear regression analysis, the following coefficients were determined: $a = 0.514$, $b = -0.961$ and $c = -0.557$. Substituting these coefficients into equation 5.12 provided a new weir contraction coefficient which was used to re-calculate the weir flow depth (h_{weir}) for each of the numerical model simulations using Equation 5.13.

$$h_{weir} = \left(\frac{Q}{\frac{2}{3} L_t \cdot 0.514 \left(\frac{D_{50}}{Z_u} \right)^{-0.961} \left(\frac{L_t}{T_w} \right)^{-0.557} \cdot \sqrt{2g}} \right)^{\frac{2}{3}} \quad \text{Equation 5.13}$$

Further analysis of the regression found that the equation tended to over predict the weir flow depth for flows greater than $2/3Q_{bkf}$ and slightly under predict for flows less than $2/3Q_{bkf}$. From the results of the flow magnification analysis described in Section 5.2, the greatest change in weir flow depth was found to occur at flows less than $2/3Q_{bkf}$ and therefore a piecewise regression was conducted using $2/3Q_{bkf}$ as the separator. Using the output from the numerical model and conducting a piecewise regression for flows less than $2/3Q_{bkf}$ and flows greater than $2/3Q_{bkf}$, the following coefficients were determined:

- $a = 0.637$, $b = -0.9503$ and $c = 0.607$ for flows greater than $2/3Q_{bkf}$
- $a = 0.446$, $b = -0.968$ and $c = 0.524$ for flows less than $2/3Q_{bkf}$

Using the results of the piecewise regression analysis described above, the upstream weir flow depth was calculated for each numerical model simulation using equations 5.14 and 5.15.

$$h_{weir} = \left(\frac{Q}{\frac{2}{3} L_t \cdot 0.446 \left(\frac{D_{50}}{Z_u} \right)^{-0.968} \left(\frac{L_t}{T_w} \right)^{-0.524} \cdot \sqrt{2g}} \right)^{\frac{2}{3}} \quad \text{for } Q < \frac{2}{3} Q_{bkf} \quad \text{Equation 5.14}$$

$$h_{weir} = \left(\frac{Q}{\frac{2}{3} L_T \cdot 0.637 \left(\frac{D_{50}}{Z_u} \right)^{-0.9503} \left(\frac{L_t}{T_w} \right)^{-0.607} \cdot \sqrt{2g}} \right)^{\frac{2}{3}} \quad \text{for } Q > \frac{2}{3} Q_{bkf} \quad \text{Equation 5.15}$$

Figure 5.16 shows the observed versus predicted weir flow depth utilizing the new piecewise regression coefficients. The results of the modified equation show an increase in the ability to predict the upstream stage for a given weir geometry and reach characteristics. While the updated equation provides a better estimate of upstream stage ($R^2=0.94$) compared to the original equations developed by Meneghetti (2009) and Thornton et al. (2011) ($R^2=0.71$ and 0.75 respectively), there is still a significant amount of error present (absolute mean error=10.2% and standard deviation=7.5%).

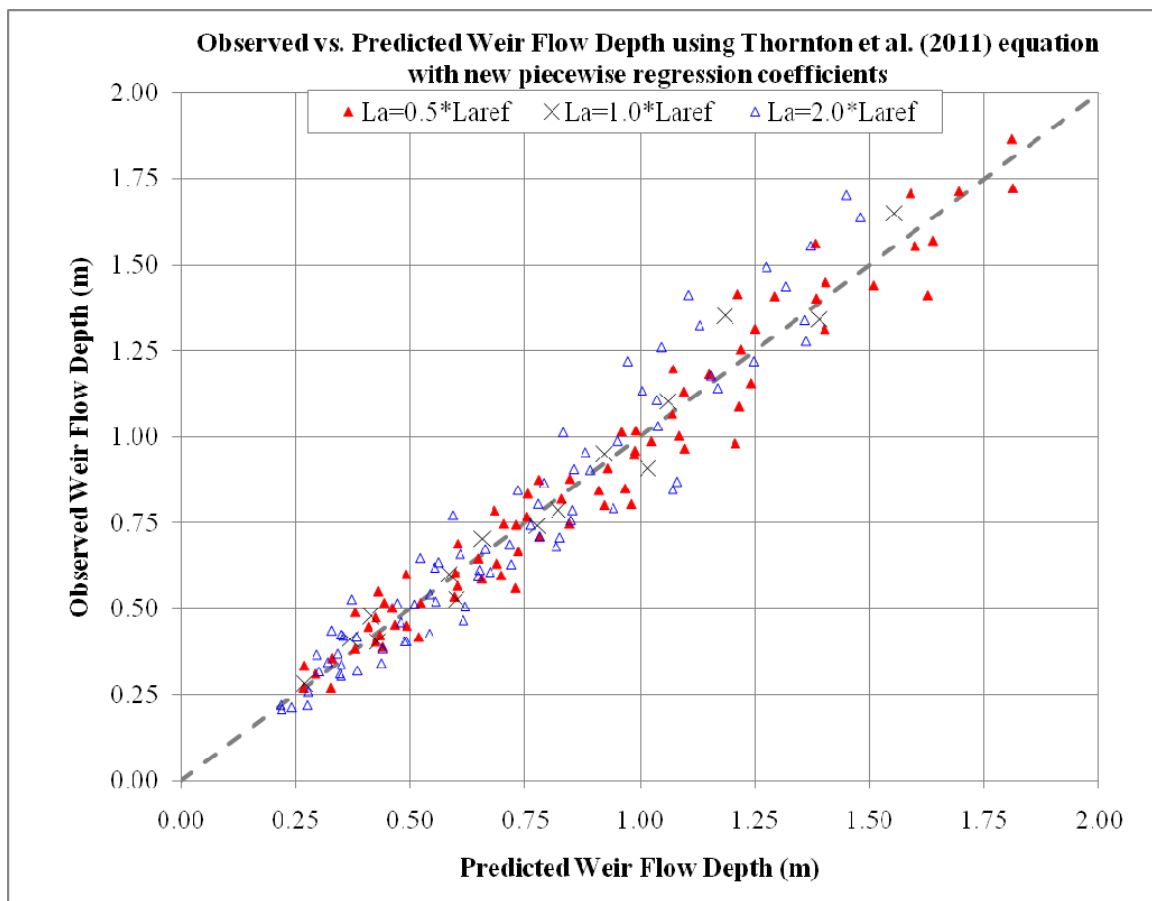


Figure 5.16 – Observed versus predicted flow depth using original equation developed by Thornton et al. (2011) with new piecewise regression coefficients.

Further investigation of the individual terms used in the stage-discharge equation provided some insight into potential reasons for the large standard deviation (scatter in the data). Using the total weir length (L_t) in place of the weir width (b) in the general

broad crested weir equation seems to over emphasize the influence of the effective weir height used in the calculation of flow depth. Therefore, identifying a variable that is more representative of the weir width in the broad crested weir equation is important.

Since the effective rock weir height is used to replace weir height in the original broad crested weir equation, an effective rock weir width seems appropriate to replace weir width. Effective weir width for a given structure geometry was calculated using Equation 5.16:

$$W_U = W_t + 2 \left(\frac{(Z_u - Z_d) \sin \theta}{\tan \phi} \right) \quad \text{Equation 5.16}$$

Where:

W_u = effective weir width and all other terms previously described.

Another term that was investigated was the weir thickness divided by the effective weir height (D_{50}/Z_u) used in calculating the weir coefficient term C_d . In general, variations in structure geometry for a given channel do not alter the size of the rock used to construct the weir and therefore the weir thickness (D_{50}) is not a function of the weir geometry and remains constant. Since the weir coefficient (C_d) is used to account for the flow constriction caused by the geometry of the weir, the effective weir width divided by effective weir height was investigated. Dividing the effective weir width (equation 5.14) by the effective weir height provides a method to account for the variation in flow constriction caused by differing structure geometries. Therefore, the D_{50}/Z_u term in the original equation developed by Thornton et al. (2011) was replaced with W_u/Z_u as shown in Equation 5.17.

$$C_d = a \left(\frac{W_u}{Z_u} \right)^b \left(\frac{L_t}{T_w} \right)^c \quad \text{Equation 5.17}$$

Regression techniques were used to obtain empirical coefficients for the dimensionless terms presented in Equation 5.17. Using the output from the numerical model and conducting a multivariate nonlinear regression analysis, the following coefficients were determined: $a = 6.042$, $b = -0.653$ and $c = 0.401$. These coefficients along with the effective weir width were used to develop a new stage-discharge relationship (Equation 5.18) to calculate the weir flow depth (h_{weir}) for each of the numerical model simulations.

$$h_{weir} = \left(\frac{Q}{\frac{2}{3} W_u \cdot 6.042 \left(\frac{W_u}{Z_u} \right)^{-0.653} \left(\frac{L_t}{T_w} \right)^{0.401} \cdot \sqrt{2g}} \right)^{\frac{2}{3}} \quad \text{Equation 5.18}$$

Figure 5.17 shows the observed versus predicted weir flow depth utilizing the new U-weir stage-discharge relationship described above. While the new equation provided a better fit ($R^2=0.97$) compared to the modified equation ($R^2=0.94$), there was a significant amount of error for flow depths greater than one meter. Further analysis of the regression found that the equation tended to over predict the weir flow depth for flows greater than $2/3Q_{bkf}$ as shown in Figure 5.17 and slightly under predict for flows less than $2/3Q_{bkf}$. A previously described, the greatest change in weir flow depth was found to occur at flows less than $2/3Q_{bkf}$ and therefore a piecewise regression was conducted using $2/3Q_{bkf}$ as the separator.

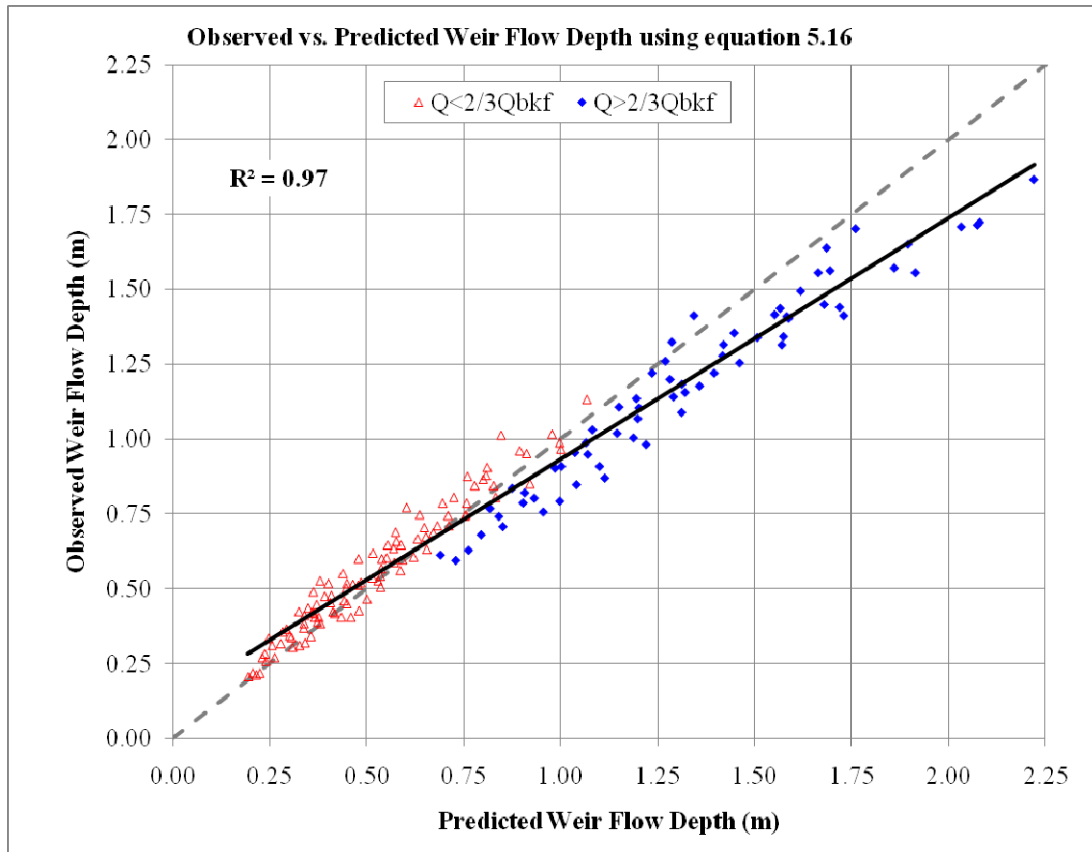


Figure 5.17 – Observed versus predicted flow depth using equation 5.18 regression for all flows.

Using the output from the numerical model and conducting a piecewise regression for flows less than $2/3Q_{bkf}$ and flows greater than $2/3Q_{bkf}$, the following coefficients were determined:

- $a = 9.766$, $b = -0.7305$ and $c = 0.3593$ for flows greater than $2/3Q_{bkf}$
- $a = 4.386$, $b = -0.6014$ and $c = 0.4292$ for flows less than $2/3Q_{bkf}$

Using the results of the piecewise regression analysis described above, the upstream weir flow depth was calculated for each numerical model simulation using equations 5.19 and 5.20.

$$h_{weir} = \left(\frac{Q}{\frac{2}{3} W_u \cdot 4.386 \left(\frac{W_u}{Z_u} \right)^{-0.601} \left(\frac{L_t}{T_w} \right)^{-0.429} \cdot \sqrt{2g}} \right)^{\frac{2}{3}} \quad \text{for } Q < \frac{2}{3} Q_{bkf} \quad \text{Equation 5.19}$$

$$h_{weir} = \left(\frac{Q}{\frac{2}{3} W_u \cdot 9.766 \left(\frac{W_u}{Z_u} \right)^{-0.73} \left(\frac{L_t}{T_w} \right)^{-0.359} \cdot \sqrt{2g}} \right)^{\frac{2}{3}} \quad \text{for } Q > \frac{2}{3} Q_{bkf} \quad \text{Equation 5.20}$$

The predicted weir flow depths for all 165 simulations are presented in Appendix B. Figure 5.18 shows observed (modeled) versus predicted weir flow depths using equations 5.19 and 5.20 for the current study.

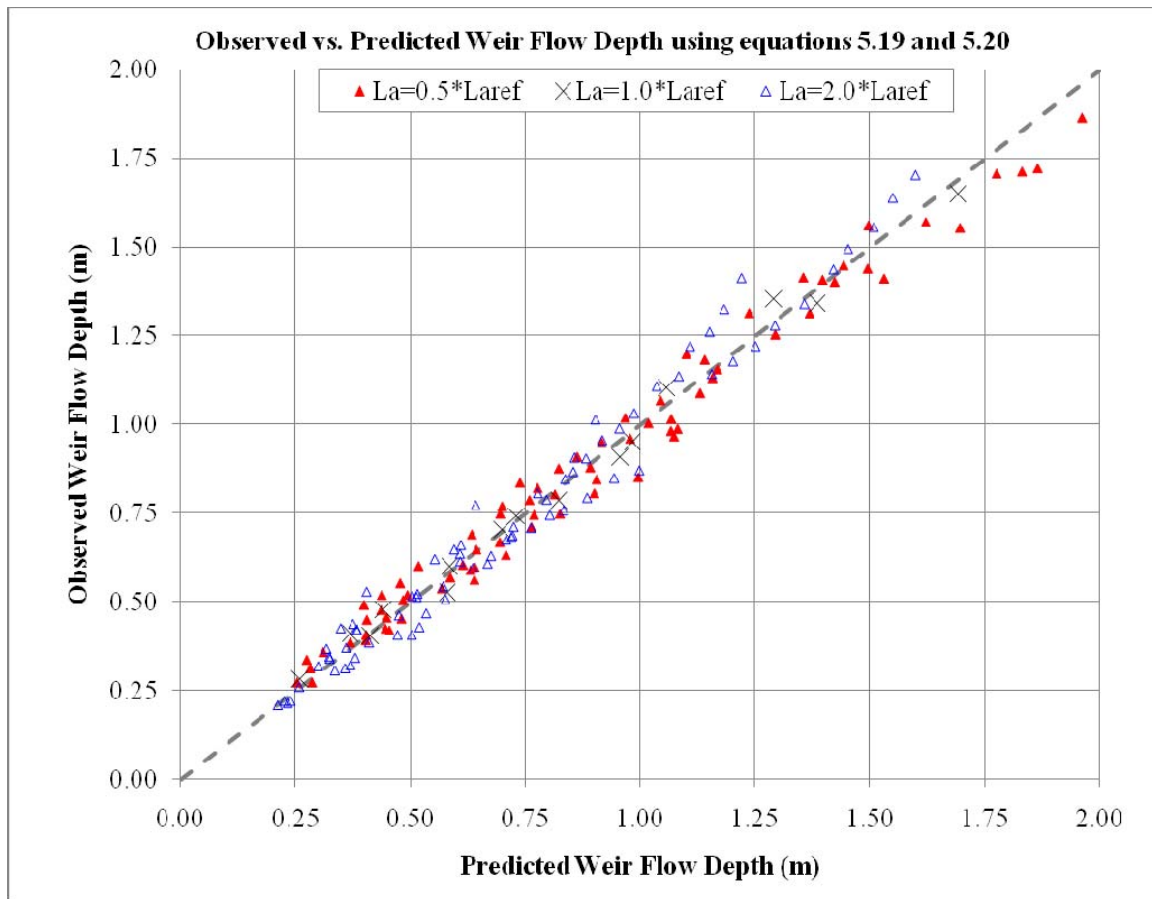
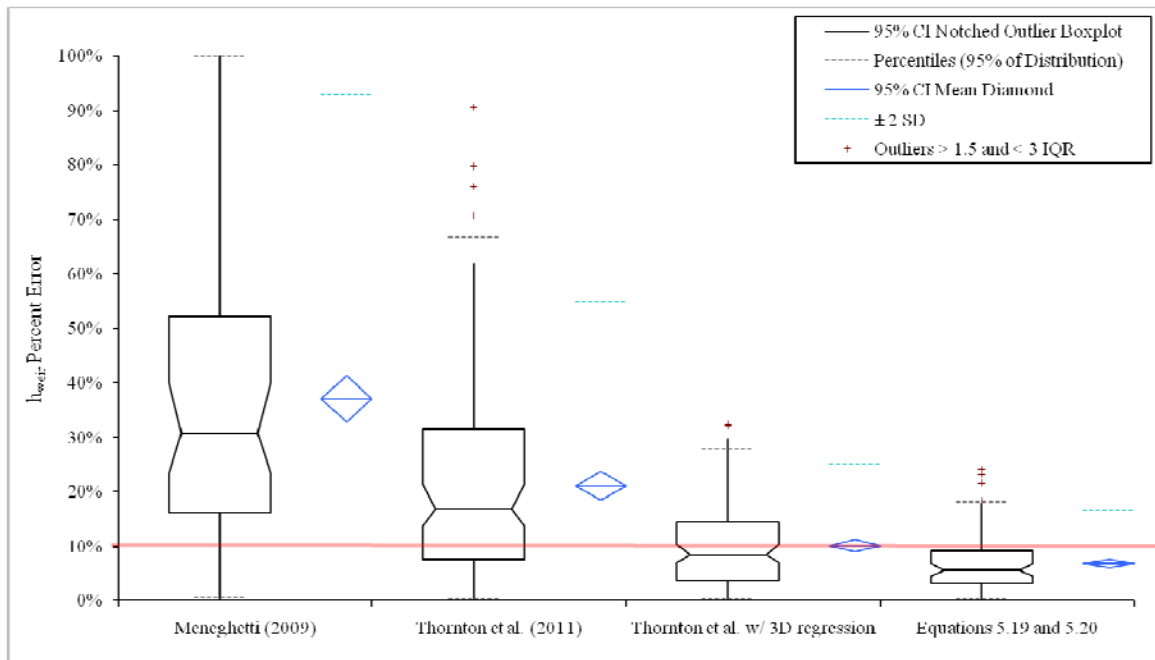


Figure 5.18 – Observed versus predicted weir flow depth using equations 5.19 and 5.20.

The results of the new U-weir stage-discharge equation showed an increase in the ability to predict the upstream stage for a given weir geometry and reach characteristics with an absolute mean error of 6.74 percent and standard deviation of 4.9 percent. Calculating the weir flow depth using the effective weir width associated with the effective weir height provided a better representation of the effects of variations in structure geometry compared to the total weir length used by Thornton et al. (2011). A box and whisker plot showing the variation in percent error in predicted weir flow depth between the four stage-discharge equations described above is presented in Figure 5.19.



	n	Mean	95% Confidence Interval	Standard Error	Standard Deviation
Meneghetti (2009)	165	37.09%	32.80% to 41.37%	2.17%	27.88%
Thornton et al. (2011)	165	21.09%	18.51% to 23.68%	1.31%	16.83%
Thornton et al. w/ 3D regression	165	10.13%	8.98% to 11.28%	0.58%	7.47%
Equations 5.19 and 5.20	165	6.74%	5.98% to 7.49%	0.38%	4.92%

	n	Min	1st Quartile	Median	95% Confidence Interval	3rd Quartile	Max	IQR
Meneghetti (2009)	165	0.40%	16.03%	30.87%	23.39% to 39.93%	52.32%	113.39%	36.30%
Thornton et al. (2011)	165	0.10%	7.52%	16.87%	13.66% to 21.34%	31.56%	90.57%	24.05%
Thornton et al. w/ 3D regression	165	0.17%	3.83%	8.48%	6.91% to 10.44%	14.51%	32.30%	10.68%
Equations 5.19 and 5.20	165	0.10%	3.19%	5.58%	4.58% to 6.81%	9.20%	24.07%	6.01%

Figure 5.19 – Percent error magnitude box-plot comparison of stage-discharge relationships developed by Meneghetti (2009), Thornton et al. (2011), and the current study.

It is evident from the comparison that of the four stage-discharge relationships, the new stage-discharge relationship (equations 5.19 and 5.20) provides a better overall prediction of the weir flow depth with a 95 percent confidence interval of 5.98%-7.49% compared to 32.8%-41% and 18.5%-23% for the equations developed by Meneghetti (2009) and Thornton et al. (2011) respectively. Since equations 5.19 and 5.20 were developed using output from the numerical model, testing the applicability of the equations with measured field and laboratory data was essential. Therefore, the new stage-discharge relationship developed from the numerical modeling was applied to the field case described in Section 3.2 and the laboratory data set from Thornton et al. (2011) to test the applicability of the new relationship to measured data. The following section describes the results of the comparison with the field case and laboratory test data.

5.4.3 APPLICATION OF MODIFIED EQUATION

Utilizing data collected from the field site described in section 3.2 and the laboratory case described in section 3.3, weir flow depth was predicted and compared with measured values. Comparing the measured flow depths with predicted values from equations 5.19 and 5.20 provides a method to test the applicability of the equations to data that was not used in the development of the new stage-discharge relationship. Although the field site is limited, the equations developed by Meneghetti (2009) and Thornton et al. (2011) were also used to predict the weir flow depth for the field site and compared with the results from the current study.

Figure 5.20 shows the observed versus predicted weir flow depth for the field site and laboratory data set utilizing the three equations described above. The results show that equations 5.19 and 5.20 predicted the weir flow depth for the field site and laboratory data set very well with an absolute mean error of 4.5 percent and standard deviation of

4.02 percent. Comparing the observed versus predicted values for the field and laboratory data independently from the numerical model data set demonstrates the applicability of equations 5.19 and 5.20 to measured data in the field and in the laboratory setting. Figure 5.20 also shows that the equations differ in their ability to predict the weir flow depth for the field site. The percent errors associated with each equation for the field site are as follows: Meneghetti (2009) percent error = 48.3%, Thornton et al. (2011) percent error = 32.85%, and the current study (equation 5.18) percent error = 10.58%.

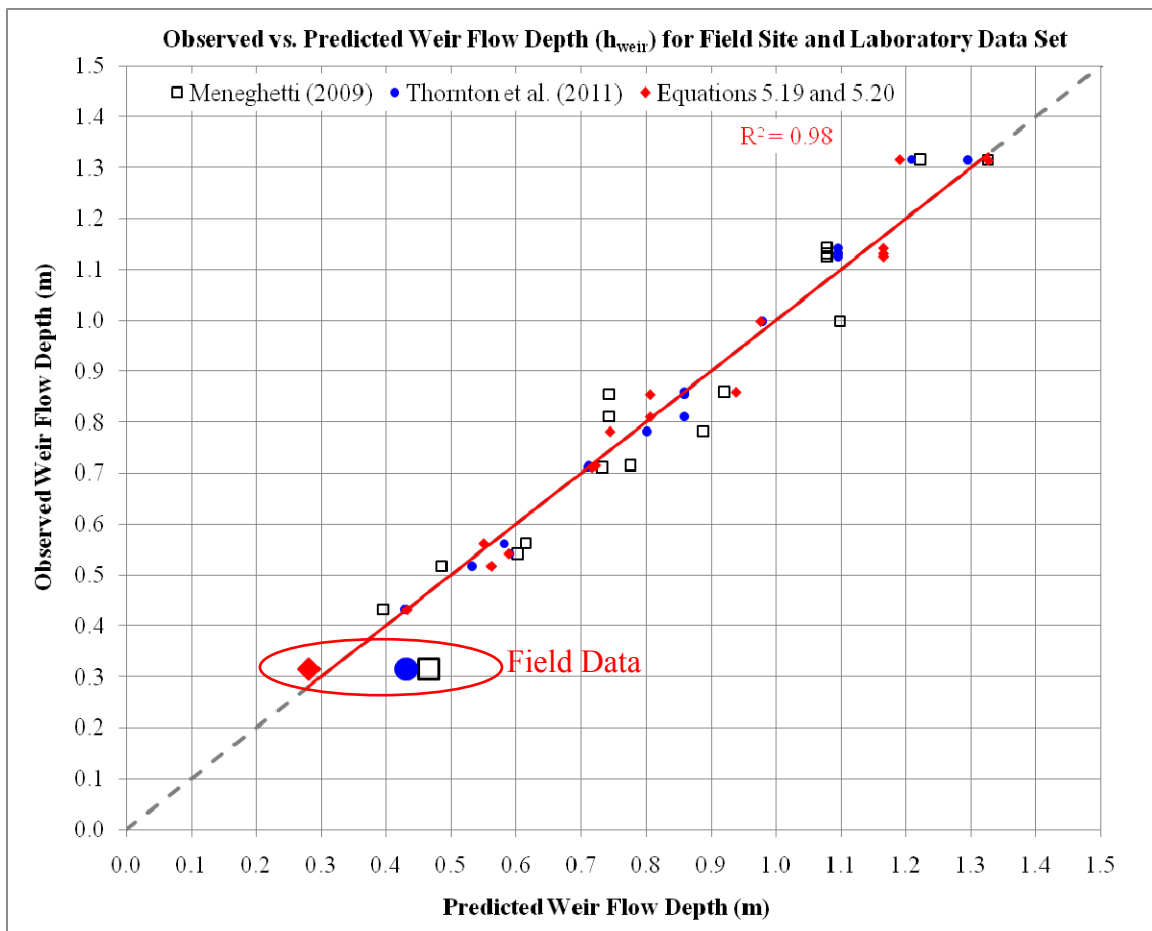
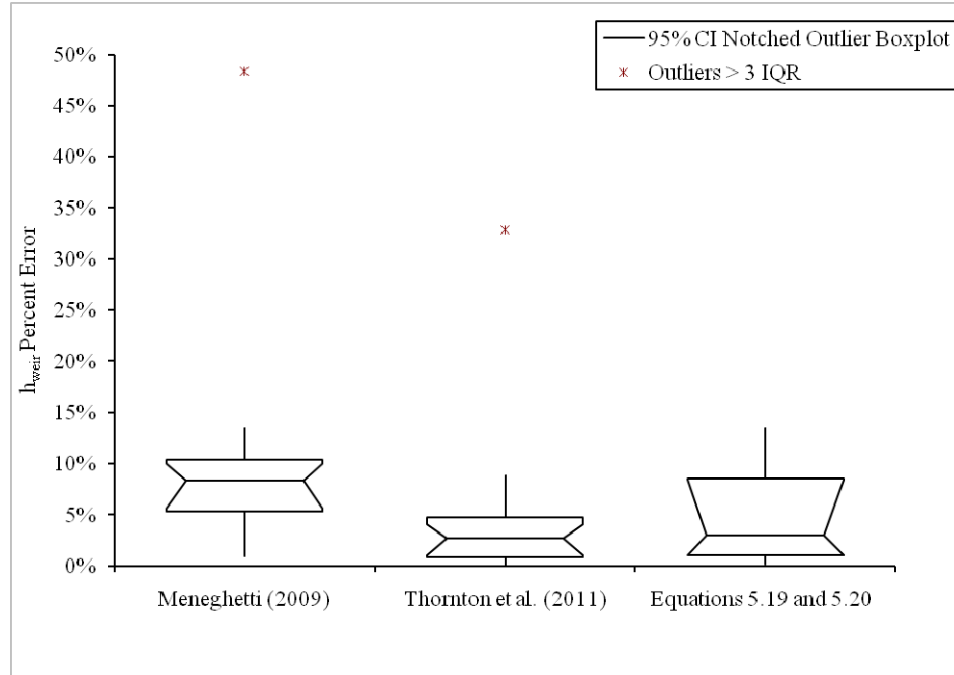


Figure 5.20 – Observed versus Predicted weir flow depth using stage-discharge relationships for field site and laboratory data set.

A box and whisker plot showing the absolute percent error in predicted weir flow depth for the field site and laboratory data set using each of the stage-discharge equations described above is presented in Figure 5.21.



	n	Mean	95% Confidence Interval	Standard Error	Standard Deviation
Meneghetti (2009)	17	9.98%	4.61% to 15.35%	2.53%	10.45%
Thornton et al. (2011)	17	4.72%	0.77% to 8.68%	1.87%	7.70%
Equations 5.19 and 5.20	17	4.45%	2.38% to 6.51%	0.97%	4.02%

	n	Min	1st Quartile	Median	95% Confidence Interval	3rd Quartile	Max	IQR
Meneghetti (2009)	17	0.90%	5.30%	8.33%	5.59% to 9.96%	10.38%	48.35%	5.08%
Thornton et al. (2011)	17	0.08%	0.82%	2.73%	1.00% to 4.10%	4.71%	32.85%	3.89%
Equations 5.19 and 5.20	17	0.14%	1.00%	2.95%	1.03% to 8.47%	8.51%	13.52%	7.51%

Figure 5.21 – Percent error box-plot comparison of stage-discharge relationships developed by Meneghetti (2009), Thornton et al. (2011), and equations 5.19 and 5.20 applied to a field site and laboratory data set.

It is evident from the comparison that the new stage-discharge relationship (equations 5.19 and 5.20) provides a better prediction of the weir flow depth for the field case and similar results for the laboratory data. Since the stage-discharge relationships developed by Meneghetti (2009) and Thornton et al. (2011) utilized the laboratory data in their analysis, it is expected that the error associated with their equations would be less

than the error of the relationship from the current study. Being able to predict the weir flow depth associated with a given U-weir geometry and channel characteristics within ten percent for the laboratory data and field site demonstrates the applicability of the new stage-discharge equations developed from the current study. It should be noted that these equations are meant to be used for guidance in the design process and may not be adequately predictable for natural streams where discharge, reach characteristics, structure geometry, and other conditions are considerably different from those included in the current study.

5.5 ANALYSIS SUMMARY

Numerical model simulations were used to examine how variations in rock weir geometry affected local flow patterns. The results clearly showed that by altering the structure geometry associate with U-weirs, local flow patterns such as upstream flow depth, downstream velocity, and bed shear stress distributions could be altered significantly. With the range of parameters tested, the maximum increase in channel velocity ranged from 1.24 to 4.04 times the reference velocity in the channel with no structure present. Similarly, the maximum increase in bed shear stress caused by altering structure geometry ranged from 1.57 to 7.59 times the critical bed shear stress in the channel for a given bed material size. For the range of structure parameters and channel characteristics modeled, stage-discharge relationships were also developed utilizing output from the numerical model simulations.

An empirical approach and regression analysis were used to examine current stage-discharge relationships for U-weirs using numerical modeling output consisting of discharge, depth of flow upstream from the weir crest, and weir geometry. Comparisons

were made between existing stage-discharge relationships and output from the numerical model to examine the applicability of the relationships to the range of variables identified in the current study. The comparisons showed that current relationships had limited applicability to a range of structure geometries not included in the original development and that additional analyses were needed. Utilizing output from the numerical model, regression analyses were conducted to develop new stage-discharge relationships that were applicable to a wide range of structure parameters and flow conditions. A comparison of predicted weir flow depths using the regression equations developed from the numerical modeling versus existing relationships showed an increase in predictive ability for the newly developed stage-discharge relationship for the range of channel conditions and structure geometry tested. Results from the stage-discharge analysis showed that the weir flow depth for a given weir geometry, channel characteristic, and flow rate could be predicted with an average error of 6.74 percent (standard deviation = 4.9 percent).

6 SUMMARY AND RECOMMENDATIONS

River spanning rock weirs are being constructed for water delivery as well as to enable fish passage at barriers and provide or improve the aquatic habitat for endangered fish species. Current design guidelines associated with river spanning rock weirs tend to rely heavily on field experience and engineering judgment. Until recently, rock weirs had met the approval of many in the conservation community, but very high maintenance and the lack of engineering performance criteria have limited their use to applications where structure stability, loss of function (i.e. irrigation diversions), and associated liability to the designer are minimized.

6.1 CONTRIBUTIONS

The primary contribution of this research, which included valuable contributions by Reclamation and Colorado State University, was to begin the development of process-based engineering design criteria for river spanning rock U-weirs that may be applicable for irrigation diversion and bed stabilization allowing fish passage and improved aquatic habit. In this research process, field and engineering laboratory data were developed and utilized to validate the use of a 3D numerical model to study the physical processes associated with an expanded range of U-weir geometries.

The contributions of this research include:

1. a better understanding of the physical processes associated with river spanning rock U-weirs and how changes in structure geometry ultimately

affect upstream flow depth and downstream velocity and bed shear stress distributions;

2. equations for predicting stage-discharge relationships for an expanded range of variations in U-weir geometry; and
3. development of a numerical method for generating and comparing various U-weir configurations and resulting flow depth, velocity, and bed shear stress distributions to improve the design process for constructing river spanning rock weirs that meet specific project objectives associated with flow diversion, fish passage, and stream restoration .

The rock weir mesh generation program and numerical modeling output provides a processed-based method for comparing the relative change in flow patterns (e.g. velocity, bed shear stress, water surface elevation) generated by variations in rock weir geometry. The results of such comparisons can be used in the design process to assist designers in determining which rock weir geometry configuration best meets their project objectives.

In making these expected contributions, there is also an expected practical, engineering design component that is in the process of being implemented. This research will be tested and the results applied to a current river spanning rock structure design guidelines project at the Bureau of Reclamation's Technical Service Center. Results from laboratory testing (Meneghetti 2009 and Scurlock 2010), field reconnaissance (Mooney et al. 2007a, 2007b, Holburn et al. 2009a, and 2009b), and numerical modeling from the current research will be summarized and compiled into a single Reclamation report providing guidelines for designing river spanning rock weirs. Integration of field

reconnaissance, laboratory experiments, and numerical modeling provides a scientific basis for predicting structure performance under various river conditions. The design guidelines manual, which will include the stage-discharge prediction equations and numerical modeling methods developed through this dissertation, will enable practitioners to design, test, and build sustainable river spanning rock weirs that meet their design goals related to flow diversion, fish passage, and stream restoration.

6.2 RESEARCH SUMMARY

The research presented in this dissertation included a review of the literature pertaining to river spanning rock weirs, development and implementation of a rock weir mesh generator and numerical model testing matrix, comparison and validation of numerical modeling methods for a field site and laboratory data, analysis of the numerical model output and development of stage-discharge relationships for U-weirs. The numerical model U²RANS was used to investigate the effects of variations in structure geometry on upstream flow depths and downstream velocity and bed shears stress distributions. A rock weir mesh generation program was developed to expedite the process of generating 33 different structure geometries in a simulated straight trapezoidal channel. Variations in structure geometry included: arm angle, arm slope, drop height, and throat width. Various combinations of each of these parameters were modeled at five different flow rates ($1/10Q_{\text{bankfull}}$, $1/5Q_{\text{bankfull}}$, $1/3Q_{\text{bankfull}}$, $2/3Q_{\text{bankfull}}$, and Q_{bankfull}) for a total of 165 simulations. Output from the numerical modeling was analyzed to quantify the effects that variations in structure geometry had on local velocity and bed shears stress distributions and develop a stage-discharge relationship for U-weirs. Conclusions from the numerical modeling of U-weirs are presented below.

As water flows over a river spanning rock U-weir it is redirected at a right angle to the structure crest and results in a concentration of flow in the center of the channel and away from the stream banks. As a result, near bank velocities and shear stresses are reduced while those in the middle of the channel are increased. Understanding the relationship between structure geometry and velocity and bed shear stress distributions may provide valuable insight to improve the performance and stability of the designed structure. Results of the velocity magnification analysis showed that, for the range of conditions tested the maximum velocity downstream from U-weirs was increased by 1.24 to 4.04 times the original channel velocity with no structure present. Results of the bed shear stress magnification analysis showed that the maximum bed shear stress downstream from U-weirs was altered by 1.57 to 7.59 times the critical bed shear stress and varied in location from 0.1 to 1.25 times the arm length downstream of the structure crest. The ability to compare the location and differences in channel velocity and bed shear stress associated with various rock weir geometries is important in the design process to ensure that the structure is not undermined by scour and will maintain sediment transport continuity through the structure.

The magnitude and location of these increases are important in the design of rock weirs because they can affect sediment transport through the structure, scour development, fish passage, and overall structure performance. Utilizing the numerical model results, designers can determine where a structure design falls within the range of investigated conditions and estimate the maximum velocity magnification and bed shear stress that is associated with that configuration. The results also provide the designer a way to compare variations in structure geometry and whether the resulting hydraulic

conditions fall within prescribed guidelines and meet project objectives. If a more detailed analysis is required or the structure configuration does not fall within the range of the current data, the rock weir mesh generation program could be used in conjunction with the numerical model to estimate how variations in specific channel characteristics and/or structure configurations would alter local flow depths and velocity and bed shear stress distributions.

Stage-discharge relationships allow designers to estimate stage upstream of a structure for diversion purposes in addition to spacing between structures to ensure that tail water conditions for an upstream structure are met. Results of the stage-discharge analysis found that the relationship developed from the current study (equations 5.17 and 5.18) provided a method to predicted the weir flow depth for a given weir geometry and reach characteristics with an absolute mean error of 6.74 percent and standard deviation of 4.9 percent. The developed stage-discharge relationship provides designers a way to compare variations in the structure design and determine whether a specific design provides the appropriate backwater affects to meet project objectives (e.g. irrigation diversion, fish passage).

From the results described above, it can be seen that placing a river spanning rock weir in the channel can greatly affect the local hydraulics, scour development, and sediment transport through the structure. The degree to which these effects occur depends on a number of important variables that influence the way in which a structure functions in the stream. When designing rock weirs, designers are advised to use due diligence in using existing design guidelines and apply formulas and methods (in addition to those

used in this dissertation) to estimate the resulting effects a specific rock weir design has on local hydraulics, scour development, and overall structure performance.

Hydraulic parameters used in designing rock weirs include flow depth, velocity and bed shear stress. These parameters should be determined for a range of flows for existing and post-project conditions. Common design discharges applied to the design of river spanning rock weirs are related to both high flow (ie. bankfull flow) and low flow conditions (ie. base flow). These parameters are used to size the weir rock as well as rock used for scour protection, demonstrate that project goals such as irrigation diversion and fish passage are being met, and determine overall structure performance. It should be noted that design of river spanning rock weirs in a natural environment, using natural materials, involves a significant degree of uncertainty. This research project focused on the relative change in local hydraulics (flow depth, velocity, and bed shear stress) associated with variations in structure geometry and developed a stage-discharge relationship applicable to U-weirs. The methods and equations presented in this dissertation provide an increased understanding of the physical processes associated with U-weirs.

Utilizing the methods and results of the current research provides designers an additional tool that can be used in conjunction with the general steps and considerations found in the literature (Holburn et al. 2010a, Mooney et al. 2007a, Rosgen 2006, Thomas et al. 2000, and WDFW 2004) for the design of river spanning rock weirs. However, these tools should be employed with an understanding of the variability occurring in natural stream systems and sound professional judgment. The installation of river spanning rock weirs should never be conducted without adequate site, reach, and

watershed assessments to determine the nature and extent of problems in the watershed and to establish realistic project goals, objectives, and priorities.

6.3 RECOMMENDATIONS FOR FURTHER RESEARCH

The analysis and results presented in this dissertation were associated with fixed bed numerical model simulations for a simplified flat bed trapezoidal channel with symmetric weir configurations. The methods employed and outcomes from the research provide additional guidance for the design and construction of U-weirs; however, several areas still need further research to provide comprehensive design guidelines. Recommendations for future research of river spanning rock weirs are presented in the following sections.

6.3.1 COMPARISON WITH ADDITIONAL FIELD SITES AND LABORATORY DATA

Validation of the presented research with additional field sites and laboratory data is advised, especially for the stage-discharge relationships presented. Results from the current study demonstrated the applicability of the new stage-discharge relationship for a field site and a particular laboratory data set. Calibrating these equations using additional field and laboratory data would increase the reliability and range of applicability of these equations for design purposes. Additional numerical modeling could also be conducted to determine weir flow depths for channel conditions and structure geometries not included in the current study.

6.3.2 INVESTIGATE EFFECTS OF PRE-EXCAVATED SCOUR HOLES

Construction of river spanning rock weirs in the field typically involves a pre-excavated scour hole downstream of the structure crest. However, design guidelines related to the location and size of the scour hole and its effects on the local hydraulics of

the weir do not exist. Being able to understand how variations in the channel geometry (scour holes) downstream from rock weirs affect the local hydraulics (velocity and bed shear stress) and resulting scour development and sediment continuity is important in the design and sustainability of the structure. The effects of pre-excavated scour holes could be investigated through additional numerical modeling and/or through physical model testing in the laboratory.

6.3.3 CHANNEL CHARACTERISTICS AND MOBILE BED SIMULATIONS

Further research is recommended for rock weirs in a sinuous, mobile-bed channel with symmetric and non-symmetric weir configurations. Investigations of variations in channel characteristics, non-symmetric structure geometries, and mobile bed simulations would provide valuable data for addition to the current data set. Investigation of these conditions should include a range of approach conditions, structure configurations, and channel geometry that would alter the resulting local hydraulics, scour development, and potential stability of the structure. Such research could be conducted in the laboratory setting as well as through the use of a mobile bed numerical model. Incorporating a testing scheme that includes both physical and numerical modeling components is recommended.

Several research recommendations have been presented for future investigation of river spanning rock weirs. Testing river spanning rock weirs under varying conditions including structure geometry and mobile bed channel conditions would provide more comprehensive background data for the development of river spanning rock weir design guidelines.

6.4 CONCLUSION

Utilizing output from numerical modeling simulations, analyses were conducted to develop stage-discharge relationships and identify the effects that variations in structure geometry have on local velocity and bed shear stress distributions. The ability to describe the physical processes associated with alterations in structure geometry and the effects on local hydraulics provides critical information for designers and facilitates additional design guidance for river spanning rock weirs.

The analysis and results from this dissertation as well as the valuable contributions from laboratory studies conducted by Colorado State University (Meneghetti, 2009 and Scurlock, 2010) and the field data set collected by the Bureau of Reclamation (Mooney et al. 2007b and Holburn et al. 2009a, 2009b) provide a process-based method for understanding how structure geometry affects flow characteristics, scour development, fish passage, water delivery, and overall structure stability. Numerical modeling results allow designers to utilize the analysis to identify the most appropriate weir geometry for generating desirable flow parameters (i.e. upstream flow depth, maximum velocity, and critical bed shear stress distribution) to meet project-specific goals.

When designing rock weirs, providing fish passage and related habitat in gravel-bed streams is very important to water resources development. The alternatives to river spanning rock weirs that function efficiently and garner the approval of ecological regulatory agencies are limited. This dissertation and related research has provided a foundation for design of these structures based upon predictable engineering and hydraulic performance criteria that may be accepted by the engineering profession.

While results from this research provide fundamental information related to physical processes associated with rock weirs, recommendations for additional research were discussed that would further expand the current state of knowledge related to river spanning rock weirs.

7 REFERENCES

- Abrahams, A.D., Li, G. and Atkinson, J.F. (1995) Step-pool streams: adjustment to maximum flow resistance. *Water Resources Research*. 31:593-602.
- Bhuiyan, F. and Hey R. (2007). Computation of three-dimensional flow field created by weir-type structures. *Engineering Applications of Computational Fluid Mechanics*. 1(4):350-360.
- Bhuiyan, F., Hey R., and Wormleaton P.R., (2007). Hydraulic evaluation of W-weir for river restoration. *Journal of Hydraulic Engineering*. ASCE 133(4):596-609.
- Castro, J., (2000). Design of rock weirs. U.S. Department of Agriculture, Natural Resources Conservation Service. Engineering Technical Note No.13.
- Chin, A., (1989). Step pools in stream channels. *Progress in Physical Geography*. v. 13, p. 391-407.
- Chow, V.T. (1959). *Open-channel Hydraulics*. McGraw-Hill.
- Cox, A., (2005). A study of in-stream rehabilitation structures in sand-bed channels. M.S. Thesis, Colorado State University, Department of Civil Engineering, Fort Collins, Colorado.
- D'Agostino, V., and Ferro, V., (2004). Scour on Alluvial Bed Downstream of Grade-Control Structures. *Journal of Hydraulic Engineering*, v. 130 (1), p. 24-37.
- FHWA. 1979. Restoration of fish habitat in relocated streams, FHWA-IP-79-3. U.S. Department of Transportation, Federal Highway Administration.
- Fischenich, C., and Seal, R. 1999. Boulder Clusters. U.S. Army Engineer Research and Development Center, Vicksburg, MS.
- Frissell, C.A. and Nawa, R.K., (1992). Incidence and causes of physical failure or artificial habitat structures in streams of Western Oregon and Washington. *North American Journal of Fisheries Management*, 12: 182-197.
- Fritz, H.M. and Hager, W.H., (1998). Hydraulics of embankment weirs. *Journal of Hydraulic Engineering*. ASCE 124(9):963-971.
- Hargreaves, D.M., Morvan, H.P., and Wright, N.G., (2007). Validation of the volume of fluid method for free surface calculation: The broad-crested weir. *Engineering Applications of Computational Mechanics*. v.1(2):136-146.
- Holburn, E., Varyu, D., and Russell, K. (2009a). Quantitative investigation of the field performance of rock weirs :SRH-2009-46. Bureau of Reclamation, Technical Service Center, Sedimentation and River Hydraulics Group, Denver, CO.

- Holburn, E., Russell, K., and Holmquist-Johnson, C.L. (2009b). River Spanning Rock Structures Field Investigations 2008 :SRH-2009-47. Bureau of Reclamation, Technical Service Center, Sedimentation and River Hydraulics Group, Denver, CO.
- Humbles, E. (2009). Personal Communication.
- Jia, Yafei, Scott, S., Xu, Y., Huang, S., and Wang, S., (2005). Three-dimensional numerical simulation and analysis of flows around submerged weir in a channel bendway. *Journal of Hydraulic Engineering*. ASCE 131(8):682–693.
- Julien, P.Y. (2002). *River Mechanics*. Cambridge University Press, Cambridge, UK.
- Knighton, D. (1998). *Fluvial Forms and Processes: A New Perspective*. Oxford University Press Inc., New York, NY, 383 p.
- Kondolf, G.M., and E.R. Micheli. (1995). Evaluating stream restoration projects. *Environmental Management* 19(1):1-15.
- Lai, Y. G., Weber, L. J., and Patel, V. C., (2003). Nonhydrostatic threedimensional model for hydraulic flow simulation. I: Formulation and verification. *Journal of Hydraulic Engineering*. ASCE 129(3):196–205.
- Lai, Y. G., Weber, L. J., and Patel, V. C., (2003). Nonhydrostatic three-dimensional model for hydraulic flow simulation. II: validation and application. *Journal of Hydraulic Engineering*. ASCE 129(3):206–214.
- Lai, Y.G. and Patel, V.C., (1999). CFD simulation and assessment of the draft tube flow. Turbvie-99 – ERCOFTAC Workshop on draft tube flows. Porjus Hydropower Center, Sweden, June 1999.
- Lai, Y.G., (1999). An unstructured grid arbitrarily shaped element method for fluid flow simulation. AIAA paper 99-3711, 30th AIAA Fluid Dynamics Conference, Norfolk, VA, July 1999.
- Lai, Y.G. (2008). SRH-2D version2: Theory and User's Manual. Bureau of Reclamation, Technical Service Center, Sedimentation and River Hydraulics Group, Denver, CO.
- Lai, Y.G. (2001). U2RANS User's Manual. IHR-Hydroscience and Engineering, University of Iowa. <http://www.usbr.gov/pmts/sediment/model/u2rans/index.html>.
- Lane, E. W., (1947). Report of the Subcommittee on Sediment Terminology, Transactions, American Geophysical Union, Washington, DC. Vol. 28, No.6:936-938.
- Leopold, L.B., and T. Maddock, (1953). The hydraulic geometry of stream channels and some physiographic implications, U.S. Geological Survey Professional Paper, 252.
- Leopold, L.B., M.G. Wolman, and J.P. Miller, (1964). *Fluvial Processes in Geomorphology*, W. H. Freeman, London.
- Mefford, B. (2005) Lecture Notes. Bureau of Reclamation, Technical Service Center, Denver, CO.
- Meneghetti, Anthony M., (2009). Stage discharge relationships for U-, W-, and A-weirs. M.S. Thesis, Colorado State University, Department of Civil Engineering, Fort Collins, Colorado.

- Millar, R.G. (2005), Theoretical regime equations for mobile gravel-bed rivers with stable banks. *Geomorphology*, 67:204– 220.
- Mooney, D., Holmquist-Johnson, C.L., and Broderick, S. (2007a). Rock Ramp Design Guidelines. Bureau of Reclamation, Technical Service Center, Sedimentation and River Hydraulics Group, Denver, CO.
- Mooney, D., Holmquist-Johnson, C.L., and Holburn, E. (2007b). Qualitative Evaluation of Rock Weir Field Performance. Bureau of Reclamation, Technical Service Center, Sedimentation and River Hydraulics Group, Denver, CO.
- Nakato, T. (1989). A Review of International Literature of Design Practice and Experience with Low-Head Alluvial-Channel Grade-Control Structures, Prepared by the Iowa Institute of Hydraulic Research for the Us Army Engineer Waterways Experiment Station, Vicksburg M.S.
- NOAA Fisheries (2004). Anadromous Salmonid Passage Facility Guidelines and Criteria (draft document). Online at:
http://www.cbfwa.org/Committees/FSOC/Meetings/2003_0304/ReleaseDraftCriteria.doc
- Oregon Department of Fish and Wildlife (2004). Fish Passage Criteria. Online at:
<http://www.dfw.state.or.us/fish/passage/criteria.pdf>
- Parker, G., Wilcock, P.R., Paola, C., Dietrich, W.E., and Pitlick, J. (2007), Physical basis for quasi-universal relations describing bankfull hydraulic geometry of single-thread gravel bed rivers. *Journal of Geophysical Research*. v.112.
- Province of Alberta (2001). Fish Habitat Manual, Fact Sheet C14.
<http://www.trans.gov.ab.ca/Content/doctype123/production/fishhabitatmanual.htm>
- Roni, P., Beechie, T.J., Bilby, R.E., Leonetti, F.E., Pollock, M.M., and Pess, G.R. (2002). A review of stream restoration techniques and a hierarchical strategy for prioritizing restoration in Pacific Northwest watersheds. *North American Journal of Fisheries Management*. 22:1-20.
- Rosgen, D.L. (1996). Applied river morphology. Wildland Hydrology. Pagosa Springs, Colorado.
- Rosgen, D.L. (2006). The Cross-vane, W-weir and J-hook Vane Structures (Updated 2006)...Their Description, Design and Application for Stream Stabilization and River Restoration. Pagosa Springs, CO.
- Ruttenburg, D. (2007). An Evaluation of Fish Passage at Rock Vortex Weirs. M.S. Thesis, University of Idaho, College of Engineering, Moscow, ID.
- Schmetterling, D.A., and R. Pierce (1999). Success of Instream Habitat Structures after a 50-year Flood in Gold Creek, Montana. *Restoration Ecology*, 7 (4):369-375.
- Scurlock, Michael S., (2009). Equilibrium scour downstream of three-dimensional grade-control structures. M.S. Thesis, Colorado State University, Department of Civil Engineering, Fort Collins, Colorado.
- Simons, D.B., Sentürk, F. 1992. *Sediment Transport Technology Water and Sediment Dynamics*. Water Resources Publication, Littleton, Colorado.

- Thomas, D.B., Abt, S.R., Mussetter, R.A., and Harvey, M.D., (2000). A Design for Sizing Step-Pool Structures. Water Resources proceedings, ASCE.
- Thompson D.M., (2005). The long-term stability and morphologic influence of the use of instream structures in channel restoration design. In *Managing Watersheds for Human and Natural Impacts*, edited by G.E. Moglen. Proceedings of the 2005 Watershed Management Conference, p. 1-9.
- Thompson, D.M., (2005). The history of the use and effectiveness of instream structures in the United States. In *Humans as Geologic Agents*, edited by J. Ehlen, B. Haneberg and R. Larson, Geological Society of America Reviews in Engineering Geology. 16:35-50.
- Thornton, C. I., Meneghetti, A.M., Collins, K., Abt, S.R., and Scurlock, M.S., (2011). Stage-Discharge Relationships for U-, A-, and W-Weirs in Un-submerged Flow Conditions. *Journal of the American Water Resources Association (JAWRA)* 47(1):169-178.
- Washington Department of Fish and Wildlife (WDFW) (2000). Fishway Guidelines for Washington State. Online at: <http://wdfw.wa.gov/hab/ahg/ahguides.htm>
- Washington Department of Fish and Wildlife (WDFW) (2004). Stream habitat restoration guidelines: Final draft 2004. Olympia, Washington.
- Whittaker, J.G. and Jaeggi, M.N.R., (1982). Origin of step-pool systems in mountain streams. *Journal of the Hydraulics Division, Proceedings of the American Society of Civil Engineers*, v. 108, p.758-773.
- Wohl, E., Angermeier, P.L., Bledsoe, B., Kondolf, G.M., MacDonnell, L., Merritt, D.M., Palmer, M.A., Poff, N.L., and Tarboton, D. (2005). River Restoration. *Water Resources Research* 41(W10301): 1-12.
- Yang, C.T. (2003) *Sediment Transport Theory and Practice*. Krieger Publishing Co., Malabar, FL.

APPENDIX A

NUMERICAL MODEL TESTING MATRIX CONFIGURATIONS

Table A1 page 1 (records 1-25) – Numerical model testing matrix configuration data.

Record ID	Config ID	River	Reach	Structure Reference	Design Discharge (cms)	Oberbank Width (m)	Slope	Channel Width (m)	Channel Depth (m)	Top Width (m)	Side Slope (H/V)	Grain size (mm)	Manning n
1	1.01	P1.01_1	22.63mm-Qb	0.8ft-.3W-1ArmL	162	0.076	0.001	52.14	1.850	54.92	.75	22.63	0.024
2	1.01	P1.01_2	22.63mm-2/3Qb	0.8ft-.3W-1ArmL	108	0.076	0.001	52.14	1.850	54.92	.75	22.63	0.025
3	1.01	P1.01_3	22.63mm-1/3Qb	0.8ft-.3W-1ArmL	54	0.076	0.001	52.14	1.850	54.92	.75	22.63	0.027
4	1.01	P1.01_4	22.63mm-1/5Qb	0.8ft-.3W-1ArmL	32	0.076	0.001	52.11	1.850	54.92	.76	22.63	0.027
5	1.01	P1.01_5	22.63mm-1/10Qb	0.8ft-.3W-1ArmL	16	0.076	0.001	52.07	1.850	54.92	.77	22.63	0.027
6	1.02	P1.02_6	22.63mm-Qb	0.4ft-.25W-0.5ArmL	162	0.076	0.001	52.14	1.850	54.92	.75	22.63	0.024
7	1.02	P1.02_7	22.63mm-2/3Qb	0.4ft-.25W-0.5ArmL	108	0.076	0.001	52.14	1.850	54.92	.75	22.63	0.025
8	1.02	P1.02_8	22.63mm-1/3Qb	0.4ft-.25W-0.5ArmL	54	0.076	0.001	52.14	1.850	54.92	.75	22.63	0.027
9	1.02	P1.02_9	22.63mm-1/5Qb	0.4ft-.25W-0.5ArmL	32	0.076	0.001	52.14	1.850	54.92	.75	22.63	0.027
10	1.02	P1.02_10	22.63mm-1/10Qb	0.4ft-.25W-0.5ArmL	16	0.076	0.001	52.14	1.850	54.92	.75	22.63	0.027
11	1.03	P1.03_11	22.63mm-Qb	0.4ft-.25W-2ArmL	162	0.076	0.001	52.14	1.850	54.92	.75	22.63	0.024
12	1.03	P1.03_12	22.63mm-2/3Qb	0.4ft-.25W-2ArmL	108	0.076	0.001	52.14	1.850	54.92	.75	22.63	0.025
13	1.03	P1.03_13	22.63mm-1/3Qb	0.4ft-.25W-2ArmL	54	0.076	0.001	52.14	1.850	54.92	.75	22.63	0.027
14	1.03	P1.03_14	22.63mm-1/5Qb	0.4ft-.25W-2ArmL	32	0.076	0.001	52.14	1.850	54.92	.75	22.63	0.027
15	1.03	P1.03_15	22.63mm-1/10Qb	0.4ft-.25W-2ArmL	16	0.076	0.001	52.14	1.850	54.92	.75	22.63	0.027
16	1.04	P1.04_16	22.63mm-Qb	0.4ft-.5W-0.5ArmL	162	0.076	0.001	52.14	1.850	54.92	.75	22.63	0.024
17	1.04	P1.04_17	22.63mm-2/3Qb	0.4ft-.5W-0.5ArmL	108	0.076	0.001	52.14	1.850	54.92	.75	22.63	0.025
18	1.04	P1.04_18	22.63mm-1/3Qb	0.4ft-.5W-0.5ArmL	54	0.076	0.001	52.14	1.850	54.92	.75	22.63	0.027
19	1.04	P1.04_19	22.63mm-1/5Qb	0.4ft-.5W-0.5ArmL	32	0.076	0.001	52.14	1.850	54.92	.75	22.63	0.027
20	1.04	P1.04_20	22.63mm-1/10Qb	0.4ft-.5W-0.5ArmL	16	0.076	0.001	52.14	1.850	54.92	.75	22.63	0.027
21	1.05	P1.05_21	22.63mm-Qb	0.4ft-.5W-2ArmL	162	0.076	0.001	52.14	1.850	54.92	.75	22.63	0.024
22	1.05	P1.05_22	22.63mm-2/3Qb	0.4ft-.5W-2ArmL	108	0.076	0.001	52.14	1.850	54.92	.75	22.63	0.025
23	1.05	P1.05_23	22.63mm-1/3Qb	0.4ft-.5W-2ArmL	54	0.076	0.001	52.14	1.850	54.92	.75	22.63	0.027
24	1.05	P1.05_24	22.63mm-1/5Qb	0.4ft-.5W-2ArmL	32	0.076	0.001	52.14	1.850	54.92	.75	22.63	0.027
25	1.05	P1.05_25	22.63mm-1/10Qb	0.4ft-.5W-2ArmL	16	0.076	0.001	52.14	1.850	54.92	.75	22.63	0.027

Table A1 page 1 (records 1-25) cont.

Record ID	Normal Depth (m)	US XS Station (m)	Crest Station (m)	DS XS Station (m)	Structure Rock Size Width (m)	Structure Rock Size Height (m)	Weir Crest Elevation (m)	Drop Height (m)	Throat Width (m)	Lft Arm Angle (degrees)	Lft Arm Slope (degrees)	Lft Arm Length (m)	Rt Arm Angle (degrees)	Rt Arm Slope (degrees)	Rt Arm Length (m)
1	1.710	-164.76	0.00	274.59	1.219	0.813	30.724	0.244	18.306	27.34	2.26	35.403	27.34	2.26	35.403
2	1.369	-164.76	0.00	274.59	1.219	0.813	30.724	0.244	18.306	27.34	2.26	35.403	27.34	2.26	35.403
3	0.939	-164.76	0.00	274.59	1.219	0.813	30.724	0.244	18.306	27.34	2.26	35.403	27.34	2.26	35.403
4	0.689	-164.76	0.00	274.59	1.219	0.813	30.724	0.244	18.306	27.34	2.26	35.403	27.34	2.26	35.403
5	0.454	-164.76	0.00	274.59	1.219	0.813	30.724	0.244	18.306	27.34	2.26	35.403	27.34	2.26	35.403
6	1.707	-164.76	0.00	274.59	1.219	0.813	30.602	0.122	13.728	46.44	3.44	19.583	46.44	3.44	19.583
7	1.369	-164.76	0.00	274.59	1.219	0.813	30.602	0.122	13.728	46.44	3.44	19.583	46.44	3.44	19.583
8	0.939	-164.76	0.00	274.59	1.219	0.813	30.602	0.122	13.728	46.44	3.44	19.583	46.44	3.44	19.583
9	0.689	-164.76	0.00	274.59	1.219	0.813	30.602	0.122	13.728	46.44	3.44	19.583	46.44	3.44	19.583
10	0.454	-164.76	0.00	274.59	1.219	0.813	30.602	0.122	13.728	46.44	3.44	19.583	46.44	3.44	19.583
11	1.707	-164.76	0.00	313.35	1.219	0.813	30.602	0.122	13.728	14.73	1.17	78.337	14.73	1.17	78.337
12	1.369	-164.76	0.00	313.35	1.219	0.813	30.602	0.122	13.728	14.73	1.17	78.337	14.73	1.17	78.337
13	0.939	-164.76	0.00	313.35	1.219	0.813	30.602	0.122	13.728	14.73	1.17	78.337	14.73	1.17	78.337
14	0.689	-164.76	0.00	313.35	1.219	0.813	30.602	0.122	13.728	14.73	1.17	78.337	14.73	1.17	78.337
15	0.454	-164.76	0.00	313.35	1.219	0.813	30.602	0.122	13.728	14.73	1.17	78.337	14.73	1.17	78.337
16	1.707	-164.76	0.00	274.59	1.219	0.813	30.602	0.122	27.459	40.29	4.61	16.194	40.29	4.61	16.194
17	1.369	-164.76	0.00	274.59	1.219	0.813	30.602	0.122	27.459	40.29	4.61	16.194	40.29	4.61	16.194
18	0.939	-164.76	0.00	274.59	1.219	0.813	30.602	0.122	27.459	40.29	4.61	16.194	40.29	4.61	16.194
19	0.689	-164.76	0.00	274.59	1.219	0.813	30.602	0.122	27.459	40.29	4.61	16.194	40.29	4.61	16.194
20	0.454	-164.76	0.00	274.59	1.219	0.813	30.602	0.122	27.459	40.29	4.61	16.194	40.29	4.61	16.194
21	1.707	-164.76	0.00	274.59	1.219	0.813	30.602	0.122	27.459	11.97	1.44	64.779	11.97	1.44	64.779
22	1.369	-164.76	0.00	274.59	1.219	0.813	30.602	0.122	27.459	11.97	1.44	64.779	11.97	1.44	64.779
23	0.939	-164.76	0.00	274.59	1.219	0.813	30.602	0.122	27.459	11.97	1.44	64.779	11.97	1.44	64.779
24	0.689	-164.76	0.00	274.59	1.219	0.813	30.602	0.122	27.459	11.97	1.44	64.779	11.97	1.44	64.779
25	0.454	-164.76	0.00	274.59	1.219	0.813	30.602	0.122	27.459	11.97	1.44	64.779	11.97	1.44	64.779

Table A1 page 2 (records 26-50) – Numerical model testing matrix configuration data.

Record ID	Config ID	River	Reach	Structure Reference	Design Discharge (cms)	Oberbank Width (m)	Slope	Channel Width (m)	Channel Depth (m)	Top Width (m)	Side Slope (H/V)	Grain size (mm)	Manning n
26	1.06	P1.06_26	22.63mm-Qb	1.2ft-.25W-0.5ArmL	162	0.076	0.001	52.14	1.850	54.92	.75	22.63	0.024
27	1.06	P1.06_27	22.63mm-2/3Qb	1.2ft-.25W-0.5ArmL	108	0.076	0.001	52.14	1.850	54.92	.75	22.63	0.025
28	1.06	P1.06_28	22.63mm-1/3Qb	1.2ft-.25W-0.5ArmL	54	0.076	0.001	52.14	1.850	54.92	.75	22.63	0.027
29	1.06	P1.06_29	22.63mm-1/5Qb	1.2ft-.25W-0.5ArmL	32	0.076	0.001	52.14	1.850	54.92	.75	22.63	0.027
30	1.06	P1.06_30	22.63mm-1/10Qb	1.2ft-.25W-0.5ArmL	16	0.076	0.001	52.14	1.850	54.92	.75	22.63	0.027
31	1.07	P1.07_31	22.63mm-Qb	1.2ft-.25W-2ArmL	162	0.076	0.001	52.14	1.850	54.92	.75	22.63	0.024
32	1.07	P1.07_32	22.63mm-2/3Qb	1.2ft-.25W-2ArmL	108	0.076	0.001	52.14	1.850	54.92	.75	22.63	0.025
33	1.07	P1.07_33	22.63mm-1/3Qb	1.2ft-.25W-2ArmL	54	0.076	0.001	52.14	1.850	54.92	.75	22.63	0.027
34	1.07	P1.07_34	22.63mm-1/5Qb	1.2ft-.25W-2ArmL	32	0.076	0.001	52.14	1.850	54.92	.75	22.63	0.027
35	1.07	P1.07_35	22.63mm-1/10Qb	1.2ft-.25W-2ArmL	16	0.076	0.001	52.14	1.850	54.92	.75	22.63	0.027
36	1.08	P1.08_36	22.63mm-Qb	1.2ft-.5W-0.5ArmL	162	0.076	0.001	52.14	1.850	54.92	.75	22.63	0.024
37	1.08	P1.08_37	22.63mm-2/3Qb	1.2ft-.5W-0.5ArmL	108	0.076	0.001	52.14	1.850	54.92	.75	22.63	0.025
38	1.08	P1.08_38	22.63mm-1/3Qb	1.2ft-.5W-0.5ArmL	54	0.076	0.001	52.14	1.850	54.92	.75	22.63	0.027
39	1.08	P1.08_39	22.63mm-1/5Qb	1.2ft-.5W-0.5ArmL	32	0.076	0.001	52.14	1.850	54.92	.75	22.63	0.027
40	1.08	P1.08_40	22.63mm-1/10Qb	1.2ft-.5W-0.5ArmL	16	0.076	0.001	52.14	1.850	54.92	.75	22.63	0.027
41	1.09	P1.09_41	22.63mm-Qb	1.2ft-.5W-2ArmL	162	0.076	0.001	52.14	1.850	54.92	.75	22.63	0.024
42	1.09	P1.09_42	22.63mm-2/3Qb	1.2ft-.5W-2ArmL	108	0.076	0.001	52.14	1.850	54.92	.75	22.63	0.025
43	1.09	P1.09_43	22.63mm-1/3Qb	1.2ft-.5W-2ArmL	54	0.076	0.001	52.14	1.850	54.92	.75	22.63	0.027
44	1.09	P1.09_44	22.63mm-1/5Qb	1.2ft-.5W-2ArmL	32	0.076	0.001	52.14	1.850	54.92	.75	22.63	0.027
45	1.09	P1.09_45	22.63mm-1/10Qb	1.2ft-.5W-2ArmL	16	0.076	0.001	52.14	1.850	54.92	.75	22.63	0.027
46	1.10	P1.10_46	22.63mm-Qb	0.8ft-.3W-0.5ArmL	162	0.076	0.001	52.14	1.850	54.92	.75	22.63	0.024
47	1.10	P1.10_47	22.63mm-2/3Qb	0.8ft-.3W-0.5ArmL	108	0.076	0.001	52.14	1.850	54.92	.75	22.63	0.025
48	1.10	P1.10_48	22.63mm-1/3Qb	0.8ft-.3W-0.5ArmL	54	0.076	0.001	52.14	1.850	54.92	.75	22.63	0.027
49	1.10	P1.10_49	22.63mm-1/5Qb	0.8ft-.3W-0.5ArmL	32	0.076	0.001	52.14	1.850	54.92	.75	22.63	0.027
50	1.10	P1.10_50	22.63mm-1/10Qb	0.8ft-.3W-0.5ArmL	16	0.076	0.001	52.14	1.850	54.92	.75	22.63	0.027

Table A1 page 2 (records 26-50) cont.

Record ID	Normal Depth (m)	US XS Station (m)	Crest Station (m)	DS XS Station (m)	Structure Rock Size Width (m)	Structure Rock Size Height (m)	Weir Crest Elevation (m)	Drop Height (m)	Throat Width (m)	Lft Arm Angle (degrees)	Lft Arm Slope (degrees)	Lft Arm Length (m)	Rt Arm Angle (degrees)	Rt Arm Slope (degrees)	Rt Arm Length (m)
26	1.707	-164.76	0.00	274.59	1.219	0.813	30.846	0.366	13.728	47.72	3.02	18.724	47.72	3.02	18.724
27	1.369	-164.76	0.00	274.59	1.219	0.813	30.846	0.366	13.728	47.72	3.02	18.724	47.72	3.02	18.724
28	0.939	-164.76	0.00	274.59	1.219	0.813	30.846	0.366	13.728	47.72	3.02	18.724	47.72	3.02	18.724
29	0.689	-164.76	0.00	274.59	1.219	0.813	30.846	0.366	13.728	47.72	3.02	18.724	47.72	3.02	18.724
30	0.454	-164.76	0.00	274.59	1.219	0.813	30.846	0.366	13.728	47.72	3.02	18.724	47.72	3.02	18.724
31	1.707	-164.76	0.00	299.59	1.219	0.813	30.846	0.366	13.728	15.37	1.04	74.899	15.37	1.04	74.899
32	1.369	-164.76	0.00	299.59	1.219	0.813	30.846	0.366	13.728	15.37	1.04	74.899	15.37	1.04	74.899
33	0.939	-164.76	0.00	299.59	1.219	0.813	30.846	0.366	13.728	15.37	1.04	74.899	15.37	1.04	74.899
34	0.689	-164.76	0.00	299.59	1.219	0.813	30.846	0.366	13.728	15.37	1.04	74.899	15.37	1.04	74.899
35	0.454	-164.76	0.00	299.59	1.219	0.813	30.846	0.366	13.728	15.37	1.04	74.899	15.37	1.04	74.899
36	1.707	-164.76	0.00	274.59	1.219	0.813	30.846	0.366	27.459	43.06	4.18	14.688	43.06	4.18	14.688
37	1.369	-164.76	0.00	274.59	1.219	0.813	30.846	0.366	27.459	43.06	4.18	14.688	43.06	4.18	14.688
38	0.939	-164.76	0.00	274.59	1.219	0.813	30.846	0.366	27.459	43.06	4.18	14.688	43.06	4.18	14.688
39	0.689	-164.76	0.00	274.59	1.219	0.813	30.846	0.366	27.459	43.06	4.18	14.688	43.06	4.18	14.688
40	0.454	-164.76	0.00	274.59	1.219	0.813	30.846	0.366	27.459	43.06	4.18	14.688	43.06	4.18	14.688
41	1.707	-164.76	0.00	274.59	1.219	0.813	30.846	0.366	27.459	13.15	1.35	58.759	13.15	1.35	58.759
42	1.369	-164.76	0.00	274.59	1.219	0.813	30.846	0.366	27.459	13.15	1.35	58.759	13.15	1.35	58.759
43	0.939	-164.76	0.00	274.59	1.219	0.813	30.846	0.366	27.459	13.15	1.35	58.759	13.15	1.35	58.759
44	0.689	-164.76	0.00	274.59	1.219	0.813	30.846	0.366	27.459	13.15	1.35	58.759	13.15	1.35	58.759
45	0.454	-164.76	0.00	274.59	1.219	0.813	30.846	0.366	27.459	13.15	1.35	58.759	13.15	1.35	58.759
46	1.710	-164.76	0.00	274.59	1.219	0.813	30.724	0.244	18.306	45.96	3.57	17.703	45.96	3.57	17.703
47	1.369	-164.76	0.00	274.59	1.219	0.813	30.724	0.244	18.306	45.96	3.57	17.703	45.96	3.57	17.703
48	0.939	-164.76	0.00	274.59	1.219	0.813	30.724	0.244	18.306	45.96	3.57	17.703	45.96	3.57	17.703
49	0.689	-164.76	0.00	274.59	1.219	0.813	30.724	0.244	18.306	45.96	3.57	17.703	45.96	3.57	17.703
50	0.454	-164.76	0.00	274.59	1.219	0.813	30.724	0.244	18.306	45.96	3.57	17.703	45.96	3.57	17.703

Table A1 page3 (records 51-75) – Numerical model testing matrix configuration data.

Record ID	Config ID	River	Reach	Structure Reference	Design Discharge (cms)	Oberbank Width (m)	Slope	Channel Width (m)	Channel Depth (m)	Top Width (m)	Side Slope (H/V)	Grain size (mm)	Manning n
51	1.11	P1.11_51	22.63mm-Qb	0.8ft-.3W-2ArmL	162	0.076	0.001	52.14	1.850	54.92	.75	22.63	0.024
52	1.11	P1.11_52	22.63mm-2/3Qb	0.8ft-.3W-2ArmL	108	0.076	0.001	52.14	1.850	54.92	.75	22.63	0.025
53	1.11	P1.11_53	22.63mm-1/3Qb	0.8ft-.3W-2ArmL	54	0.076	0.001	52.14	1.850	54.92	.75	22.63	0.027
54	1.11	P1.11_54	22.63mm-1/5Qb	0.8ft-.3W-2ArmL	32	0.076	0.001	52.14	1.850	54.92	.75	22.63	0.027
55	1.11	P1.11_55	22.63mm-1/10Qb	0.8ft-.3W-2ArmL	16	0.076	0.001	52.14	1.850	54.92	.75	22.63	0.027
56	2.01	P2.01_56	90.51mm-Qb	0.8ft-.3W-1ArmL	92	0.076	0.004	31.26	1.475	33.47	.75	90.51	0.034
57	2.01	P2.01_57	90.51mm-2/3Qb	0.8ft-.3W-1ArmL	61	0.076	0.004	31.26	1.475	33.47	.75	90.51	0.035
58	2.01	P2.01_58	90.51mm-1/3Qb	0.8ft-.3W-1ArmL	31	0.076	0.004	31.26	1.475	33.47	.75	90.51	0.037
59	2.01	P2.01_59	90.51mm-1/5Qb	0.8ft-.3W-1ArmL	18	0.076	0.004	31.26	1.475	33.47	.75	90.51	0.037
60	2.01	P2.01_60	90.51mm-1/10Qb	0.8ft-.3W-1ArmL	9	0.076	0.004	31.26	1.475	33.47	.75	90.51	0.037
61	2.02	P2.02_61	90.51mm-Qb	0.4ft-.25W-0.5ArmL	92	0.076	0.004	31.26	1.475	33.47	.75	90.51	0.034
62	2.02	P2.02_62	90.51mm-2/3Qb	0.4ft-.25W-0.5ArmL	61	0.076	0.004	31.26	1.475	33.47	.75	90.51	0.035
63	2.02	P2.02_63	90.51mm-1/3Qb	0.4ft-.25W-0.5ArmL	31	0.076	0.004	31.26	1.475	33.47	.75	90.51	0.037
64	2.02	P2.02_64	90.51mm-1/5Qb	0.4ft-.25W-0.5ArmL	18	0.076	0.004	31.26	1.475	33.47	.75	90.51	0.037
65	2.02	P2.02_65	90.51mm-1/10Qb	0.4ft-.25W-0.5ArmL	9	0.076	0.004	31.26	1.475	33.47	.75	90.51	0.037
66	2.03	P2.03_66	90.51mm-Qb	0.4ft-.25W-2ArmL	92	0.076	0.004	31.26	1.475	33.47	.75	90.51	0.034
67	2.03	P2.03_67	90.51mm-2/3Qb	0.4ft-.25W-2ArmL	61	0.076	0.004	31.26	1.475	33.47	.75	90.51	0.035
68	2.03	P2.03_68	90.51mm-1/3Qb	0.4ft-.25W-2ArmL	31	0.076	0.004	31.26	1.475	33.47	.75	90.51	0.037
69	2.03	P2.03_69	90.51mm-1/5Qb	0.4ft-.25W-2ArmL	18	0.076	0.004	31.26	1.475	33.47	.75	90.51	0.037
70	2.03	P2.03_70	90.51mm-1/10Qb	0.4ft-.25W-2ArmL	9	0.076	0.004	31.26	1.475	33.47	.75	90.51	0.037
71	2.04	P2.04_71	90.51mm-Qb	0.4ft-.5W-0.5ArmL	92	0.076	0.004	31.26	1.475	33.47	.75	90.51	0.034
72	2.04	P2.04_72	90.51mm-2/3Qb	0.4ft-.5W-0.5ArmL	61	0.076	0.004	31.26	1.475	33.47	.75	90.51	0.035
73	2.04	P2.04_73	90.51mm-1/3Qb	0.4ft-.5W-0.5ArmL	31	0.076	0.004	31.26	1.475	33.47	.75	90.51	0.037
74	2.04	P2.04_74	90.51mm-1/5Qb	0.4ft-.5W-0.5ArmL	18	0.076	0.004	31.26	1.475	33.47	.75	90.51	0.037
75	2.04	P2.04_75	90.51mm-1/10Qb	0.4ft-.5W-0.5ArmL	9	0.076	0.004	31.26	1.475	33.47	.75	90.51	0.037

Table A1 page 3 (records 51-75) cont.

Record ID	Normal Depth (m)	US XS Station (m)	Crest Station (m)	DS XS Station (m)	Structure Rock Size Width (m)	Structure Rock Size Height (m)	Weir Crest Elevation (m)	Drop Height (m)	Throat Width (m)	Lft Arm Angle (degrees)	Lft Arm Slope (degrees)	Lft Arm Length (m)	Rt Arm Angle (degrees)	Rt Arm Slope (degrees)	Rt Arm Length (m)
51	1.710	-164.76	0.00	283.23	1.219	0.813	30.724	0.244	18.306	14.5	1.2	70.808	14.50	1.20	70.808
52	1.369	-164.76	0.00	283.23	1.219	0.813	30.724	0.244	18.306	14.5	1.2	70.808	14.50	1.20	70.808
53	0.939	-164.76	0.00	283.23	1.219	0.813	30.724	0.244	18.306	14.50	1.20	70.808	14.50	1.20	70.808
54	0.689	-164.76	0.00	283.23	1.219	0.813	30.724	0.244	18.306	14.50	1.20	70.808	14.50	1.20	70.808
55	0.454	-164.76	0.00	283.23	1.219	0.813	30.724	0.244	18.306	14.50	1.20	70.808	14.50	1.20	70.808
56	1.350	-100.41	0.00	167.35	0.914	0.610	30.724	0.244	11.156	25.53	2.52	23.354	25.53	2.52	23.354
57	1.073	-100.41	0.00	167.35	0.914	0.610	30.724	0.244	11.156	25.53	2.52	23.354	25.53	2.52	23.354
58	0.728	-100.41	0.00	167.35	0.914	0.610	30.724	0.244	11.156	25.53	2.52	23.354	25.53	2.52	23.354
59	0.533	-100.41	0.00	167.35	0.914	0.610	30.724	0.244	11.156	25.53	2.52	23.354	25.53	2.52	23.354
60	0.354	-100.41	0.00	167.35	0.914	0.610	30.724	0.244	11.156	25.53	2.52	23.354	25.53	2.52	23.354
61	1.350	-100.41	0.00	167.35	0.914	0.610	30.602	0.122	8.367	44.08	4.13	12.963	44.08	4.13	12.963
62	1.073	-100.41	0.00	167.35	0.914	0.610	30.602	0.122	8.367	44.08	4.13	12.963	44.08	4.13	12.963
63	0.728	-100.41	0.00	167.35	0.914	0.610	30.602	0.122	8.367	44.08	4.13	12.963	44.08	4.13	12.963
64	0.533	-100.41	0.00	167.35	0.914	0.610	30.602	0.122	8.367	44.08	4.13	12.963	44.08	4.13	12.963
65	0.354	-100.41	0.00	167.35	0.914	0.610	30.602	0.122	8.367	44.08	4.13	12.963	44.08	4.13	12.963
66	1.350	-100.41	0.00	207.39	0.914	0.610	30.602	0.122	8.367	13.61	1.23	51.846	13.61	1.23	51.846
67	1.073	-100.41	0.00	207.39	0.914	0.610	30.602	0.122	8.367	13.61	1.23	51.846	13.61	1.23	51.846
68	0.728	-100.41	0.00	207.39	0.914	0.610	30.602	0.122	8.367	13.61	1.23	51.846	13.61	1.23	51.846
69	0.533	-100.41	0.00	207.39	0.914	0.610	30.602	0.122	8.367	13.61	1.23	51.846	13.61	1.23	51.846
70	0.354	-100.41	0.00	207.39	0.914	0.610	30.602	0.122	8.367	13.61	1.23	51.846	13.61	1.23	51.846
71	1.350	-100.41	0.00	167.35	0.914	0.610	30.602	0.122	16.734	36.05	5.26	11.494	36.05	5.26	11.494
72	1.073	-100.41	0.00	167.35	0.914	0.610	30.602	0.122	16.734	36.05	5.26	11.494	36.05	5.26	11.494
73	0.728	-100.41	0.00	167.35	0.914	0.610	30.602	0.122	16.734	36.05	5.26	11.494	36.05	5.26	11.494
74	0.533	-100.41	0.00	167.35	0.914	0.610	30.602	0.122	16.734	36.05	5.26	11.494	36.05	5.26	11.494
75	0.354	-100.41	0.00	167.35	0.914	0.610	30.602	0.122	16.734	36.05	5.26	11.494	36.05	5.26	11.494

Table A1 page 4 (records 76-100) – Numerical model testing matrix configuration data.

Record ID	Config ID	River	Reach	Structure Reference	Design Discharge (cms)	Oberbank Width (m)	Slope	Channel Width (m)	Channel Depth (m)	Top Width (m)	Side Slope (H/V)	Grain size (mm)	Manning n
76	2.05	P2.05_76	90.51mm-Qb	0.4ft-.5W-2ArmL	92	0.076	0.004	31.26	1.475	33.47	.75	90.51	0.034
77	2.05	P2.05_77	90.51mm-2/3Qb	0.4ft-.5W-2ArmL	61	0.076	0.004	31.26	1.475	33.47	.75	90.51	0.035
78	2.05	P2.05_78	90.51mm-1/3Qb	0.4ft-.5W-2ArmL	31	0.076	0.004	31.26	1.475	33.47	.75	90.51	0.037
79	2.05	P2.05_79	90.51mm-1/5Qb	0.4ft-.5W-2ArmL	18	0.076	0.004	31.26	1.475	33.47	.75	90.51	0.037
80	2.05	P2.05_80	90.51mm-1/10Qb	0.4ft-.5W-2ArmL	9	0.076	0.004	31.26	1.475	33.47	.75	90.51	0.037
81	2.06	P2.06_81	90.51mm-Qb	1.2ft-.25W-0.5ArmL	92	0.076	0.004	31.26	1.475	33.47	.75	90.51	0.034
82	2.06	P2.06_82	90.51mm-2/3Qb	1.2ft-.25W-0.5ArmL	61	0.076	0.004	31.26	1.475	33.47	.75	90.51	0.035
83	2.06	P2.06_83	90.51mm-1/3Qb	1.2ft-.25W-0.5ArmL	31	0.076	0.004	31.26	1.475	33.47	.75	90.51	0.037
84	2.06	P2.06_84	90.51mm-1/5Qb	1.2ft-.25W-0.5ArmL	18	0.076	0.004	31.26	1.475	33.47	.75	90.51	0.037
85	2.06	P2.06_85	90.51mm-1/10Qb	1.2ft-.25W-0.5ArmL	9	0.076	0.004	31.26	1.475	33.47	.75	90.51	0.037
86	2.07	P2.07_86	90.51mm-Qb	1.2ft-.25W-2ArmL	92	0.076	0.004	31.26	1.475	33.47	.75	90.51	0.034
87	2.07	P2.07_87	90.51mm-2/3Qb	1.2ft-.25W-2ArmL	61	0.076	0.004	31.26	1.475	33.47	.75	90.51	0.035
88	2.07	P2.07_88	90.51mm-1/3Qb	1.2ft-.25W-2ArmL	31	0.076	0.004	31.26	1.475	33.47	.75	90.51	0.037
89	2.07	P2.07_89	90.51mm-1/5Qb	1.2ft-.25W-2ArmL	18	0.076	0.004	31.26	1.475	33.47	.75	90.51	0.037
90	2.07	P2.07_90	90.51mm-1/10Qb	1.2ft-.25W-2ArmL	9	0.076	0.004	31.26	1.475	33.47	.75	90.51	0.037
91	2.08	P2.08_91	90.51mm-Qb	1.2ft-.5W-0.5ArmL	92	0.076	0.004	31.26	1.475	33.47	.75	90.51	0.034
92	2.08	P2.08_92	90.51mm-2/3Qb	1.2ft-.5W-0.5ArmL	61	0.076	0.004	31.26	1.475	33.47	.75	90.51	0.035
93	2.08	P2.08_93	90.51mm-1/3Qb	1.2ft-.5W-0.5ArmL	31	0.076	0.004	31.26	1.475	33.47	.75	90.51	0.037
94	2.08	P2.08_94	90.51mm-1/5Qb	1.2ft-.5W-0.5ArmL	18	0.076	0.004	31.26	1.475	33.47	.75	90.51	0.037
95	2.08	P2.08_95	90.51mm-1/10Qb	1.2ft-.5W-0.5ArmL	9	0.076	0.004	31.26	1.475	33.47	.75	90.51	0.037
96	2.09	P2.09_96	90.51mm-Qb	1.2ft-.5W-2ArmL	92	0.076	0.004	31.26	1.475	33.47	.75	90.51	0.034
97	2.09	P2.09_97	90.51mm-2/3Qb	1.2ft-.5W-2ArmL	61	0.076	0.004	31.26	1.475	33.47	.75	90.51	0.035
98	2.09	P2.09_98	90.51mm-1/3Qb	1.2ft-.5W-2ArmL	31	0.076	0.004	31.26	1.475	33.47	.75	90.51	0.037
99	2.09	P2.09_99	90.51mm-1/5Qb	1.2ft-.5W-2ArmL	18	0.076	0.004	31.26	1.475	33.47	.75	90.51	0.037
100	2.09	P2.09_100	90.51mm-1/10Qb	1.2ft-.5W-2ArmL	9	0.076	0.004	31.26	1.475	33.47	.75	90.51	0.037

Table A1 page 4 (records 76-100) cont.

Record ID	Normal Depth (m)	US XS Station (m)	Crest Station (m)	DS XS Station (m)	Structure Rock Size Width (m)	Structure Rock Size Height (m)	Weir Crest Elevation (m)	Drop Height (m)	Throat Width (m)	Lft Arm Angle (degrees)	Lft Arm Slope (degrees)	Lft Arm Length (m)	Rt Arm Angle (degrees)	Rt Arm Slope (degrees)	Rt Arm Length (m)
76	1.350	-100.41	0.00	183.92	0.914	0.610	30.602	0.122	16.734	10.31	1.43	45.979	10.31	1.43	45.979
77	1.073	-100.41	0.00	183.92	0.914	0.610	30.602	0.122	16.734	10.31	1.43	45.979	10.31	1.43	45.979
78	0.728	-100.41	0.00	183.92	0.914	0.610	30.602	0.122	16.734	10.31	1.43	45.979	10.31	1.43	45.979
79	0.533	-100.41	0.00	183.92	0.914	0.610	30.602	0.122	16.734	10.31	1.43	45.979	10.31	1.43	45.979
80	0.354	-100.41	0.00	183.92	0.914	0.610	30.602	0.122	16.734	10.31	1.43	45.979	10.31	1.43	45.979
81	1.350	-100.41	0.00	167.35	0.914	0.610	30.846	0.366	8.367	46.76	3.53	11.802	46.76	3.53	11.802
82	1.073	-100.41	0.00	167.35	0.914	0.610	30.846	0.366	8.367	46.76	3.53	11.802	46.76	3.53	11.802
83	0.728	-100.41	0.00	167.35	0.914	0.610	30.846	0.366	8.367	46.76	3.53	11.802	46.76	3.53	11.802
84	0.533	-100.41	0.00	167.35	0.914	0.610	30.846	0.366	8.367	46.76	3.53	11.802	46.76	3.53	11.802
85	0.354	-100.41	0.00	167.35	0.914	0.610	30.846	0.366	8.367	46.76	3.53	11.802	46.76	3.53	11.802
86	1.350	-100.41	0.00	188.82	0.914	0.610	30.846	0.366	8.367	14.89	1.08	47.204	14.89	1.08	47.204
87	1.073	-100.41	0.00	188.82	0.914	0.610	30.846	0.366	8.367	14.89	1.08	47.204	14.89	1.08	47.204
88	0.728	-100.41	0.00	188.82	0.914	0.610	30.846	0.366	8.367	14.89	1.08	47.204	14.89	1.08	47.204
89	0.533	-100.41	0.00	188.82	0.914	0.610	30.846	0.366	8.367	14.89	1.08	47.204	14.89	1.08	47.204
90	0.354	-100.41	0.00	188.82	0.914	0.610	30.846	0.366	8.367	14.89	1.08	47.204	14.89	1.08	47.204
91	1.350	-100.41	0.00	167.35	0.914	0.610	30.846	0.366	16.734	40.26	4.73	9.879	40.26	4.73	9.879
92	1.073	-100.41	0.00	167.35	0.914	0.610	30.846	0.366	16.734	40.26	4.73	9.879	40.26	4.73	9.879
93	0.728	-100.41	0.00	167.35	0.914	0.610	30.846	0.366	16.734	40.26	4.73	9.879	40.26	4.73	9.879
94	0.533	-100.41	0.00	167.35	0.914	0.610	30.846	0.366	16.734	40.26	4.73	9.879	40.26	4.73	9.879
95	0.354	-100.41	0.00	167.35	0.914	0.610	30.846	0.366	16.734	40.26	4.73	9.879	40.26	4.73	9.879
96	1.350	-100.41	0.00	167.35	0.914	0.610	30.846	0.366	16.734	11.95	1.35	39.517	11.95	1.35	39.517
97	1.073	-100.41	0.00	167.35	0.914	0.610	30.846	0.366	16.734	11.95	1.35	39.517	11.95	1.35	39.517
98	0.728	-100.41	0.00	167.35	0.914	0.610	30.846	0.366	16.734	11.95	1.35	39.517	11.95	1.35	39.517
99	0.533	-100.41	0.00	167.35	0.914	0.610	30.846	0.366	16.734	11.95	1.35	39.517	11.95	1.35	39.517
100	0.354	-100.41	0.00	167.35	0.914	0.610	30.846	0.366	16.734	11.95	1.35	39.517	11.95	1.35	39.517

Table A1 page 5 (records 101-125) – Numerical model testing matrix configuration data.

Record ID	Config ID	River	Reach	Structure Reference	Design Discharge (cms)	Oberbank Width (m)	Slope	Channel Width (m)	Channel Depth (m)	Top Width (m)	Side Slope (H/V)	Grain size (mm)	Manning n
101	2.10	P2.10_101	90.51mm-Qb	0.8ft-.3W-0.5ArmL	92	0.076	0.004	31.26	1.475	33.47	.75	90.51	0.034
102	2.10	P2.10_102	90.51mm-2/3Qb	0.8ft-.3W-0.5ArmL	61	0.076	0.004	31.26	1.475	33.47	.75	90.51	0.035
103	2.10	P2.10_103	90.51mm-1/3Qb	0.8ft-.3W-0.5ArmL	31	0.076	0.004	31.26	1.475	33.47	.75	90.51	0.037
104	2.10	P2.10_104	90.51mm-1/5Qb	0.8ft-.3W-0.5ArmL	18	0.076	0.004	31.26	1.475	33.47	.75	90.51	0.037
105	2.10	P2.10_105	90.51mm-1/10Qb	0.8ft-.3W-0.5ArmL	9	0.076	0.004	31.26	1.475	33.47	.75	90.51	0.037
106	2.11	P2.11_106	90.51mm-Qb	0.8ft-.3W-2ArmL	92	0.076	0.004	31.26	1.475	33.47	.75	90.51	0.034
107	2.11	P2.11_107	90.51mm-2/3Qb	0.8ft-.3W-2ArmL	61	0.076	0.004	31.26	1.475	33.47	.75	90.51	0.035
108	2.11	P2.11_108	90.51mm-1/3Qb	0.8ft-.3W-2ArmL	31	0.076	0.004	31.26	1.475	33.47	.75	90.51	0.037
109	2.11	P2.11_109	90.51mm-1/5Qb	0.8ft-.3W-2ArmL	18	0.076	0.004	31.26	1.475	33.47	.75	90.51	0.037
110	2.11	P2.11_110	90.51mm-1/10Qb	0.8ft-.3W-2ArmL	9	0.076	0.004	31.26	1.475	33.47	.75	90.51	0.037
111	3.01	P3.01_111	181mm-Qb	0.8ft-.3W-1ArmL	36	0.076	0.01	17.72	1.015	19.24	.75	181	0.040
112	3.01	P3.01_112	181mm-2/3Qb	0.8ft-.3W-1ArmL	24	0.076	0.01	17.72	1.015	19.24	.75	181	0.042
113	3.01	P3.01_113	181mm-1/3Qb	0.8ft-.3W-1ArmL	12	0.076	0.01	17.72	1.015	19.24	.75	181	0.045
114	3.01	P3.01_114	181mm-1/5Qb	0.8ft-.3W-1ArmL	7	0.076	0.01	17.72	1.015	19.24	.75	181	0.045
115	3.01	P3.01_115	181mm-1/10Qb	0.8ft-.3W-1ArmL	4	0.076	0.01	17.72	1.015	19.24	.75	181	0.045
116	3.02	P3.02_116	181mm-Qb	0.4ft-.25W-0.5ArmL	36	0.076	0.01	17.72	1.015	19.24	.75	181	0.040
117	3.02	P3.02_117	181mm-2/3Qb	0.4ft-.25W-0.5ArmL	24	0.076	0.01	17.72	1.015	19.24	.75	181	0.042
118	3.02	P3.02_118	181mm-1/3Qb	0.4ft-.25W-0.5ArmL	12	0.076	0.01	17.72	1.015	19.24	.75	181	0.045
119	3.02	P3.02_119	181mm-1/5Qb	0.4ft-.25W-0.5ArmL	7	0.076	0.01	17.72	1.015	19.24	.75	181	0.045
120	3.02	P3.02_120	181mm-1/10Qb	0.4ft-.25W-0.5ArmL	4	0.076	0.01	17.72	1.015	19.24	.75	181	0.045
121	3.03	P3.03_121	181mm-Qb	0.4ft-.25W-2ArmL	36	0.076	0.01	17.72	1.015	19.24	.75	181	0.040
122	3.03	P3.03_122	181mm-2/3Qb	0.4ft-.25W-2ArmL	24	0.076	0.01	17.72	1.015	19.24	.75	181	0.042
123	3.03	P3.03_123	181mm-1/3Qb	0.4ft-.25W-2ArmL	12	0.076	0.01	17.72	1.015	19.24	.75	181	0.045
124	3.03	P3.03_124	181mm-1/5Qb	0.4ft-.25W-2ArmL	7	0.076	0.01	17.72	1.015	19.24	.75	181	0.045
125	3.03	P3.03_125	181mm-1/10Qb	0.4ft-.25W-2ArmL	4	0.076	0.01	17.72	1.015	19.24	.75	181	0.045

Table A1 page 5 (records 101-125) cont.

Record ID	Normal Depth (m)	US XS Station (m)	Crest Station (m)	DS XS Station (m)	Structure Rock Size Width (m)	Structure Rock Size Height (m)	Weir Crest Elevation (m)	Drop Height (m)	Throat Width (m)	Lft Arm Angle (degrees)	Lft Arm Slope (degrees)	Lft Arm Length (m)	Rt Arm Angle (degrees)	Rt Arm Slope (degrees)	Rt Arm Length (m)
101	1.350	-100.41	0.00	167.35	0.914	0.610	30.724	0.244	11.156	43.69	4.2	11.677	43.69	4.20	11.677
102	1.073	-100.41	0.00	167.35	0.914	0.610	30.724	0.244	11.156	43.69	4.2	11.677	43.69	4.20	11.677
103	0.728	-100.41	0.00	167.35	0.914	0.610	30.724	0.244	11.156	43.69	4.2	11.677	43.69	4.20	11.677
104	0.533	-100.41	0.00	167.35	0.914	0.610	30.724	0.244	11.156	43.69	4.2	11.677	43.69	4.20	11.677
105	0.354	-100.41	0.00	167.35	0.914	0.610	30.724	0.244	11.156	43.69	4.2	11.677	43.69	4.20	11.677
106	1.350	-100.41	0.00	186.83	0.914	0.610	30.724	0.244	11.156	13.43	1.25	46.708	13.43	1.25	46.708
107	1.073	-100.41	0.00	186.83	0.914	0.610	30.724	0.244	11.156	13.43	1.25	46.708	13.43	1.25	46.708
108	0.728	-100.41	0.00	186.83	0.914	0.610	30.724	0.244	11.156	13.43	1.25	46.708	13.43	1.25	46.708
109	0.533	-100.41	0.00	186.83	0.914	0.610	30.724	0.244	11.156	13.43	1.25	46.708	13.43	1.25	46.708
110	0.354	-100.41	0.00	186.83	0.914	0.610	30.724	0.244	11.156	13.43	1.25	46.708	13.43	1.25	46.708
111	0.908	-57.73	0.00	96.21	0.610	0.610	30.724	0.244	6.413	25.91	2.49	13.201	25.91	2.49	13.201
112	0.732	-57.73	0.00	96.21	0.610	0.610	30.724	0.244	6.413	25.91	2.49	13.201	25.91	2.49	13.201
113	0.497	-57.73	0.00	96.21	0.610	0.610	30.724	0.244	6.413	25.91	2.49	13.201	25.91	2.49	13.201
114	0.369	-57.73	0.00	96.21	0.610	0.610	30.724	0.244	6.413	25.91	2.49	13.201	25.91	2.49	13.201
115	0.238	-57.73	0.00	96.21	0.610	0.610	30.724	0.244	6.413	25.91	2.49	13.201	25.91	2.49	13.201
116	0.908	-57.73	0.00	96.21	0.610	0.610	30.602	0.122	4.810	43.65	4.47	7.565	43.65	4.47	7.565
117	0.732	-57.73	0.00	96.21	0.610	0.610	30.602	0.122	4.810	43.65	4.47	7.565	43.65	4.47	7.565
118	0.497	-57.73	0.00	96.21	0.610	0.610	30.602	0.122	4.810	43.65	4.47	7.565	43.65	4.47	7.565
119	0.369	-57.73	0.00	96.21	0.610	0.610	30.602	0.122	4.810	43.65	4.47	7.565	43.65	4.47	7.565
120	0.238	-57.73	0.00	96.21	0.610	0.610	30.602	0.122	4.810	43.65	4.47	7.565	43.65	4.47	7.565
121	0.908	-57.73	0.00	121.04	0.610	0.610	30.602	0.122	4.810	13.41	1.09	30.261	13.41	1.09	30.261
122	0.732	-57.73	0.00	121.04	0.610	0.610	30.602	0.122	4.810	13.41	1.09	30.261	13.41	1.09	30.261
123	0.497	-57.73	0.00	121.04	0.610	0.610	30.602	0.122	4.810	13.41	1.09	30.261	13.41	1.09	30.261
124	0.369	-57.73	0.00	121.04	0.610	0.610	30.602	0.122	4.810	13.41	1.09	30.261	13.41	1.09	30.261
125	0.238	-57.73	0.00	121.04	0.610	0.610	30.602	0.122	4.810	13.41	1.09	30.261	13.41	1.09	30.261

Table A1 page 6 (records 125-150) – Numerical model testing matrix configuration data.

Record ID	Config ID	River	Reach	Structure Reference	Design Discharge (cms)	Oberbank Width (m)	Slope	Channel Width (m)	Channel Depth (m)	Top Width (m)	Side Slope (H/V)	Grain size (mm)	Manning n
126	3.04	P3.04_126	181mm-Qb	0.4ft-.5W-0.5ArmL	36	0.076	0.01	17.72	1.015	19.24	.75	181	0.040
127	3.04	P3.04_127	181mm-2/3Qb	0.4ft-.5W-0.5ArmL	24	0.076	0.01	17.72	1.015	19.24	.75	181	0.042
128	3.04	P3.04_128	181mm-1/3Qb	0.4ft-.5W-0.5ArmL	12	0.076	0.01	17.72	1.015	19.24	.75	181	0.045
129	3.04	P3.04_129	181mm-1/5Qb	0.4ft-.5W-0.5ArmL	7	0.076	0.01	17.72	1.015	19.24	.75	181	0.045
130	3.04	P3.04_130	181mm-1/10Qb	0.4ft-.5W-0.5ArmL	4	0.076	0.01	17.72	1.015	19.24	.75	181	0.045
131	3.05	P3.05_131	181mm-Qb	0.4ft-.5W-2ArmL	36	0.076	0.01	17.72	1.015	19.24	.75	181	0.040
132	3.05	P3.05_132	181mm-2/3Qb	0.4ft-.5W-2ArmL	24	0.076	0.01	17.72	1.015	19.24	.75	181	0.042
133	3.05	P3.05_133	181mm-1/3Qb	0.4ft-.5W-2ArmL	12	0.076	0.01	17.72	1.015	19.24	.75	181	0.045
134	3.05	P3.05_134	181mm-1/5Qb	0.4ft-.5W-2ArmL	7	0.076	0.01	17.72	1.015	19.24	.75	181	0.045
135	3.05	P3.05_135	181mm-1/10Qb	0.4ft-.5W-2ArmL	4	0.076	0.01	17.72	1.015	19.24	.75	181	0.045
136	3.06	P3.06_136	181mm-Qb	1.2ft-.25W-0.5ArmL	36	0.076	0.01	17.72	1.015	19.24	.75	181	0.040
137	3.06	P3.06_137	181mm-2/3Qb	1.2ft-.25W-0.5ArmL	24	0.076	0.01	17.72	1.015	19.24	.75	181	0.042
138	3.06	P3.06_138	181mm-1/3Qb	1.2ft-.25W-0.5ArmL	12	0.076	0.01	17.72	1.015	19.24	.75	181	0.045
139	3.06	P3.06_139	181mm-1/5Qb	1.2ft-.25W-0.5ArmL	7	0.076	0.01	17.72	1.015	19.24	.75	181	0.045
140	3.06	P3.06_140	181mm-1/10Qb	1.2ft-.25W-0.5ArmL	4	0.076	0.01	17.72	1.015	19.24	.75	181	0.045
141	3.07	P3.07_141	181mm-Qb	1.2ft-.25W-2ArmL	36	0.076	0.01	17.72	1.015	19.24	.75	181	0.040
142	3.07	P3.07_142	181mm-2/3Qb	1.2ft-.25W-2ArmL	24	0.076	0.01	17.72	1.015	19.24	.75	181	0.042
143	3.07	P3.07_143	181mm-1/3Qb	1.2ft-.25W-2ArmL	12	0.076	0.01	17.72	1.015	19.24	.75	181	0.045
144	3.07	P3.07_144	181mm-1/5Qb	1.2ft-.25W-2ArmL	7	0.076	0.01	17.72	1.015	19.24	.75	181	0.045
145	3.07	P3.07_145	181mm-1/10Qb	1.2ft-.25W-2ArmL	4	0.076	0.01	17.72	1.015	19.24	.75	181	0.045
146	3.08	P3.08_146	181mm-Qb	1.2ft-.5W-0.5ArmL	36	0.076	0.01	17.72	1.015	19.24	.75	181	0.040
147	3.08	P3.08_147	181mm-2/3Qb	1.2ft-.5W-0.5ArmL	24	0.076	0.01	17.72	1.015	19.24	.75	181	0.042
148	3.08	P3.08_148	181mm-1/3Qb	1.2ft-.5W-0.5ArmL	12	0.076	0.01	17.72	1.015	19.24	.75	181	0.045
149	3.08	P3.08_149	181mm-1/5Qb	1.2ft-.5W-0.5ArmL	7	0.076	0.01	17.72	1.015	19.24	.75	181	0.045
150	3.08	P3.08_150	181mm-1/10Qb	1.2ft-.5W-0.5ArmL	4	0.076	0.01	17.72	1.015	19.24	.75	181	0.045

Table A1 page 6 (records 125-150) cont.

Record ID	Normal Depth (m)	US XS Station (m)	Crest Station (m)	DS XS Station (m)	Structure Rock Size Width (m)	Structure Rock Size Height (m)	Weir Crest Elevation (m)	Drop Height (m)	Throat Width (m)	Lft Arm Angle (degrees)	Lft Arm Slope (degrees)	Lft Arm Length (m)	Rt Arm Angle (degrees)	Rt Arm Slope (degrees)	Rt Arm Length (m)
126	0.908	-57.73	0.00	96.21	0.610	0.610	30.602	0.122	9.623	36.05	5.77	6.608	36.05	5.77	6.608
127	0.732	-57.73	0.00	96.21	0.610	0.610	30.602	0.122	9.623	36.05	5.77	6.608	36.05	5.77	6.608
128	0.497	-57.73	0.00	96.21	0.610	0.610	30.602	0.122	9.623	36.05	5.77	6.608	36.05	5.77	6.608
129	0.369	-57.73	0.00	96.21	0.610	0.610	30.602	0.122	9.623	36.05	5.77	6.608	36.05	5.77	6.608
130	0.238	-57.73	0.00	96.21	0.610	0.610	30.602	0.122	9.623	36.05	5.77	6.608	36.05	5.77	6.608
131	0.908	-57.73	0.00	105.74	0.610	0.610	30.602	0.122	9.623	10.31	1.34	26.435	10.31	1.34	26.435
132	0.732	-57.73	0.00	105.74	0.610	0.610	30.602	0.122	9.623	10.31	1.34	26.435	10.31	1.34	26.435
133	0.497	-57.73	0.00	105.74	0.610	0.610	30.602	0.122	9.623	10.31	1.34	26.435	10.31	1.34	26.435
134	0.369	-57.73	0.00	105.74	0.610	0.610	30.602	0.122	9.623	10.31	1.34	26.435	10.31	1.34	26.435
135	0.238	-57.73	0.00	105.74	0.610	0.610	30.602	0.122	9.623	10.31	1.34	26.435	10.31	1.34	26.435
136	0.908	-57.73	0.00	96.21	0.610	0.610	30.846	0.366	4.810	48.35	3.46	6.419	48.35	3.46	6.419
137	0.732	-57.73	0.00	96.21	0.610	0.610	30.846	0.366	4.810	48.35	3.46	6.419	48.35	3.46	6.419
138	0.497	-57.73	0.00	96.21	0.610	0.610	30.846	0.366	4.810	48.35	3.46	6.419	48.35	3.46	6.419
139	0.369	-57.73	0.00	96.21	0.610	0.610	30.846	0.366	4.810	48.35	3.46	6.419	48.35	3.46	6.419
140	0.238	-57.73	0.00	96.21	0.610	0.610	30.846	0.366	4.810	48.35	3.46	6.419	48.35	3.46	6.419
141	0.908	-57.73	0.00	102.71	0.610	0.610	30.846	0.366	4.810	15.7	0.84	25.676	15.70	0.84	25.676
142	0.732	-57.73	0.00	102.71	0.610	0.610	30.846	0.366	4.810	15.7	0.84	25.676	15.70	0.84	25.676
143	0.497	-57.73	0.00	102.71	0.610	0.610	30.846	0.366	4.810	15.7	0.84	25.676	15.70	0.84	25.676
144	0.369	-57.73	0.00	102.71	0.610	0.610	30.846	0.366	4.810	15.7	0.84	25.676	15.70	0.84	25.676
145	0.238	-57.73	0.00	102.71	0.610	0.610	30.846	0.366	4.810	15.7	0.84	25.676	15.70	0.84	25.676
146	0.908	-57.73	0.00	96.21	0.610	0.610	30.846	0.366	9.623	41.96	4.73	5.349	41.96	4.73	5.349
147	0.732	-57.73	0.00	96.21	0.610	0.610	30.846	0.366	9.623	41.96	4.73	5.349	41.96	4.73	5.349
148	0.497	-57.73	0.00	96.21	0.610	0.610	30.846	0.366	9.623	41.96	4.73	5.349	41.96	4.73	5.349
149	0.369	-57.73	0.00	96.21	0.610	0.610	30.846	0.366	9.623	41.96	4.73	5.349	41.96	4.73	5.349
150	0.238	-57.73	0.00	96.21	0.610	0.610	30.846	0.366	9.623	41.96	4.73	5.349	41.96	4.73	5.349

Table A1 page 7 (records 151-165) – Numerical model testing matrix configuration data.

Record ID	Config ID	River	Reach	Structure Reference	Design Discharge (cms)	Oberbank Width (m)	Slope	Channel Width (m)	Channel Depth (m)	Top Width (m)	Side Slope (H/V)	Grain size (mm)	Manning n
151	3.09	P3.09_151	181mm-Qb	1.2ft-.5W-2ArmL	36	0.076	0.01	17.72	1.015	19.24	.75	181	0.040
152	3.09	P3.09_152	181mm-2/3Qb	1.2ft-.5W-2ArmL	24	0.076	0.01	17.72	1.015	19.24	.75	181	0.042
153	3.09	P3.09_153	181mm-1/3Qb	1.2ft-.5W-2ArmL	12	0.076	0.01	17.72	1.015	19.24	.75	181	0.045
154	3.09	P3.09_154	181mm-1/5Qb	1.2ft-.5W-2ArmL	7	0.076	0.01	17.72	1.015	19.24	.75	181	0.045
155	3.09	P3.09_155	181mm-1/10Qb	1.2ft-.5W-2ArmL	4	0.076	0.01	17.72	1.015	19.24	.75	181	0.045
156	3.10	P3.10_156	181mm-Qb	0.8ft-.3W-0.5ArmL	36	0.076	0.01	17.72	1.015	19.24	.75	181	0.040
157	3.10	P3.10_157	181mm-2/3Qb	0.8ft-.3W-0.5ArmL	24	0.076	0.01	17.72	1.015	19.24	.75	181	0.042
158	3.10	P3.10_158	181mm-1/3Qb	0.8ft-.3W-0.5ArmL	12	0.076	0.01	17.72	1.015	19.24	.75	181	0.045
159	3.10	P3.10_159	181mm-1/5Qb	0.8ft-.3W-0.5ArmL	7	0.076	0.01	17.72	1.015	19.24	.75	181	0.045
160	3.10	P3.10_160	181mm-1/10Qb	0.8ft-.3W-0.5ArmL	4	0.076	0.01	17.72	1.015	19.24	.75	181	0.045
161	3.11	P3.11_161	181mm-Qb	0.8ft-.3W-2ArmL	36	0.076	0.01	17.72	1.015	19.24	.75	181	0.040
162	3.11	P3.11_162	181mm-2/3Qb	0.8ft-.3W-2ArmL	24	0.076	0.01	17.72	1.015	19.24	.75	181	0.042
163	3.11	P3.11_163	181mm-1/3Qb	0.8ft-.3W-2ArmL	12	0.076	0.01	17.72	1.015	19.24	.75	181	0.045
164	3.11	P3.11_164	181mm-1/5Qb	0.8ft-.3W-2ArmL	7	0.076	0.01	17.72	1.015	19.24	.75	181	0.045
165	3.11	P3.11_165	181mm-1/10Qb	0.8ft-.3W-2ArmL	4	0.076	0.01	17.72	1.015	19.24	.75	181	0.045

Table A1 page7 (records 151-165) cont.

Record ID	Normal Depth (m)	US XS Station (m)	Crest Station (m)	DS XS Station (m)	Structure Rock Size Width (m)	Structure Rock Size Height (m)	Weir Crest Elevation (m)	Drop Height (m)	Throat Width (m)	Lft Arm Angle (degrees)	Lft Arm Slope (degrees)	Lft Arm Length (m)	Rt Arm Angle (degrees)	Rt Arm Slope (degrees)	Rt Arm Length (m)
151	0.908	-57.73	0.00	96.21	0.610	0.610	30.846	0.366	9.623	12.67	1.13	21.400	12.67	1.13	21.400
152	0.732	-57.73	0.00	96.21	0.610	0.610	30.846	0.366	9.623	12.67	1.13	21.400	12.67	1.13	21.400
153	0.497	-57.73	0.00	96.21	0.610	0.610	30.846	0.366	9.623	12.67	1.13	21.400	12.67	1.13	21.400
154	0.369	-57.73	0.00	96.21	0.610	0.610	30.846	0.366	9.623	12.67	1.13	21.400	12.67	1.13	21.400
155	0.238	-57.73	0.00	96.21	0.610	0.610	30.846	0.366	9.623	12.67	1.13	21.400	12.67	1.13	21.400
156	0.908	-57.73	0.00	96.21	0.610	0.610	30.724	0.244	6.413	44.18	4.38	6.602	44.18	4.38	6.602
157	0.732	-57.73	0.00	96.21	0.610	0.610	30.724	0.244	6.413	44.18	4.38	6.602	44.18	4.38	6.602
158	0.497	-57.73	0.00	96.21	0.610	0.610	30.724	0.244	6.413	44.18	4.38	6.602	44.18	4.38	6.602
159	0.369	-57.73	0.00	96.21	0.610	0.610	30.724	0.244	6.413	44.18	4.38	6.602	44.18	4.38	6.602
160	0.238	-57.73	0.00	96.21	0.610	0.610	30.724	0.244	6.413	44.18	4.38	6.602	44.18	4.38	6.602
161	0.908	-57.73	0.00	105.62	0.610	0.610	30.724	0.244	6.413	13.65	1.07	26.405	13.65	1.07	26.405
162	0.732	-57.73	0.00	105.62	0.610	0.610	30.724	0.244	6.413	13.65	1.07	26.405	13.65	1.07	26.405
163	0.497	-57.73	0.00	105.62	0.610	0.610	30.724	0.244	6.413	13.65	1.07	26.405	13.65	1.07	26.405
164	0.369	-57.73	0.00	105.62	0.610	0.610	30.724	0.244	6.413	13.65	1.07	26.405	13.65	1.07	26.405
165	0.238	-57.73	0.00	105.62	0.610	0.610	30.724	0.244	6.413	13.65	1.07	26.405	13.65	1.07	26.405

APPENDIX B

SUMMARY OF NUMERICAL MODEL RESULTS FOR EACH STRUCTURE CONFIGURATION

Table B1 page 1 (records 1-25) – Summary of numerical model results.

Record ID	Reach	Qratio	StrucRef	Q (cms)	d ₅₀ (mm)	S _o	H _{bkf} (m)	T _w (m)	Z _d (m)	W _t (m)	W _t /T _w	L _a (m)	L _a _{ref}
1	22.63mm-Qb	Qb	0.8ft-.3W-1ArmL	162	22.63	0.001	1.85	54.92	0.24	18.31	0.33	35.40	1.0
2	22.63mm-2/3Qb	2/3Qb	0.8ft-.3W-1ArmL	108	22.63	0.001	1.85	54.92	0.24	18.31	0.33	35.40	1.0
3	22.63mm-1/3Qb	1/3Qb	0.8ft-.3W-1ArmL	54	22.63	0.001	1.85	54.92	0.24	18.31	0.33	35.40	1.0
4	22.63mm-1/5Qb	1/5Qb	0.8ft-.3W-1ArmL	32	22.63	0.001	1.85	54.92	0.24	18.31	0.33	35.40	1.0
5	22.63mm-1/10Qb	1/10Qb	0.8ft-.3W-1ArmL	16	22.63	0.001	1.85	54.92	0.24	18.31	0.33	35.40	1.0
6	22.63mm-Qb	Qb	0.4ft-.25W-0.5ArmL	162	22.63	0.001	1.85	54.92	0.12	13.73	0.25	19.58	0.5
7	22.63mm-2/3Qb	2/3Qb	0.4ft-.25W-0.5ArmL	108	22.63	0.001	1.85	54.92	0.12	13.73	0.25	19.58	0.5
8	22.63mm-1/3Qb	1/3Qb	0.4ft-.25W-0.5ArmL	54	22.63	0.001	1.85	54.92	0.12	13.73	0.25	19.58	0.5
9	22.63mm-1/5Qb	1/5Qb	0.4ft-.25W-0.5ArmL	32	22.63	0.001	1.85	54.92	0.12	13.73	0.25	19.58	0.5
10	22.63mm-1/10Qb	1/10Qb	0.4ft-.25W-0.5ArmL	16	22.63	0.001	1.85	54.92	0.12	13.73	0.25	19.58	0.5
11	22.63mm-Qb	Qb	0.4ft-.25W-2ArmL	162	22.63	0.001	1.85	54.92	0.12	13.73	0.25	78.34	2.0
12	22.63mm-2/3Qb	2/3Qb	0.4ft-.25W-2ArmL	108	22.63	0.001	1.85	54.92	0.12	13.73	0.25	78.34	2.0
13	22.63mm-1/3Qb	1/3Qb	0.4ft-.25W-2ArmL	54	22.63	0.001	1.85	54.92	0.12	13.73	0.25	78.34	2.0
14	22.63mm-1/5Qb	1/5Qb	0.4ft-.25W-2ArmL	32	22.63	0.001	1.85	54.92	0.12	13.73	0.25	78.34	2.0
15	22.63mm-1/10Qb	1/10Qb	0.4ft-.25W-2ArmL	16	22.63	0.001	1.85	54.92	0.12	13.73	0.25	78.34	2.0
16	22.63mm-Qb	Qb	0.4ft-.5W-0.5ArmL	162	22.63	0.001	1.85	54.92	0.12	27.46	0.50	16.19	0.5
17	22.63mm-2/3Qb	2/3Qb	0.4ft-.5W-0.5ArmL	108	22.63	0.001	1.85	54.92	0.12	27.46	0.50	16.19	0.5
18	22.63mm-1/3Qb	1/3Qb	0.4ft-.5W-0.5ArmL	54	22.63	0.001	1.85	54.92	0.12	27.46	0.50	16.19	0.5
19	22.63mm-1/5Qb	1/5Qb	0.4ft-.5W-0.5ArmL	32	22.63	0.001	1.85	54.92	0.12	27.46	0.50	16.19	0.5
20	22.63mm-1/10Qb	1/10Qb	0.4ft-.5W-0.5ArmL	16	22.63	0.001	1.85	54.92	0.12	27.46	0.50	16.19	0.5
21	22.63mm-Qb	Qb	0.4ft-.5W-2ArmL	162	22.63	0.001	1.85	54.92	0.12	27.46	0.50	64.78	2.0
22	22.63mm-2/3Qb	2/3Qb	0.4ft-.5W-2ArmL	108	22.63	0.001	1.85	54.92	0.12	27.46	0.50	64.78	2.0
23	22.63mm-1/3Qb	1/3Qb	0.4ft-.5W-2ArmL	54	22.63	0.001	1.85	54.92	0.12	27.46	0.50	64.78	2.0
24	22.63mm-1/5Qb	1/5Qb	0.4ft-.5W-2ArmL	32	22.63	0.001	1.85	54.92	0.12	27.46	0.50	64.78	2.0
25	22.63mm-1/10Qb	1/10Qb	0.4ft-.5W-2ArmL	16	22.63	0.001	1.85	54.92	0.12	27.46	0.50	64.78	2.0

Table B1 page 1 (records 1-25) cont.

Record ID	Arm Angle	Arm Slope	Arm Slope %	L _t (m)	Z _u (m)	W _u (m)	V _o (m/s)	τ _c (Pa)	D _q (m)	h _{weir} (m)	D _{nref} (m)	V _{max} /V _o	V _{max} Loc	τ _{max} /τ _c	τ _{max} Loc
1	27.34	2.26	3.95%	98.09	0.77	30.51	1.77	18.30	1.89	1.65	1.71	1.91	15.4	3.96	14.4
2	27.34	2.26	3.95%	98.09	0.77	30.51	1.48	18.30	1.60	1.35	1.37	2.24	14.4	4.00	11.4
3	27.34	2.26	3.95%	98.09	0.77	30.51	1.09	18.30	1.20	0.95	0.94	2.65	11.4	3.30	9.4
4	27.34	2.26	3.95%	98.09	0.77	30.51	0.89	18.30	0.95	0.70	0.69	2.97	9.4	N/A	N/A
5	27.34	2.26	3.95%	98.09	0.77	30.51	0.68	18.30	0.72	0.48	0.45	3.41	7.4	N/A	N/A
6	46.44	3.44	6.01%	70.67	0.69	27.46	1.78	18.30	1.99	1.87	1.71	2.36	17.45	6.00	15.4
7	46.44	3.44	6.01%	70.67	0.69	27.46	1.48	18.30	1.68	1.56	1.37	2.72	16.45	5.68	14.4
8	46.44	3.44	6.01%	70.67	0.69	27.46	1.09	18.30	1.25	1.13	0.94	3.17	14.45	4.45	13.45
9	46.44	3.44	6.01%	70.67	0.69	27.46	0.89	18.30	1.00	0.88	0.69	3.43	12.5	N/A	N/A
10	46.44	3.44	6.01%	70.67	0.69	27.46	0.68	18.30	0.72	0.60	0.45	3.74	11.5	N/A	N/A
11	14.73	1.17	2.04%	175.76	0.67	27.46	1.78	18.30	1.82	1.70	1.71	1.48	13.45	2.39	11.35
12	14.73	1.17	2.04%	175.76	0.67	27.46	1.48	18.30	1.53	1.41	1.37	1.76	11.45	2.43	11.4
13	14.73	1.17	2.04%	175.76	0.67	27.46	1.09	18.30	1.13	1.01	0.94	2.24	9.45	2.29	9.45
14	14.73	1.17	2.04%	175.76	0.67	27.46	0.89	18.30	0.89	0.77	0.69	2.54	8.45	N/A	N/A
15	14.73	1.17	2.04%	175.76	0.67	27.46	0.68	18.30	0.65	0.53	0.45	2.78	8.45	N/A	N/A
16	40.29	4.61	8.06%	70.06	0.69	36.61	1.78	18.30	1.84	1.72	1.71	1.79	19.35	3.52	16.3
17	40.29	4.61	8.06%	70.06	0.69	36.61	1.48	18.30	1.52	1.40	1.37	1.94	18.35	2.98	13.3
18	40.29	4.61	8.06%	70.06	0.69	36.61	1.09	18.30	1.09	0.97	0.94	2.16	16.35	2.12	15.35
19	40.29	4.61	8.06%	70.06	0.69	36.61	0.89	18.30	0.83	0.71	0.69	2.23	15.35	N/A	N/A
20	40.29	4.61	8.06%	70.06	0.69	36.61	0.68	18.30	0.57	0.45	0.45	2.31	15.5	N/A	N/A
21	11.97	1.44	2.51%	159.90	0.68	36.61	1.78	18.30	1.76	1.64	1.71	1.24	13.3	1.79	12.25
22	11.97	1.44	2.51%	159.90	0.68	36.61	1.48	18.30	1.45	1.32	1.37	1.37	12.3	1.54	10.3
23	11.97	1.44	2.51%	159.90	0.68	36.61	1.09	18.30	1.03	0.91	0.94	1.64	9.35	1.28	9.35
24	11.97	1.44	2.51%	159.90	0.68	36.61	0.89	18.30	0.78	0.66	0.69	1.83	8.35	N/A	N/A
25	11.97	1.44	2.51%	159.90	0.68	36.61	0.68	18.30	0.54	0.42	0.45	2.03	8.35	N/A	N/A

Table B1 page 2 (records 26-50) – Summary of numerical model results.

Record ID	Reach	Qratio	StrucRef	Q (cms)	d ₅₀ (mm)	S _o	H _{bkf} (m)	T _w (m)	Z _d (m)	W _t (m)	W _t /T _w	L _a (m)	L _a _{ref}
26	22.63mm-Qb	Qb	1.2ft-.25W-0.5ArmL	162	22.63	0.001	1.85	54.92	0.37	13.73	0.25	18.72	0.5
27	22.63mm-2/3Qb	2/3Qb	1.2ft-.25W-0.5ArmL	108	22.63	0.001	1.85	54.92	0.37	13.73	0.25	18.72	0.5
28	22.63mm-1/3Qb	1/3Qb	1.2ft-.25W-0.5ArmL	54	22.63	0.001	1.85	54.92	0.37	13.73	0.25	18.72	0.5
29	22.63mm-1/5Qb	1/5Qb	1.2ft-.25W-0.5ArmL	32	22.63	0.001	1.85	54.92	0.37	13.73	0.25	18.72	0.5
30	22.63mm-1/10Qb	1/10Qb	1.2ft-.25W-0.5ArmL	16	22.63	0.001	1.85	54.92	0.37	13.73	0.25	18.72	0.5
31	22.63mm-Qb	Qb	1.2ft-.25W-2ArmL	162	22.63	0.001	1.85	54.92	0.37	13.73	0.25	74.90	2.0
32	22.63mm-2/3Qb	2/3Qb	1.2ft-.25W-2ArmL	108	22.63	0.001	1.85	54.92	0.37	13.73	0.25	74.90	2.0
33	22.63mm-1/3Qb	1/3Qb	1.2ft-.25W-2ArmL	54	22.63	0.001	1.85	54.92	0.37	13.73	0.25	74.90	2.0
34	22.63mm-1/5Qb	1/5Qb	1.2ft-.25W-2ArmL	32	22.63	0.001	1.85	54.92	0.37	13.73	0.25	74.90	2.0
35	22.63mm-1/10Qb	1/10Qb	1.2ft-.25W-2ArmL	16	22.63	0.001	1.85	54.92	0.37	13.73	0.25	74.90	2.0
36	22.63mm-Qb	Qb	1.2ft-.5W-0.5ArmL	162	22.63	0.001	1.85	54.92	0.37	27.46	0.50	14.69	0.5
37	22.63mm-2/3Qb	2/3Qb	1.2ft-.5W-0.5ArmL	108	22.63	0.001	1.85	54.92	0.37	27.46	0.50	14.69	0.5
38	22.63mm-1/3Qb	1/3Qb	1.2ft-.5W-0.5ArmL	54	22.63	0.001	1.85	54.92	0.37	27.46	0.50	14.69	0.5
39	22.63mm-1/5Qb	1/5Qb	1.2ft-.5W-0.5ArmL	32	22.63	0.001	1.85	54.92	0.37	27.46	0.50	14.69	0.5
40	22.63mm-1/10Qb	1/10Qb	1.2ft-.5W-0.5ArmL	16	22.63	0.001	1.85	54.92	0.37	27.46	0.50	14.69	0.5
41	22.63mm-Qb	Qb	1.2ft-.5W-2ArmL	162	22.63	0.001	1.85	54.92	0.37	27.46	0.50	58.76	2.0
42	22.63mm-2/3Qb	2/3Qb	1.2ft-.5W-2ArmL	108	22.63	0.001	1.85	54.92	0.37	27.46	0.50	58.76	2.0
43	22.63mm-1/3Qb	1/3Qb	1.2ft-.5W-2ArmL	54	22.63	0.001	1.85	54.92	0.37	27.46	0.50	58.76	2.0
44	22.63mm-1/5Qb	1/5Qb	1.2ft-.5W-2ArmL	32	22.63	0.001	1.85	54.92	0.37	27.46	0.50	58.76	2.0
45	22.63mm-1/10Qb	1/10Qb	1.2ft-.5W-2ArmL	16	22.63	0.001	1.85	54.92	0.37	27.46	0.50	58.76	2.0
46	22.63mm-Qb	Qb	0.8ft-.3W-0.5ArmL	162	22.63	0.001	1.85	54.92	0.24	18.31	0.33	17.70	0.5
47	22.63mm-2/3Qb	2/3Qb	0.8ft-.3W-0.5ArmL	108	22.63	0.001	1.85	54.92	0.24	18.31	0.33	17.70	0.5
48	22.63mm-1/3Qb	1/3Qb	0.8ft-.3W-0.5ArmL	54	22.63	0.001	1.85	54.92	0.24	18.31	0.33	17.70	0.5
49	22.63mm-1/5Qb	1/5Qb	0.8ft-.3W-0.5ArmL	32	22.63	0.001	1.85	54.92	0.24	18.31	0.33	17.70	0.5
50	22.63mm-1/10Qb	1/10Qb	0.8ft-.3W-0.5ArmL	16	22.63	0.001	1.85	54.92	0.24	18.31	0.33	17.70	0.5

Table B1 page 2 (records 1-25) cont.

Record ID	Arm Angle	Arm Slope	Arm Slope %	L _t (m)	Z _u (m)	W _u (m)	V _o (m/s)	τ _c (Pa)	D _q (m)	h _{weir} (m)	D _{nref} (m)	V _{max} /V _o	V _{max} Loc	τ _{max} /τ _c	τ _{max} Loc
26	47.72	3.02	5.28%	69.48	0.86	27.46	1.78	18.30	2.07	1.71	1.71	2.65	16.45	7.59	15.4
27	47.72	3.02	5.28%	69.48	0.86	27.46	1.48	18.30	1.78	1.41	1.37	3.11	15.45	7.32	13.4
28	47.72	3.02	5.28%	69.48	0.86	27.46	1.09	18.30	1.38	1.02	0.94	3.70	13.45	5.01	12.45
29	47.72	3.02	5.28%	69.48	0.86	27.46	0.89	18.30	1.15	0.79	0.69	3.82	11.45	N/A	N/A
30	47.72	3.02	5.28%	69.48	0.86	27.46	0.68	18.30	0.92	0.55	0.45	3.77	11.5	N/A	N/A
31	15.37	1.04	1.82%	169.16	0.84	27.46	1.78	18.30	1.86	1.49	1.71	1.59	13.45	3.05	12.4
32	15.37	1.04	1.82%	169.16	0.84	27.46	1.48	18.30	1.59	1.22	1.37	1.97	11.45	3.27	10.4
33	15.37	1.04	1.82%	169.16	0.84	27.46	1.09	18.30	1.21	0.84	0.94	2.58	8.45	3.19	8.45
34	15.37	1.04	1.82%	169.16	0.84	27.46	0.89	18.30	1.01	0.65	0.69	2.67	7.45	N/A	N/A
35	15.37	1.04	1.82%	169.16	0.84	27.46	0.68	18.30	0.80	0.44	0.45	3.49	7.45	N/A	N/A
36	43.06	4.18	7.31%	67.78	0.86	36.61	1.78	18.30	1.92	1.55	1.71	1.95	19.35	4.30	15.3
37	43.06	4.18	7.31%	67.78	0.86	36.61	1.48	18.30	1.62	1.25	1.37	2.18	17.35	3.89	5.5
38	43.06	4.18	7.31%	67.78	0.86	36.61	1.09	18.30	1.22	0.85	0.94	2.50	16.35	3.41	5.5
39	43.06	4.18	7.31%	67.78	0.86	36.61	0.89	18.30	1.00	0.63	0.69	2.79	7.3	N/A	N/A
40	43.06	4.18	7.31%	67.78	0.86	36.61	0.68	18.30	0.79	0.42	0.45	2.93	5.5	N/A	N/A
41	13.15	1.35	2.36%	148.19	0.84	36.61	1.78	18.30	1.80	1.44	1.71	1.37	13.3	2.28	11.3
42	13.15	1.35	2.36%	148.19	0.84	36.61	1.48	18.30	1.50	1.13	1.37	1.57	11.35	2.15	10.3
43	13.15	1.35	2.36%	148.19	0.84	36.61	1.09	18.30	1.11	0.74	0.94	1.98	8.35	1.94	8.35
44	13.15	1.35	2.36%	148.19	0.84	36.61	0.89	18.30	0.91	0.54	0.69	2.32	7.35	N/A	N/A
45	13.15	1.35	2.36%	148.19	0.84	36.61	0.68	18.30	0.74	0.37	0.45	2.81	5.3	N/A	N/A
46	45.96	3.57	6.24%	69.34	0.77	30.51	1.77	18.30	1.96	1.71	1.71	2.30	17.4	5.48	15.35
47	45.96	3.57	6.24%	69.34	0.77	30.51	1.48	18.30	1.65	1.41	1.37	2.64	16.4	5.33	15.4
48	45.96	3.57	6.24%	69.34	0.77	30.51	1.09	18.30	1.23	0.99	0.94	3.04	15.4	4.14	13.4
49	45.96	3.57	6.24%	69.34	0.77	30.51	0.89	18.30	0.99	0.74	0.69	3.27	13.4	N/A	N/A
50	45.96	3.57	6.24%	69.34	0.77	30.51	0.68	18.30	0.75	0.50	0.45	3.56	11.4	N/A	N/A

Table B1 page 3 (records 51-75) – Summary of numerical model results.

Record ID	Reach	Qratio	StrucRef	Q (cms)	d ₅₀ (mm)	S _o	H _{bkf} (m)	T _w (m)	Z _d (m)	W _t (m)	W _t /T _w	L _a (m)	L _a _{ref}
51	22.63mm-Qb	Qb	0.8ft-.3W-2ArmL	162	22.63	0.001	1.85	54.92	0.24	18.31	0.33	70.81	2.0
52	22.63mm-2/3Qb	2/3Qb	0.8ft-.3W-2ArmL	108	22.63	0.001	1.85	54.92	0.24	18.31	0.33	70.81	2.0
53	22.63mm-1/3Qb	1/3Qb	0.8ft-.3W-2ArmL	54	22.63	0.001	1.85	54.92	0.24	18.31	0.33	70.81	2.0
54	22.63mm-1/5Qb	1/5Qb	0.8ft-.3W-2ArmL	32	22.63	0.001	1.85	54.92	0.24	18.31	0.33	70.81	2.0
55	22.63mm-1/10Qb	1/10Qb	0.8ft-.3W-2ArmL	16	22.63	0.001	1.85	54.92	0.24	18.31	0.33	70.81	2.0
56	90.51mm-Qb	Qb	0.8ft-.3W-1ArmL	92	90.51	0.004	1.48	33.47	0.24	11.16	0.33	23.35	1.0
57	90.51mm-2/3Qb	2/3Qb	0.8ft-.3W-1ArmL	61	90.51	0.004	1.48	33.47	0.24	11.16	0.33	23.35	1.0
58	90.51mm-1/3Qb	1/3Qb	0.8ft-.3W-1ArmL	31	90.51	0.004	1.48	33.47	0.24	11.16	0.33	23.35	1.0
59	90.51mm-1/5Qb	1/5Qb	0.8ft-.3W-1ArmL	18	90.51	0.004	1.48	33.47	0.24	11.16	0.33	23.35	1.0
60	90.51mm-1/10Qb	1/10Qb	0.8ft-.3W-1ArmL	9	90.51	0.004	1.48	33.47	0.24	11.16	0.33	23.35	1.0
61	90.51mm-Qb	Qb	0.4ft-.25W-0.5ArmL	92	90.51	0.004	1.48	33.47	0.12	8.37	0.25	12.96	0.5
62	90.51mm-2/3Qb	2/3Qb	0.4ft-.25W-0.5ArmL	61	90.51	0.004	1.48	33.47	0.12	8.37	0.25	12.96	0.5
63	90.51mm-1/3Qb	1/3Qb	0.4ft-.25W-0.5ArmL	31	90.51	0.004	1.48	33.47	0.12	8.37	0.25	12.96	0.5
64	90.51mm-1/5Qb	1/5Qb	0.4ft-.25W-0.5ArmL	18	90.51	0.004	1.48	33.47	0.12	8.37	0.25	12.96	0.5
65	90.51mm-1/10Qb	1/10Qb	0.4ft-.25W-0.5ArmL	9	90.51	0.004	1.48	33.47	0.12	8.37	0.25	12.96	0.5
66	90.51mm-Qb	Qb	0.4ft-.25W-2ArmL	92	90.51	0.004	1.48	33.47	0.12	8.37	0.25	51.85	2.0
67	90.51mm-2/3Qb	2/3Qb	0.4ft-.25W-2ArmL	61	90.51	0.004	1.48	33.47	0.12	8.37	0.25	51.85	2.0
68	90.51mm-1/3Qb	1/3Qb	0.4ft-.25W-2ArmL	31	90.51	0.004	1.48	33.47	0.12	8.37	0.25	51.85	2.0
69	90.51mm-1/5Qb	1/5Qb	0.4ft-.25W-2ArmL	18	90.51	0.004	1.48	33.47	0.12	8.37	0.25	51.85	2.0
70	90.51mm-1/10Qb	1/10Qb	0.4ft-.25W-2ArmL	9	90.51	0.004	1.48	33.47	0.12	8.37	0.25	51.85	2.0
71	90.51mm-Qb	Qb	0.4ft-.5W-0.5ArmL	92	90.51	0.004	1.48	33.47	0.12	16.74	0.50	11.49	0.5
72	90.51mm-2/3Qb	2/3Qb	0.4ft-.5W-0.5ArmL	61	90.51	0.004	1.48	33.47	0.12	16.74	0.50	11.49	0.5
73	90.51mm-1/3Qb	1/3Qb	0.4ft-.5W-0.5ArmL	31	90.51	0.004	1.48	33.47	0.12	16.74	0.50	11.49	0.5
74	90.51mm-1/5Qb	1/5Qb	0.4ft-.5W-0.5ArmL	18	90.51	0.004	1.48	33.47	0.12	16.74	0.50	11.49	0.5
75	90.51mm-1/10Qb	1/10Qb	0.4ft-.5W-0.5ArmL	9	90.51	0.004	1.48	33.47	0.12	16.74	0.50	11.49	0.5

Table B1 page 3 (records 51-75) cont.

Record ID	Arm Angle	Arm Slope	Arm Slope %	L _t (m)	Z _u (m)	W _u (m)	V _o (m/s)	τ _c (Pa)	D _q (m)	h _{weir} (m)	D _{nref} (m)	V _{max} /V _o	V _{max} Loc	τ _{max} /τ _c	τ _{max} Loc
51	14.5	1.2	2.09%	164.57	0.75	30.51	1.77	18.30	1.80	1.55	1.71	1.46	13.4	2.34	11.35
52	14.5	1.2	2.09%	164.57	0.75	30.51	1.48	18.30	1.50	1.26	1.37	1.75	11.4	2.50	10.4
53	14.5	1.2	2.09%	164.57	0.75	30.51	1.09	18.30	1.11	0.87	0.94	2.16	9.45	2.25	8.4
54	14.5	1.2	2.09%	164.57	0.75	30.51	0.89	18.30	0.88	0.63	0.69	2.50	7.45	N/A	N/A
55	14.5	1.2	2.09%	164.57	0.75	30.51	0.68	18.30	0.66	0.42	0.45	2.91	8.45	N/A	N/A
56	25.53	2.52	4.40%	62.98	0.62	18.59	2.11	73.20	1.59	1.34	1.35	1.81	14.4	3.53	14.4
57	25.53	2.52	4.40%	62.98	0.62	18.59	1.78	73.20	1.35	1.10	1.07	2.11	14.4	3.70	12.4
58	25.53	2.52	4.40%	62.98	0.62	18.59	1.32	73.20	1.03	0.79	0.73	2.45	11.4	2.99	10.4
59	25.53	2.52	4.40%	62.98	0.62	18.59	1.09	73.20	0.84	0.60	0.53	2.70	9.4	N/A	N/A
60	25.53	2.52	4.40%	62.98	0.62	18.59	0.83	73.20	0.66	0.41	0.35	2.95	7.4	N/A	N/A
61	44.08	4.13	7.22%	44.55	0.56	16.74	2.11	73.20	1.69	1.57	1.35	2.21	16.45	5.41	15.4
62	44.08	4.13	7.22%	44.55	0.56	16.74	1.78	73.20	1.44	1.31	1.07	2.50	16.45	5.07	15.4
63	44.08	4.13	7.22%	44.55	0.56	16.74	1.32	73.20	1.08	0.96	0.73	2.88	15.5	4.01	13.45
64	44.08	4.13	7.22%	44.55	0.56	16.74	1.09	73.20	0.87	0.75	0.53	3.11	14.5	N/A	N/A
65	44.08	4.13	7.22%	44.55	0.56	16.74	0.83	73.20	0.64	0.52	0.35	3.31	11.5	N/A	N/A
66	13.61	1.23	2.15%	115.07	0.50	16.74	2.11	73.20	1.46	1.34	1.35	1.45	13.45	2.30	12.4
67	13.61	1.23	2.15%	115.07	0.50	16.74	1.78	73.20	1.23	1.11	1.07	1.64	12.45	2.23	12.4
68	13.61	1.23	2.15%	115.07	0.50	16.74	1.32	73.20	0.93	0.81	0.73	1.95	10.45	1.86	9.45
69	13.61	1.23	2.15%	115.07	0.50	16.74	1.09	73.20	0.74	0.62	0.53	2.18	8.45	N/A	N/A
70	13.61	1.23	2.15%	115.07	0.50	16.74	0.83	73.20	0.55	0.42	0.35	2.38	7.45	N/A	N/A
71	36.05	5.26	9.21%	45.29	0.56	22.31	2.11	73.20	1.53	1.41	1.35	1.75	17.35	3.41	15.3
72	36.05	5.26	9.21%	45.29	0.56	22.31	1.78	73.20	1.28	1.16	1.07	1.92	17.5	2.97	16.4
73	36.05	5.26	9.21%	45.29	0.56	22.31	1.32	73.20	0.93	0.81	0.73	2.08	16.5	2.17	13.35
74	36.05	5.26	9.21%	45.29	0.56	22.31	1.09	73.20	0.72	0.60	0.53	2.17	15.5	N/A	N/A
75	36.05	5.26	9.21%	45.29	0.56	22.31	0.83	73.20	0.51	0.39	0.35	2.23	12.35	N/A	N/A

Table B1 page 4 (records 76-100) – Summary of numerical model results.

Record ID	Reach	Qratio	StrucRef	Q (cms)	d ₅₀ (mm)	S _o	H _{bkf} (m)	T _w (m)	Z _d (m)	W _t (m)	W _t /T _w	L _a (m)	L _a _{ref}
76	90.51mm-Qb	Qb	0.4ft-.5W-2ArmL	92	90.51	0.004	1.48	33.47	0.12	16.74	0.50	45.98	2.0
77	90.51mm-2/3Qb	2/3Qb	0.4ft-.5W-2ArmL	61	90.51	0.004	1.48	33.47	0.12	16.74	0.50	45.98	2.0
78	90.51mm-1/3Qb	1/3Qb	0.4ft-.5W-2ArmL	31	90.51	0.004	1.48	33.47	0.12	16.74	0.50	45.98	2.0
79	90.51mm-1/5Qb	1/5Qb	0.4ft-.5W-2ArmL	18	90.51	0.004	1.48	33.47	0.12	16.74	0.50	45.98	2.0
80	90.51mm-1/10Qb	1/10Qb	0.4ft-.5W-2ArmL	9	90.51	0.004	1.48	33.47	0.12	16.74	0.50	45.98	2.0
81	90.51mm-Qb	Qb	1.2ft-.25W-0.5ArmL	92	90.51	0.004	1.48	33.47	0.37	8.37	0.25	11.80	0.5
82	90.51mm-2/3Qb	2/3Qb	1.2ft-.25W-0.5ArmL	61	90.51	0.004	1.48	33.47	0.37	8.37	0.25	11.80	0.5
83	90.51mm-1/3Qb	1/3Qb	1.2ft-.25W-0.5ArmL	31	90.51	0.004	1.48	33.47	0.37	8.37	0.25	11.80	0.5
84	90.51mm-1/5Qb	1/5Qb	1.2ft-.25W-0.5ArmL	18	90.51	0.004	1.48	33.47	0.37	8.37	0.25	11.80	0.5
85	90.51mm-1/10Qb	1/10Qb	1.2ft-.25W-0.5ArmL	9	90.51	0.004	1.48	33.47	0.37	8.37	0.25	11.80	0.5
86	90.51mm-Qb	Qb	1.2ft-.25W-2ArmL	92	90.51	0.004	1.48	33.47	0.37	8.37	0.25	47.20	2.0
87	90.51mm-2/3Qb	2/3Qb	1.2ft-.25W-2ArmL	61	90.51	0.004	1.48	33.47	0.37	8.37	0.25	47.20	2.0
88	90.51mm-1/3Qb	1/3Qb	1.2ft-.25W-2ArmL	31	90.51	0.004	1.48	33.47	0.37	8.37	0.25	47.20	2.0
89	90.51mm-1/5Qb	1/5Qb	1.2ft-.25W-2ArmL	18	90.51	0.004	1.48	33.47	0.37	8.37	0.25	47.20	2.0
90	90.51mm-1/10Qb	1/10Qb	1.2ft-.25W-2ArmL	9	90.51	0.004	1.48	33.47	0.37	8.37	0.25	47.20	2.0
91	90.51mm-Qb	Qb	1.2ft-.5W-0.5ArmL	92	90.51	0.004	1.48	33.47	0.37	16.74	0.50	9.88	0.5
92	90.51mm-2/3Qb	2/3Qb	1.2ft-.5W-0.5ArmL	61	90.51	0.004	1.48	33.47	0.37	16.74	0.50	9.88	0.5
93	90.51mm-1/3Qb	1/3Qb	1.2ft-.5W-0.5ArmL	31	90.51	0.004	1.48	33.47	0.37	16.74	0.50	9.88	0.5
94	90.51mm-1/5Qb	1/5Qb	1.2ft-.5W-0.5ArmL	18	90.51	0.004	1.48	33.47	0.37	16.74	0.50	9.88	0.5
95	90.51mm-1/10Qb	1/10Qb	1.2ft-.5W-0.5ArmL	9	90.51	0.004	1.48	33.47	0.37	16.74	0.50	9.88	0.5
96	90.51mm-Qb	Qb	1.2ft-.5W-2ArmL	92	90.51	0.004	1.48	33.47	0.37	16.74	0.50	39.52	2.0
97	90.51mm-2/3Qb	2/3Qb	1.2ft-.5W-2ArmL	61	90.51	0.004	1.48	33.47	0.37	16.74	0.50	39.52	2.0
98	90.51mm-1/3Qb	1/3Qb	1.2ft-.5W-2ArmL	31	90.51	0.004	1.48	33.47	0.37	16.74	0.50	39.52	2.0
99	90.51mm-1/5Qb	1/5Qb	1.2ft-.5W-2ArmL	18	90.51	0.004	1.48	33.47	0.37	16.74	0.50	39.52	2.0
100	90.51mm-1/10Qb	1/10Qb	1.2ft-.5W-2ArmL	9	90.51	0.004	1.48	33.47	0.37	16.74	0.50	39.52	2.0

Table B1 page 4 (records 76-100) cont.

Record ID	Arm Angle	Arm Slope	Arm Slope %	L _t (m)	Z _u (m)	W _u (m)	V _o (m/s)	τ _c (Pa)	D _q (m)	h _{weir} (m)	D _{nref} (m)	V _{max} /V _o	V _{max} Loc	τ _{max} /τ _c	τ _{max} Loc
76	10.31	1.43	2.50%	110.27	0.51	22.31	2.11	73.20	1.40	1.28	1.35	1.24	14.25	1.77	12.25
77	10.31	1.43	2.50%	110.27	0.51	22.31	1.78	73.20	1.15	1.03	1.07	1.33	12.35	1.48	12.35
78	10.31	1.43	2.50%	110.27	0.51	22.31	1.32	73.20	0.83	0.71	0.73	1.56	10.35	1.24	9.35
79	10.31	1.43	2.50%	110.27	0.51	22.31	1.09	73.20	0.64	0.52	0.53	1.73	8.35	N/A	N/A
80	10.31	1.43	2.50%	110.27	0.51	22.31	0.83	73.20	0.46	0.34	0.35	1.94	7.35	N/A	N/A
81	46.76	3.53	6.17%	42.89	0.72	16.74	2.11	73.20	1.81	1.45	1.35	2.42	16.45	6.47	16.4
82	46.76	3.53	6.17%	42.89	0.72	16.74	1.78	73.20	1.56	1.20	1.07	2.75	16.45	6.01	15.4
83	46.76	3.53	6.17%	42.89	0.72	16.74	1.32	73.20	1.24	0.88	0.73	3.24	14.45	5.13	6.35
84	46.76	3.53	6.17%	42.89	0.72	16.74	1.09	73.20	1.06	0.69	0.53	3.41	13.45	N/A	N/A
85	46.76	3.53	6.17%	42.89	0.72	16.74	0.83	73.20	0.86	0.49	0.35	3.63	6.4	N/A	N/A
86	14.89	1.08	1.89%	106.07	0.67	16.74	2.11	73.20	1.54	1.18	1.35	1.63	13.45	3.20	12.4
87	14.89	1.08	1.89%	106.07	0.67	16.74	1.78	73.20	1.32	0.95	1.07	1.89	11.45	3.08	10.4
88	14.89	1.08	1.89%	106.07	0.67	16.74	1.32	73.20	1.04	0.67	0.73	2.30	9.45	2.69	8.45
89	14.89	1.08	1.89%	106.07	0.67	16.74	1.09	73.20	0.88	0.52	0.53	2.68	7.45	N/A	N/A
90	14.89	1.08	1.89%	106.07	0.67	16.74	0.83	73.20	0.73	0.37	0.35	3.01	8.45	N/A	N/A
91	40.26	4.73	8.27%	42.72	0.72	22.31	2.11	73.20	1.68	1.31	1.35	1.96	17.35	4.41	16.3
92	40.26	4.73	8.27%	42.72	0.72	22.31	1.78	73.20	1.43	1.07	1.07	2.15	16.35	3.92	5.5
93	40.26	4.73	8.27%	42.72	0.72	22.31	1.32	73.20	1.11	0.75	0.73	2.41	7.3	3.23	9.3
94	40.26	4.73	8.27%	42.72	0.72	22.31	1.09	73.20	0.93	0.57	0.53	2.49	7.3	N/A	N/A
95	40.26	4.73	8.27%	42.72	0.72	22.31	0.83	73.20	0.75	0.38	0.35	3.12	6.5	N/A	N/A
96	11.95	1.35	2.36%	97.58	0.68	22.31	2.11	73.20	1.51	1.14	1.35	1.39	13.3	2.39	11.25
97	11.95	1.35	2.36%	97.58	0.68	22.31	1.78	73.20	1.27	0.90	1.07	1.58	12.35	2.19	10.35
98	11.95	1.35	2.36%	97.58	0.68	22.31	1.32	73.20	0.97	0.61	0.73	1.94	9.35	2.00	8.35
99	11.95	1.35	2.36%	97.58	0.68	22.31	1.09	73.20	0.83	0.46	0.53	2.15	7.35	N/A	N/A
100	11.95	1.35	2.36%	97.58	0.68	22.31	0.83	73.20	0.68	0.32	0.35	2.02	5.5	N/A	N/A

Table B1 page 5 (records 101-125) – Summary of numerical model results.

Record ID	Reach	Qratio	StrucRef	Q (cms)	d ₅₀ (mm)	S _o	H _{bkf} (m)	T _w (m)	Z _d (m)	W _t (m)	W _t /T _w	L _a (m)	L _a _{ref}
101	90.51mm-Qb	Qb	0.8ft-.3W-0.5ArmL	92	90.51	0.004	1.48	33.47	0.24	11.16	0.33	11.68	0.5
102	90.51mm-2/3Qb	2/3Qb	0.8ft-.3W-0.5ArmL	61	90.51	0.004	1.48	33.47	0.24	11.16	0.33	11.68	0.5
103	90.51mm-1/3Qb	1/3Qb	0.8ft-.3W-0.5ArmL	31	90.51	0.004	1.48	33.47	0.24	11.16	0.33	11.68	0.5
104	90.51mm-1/5Qb	1/5Qb	0.8ft-.3W-0.5ArmL	18	90.51	0.004	1.48	33.47	0.24	11.16	0.33	11.68	0.5
105	90.51mm-1/10Qb	1/10Qb	0.8ft-.3W-0.5ArmL	9	90.51	0.004	1.48	33.47	0.24	11.16	0.33	11.68	0.5
106	90.51mm-Qb	Qb	0.8ft-.3W-2ArmL	92	90.51	0.004	1.48	33.47	0.24	11.16	0.33	46.71	2.0
107	90.51mm-2/3Qb	2/3Qb	0.8ft-.3W-2ArmL	61	90.51	0.004	1.48	33.47	0.24	11.16	0.33	46.71	2.0
108	90.51mm-1/3Qb	1/3Qb	0.8ft-.3W-2ArmL	31	90.51	0.004	1.48	33.47	0.24	11.16	0.33	46.71	2.0
109	90.51mm-1/5Qb	1/5Qb	0.8ft-.3W-2ArmL	18	90.51	0.004	1.48	33.47	0.24	11.16	0.33	46.71	2.0
110	90.51mm-1/10Qb	1/10Qb	0.8ft-.3W-2ArmL	9	90.51	0.004	1.48	33.47	0.24	11.16	0.33	46.71	2.0
111	181mm-Qb	Qb	0.8ft-.3W-1ArmL	36	181	0.01	1.01	19.24	0.24	6.41	0.33	13.20	1.0
112	181mm-2/3Qb	2/3Qb	0.8ft-.3W-1ArmL	24	181	0.01	1.01	19.24	0.24	6.41	0.33	13.20	1.0
113	181mm-1/3Qb	1/3Qb	0.8ft-.3W-1ArmL	12	181	0.01	1.01	19.24	0.24	6.41	0.33	13.20	1.0
114	181mm-1/5Qb	1/5Qb	0.8ft-.3W-1ArmL	7	181	0.01	1.01	19.24	0.24	6.41	0.33	13.20	1.0
115	181mm-1/10Qb	1/10Qb	0.8ft-.3W-1ArmL	4	181	0.01	1.01	19.24	0.24	6.41	0.33	13.20	1.0
116	181mm-Qb	Qb	0.4ft-.25W-0.5ArmL	36	181	0.01	1.01	19.24	0.12	4.81	0.25	7.57	0.5
117	181mm-2/3Qb	2/3Qb	0.4ft-.25W-0.5ArmL	24	181	0.01	1.01	19.24	0.12	4.81	0.25	7.57	0.5
118	181mm-1/3Qb	1/3Qb	0.4ft-.25W-0.5ArmL	12	181	0.01	1.01	19.24	0.12	4.81	0.25	7.57	0.5
119	181mm-1/5Qb	1/5Qb	0.4ft-.25W-0.5ArmL	7	181	0.01	1.01	19.24	0.12	4.81	0.25	7.57	0.5
120	181mm-1/10Qb	1/10Qb	0.4ft-.25W-0.5ArmL	4	181	0.01	1.01	19.24	0.12	4.81	0.25	7.57	0.5
121	181mm-Qb	Qb	0.4ft-.25W-2ArmL	36	181	0.01	1.01	19.24	0.12	4.81	0.25	30.26	2.0
122	181mm-2/3Qb	2/3Qb	0.4ft-.25W-2ArmL	24	181	0.01	1.01	19.24	0.12	4.81	0.25	30.26	2.0
123	181mm-1/3Qb	1/3Qb	0.4ft-.25W-2ArmL	12	181	0.01	1.01	19.24	0.12	4.81	0.25	30.26	2.0
124	181mm-1/5Qb	1/5Qb	0.4ft-.25W-2ArmL	7	181	0.01	1.01	19.24	0.12	4.81	0.25	30.26	2.0
125	181mm-1/10Qb	1/10Qb	0.4ft-.25W-2ArmL	4	181	0.01	1.01	19.24	0.12	4.81	0.25	30.26	2.0

Table B1 page 5 (records 101-125) cont.

Record ID	Arm Angle	Arm Slope	Arm Slope %	L _t (m)	Z _u (m)	W _u (m)	V _o (m/s)	τ _c (Pa)	D _q (m)	h _{weir} (m)	D _{nref} (m)	V _{max} /V _o	V _{max} Loc	τ _{max} /τ _c	τ _{max} Loc
101	43.69	4.2	7.34%	43.55	0.64	18.59	2.11	73.20	1.68	1.44	1.35	2.19	17.4	5.07	15.4
102	43.69	4.2	7.34%	43.55	0.64	18.59	1.78	73.20	1.43	1.18	1.07	2.45	16.4	4.83	15.4
103	43.69	4.2	7.34%	43.55	0.64	18.59	1.32	73.20	1.09	0.84	0.73	2.82	15.4	3.84	15.4
104	43.69	4.2	7.34%	43.55	0.64	18.59	1.09	73.20	0.89	0.65	0.53	3.04	13.4	N/A	N/A
105	43.69	4.2	7.34%	43.55	0.64	18.59	0.83	73.20	0.69	0.45	0.35	3.07	11.4	N/A	N/A
106	13.43	1.25	2.18%	107.25	0.59	18.59	2.11	73.20	1.46	1.22	1.35	1.47	13.4	2.43	13.4
107	13.43	1.25	2.18%	107.25	0.59	18.59	1.78	73.20	1.23	0.99	1.07	1.66	12.4	2.36	12.4
108	13.43	1.25	2.18%	107.25	0.59	18.59	1.32	73.20	0.93	0.69	0.73	1.95	10.4	1.99	9.4
109	13.43	1.25	2.18%	107.25	0.59	18.59	1.09	73.20	0.76	0.51	0.53	2.23	8.45	N/A	N/A
110	13.43	1.25	2.18%	107.25	0.59	18.59	0.83	73.20	0.59	0.34	0.35	2.50	8.5	N/A	N/A
111	25.91	2.49	4.35%	35.80	0.46	10.69	2.15	146.38	1.15	0.91	0.91	1.88	15.4	3.39	14.4
112	25.91	2.49	4.35%	35.80	0.46	10.69	1.80	146.38	0.99	0.74	0.73	2.08	14.4	3.07	14.4
113	25.91	2.49	4.35%	35.80	0.46	10.69	1.34	146.38	0.77	0.53	0.50	2.34	12.4	2.39	11.4
114	25.91	2.49	4.35%	35.80	0.46	10.69	1.08	146.38	0.65	0.41	0.37	2.59	10.4	N/A	N/A
115	25.91	2.49	4.35%	35.80	0.46	10.69	0.85	146.38	0.53	0.28	0.24	2.74	7.4	N/A	N/A
116	43.65	4.47	7.82%	25.78	0.39	9.62	2.15	146.38	1.21	1.09	0.91	2.11	17.45	4.23	16.4
117	43.65	4.47	7.82%	25.78	0.39	9.62	1.80	146.38	1.03	0.91	0.73	2.33	16.45	3.78	16.45
118	43.65	4.47	7.82%	25.78	0.39	9.62	1.34	146.38	0.79	0.67	0.50	2.59	15.5	2.80	15.5
119	43.65	4.47	7.82%	25.78	0.39	9.62	1.08	146.38	0.64	0.52	0.37	2.82	14.5	N/A	N/A
120	43.65	4.47	7.82%	25.78	0.39	9.62	0.85	146.38	0.48	0.36	0.24	2.43	12.45	N/A	N/A
121	13.41	1.09	1.90%	67.05	0.32	9.62	2.15	146.38	0.99	0.87	0.91	1.42	14.45	1.92	13.4
122	13.41	1.09	1.90%	67.05	0.32	9.62	1.80	146.38	0.83	0.71	0.73	1.56	12.45	1.71	12.4
123	13.41	1.09	1.90%	67.05	0.32	9.62	1.34	146.38	0.63	0.51	0.50	1.77	10.45	1.35	10.45
124	13.41	1.09	1.90%	67.05	0.32	9.62	1.08	146.38	0.51	0.38	0.37	1.98	9.45	N/A	N/A
125	13.41	1.09	1.90%	67.05	0.32	9.62	0.85	146.38	0.38	0.26	0.24	2.23	7.45	N/A	N/A

Table B1 page 6 (records 126-150) – Summary of numerical model results.

Record ID	Reach	Qratio	StrucRef	Q (cms)	d ₅₀ (mm)	S _o	H _{bkf} (m)	T _w (m)	Z _d (m)	W _t (m)	W _t /T _w	L _a (m)	L _a _{ref}
126	181mm-Qb	Qb	0.4ft-.5W-0.5ArmL	36	181	0.01	1.01	19.24	0.12	9.62	0.50	6.61	0.5
127	181mm-2/3Qb	2/3Qb	0.4ft-.5W-0.5ArmL	24	181	0.01	1.01	19.24	0.12	9.62	0.50	6.61	0.5
128	181mm-1/3Qb	1/3Qb	0.4ft-.5W-0.5ArmL	12	181	0.01	1.01	19.24	0.12	9.62	0.50	6.61	0.5
129	181mm-1/5Qb	1/5Qb	0.4ft-.5W-0.5ArmL	7	181	0.01	1.01	19.24	0.12	9.62	0.50	6.61	0.5
130	181mm-1/10Qb	1/10Qb	0.4ft-.5W-0.5ArmL	4	181	0.01	1.01	19.24	0.12	9.62	0.50	6.61	0.5
131	181mm-Qb	Qb	0.4ft-.5W-2ArmL	36	181	0.01	1.01	19.24	0.12	9.62	0.50	26.44	2.0
132	181mm-2/3Qb	2/3Qb	0.4ft-.5W-2ArmL	24	181	0.01	1.01	19.24	0.12	9.62	0.50	26.44	2.0
133	181mm-1/3Qb	1/3Qb	0.4ft-.5W-2ArmL	12	181	0.01	1.01	19.24	0.12	9.62	0.50	26.44	2.0
134	181mm-1/5Qb	1/5Qb	0.4ft-.5W-2ArmL	7	181	0.01	1.01	19.24	0.12	9.62	0.50	26.44	2.0
135	181mm-1/10Qb	1/10Qb	0.4ft-.5W-2ArmL	4	181	0.01	1.01	19.24	0.12	9.62	0.50	26.44	2.0
136	181mm-Qb	Qb	1.2ft-.25W-0.5ArmL	36	181	0.01	1.01	19.24	0.37	4.81	0.25	6.42	0.5
137	181mm-2/3Qb	2/3Qb	1.2ft-.25W-0.5ArmL	24	181	0.01	1.01	19.24	0.37	4.81	0.25	6.42	0.5
138	181mm-1/3Qb	1/3Qb	1.2ft-.25W-0.5ArmL	12	181	0.01	1.01	19.24	0.37	4.81	0.25	6.42	0.5
139	181mm-1/5Qb	1/5Qb	1.2ft-.25W-0.5ArmL	7	181	0.01	1.01	19.24	0.37	4.81	0.25	6.42	0.5
140	181mm-1/10Qb	1/10Qb	1.2ft-.25W-0.5ArmL	4	181	0.01	1.01	19.24	0.37	4.81	0.25	6.42	0.5
141	181mm-Qb	Qb	1.2ft-.25W-2ArmL	36	181	0.01	1.01	19.24	0.37	4.81	0.25	25.68	2.0
142	181mm-2/3Qb	2/3Qb	1.2ft-.25W-2ArmL	24	181	0.01	1.01	19.24	0.37	4.81	0.25	25.68	2.0
143	181mm-1/3Qb	1/3Qb	1.2ft-.25W-2ArmL	12	181	0.01	1.01	19.24	0.37	4.81	0.25	25.68	2.0
144	181mm-1/5Qb	1/5Qb	1.2ft-.25W-2ArmL	7	181	0.01	1.01	19.24	0.37	4.81	0.25	25.68	2.0
145	181mm-1/10Qb	1/10Qb	1.2ft-.25W-2ArmL	4	181	0.01	1.01	19.24	0.37	4.81	0.25	25.68	2.0
146	181mm-Qb	Qb	1.2ft-.5W-0.5ArmL	36	181	0.01	1.01	19.24	0.37	9.62	0.50	5.35	0.5
147	181mm-2/3Qb	2/3Qb	1.2ft-.5W-0.5ArmL	24	181	0.01	1.01	19.24	0.37	9.62	0.50	5.35	0.5
148	181mm-1/3Qb	1/3Qb	1.2ft-.5W-0.5ArmL	12	181	0.01	1.01	19.24	0.37	9.62	0.50	5.35	0.5
149	181mm-1/5Qb	1/5Qb	1.2ft-.5W-0.5ArmL	7	181	0.01	1.01	19.24	0.37	9.62	0.50	5.35	0.5
150	181mm-1/10Qb	1/10Qb	1.2ft-.5W-0.5ArmL	4	181	0.01	1.01	19.24	0.37	9.62	0.50	5.35	0.5

Table B1 page 6 (records 126-150) cont.

Record ID	Arm Angle	Arm Slope	Arm Slope %	L _t (m)	Z _u (m)	W _u (m)	V _o (m/s)	τ _c (Pa)	D _q (m)	h _{weir} (m)	D _{nref} (m)	V _{max} /V _o	V _{max} Loc	τ _{max} /τ _c	τ _{max} Loc
126	36.05	5.77	10.10%	26.05	0.40	12.83	2.15	146.38	1.10	0.98	0.91	1.70	17.35	2.79	17.3
127	36.05	5.77	10.10%	26.05	0.40	12.83	1.80	146.38	0.92	0.80	0.73	1.83	17.5	2.38	16.35
128	36.05	5.77	10.10%	26.05	0.40	12.83	1.34	146.38	0.68	0.56	0.50	1.96	15.35	1.67	14.35
129	36.05	5.77	10.10%	26.05	0.40	12.83	1.08	146.38	0.54	0.42	0.37	2.08	14.35	N/A	N/A
130	36.05	5.77	10.10%	26.05	0.40	12.83	0.85	146.38	0.39	0.27	0.24	2.11	12.35	N/A	N/A
131	10.31	1.34	2.34%	63.39	0.33	12.83	2.15	146.38	0.97	0.85	0.91	1.27	14.25	1.57	12.25
132	10.31	1.34	2.34%	63.39	0.33	12.83	1.80	146.38	0.80	0.68	0.73	1.32	13.3	1.26	13.3
133	10.31	1.34	2.34%	63.39	0.33	12.83	1.34	146.38	0.59	0.47	0.50	1.47	10.35	0.96	10.35
134	10.31	1.34	2.34%	63.39	0.33	12.83	1.08	146.38	0.46	0.34	0.37	1.61	9.35	N/A	N/A
135	10.31	1.34	2.34%	63.39	0.33	12.83	0.85	146.38	0.34	0.22	0.24	1.73	5.5	N/A	N/A
136	48.35	3.46	6.05%	24.16	0.56	9.62	2.15	146.38	1.38	1.02	0.91	2.29	17.45	5.36	6.35
137	48.35	3.46	6.05%	24.16	0.56	9.62	1.80	146.38	1.20	0.84	0.73	2.63	16.45	5.29	6.35
138	48.35	3.46	6.05%	24.16	0.56	9.62	1.34	146.38	0.97	0.60	0.50	3.07	15.45	4.61	6.35
139	48.35	3.46	6.05%	24.16	0.56	9.62	1.08	146.38	0.84	0.48	0.37	3.41	6.4	N/A	N/A
140	48.35	3.46	6.05%	24.16	0.56	9.62	0.85	146.38	0.70	0.34	0.24	4.04	6.4	N/A	N/A
141	15.7	0.84	1.47%	58.15	0.50	9.62	2.15	146.38	1.12	0.76	0.91	1.70	14.5	2.92	14.5
142	15.7	0.84	1.47%	58.15	0.50	9.62	1.80	146.38	0.96	0.59	0.73	1.94	10.45	2.79	10.4
143	15.7	0.84	1.47%	58.15	0.50	9.62	1.34	146.38	0.77	0.41	0.50	2.43	8.45	2.79	6.35
144	15.7	0.84	1.47%	58.15	0.50	9.62	1.08	146.38	0.68	0.31	0.37	2.93	8.45	N/A	N/A
145	15.7	0.84	1.47%	58.15	0.50	9.62	0.85	146.38	0.59	0.22	0.24	3.42	8.5	N/A	N/A
146	41.96	4.73	8.27%	24.06	0.56	12.83	2.15	146.38	1.31	0.95	0.91	1.97	8.3	3.97	9.3
147	41.96	4.73	8.27%	24.06	0.56	12.83	1.80	146.38	1.13	0.77	0.73	2.15	8.3	3.63	16.35
148	41.96	4.73	8.27%	24.06	0.56	12.83	1.34	146.38	0.90	0.54	0.50	2.54	6.5	2.83	9.3
149	41.96	4.73	8.27%	24.06	0.56	12.83	1.08	146.38	0.77	0.41	0.37	3.02	6.5	N/A	N/A
150	41.96	4.73	8.27%	24.06	0.56	12.83	0.85	146.38	0.64	0.27	0.24	3.54	6.5	N/A	N/A

Table B1 page 7 (records 151-165) – Summary of numerical model results.

Record ID	Reach	Qratio	StrucRef	Q (cms)	d ₅₀ (mm)	S _o	H _{bkf} (m)	T _w (m)	Z _d (m)	W _t (m)	W _t /T _w	L _a (m)	L _a _{ref}
151	181mm-Qb	Qb	1.2ft-.5W-2ArmL	36	181	0.01	1.01	19.24	0.37	9.62	0.50	21.40	2.0
152	181mm-2/3Qb	2/3Qb	1.2ft-.5W-2ArmL	24	181	0.01	1.01	19.24	0.37	9.62	0.50	21.40	2.0
153	181mm-1/3Qb	1/3Qb	1.2ft-.5W-2ArmL	12	181	0.01	1.01	19.24	0.37	9.62	0.50	21.40	2.0
154	181mm-1/5Qb	1/5Qb	1.2ft-.5W-2ArmL	7	181	0.01	1.01	19.24	0.37	9.62	0.50	21.40	2.0
155	181mm-1/10Qb	1/10Qb	1.2ft-.5W-2ArmL	4	181	0.01	1.01	19.24	0.37	9.62	0.50	21.40	2.0
156	181mm-Qb	Qb	0.8ft-.3W-0.5ArmL	36	181	0.01	1.01	19.24	0.24	6.41	0.33	6.60	0.5
157	181mm-2/3Qb	2/3Qb	0.8ft-.3W-0.5ArmL	24	181	0.01	1.01	19.24	0.24	6.41	0.33	6.60	0.5
158	181mm-1/3Qb	1/3Qb	0.8ft-.3W-0.5ArmL	12	181	0.01	1.01	19.24	0.24	6.41	0.33	6.60	0.5
159	181mm-1/5Qb	1/5Qb	0.8ft-.3W-0.5ArmL	7	181	0.01	1.01	19.24	0.24	6.41	0.33	6.60	0.5
160	181mm-1/10Qb	1/10Qb	0.8ft-.3W-0.5ArmL	4	181	0.01	1.01	19.24	0.24	6.41	0.33	6.60	0.5
161	181mm-Qb	Qb	0.8ft-.3W-2ArmL	36	181	0.01	1.01	19.24	0.24	6.41	0.33	26.40	2.0
162	181mm-2/3Qb	2/3Qb	0.8ft-.3W-2ArmL	24	181	0.01	1.01	19.24	0.24	6.41	0.33	26.40	2.0
163	181mm-1/3Qb	1/3Qb	0.8ft-.3W-2ArmL	12	181	0.01	1.01	19.24	0.24	6.41	0.33	26.40	2.0
164	181mm-1/5Qb	1/5Qb	0.8ft-.3W-2ArmL	7	181	0.01	1.01	19.24	0.24	6.41	0.33	26.40	2.0
165	181mm-1/10Qb	1/10Qb	0.8ft-.3W-2ArmL	4	181	0.01	1.01	19.24	0.24	6.41	0.33	26.40	2.0

Table B1 page 7 (records 151-165) cont.

Record ID	Arm Angle	Arm Slope	Arm Slope %	L _t (m)	Z _u (m)	W _u (m)	V _o (m/s)	τ _c (Pa)	D _q (m)	h _{weir} (m)	D _{nref} (m)	V _{max} /V _o	V _{max} Loc	τ _{max} /τ _c	τ _{max} Loc
151	12.67	1.13	1.97%	53.49	0.51	12.83	2.15	146.38	1.15	0.79	0.91	1.46	12.3	2.41	7.2
152	12.67	1.13	1.97%	53.49	0.51	12.83	1.80	146.38	0.98	0.61	0.73	1.71	10.35	2.35	7.2
153	12.67	1.13	1.97%	53.49	0.51	12.83	1.34	146.38	0.77	0.41	0.50	2.07	8.35	2.02	9.35
154	12.67	1.13	1.97%	53.49	0.51	12.83	1.08	146.38	0.67	0.31	0.37	2.15	7.35	N/A	N/A
155	12.67	1.13	1.97%	53.49	0.51	12.83	0.85	146.38	0.57	0.21	0.24	2.58	8.2	N/A	N/A
156	44.18	4.38	7.66%	24.87	0.48	10.69	2.15	146.38	1.25	1.00	0.91	2.16	17.4	4.30	17.4
157	44.18	4.38	7.66%	24.87	0.48	10.69	1.80	146.38	1.06	0.82	0.73	2.39	16.4	3.91	15.4
158	44.18	4.38	7.66%	24.87	0.48	10.69	1.34	146.38	0.83	0.59	0.50	2.65	15.4	3.07	14.4
159	44.18	4.38	7.66%	24.87	0.48	10.69	1.08	146.38	0.70	0.45	0.37	2.86	14.4	N/A	N/A
160	44.18	4.38	7.66%	24.87	0.48	10.69	0.85	146.38	0.56	0.31	0.24	2.41	12.4	N/A	N/A
161	13.65	1.07	1.87%	60.78	0.41	10.69	2.15	146.38	1.04	0.79	0.91	1.48	13.4	2.11	11.3
162	13.65	1.07	1.87%	60.78	0.41	10.69	1.80	146.38	0.87	0.63	0.73	1.67	12.4	2.02	10.4
163	13.65	1.07	1.87%	60.78	0.41	10.69	1.34	146.38	0.67	0.43	0.50	1.89	9.4	1.65	9.4
164	13.65	1.07	1.87%	60.78	0.41	10.69	1.08	146.38	0.56	0.32	0.37	2.15	8.4	N/A	N/A
165	13.65	1.07	1.87%	60.78	0.41	10.69	0.85	146.38	0.46	0.21	0.24	2.50	8.4	N/A	N/A